Report No. FHWA-RD-75-1

RELATING PAVEMENT ROUGHNESS TO VEHICLE BEHAVIOR

B. E. Quinn and E. W. Jones

October 1974
Final Report

This document is available to the public through the National Technical Information Service, Springfield, Virginia 22161

Prepared for
FEDERAL HIGHWAY ADMINISTRATION
Offices of Research & Development
Washington, D.C. 20590

NOTICE

This document is disseminated under the sponsorship of the U.S. Department of Transportation in the interest of information exchange. The United States Government assumes no liability for its contents or use thereof.

The contents of this report reflect the views of the Purdue Research Foundation which is responsible for the facts and the accuracy of the data presented herein. The contents do not necessarily reflect the official views or policy of the Department of Transportation.

This report does not constitute a standard, specification, or regulation.

FHWA DISTRIBUTION NOTICE

This report is being given limited distribution, primarily to research audiences, by FHWA transmittal memorandum. Distribution to FHWA field offices will be to Field Project Advisors in accordance with this procedure.

TECHNICAL REPORT STANDARD TITLE PAGE

1. Report No.	2. Government Accession No.	3. Recipient's Catalog No.
FHWA-RD-75-1		

4. Title and Subtitle
RELATING PAVEMENT ROUGHNESS TO VEHICLE BEHAVIOR

5. Report Date
October 1974

6. Performing Organization Code

7. Author(s)
B. E. Quinn and E. W. Jones

8. Performing Organization Report No.

9. Performing Organization Name and Address
Purdue Research Foundation
Mechanical Engineering School
Lafayette, Indiana 47907

10. Work Unit No.
FCP-31H3-112

11. Contract or Grant No.
DOT-FH-11-8056

12. Sponsoring Agency Name and Address
U.S. Department of Transportation
Federal Highway Administration
Washington, D.C. 20590

13. Type of Report and Period Covered
Final Report
May 1973 to May 1974

14. Sponsoring Agency Code
S0453

15. Supplementary Notes
Contract Manager: Glenn G. Balmer (HRS-12).

16. Abstract

A study was made of the relationship between pavement roughness as measured with the modified BPR roughometer and various criteria of vehicle behavior such as steer angle, steering wheel angle, side-slip angle, driver acceleration and lateral tire forces. The possible use of these criteria to establish limits for pavement roughness is discussed.

This is the first of three reports on pavement roughness and vehicle dynamics studies under this contract. Titles of the other two reports are listed below:

(2) "Laboratory Measurement of Vehicle Characteristics for Predicting Highway Behavior" (FHWA-RD- 75-2).

(3) Tentative Road Roughness Criteria Based Upon Vehicle Performance (FHWA-RD-75-3)

17. Key Words	18. Distribution Statement
Road Roughness Pavement Roughness Vehicle Response Safety Highway Safety	No restrictions. This document is available through the National Technical Information Service, Springfield, Virginia 22161.

19. Security Classif. (of this report)	20. Security Classif. (of this page)	21. No. of Pages	22. Price
Unclassified	Unclassified	215	

Form DOT F 1700.7 (8-69)

TABLE OF CONTENTS

LIST OF TABLES

LIST OF FIGURES

PREFACE

The surface roughness of a highway may significantly affect the behavior of a vehicle and the driver. When the road roughness produces relative motion between the wheels and the vehicle body, unanticipated steering of the wheels may be produced. Wheel hop, which is excited by the road undulations, reduces the effective value of the lateral tire force that is available to control the vehicle. The vibration of the driver contributes to operator fatigue.

This investigation shows the effects of road roughness on the behavior of the vehicle and driver system in terms of the following factors: The steer angle, the steering wheel angle, the sideslip angle, the vertical acceleration of the driver and the available lateral tire force. The steer angle, steering wheel angle, sideslip angle and acceleration of the driver were obtained by measurement. The lateral tire forces are calculated values. These quantities are reported for various roads which have known values of roughness. The roughness values were measured by the modified BPR roughometer.

The possibility of using these factors to establish tolerance limits for road roughness is discussed.

The change in vehicle sideslip angle was investigated by using measured values of steering wheel rotation as the input to the bicycle mathematical model.

The ride of the vehicle on roads of different roughness was also investigated by using the roughness power spectrum as the excitation for a linear three degree of freedom model to obtain vertical driver acceleration.

The roughness power spectrum as defined by the Zable Equation was used to generate a distance-based roughness profile for a road surface.

The steering wheel rotation, the vertical acceleration of the driver, the lateral tire force and the normal tire force appear to have the greatest potential for aiding in the establishment of tolerances for road roughness.

SUMMARY OF REPORT

OBJECTIVE

The purpose of this investigation was to study acceptable levels of road roughness by considering those aspects of vehicle behavior that are adversely influenced by pavement roughness.

PROCEDURE

In this investigation road roughness was measured by means of the modified BPR roughometer which made it possible to determine experimentally the pavement roughness spectra of the highways in question. The aspects of vehicle behavior that were studied in detail consisted of the steer angle of the left front wheel, the steering wheel angle, the sideslip angle, the driver acceleration and the lateral tire forces. In this investigation the possibility of using each of these factors as an indicator of pavement roughness was considered.

Special equipment (see pages 61-63) was developed for measuring the rotation of the left front wheel about the steer axis as the vehicle was driven down the road. The angular position of the left front wheel about the king pin axis was recorded continuously using this equipment, and this angular position is referred to as the steer angle. The vehicle was operated on different highways having different degrees of roughness and the behavior of this angle was studied.

Special equipment was also developed for measuring the rotation of the steering wheel as the vehicle was driven on the road. This is referred to as the steering wheel angle. A detailed description of the instrumentation used for measuring the steering wheel angle is given on pages 63-71 of the report.

The use of the sideslip angle of the vehicle was also considered as a possible criterion pavement roughness. A more complete discussion of the theoretical aspects of the sideslip angle and its relationship to other vehicle performance characteristics is given in the report on pages 18-42 inclusive. The instrumentation is described on pages 71-76. It was not possible to measure the sideslip angle directly while operating the vehicle on a highway, but continuous records were made of those quantities from which the value of the sideslip angle could be determined at any instant of time.

The vertical acceleration of the driver was also considered as a possible criterion of pavement roughness. An accelerometer was placed on the interface between the driver and the seat and continuous records of this acceleration were made as the vehicle was driven over the highway. The theoretical aspects of considering the vertical acceleration are discussed in the report on pages 42-47 while the instrumentation is discussed on page 76.

The lateral tire forces, sometimes referred to as the cornering forces, were also considered as a possible criterion

of the pavement roughness. These forces depend upon the properties of the tire and the pavement, and also upon the vertical forces which the vehicle exerts upon the road. Since the pavement roughness influences the vertical forces, it will also influence the lateral forces which are necessary for vehicle control. A significant variation in these forces would indicate a significant variation in the ability of the driver to maneuver the vehicle. These forces are important even on straight sections of pavement because passing maneuvers are frequently executed under these conditions. The ability of the driver to control the vehicle during a passing maneuver is directly related to highway safety. The theory involved in determing the lateral tire forces is found on pages 47-51 of the report.

When the modified BPR roughometer is used to measure the pavement roughness spectrum, experimental values are obtained for the various ordinates of the roughness spectrum curve. It is difficult to use this information when further analysis is undertaken, and an empirical equation is used to represent the pavement roughness spectrum. This equation contains two constants designated by P and Q, and these constants completely define a curve that can be fitted to the experimentally measured values of pavement roughness. In certain types of analysis it is desirable to have a pavement profile established that has certain statistical properties. The use of the values

P and Q and the procedure for establishing such a profile is also discussed in this report. The theory underlying this procedure is discussed on pages 51-59 inclusive.

RESULTS

Steer Angle

The use of the steer angle (the angular rotation of the left front wheel about the king pin axis) as a criterion of controllability is less satisfactory than other criteria. In certain situations the steer angle and the steering wheel rotation were very closely related as shown in Figures 4.1 and 4.2. Unfortunately there were other situations in which this relationship was less meaningful as shown in Figure 4.3. In this figure the steer angle shows considerable variation while the steering wheel rotation shows somewhat less change in magnitude. This was due to the relative motion between the body of the vehicle and the unsprung mass of the front suspension system. Changes in steer angle thus did not indicate effort upon the part of the driver to control the vehicle. Moreover, corresponding changes also occured in the steer angle of the right front wheel so that at times both front wheels appeared to oscillate out of phase as the vehicle was moving down the highway. The steering effect of one wheel thus cancelled the steering effect of the other wheel, although there were measurable changes in the steer angle of both wheels. Because of this condition the steer angle was less satisfactory as the criterion of the vehicle controllability than were other quantities studied in this investigation.

Steering Wheel Angle

On the other hand, the steering wheel angle was a relatively sensitive criterion of pavement roughness. The effect of pavement roughness on the steering wheel angle is shown in Figures 4.4 and 4.5. On the rougher road (Figure 4.4) the magnitudes of the steering wheel angle are considerably larger than are those measured on the smoother road (Figure 4.5).

Not only is the amplitude of the steering wheel angle influenced by pavement roughness but the frequencies present in the steering wheel angle records are also sensitive to this condition. This is shown in Figure 4.6 in which the steering wheel angle as a function of time is shown for State Road 26 (S.R. 26) which is a pavement having relatively long wavelengths in its contour but which is relatively smooth as far as the shorter wavelengths are concerned. This is characteristic of many bituminous pavements. In this record a relatively low frequency is observed in the steering wheel angle plotted as a function of time. On the other hand, in Figure 4.7 the effect of shorter wavelength disturbances are indicated by the relatively high frequency that is present in this record. This pavement was a faulted concrete pavement containing a relatively large amount of short wavelength roughness but being relatively smooth as far as the longer wavelengths are concerned. Similar curves for two other roads are shown in Figures 4.8 and 4.9.

The probability density distribution for steering wheel angles on these roads is given in Figures 4.10 to Figure 4.15

inclusive, while Table 4.2 summarizes the statistical properties of the steering wheel angle for six different highways.

The power spectral density functions of steering wheel angle versus time were also computed and are given in Figures 4.18 to 4.23 inclusive. Significant differences are shown in these spectra as can clearly be seen in Figures 4.19 and Figures 4.20. The area under these power spectrum curves represents the mean squared value of the steering wheel angle, and this value is plotted as a function of the mean squared value of the roughness of the road. This latter value was obtained by taking the area under the pavement roughness spectrum curves as described in the report. This relationship is shown in Figure 4.24, which indicated that there is a relationship between pavement roughness and the mean squared value of the steering wheel angle of a vehicle operated over the pavement in question.

Unfortunately it was not possible to measure the pavement roughness at the same time that the measurements of vehicle performance were made. Previous values of pavement roughness were therefore used in this study, and the existing roughness was therefore somewhat greater than is indicated in this report.

The steering wheel angle is relatively easy to measure and is very sensitive to pavement roughness. This investigation indicates that the steering wheel angle may be a very useful criterion in establishing levels of pavement roughness for straight pavement sections.

Sideslip Angle

Using the equipment described in the report, the sideslip angle was measured with the vehicle traveling on a circular path and also with the vehicle traveling on selected sections of pavement. Figure 3.10 shows a comparison of the radius of curvature of the vehicle path determined from the sideslip angle as compared with that obtained by another means. For a vehicle traveling on a straight section of pavement the variation in the sideslip angle was insignificant. Figures 4.26 and 4.27 indicate the relationship between the sideslip angle and the steer angle of the vehicle plotted as functions of time. A comparison of the path of the vehicle computed from the sideslip angle measurements with that of the actual path is shown in Figure 4.28.

The variation of the sideslip angle for a vehicle going around a rough curve is shown in Figure 4.29. This curve was so rough that it was diffiuclt to control the vehicle during this maneuver.

The tests indicated that the sideslip angle is relatively insensitive to pavement roughness, and that other criteria of vehicle behavior are more closely related to the pavement roughness than is the sideslip angle. The sideslip angle is a relatively difficult quantity to measure because of its small magnitude.

Vertical Driver Acceleration

The vertical acceleration of the driver was obtained by placing an accelerometer on the seat of the vehicle and making measurements while the vehicle was driven along the highway. These measurements were made with and without the rear shock absorbers being attached to the vehicle.

Typical records are shown in Figures 4.34 to 4.37 inclusive. Probability density curves were plotted and are shown in Figures 4.38 to 4.41 for those tests conducted without the rear shock absorbers while corresponding curves for tests conducted with the rear shock absorbers are shown in Figures 4.48 to 4.53 inclusive. Tables summarizing these distributions are given in Tables 4.3 and 4.4.Of greatest interest, however, are the power spectral density curves of driver acceleration. Of particular interest is the power spectrum curve of driver acceleration for S. R. 26 given in Figure 4.42. Here the largest amount of power is in the low frequency region. The corresponding curve for driver acceleration for U. S. 52 is shown in Figure 4.43 in which the largest amount of power is indicated in the higher frequency region. The curve given in Figure 4.44 indicates that the power in the power spectral density curve of the vertical acceleration of the driver for Cummberland Ave. is approximately equally split between the high and the low frequency regions. It was evident from these tests that the vertical acceleration of the driver is very sen-

sitive to both high frequency and low frequency disturbances generated by roughness in the highway. As a result the area under the roughness power spectrum curve for these highways was divided into two regions and the areas under the driver acceleration power spectrum curves were treated in the same manner. The relationships between the low frequency regions and the high frequency regions were studied independently. Figure 4.46 shows a comparison of the corresponding areas of the pavement roughness spectrum curves and the driver acceleration power spectrum curves for the low frequency region. A corresponding comparison in the high frequency region is given in Figure 4.47.

These measurements of driver acceleration provide one of the most significant results of this research effort because it appears possible to relate long wavelength roughness and short wavelength roughness with high and low frequency driver accelerations. It thus appears possible to evaluate the pavement roughness in different wavelength regions. This may be one of the more useful ways for evaluating pavement roughness, but further study is needed to determine the effect of vehicle suspension systems.

Lateral Tire Forces

The lateral tire forces (cornering forces) are parallel to the surface of the road and perpendicular to the wheel heading. These forces are necessary when the vehicle is executing a turn or undergoing a passing maneuver on a

straight section of highway. These forces are related to the vertical tire forces that in turn are influenced by the roughness of the pavement. Consequently the lateral forces are also influenced by pavement roughness, and hence the ability to control the vehicle is involved.

The lateral forces are not linearly related to the normal tire forces because of the characteristics of the tires, and a typical tire characteristic is shown in Figure 4.61. By using this tire characteristic together with the statistical distribution of the normal tire forces it is possible to plot the lateral tire force probability density distribution for a given speed. This can also be done if the pavement roughness is unknown but if the normal tire forces are available. This latter information was available because of previous research conducted on the effect of pavement roughness on normal tire forces.

The lateral tire force distribution is shown in Figure 4.62 for three different highways. Of particular interest is the higher probability of encountering lower lateral forces on a rough pavement as compared with a smooth pavement. The higher probability of lower lateral forces indicates a higher probability of having less control over the vehicle as a consequence of pavement roughness.

The statistical distribution of the lateral tire forces appears to offer a valuable criterion of pavement roughness that is directly related to safe vehicle handling conditions.

Using P and Q to Generate a Pavement Profile

Using the procedure described in this report a pavement profile was generated for the values of P and Q for a local pavement. This generated profile appeared to be similar to the actual pavement although certain assumptions were required in generating the profile. Unfortunately the elevation measurements obtained on this pavement section were made nine years prior to these calculations and so a direct comparison was not feasible. As a consequence of this study it appeared more important, however, to relate the values of P and Q to other factors in the vehicle behavior and thus use values of P and Q to establish acceptable limits for lateral tire force, driver acceleration and other behavior characteristics.

RECOMMENDATION

This investigation has indicated that the effect of pavement roughness upon vehicle behavior can be evaluated best in terms of the steering wheel angle, the vertical acceleration of the driver and the lateral tire forces. By establishing acceptable levels for these quantities it is possible to set limits for pavement roughness. It is recommended that such a study be undertaken, but that the normal tire forces (not included in this investigation) also be considered in establishing acceptable levels of pavement roughness.

NOMENCLATURE

a = Distance between vehicle center of gravity and axis of front wheel (ft)

a_1 = Upper limit of lateral tire force (lbf)

A_{CG} = Lateral acceleration of the vehicle center of gravity (ft/sec/sec)

A_f = Angular position of the front trail wheel to the x axis (deg)

A_i = Area under the i'th band of the roughness power spectrum curve (ft^2)

A_p = Distance along x axis from front wheel axis to front trail wheel hinge (ft)

A_r = Angular position of rear trail wheel to the x axis (deg)

b = Distance between rear tire axis and vehicle center of gravity (ft)

b_1 = Lower limit of lateral tire force (lbf)

B_p = Distance along x axis from rear wheel axis to the rear trail wheel hinge (ft)

c = Damping constant (lbf sec/ft)

$c(I,j)$ = Coefficients in equation relating lateral tire force to normal tire force (j = 1,2,3,4)

c_1 = Equivalent linear damping coefficient for tire (lbf sec/ft)

c_2 = Equivalent linear damping coefficient for vehicle shock absorbers (lbf sec/ft)

c_3 = Equivalent linear damping coefficient for vehicle seat (lbf sec/ft)

$c_{\alpha f}$ = Front tire cornering stiffness (lbf/deg)

$c_{\alpha r}$ = Rear tire cornering stiffness (lbf/deg)

c_α = Tire cornering stiffness (lbf/deg)

c_γ = Tire camber stiffness (lbf/deg)

D_p = Pulley diameter on potentiometer in instrumentation (in.)

D_{sw} = Pulley diameter on steering wheel (in.)

e = Base of natural logarithms

e_o = Output signal voltage

E_s = Total source voltage

f = Frequency (Hz)

F_{xi}, F_{yi}, F_{zi} = Components of inertia force in the x, y, z directions (lbf)

F_1 = Angle between x axis and R_r (deg)

F_2 = Angle between x axis and R_f (deg)

f_d = Distance based frequency (cycles/ft)

f_{d_1} = Specific value of distance based frequency (cycles/ft)

$F_{\ell f}$ = Lateral tire force, front (lbf)

$F_{\ell r}$ = Lateral tire force, rear (lbf)

F_n = Normal tire force (lbf)

F_{nN} = Normal tire force at station N (lbf)

f_t = Time based frequency (Hz)

I_x = Moment of inertia of vehicle about x axis (lbf ft sec^2)

I_y = Moment of inertia of vehicle about y axis (lbf ft sec^2)

I_z = Moment of inertia of vehicle about z axis (lbf ft sec^2)

I_{xz} = Product of inertia of vehicle about indicated axis (lbf ft sec^2)

K_1 = Tire stiffness (lbf/in)

K_2 = Vehicle spring stiffness (lbf/in)

K_3 = Vehicle seat stiffness (lbf/in)

M = Vehicle mass (lbf sec^2/ft)

M_{xi}, M_{yi}, M_{zi} = Moment components about the x, y, z axis produced by the inertia forces (lbf ft)

ma = Milliamperes

p = Angular velocity about x axis (rad/sec)

P = Highway roughness parameter in Zable equation

P_f = Distance from hinge to axis of front trail wheel (ft)

$P_\ell(F_\ell)$ = Probability density for lateral tire forces (lbf^2/lbf)

$P_n(F_{nN})$ = Probability density for normal tire forces (lbf^2/lbf)

P_r = Distance from hinge to axis of rear trail wheel (ft)

$P_r(F_\ell)$ = Probability of lateral forces being within a given range

$P_y(f_d)$ = Power spectral density of road roughness [ft^2/(cycles/ft)]

$P_{\ddot{Y}_3}(f)$ = Power spectral density of the driver acceleration (g^2/cps)

q = Angular velocity about y axis (rad/sec)

Q = Highway roughness parameter in Zable equation

r = Angular velocity about z axis (rad/sec)

R = Resistor value (ohms)

R_c = Distance from instant center to vehicle center of gravity (ft)

R_f = Distance from instant center to front trail wheel axis (ft)

R_r = Distance from instant center to rear trail wheel axis (ft)

$[S_s]^2$ = Mean square value of steering wheel angle (deg^2)

$[S_y]^2$ = Mean square value of road roughness ($in.^2$)

t = Time variable (sec)

T = Period (sec)

T_r = Track width (ft)

u = Linear velocity in the x direction (ft/sec)

v = Linear velocity in the y direction (ft/sec)

V = Vehicle velocity (ft/sec)

w = Linear velocity in the z direction (ft/sec)

W_r = Rear wheel ground reaction (lbf)

W_t = Vehicle weight (lbf)

x,y,z = Orthogonal set of axis fastened to the vehicle at the center of gravity with the x axis parrallel to the longitudinal vehicle axis

X_o = Coordinate of the vehicle instant center in the x direction (ft)

X_{max} = Maximum recommended displacement amplitude for sinusoidal vibration at frequency f (in.)

$\ddot{X}^2_{Max}$ = Maximum recommended mean square value of sinusoidal vibrations (g^2)

X(t) = Time based random variable representing a pavement profile (ft)

X,Y,Z = Stationary set of orthogonal axis

Y_o = Coordinate of the vehicle instant center in the y direction (ft)

$Y_o(f)$ = Displacement input into the system at frequency f (in.)

$\ddot{Y}_3(f)$ = Acceleration of the driver for a given excitation Y_o at a frequency of f (g)

$\ddot{Y}_3/Y_o$ = Transfer function for the linear vehicle model (g/in.)

α_f = Front tire slip angle (deg)

α_r = Rear tire slip angle (deg)

β = Vehicle sideslip angle (deg)

γ = Tire inclination angle (deg)

δ = Steer angle of front wheel (deg)

δ_{sw} = Angular rotation of the vehicle steering wheel from the straight path position (deg)

λ = Pavement wavelength (ft)

w_i = Value of the frequency at the midpoint of the i'th frequency band (rad/sec)

CHAPTER 1

INTRODUCTION

The roughness of a pavement surface has a significant influence on the dynamic behavior of the vehicle-driver system. On rough roads the driver's choice of a safe, comfortable speed may be primarily established by the pavement roughness. The roughness also affects the rate of deterioration of the vehicle and the pavement. The maintenance schedule for the pavement surface may be based on the roughness as suggested by Gronberg (13). These are some of the reasons for the efforts to measure and characterize pavement condition.

Pavement roughness should not be confused with pavement slipperiness which indicates a low coefficient of friction between the tire and pavement surface. In this investigation, the test results will only refer to dry pavements.

A historical review of devices for measuring road roughness is given by Hveem (19). Some devices for measuring pavement roughness are:

1- Bureau of Public Roads Roughometer

2- AASHO Slope Profilometer

3- CHLOE Profilometer

4- Kentucky Highway Department Accelerometer Device

5- University of Michigan Truck Mounted Profilometer

6- General Motors Profilometer

7- BPR Roughometer with Seismic System

8- Rod and Level

9- Lasers

The performance of the first five devices is reported by Yoder (42).

The BPR roughometer is one of the most popular devices for measuring pavement roughness. The device consists of a one wheel trailer with special shock absorbers and a sprung mass, which is approximately equal to one fourth of the mass of an automobile. The BPR roughometer method of evaluating pavement serviceability did consistently yield good results on all types of pavements for extensive tests as reported by Yoder (42). However, Nakamura and Michael noted some cases of poor correlation between the BPR roughometer measurements and serviceability for overlay and flexible pavements (29).

The construction of some of the roughness measuring devices may cause some distortion of the roughness measurements. Because of the sprung and unsprung masses, the BPR roughometer has two major natural frequencies, which will amplify those values of roughness which have corresponding frequencies. Since the roughometer is similar to the dynamic system of one fourth of an automobile, this modification of the data may help establish ridability for an automobile.

The modified BPR roughometer with seismic systems was developed by the Vehicle Dynamics Group at Purdue University as described by Zable (43). This unit consists of a BPR roughometer with a rigid suspension system between the wheel and frame. Four tuned beams with natural frequencies of 1/4, 2/3, 2, and 7 cps are mounted on the trailer to identify the presence of corresponding frequencies in the road profile for a given trailer velocity. This system is equipped with a notch filter to remove the four cps natural frequency of the roughometer, which would otherwise produce distortion.

The roughness of a road may be characterized in terms of a scale called the Present Serviceability Index, PSI. The PSI is defined by Carey and Irick (11) as "The ability of a specific section of pavement to serve high-speed, high-volume mixed ... traffic in its existing condition." PSI is a weighted function of roughness, rut depth, major cracking and patching. The value of roughness has the largest influence on the PSI value. The PSI rating is based on ridability and does not reflect subsurface defects. The PSI uses a single number to characterize pavement serviceability, and this number is an estimate of the rating which would be given to a pavement by a cross-section of highway users.

A statistical method is available for describing the roughness of a pavement that is based upon the distance-based frequency, f_d, and the average amplitude of each component wavelength. This method is the power spectral density analysis of the profile as described by DeVries (12).

Roughness may be considered as the vertical change in the pavement surface height relative to a grade line. The roughness profile may be simulated by the sum of many waves, which have different amplitudes and wavelengths as illustrated in Figure 1.1. The reciprocal of the wavelength is the distance based frequency given by:

$$f_d = \frac{1}{\lambda} , \tag{1.1}$$

where

f_d = distance-based frequency (cycles per foot),

λ = wavelength (feet per cycle).

The advantage of a power spectral density representation of a pavement is that it is more descriptive than a single number characterization of roughness, and it does provide a physical description of the road in terms of the presence of the various wavelengths. One disadvantage is that it is not a simple function of the subjective rating by highway users.

The response of the vehicle-driver system is usually expressed as a function of time instead of distance. A time based frequency for the vehicle-driver system may be obtained by

$$f_t = \frac{V}{\lambda} , \tag{1.2}$$

where

f_t = time-based frequency (cycles per second)

λ = wavelength (feet per cycle)

V = vehicle velocity (feet per second).

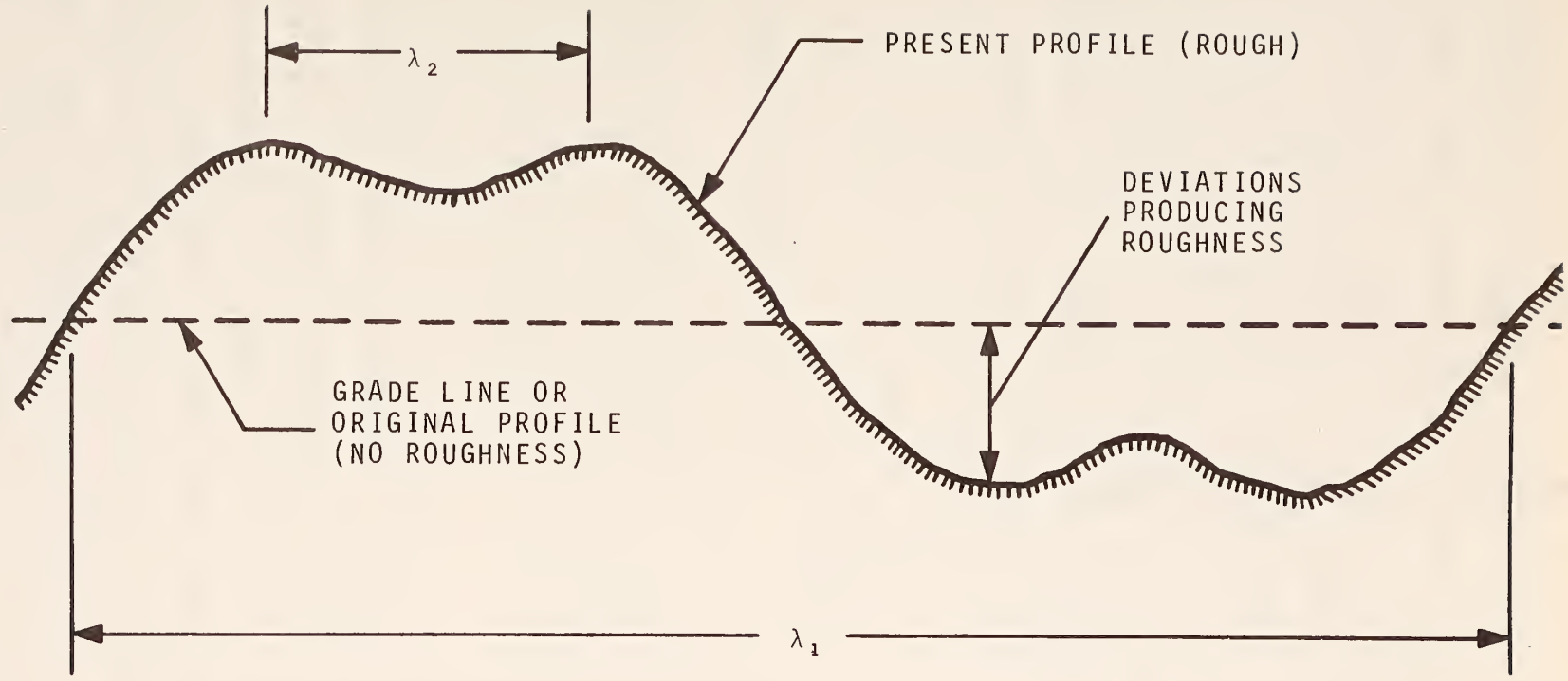

FIGURE 1.1 LONGITUDINAL PAVEMENT PROFILE

Therefore, the frequency of the system disturbance is a function of the length of the waves in the road and of the vehicle velocity. The disturbance of the system is also a function of the amplitude of the wavelengths. From a statistical viewpoint, the amplitude of the waves in the highway profile will increase as the wavelength is increased as indicated by Van Deusen (40). Therefore, when the vehicle speed is increased, the amplitude of the wavelength which occurs at a given frequency, f_t, will increase.

The influence of road roughness on the dynamic behaviour of the vehicle-driver system may be observed in changes in the following quantities:

1- The required steering correction needed to keep the vehicle under control

2- The resulting sideslip angle of the vehicle

3- The variation in the lateral tire forces

4- The vertical acceleration of the driver

The angular rotation of the steering wheel will increase as the shock absorber damping is reduced according to Belsdorf et al. (3). This observation is based upon the operation of a vehicle on a fabricated obstacle path and over a fabricated bumpy curve. A reduction in shock absorber damping allows an increase in the motion of the sprung mass and the attached steering linkage. This increase in motion may also be produced by rough roads. Therefore,

an increase in steering wheel angular rotation may be expected when the road roughness is increased.

The response of a vehicle to steering control and the concept of vehicle stability are discussed by Milliken, Whitcomb, Segel, et al. (26). The effects of speed on the response of a vehicle in a left hand turn along the hyperbolic path of Figure 1.2 are reported by Hildebrand (16). If the speed of an oversteer vehicle is increased from zero, Hildebrand's investigation shows the following:

1- The steer angle will decrease.

2- The sideslip angle will increase in magnitude. (Both the steer angle and sideslip angle are defined in Figure B.2)

These results are shown in Figure 1.3. They were obtained by an analysis of a bicycle model of a passenger car, which indicates an oversteer condition when the majority of the weight is on the rear wheels.

The response of a vehicle, when it is subjected to a wind gust or to road roughness, will indicate the effects of external disturbances on the controllability of the vehicle. The effect of wind blast on vehicle handling response is reported by Bundorf et al. (9). The effect of road roughness on handling response is reported by Hildebrand (16). Hildebrand used measured values of vertical tire forces from one rough road and one smooth road as the disturbance input to the vehicle while executing

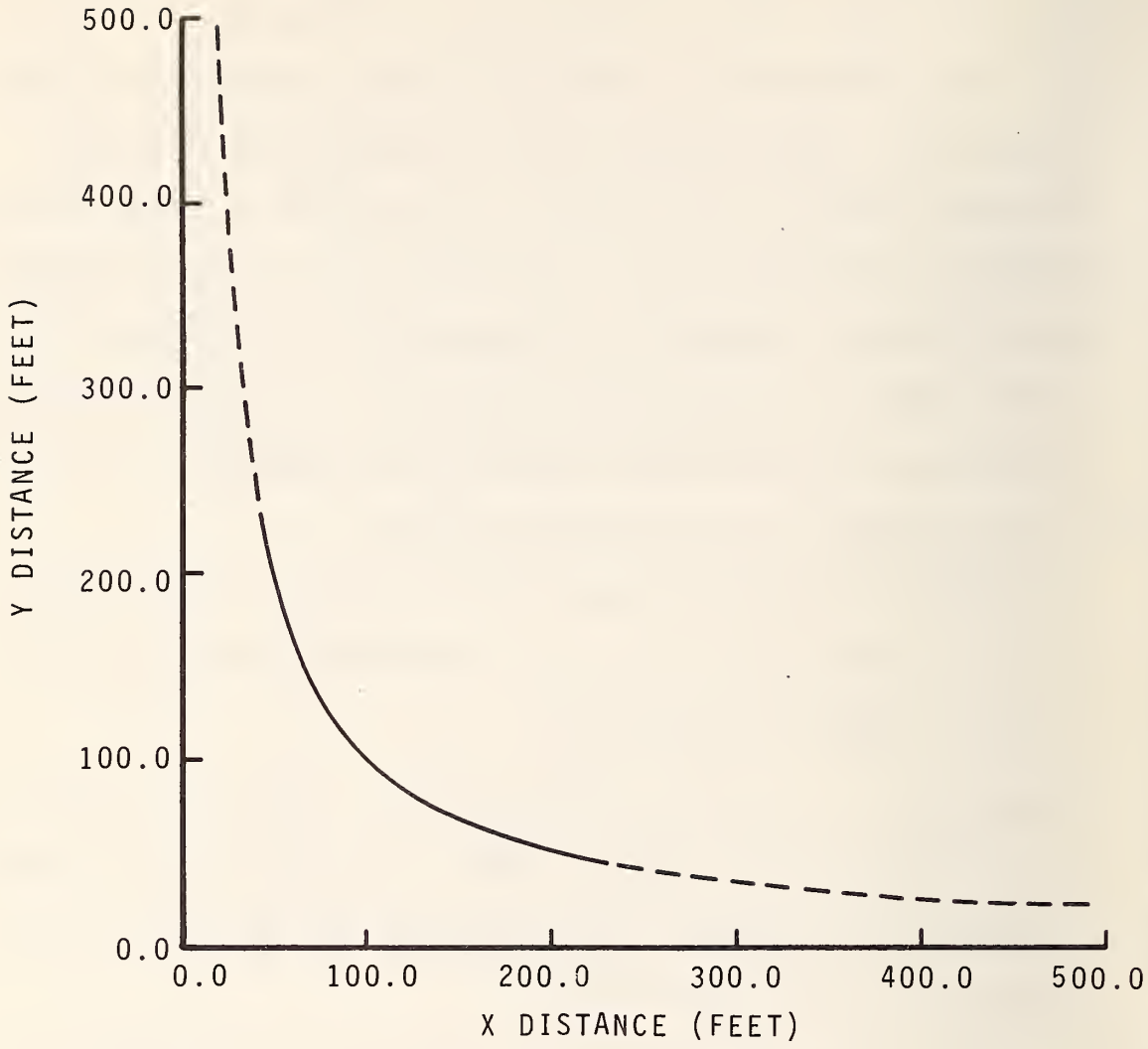

FIGURE 1.2 HYPERBOLIC PATH

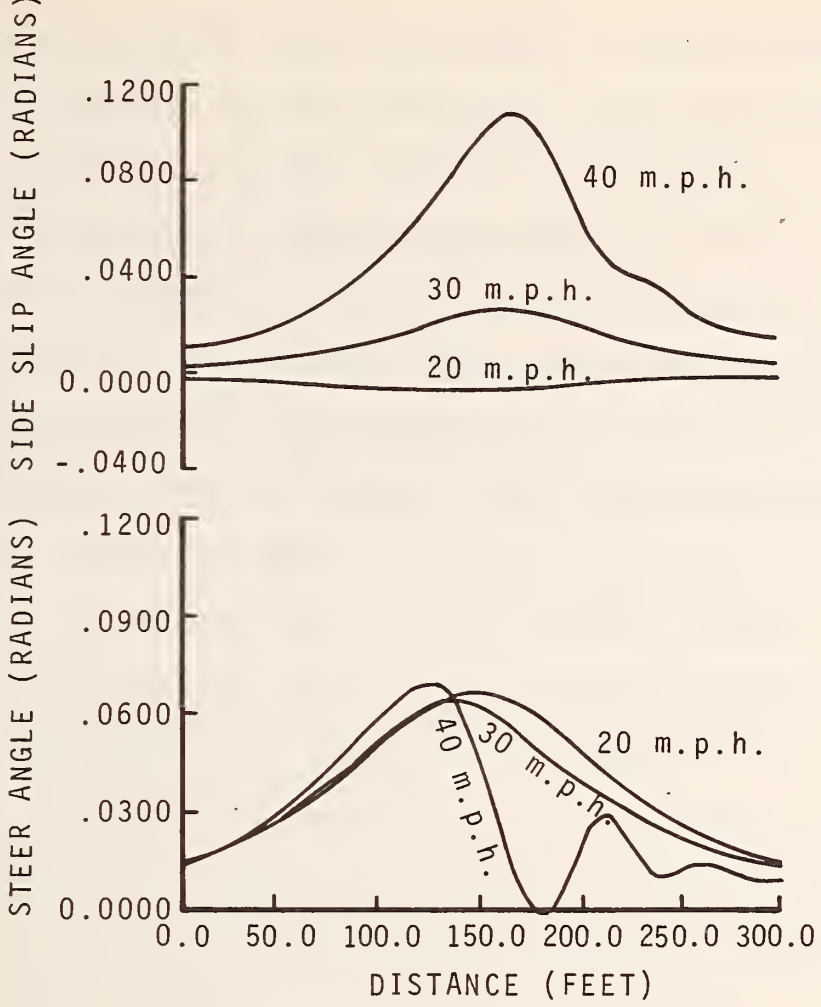

FIGURE 1.3 EFFECT OF VEHICLE SPEED ON SIDE SLIP AND STEER ANGLES FOR HYPERBOLIC PATH FOR OVERSTEER VEHICLE

a hyperbolic turn. The results show higher rates of response and larger overshoots for the rougher road.

The relationship between a vehicle response characteristic (defined as the sideslip angle acceleration) and the subjective evaluation of the ease of control of a vehicle are reported by Bergman (5). Accordingly, a 0.98 correlation coefficient exists between the sideslip angle acceleration and the ease of control for the case of transient steering. The sense of loss of control associated with large sideslip angles is partly due to the driver's observation that the vehicle is no longer aligned with its direction of travel. An excessive overshoot or oscillation of the sideslip angle response will give the driver an uncertain sense of directional control and result in excessive correctional movements, according to Beauvais et al. (2).

The direction of the vehicle is controlled by lateral forces acting on the tires. These lateral forces are proportional to the tire slip angle if the vertical force acting on the tire is constant. If the vertical tire force is reduced, the lateral force will usually be reduced even though the slip angle remains constant.

Since road roughness causes fluctuations in the magnitude of the normal (vertical) tire force, road roughness will change the magnitude of the available lateral force. The magnitude of the change in the normal tire force due to roughness is reported by Sattaripour (36). He gives the

standard deviation of the normal tire force for seven roads, and also suggests a method for calculating the normal tire force, based upon measured values of roughness and vehicle characteristics for an average vehicle.

Road roughness can increase driver fatigue. This is in part due to the increased vertical acceleration experienced by the driver as well as the need for more frequent and larger steering corrections. Fatigue as a factor in accidents is distinguished from "mere drowsiness" in Reference 24. Accordingly, fatigue is described as follows:

> ... fatigue of the type which requires a considerable period of rest for full recovery and, which if carried too far, results in exhaustion.

The result of this study on truck drivers showed a decreasing ability to perform various physical tasks as the time spent driving was increased.

The response of vehicle occupants to vibration has received considerable attention by Janeway (22), Holbrook (17) and other investigators. The roughness serves as the excitation for the vehicle-driver system. The frequencies of the high amplitude vibrations, which are transmitted to the driver are primarily established by the major natural frequencies of the vehicle. The major natural frequencies of the vehicle are 1-2 cps and 8-10 cps (28). The response of the driver is colored by the resonant frequencies (28) of the human body which are:

1- Approximately five cps for the spinal column

2- Approximately three cps for the thorax-abdomen system

3- Approximately twenty cps for the head and neck

But the general severity of the vibration is determined by the roughness of the road. The status of efforts to classify human response to random vibration has been suggested by Van Deusen (41):

> If the spectral composition of the road roughness is not fixed, then a single number for expressing ride is not very meaningful, and it is probably necessary to tabulate several numbers that represent the acceleration variances in different frequency bands.

An upper vibrational intensity limit for drivers on rough roads, which includes vibration frequency, amplitude, and duration of exposure, has been proposed (15) by the International Standardization Organization, ISO, and is illustrated in Figure 1.4.

The vertical acceleration of a vehicle passenger is used as a criterion for road roughness by the Kentucky Department of Highways. The accelerometer is mounted on the passenger's chest. The test vehicle is an ordinary automobile. The area enclosed by the acceleration versus time record is calculated for a given length of time, and this sum is expressed in terms of a roughness index. The results give a 0.90 correlation with the PSI as reported by Rizenbergs (34).

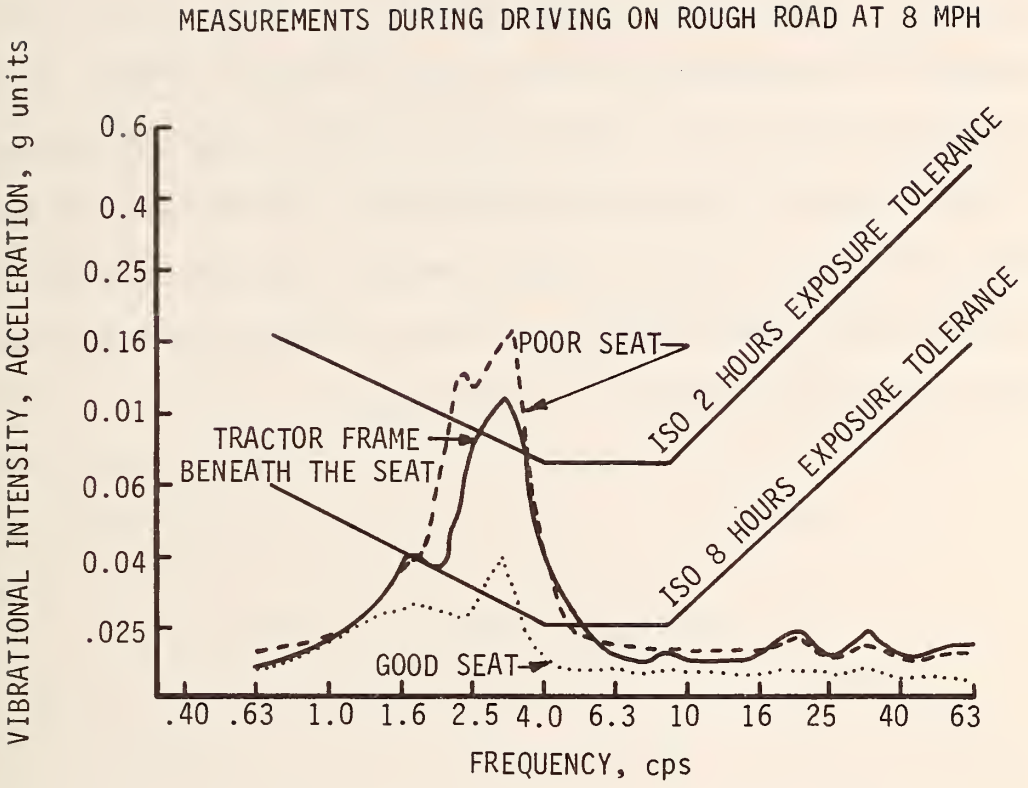

FIGURE 1.4 PROPOSED ISO UPPER LIMITS FOR VIBRATION EXPOSURE FOR TRACTOR DRIVERS

Previous investigators have thus shown that pavement roughness has a significant influence on the dynamic behaviour of the vehicle.

The objective of this investigation is to relate road roughness with those quantities which affect the control response and safety of the vehicle-driver system. These quantities include: steer angle, steering wheel angle, sideslip angle, lateral tire forces, and driver acceleration. It is desirable to determine if these parameters may be used to establish criteria for the allowable roughness on various classes of highways.

CHAPTER 2

DISCUSSION OF THEORY

Introduction

The change in steer angle, the steering wheel angle, the sideslip angle, the lateral tire forces, and the vertical acceleration of the driver are affected by the roughness of the road. The first four quantities are related to the control of the vehicle, and the last quantity is related to the comfort of the driver. An understanding of these quantities is necessary if the effects of pavement roughness are to be studied.

Steer Angle and Steering Wheel Angle

When executing a turn, the front wheels of the typical passenger vehicle rotate through slightly different steer angles in order to minimize wear on the tires. Moreover, when the vehicle is traveling straight ahead on the road, the two front wheels are frequently rotated inward a slight amount to provide stability. In this investigation, the quantity which is described as the steer angle, δ, is the rotation of the left front wheel about its steer axis, and it is measured from the mean position of the wheel when the vehicle is moving along a straight section of highway.

The angle δ is illustrated in Figure 2.1. Fluctuations in the left front wheel steer angle may occur without changing the direction of the vehicle, because of compensating movements by the right front wheel. These compensating movements by the right wheel are primarily produced by the geometry of the steering and suspension systems.

The steering wheel angle, δ_{SW}, refers to the rotation of the steering wheel from its mean position on a straight road. The angle δ_{SW} is also illustrated in Figure 2.1.

The steering wheel angle is related to the steer angle by a ratio based on the connecting gears and linkages. The ratio of the steering wheel angle to the steer angle is approximately 30:1 for the test vehicle. This ratio is not constant due to the nonlinear linkage. A change in steering wheel angle reflects the driver's desire to provide a control correction.

If the steer angle is changed, the tire slip angle will change to produce a new value for the lateral tire force. The directional control of the vehicle is maintained by this change in lateral tire force.

The roughness of the road can cause a change in the heading of a vehicle. Since road roughness tends to be a random variable, the control correction, δ_{SW}, for this disturbance will also tend to be a random variable. If a variable represents a random phenomenon, its autocovariance function will approach zero as the lag value is increased.

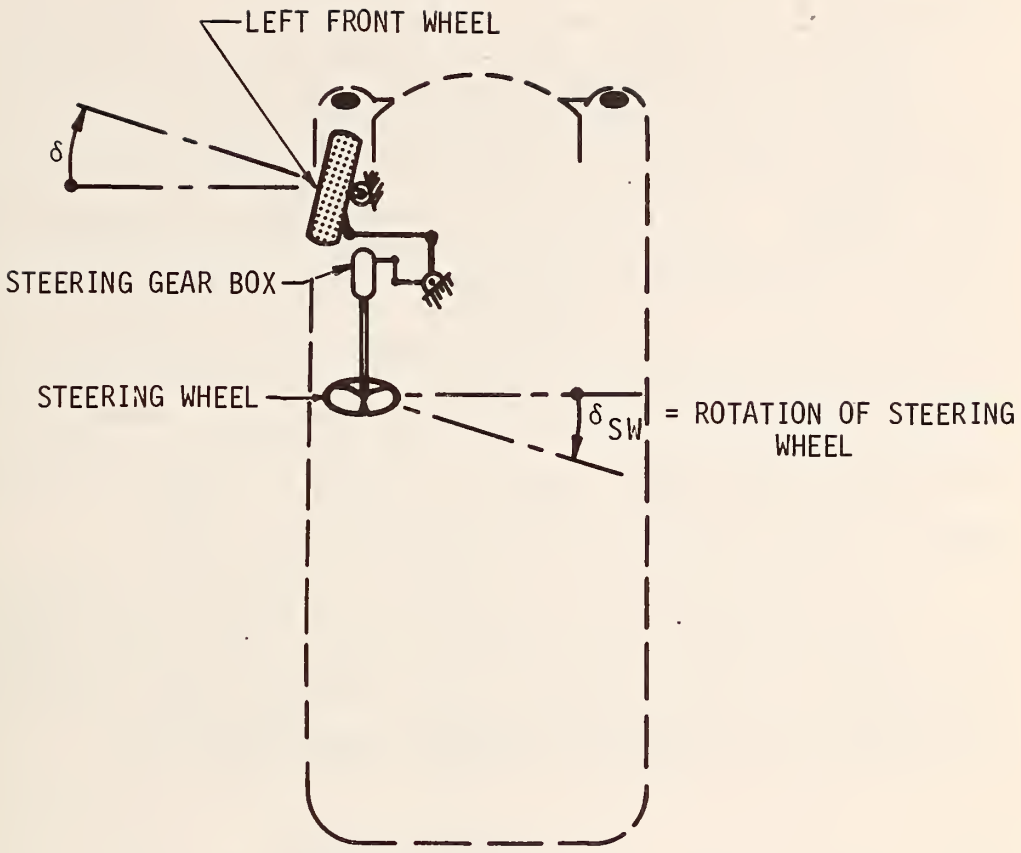

FIGURE 2.1 SCHEMATIC OF LEFT FRONT TIRE, STEERING WHEEL AND CONNECTING LINKAGE

The frequencies which make large contributions to the mean square value of a random variable, such as δ_{SW}, can be identified with the power spectral density function.

One of the uses of spectral analysis (1, 4) is to identify significant frequencies in random records in the time domain. This can be a useful tool in studying the effect of pavement roughness on the magnitude and frequency of the steering corrections, which are required by the driver to keep the vehicle under control. Moreover, the area under the power spectrum curve is equal to the total mean square value of the steering correction.

The procedure used in this investigation for making the power spectral analysis is a modification of the procedure developed by Blackman and Tukey (6).

Sideslip Angle

Various mathematical models of a vehicle, such as the bicycle model and the HVOSM, have been proposed by Bundorf (7), Tsao (39), McHenry et al. (25) and others for describing the behavior of the vehicle under specified conditions. The complexity of these models is varied, since the models depend upon the detail which is reproduced in the suspension and steering systems. The mathematical model best suited for this investigation is the one that will most accurately describe the behavior of the vehicle and will minimize costly mathematical computations. For this reason, a

simplified bicycle model, which is similar to the vehicle model proposed by Bundorf (7), is used in this investigation.

In developing this model, a stationary set of axes (X-Y-Z) is established and the displacement of the center of gravity of the vehicle relative to these axes is determined. In addition, the angular position of the vehicle relative to these axes can be evaluated.

To facilitate this calculation, an additional set of axes (x-y-z) is fastened to the vehicle at the center of gravity. The x-axis coincides with the longitudinal axis of the vehicle, the y-axis coincides with the lateral axis of the vehicle and the z-axis is mutually perpendicular to the other axes. The angular velocities (p,q,r) and linear velocities (u,v,w) are illustrated in Figure 2.2 with the two sets of axes.

The dynamic response of the vehicle shown in Figure 2.2 may be analyzed by considering the vehicle as a system of small distributed masses. A typical element, dm, of this mass system is shown in Figure 2.3. The components of linear velocity of the mass dm in the x, y and z directions are

$$u + zq - yr ,$$

$$v + xr - zp$$

and

$$w + yp - xq$$

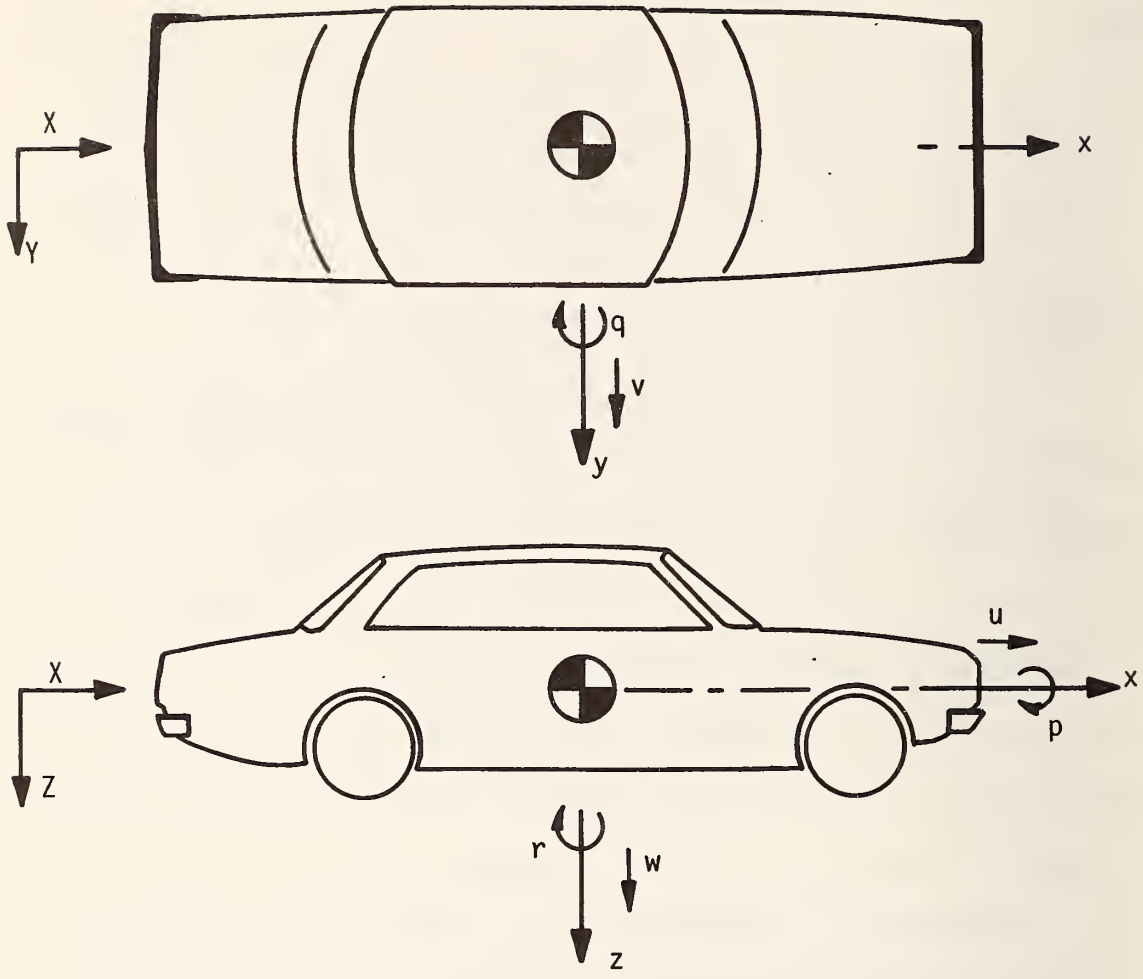

FIGURE 2.2 SCHEMATIC OF VEHICLE WITH AXES SYSTEMS

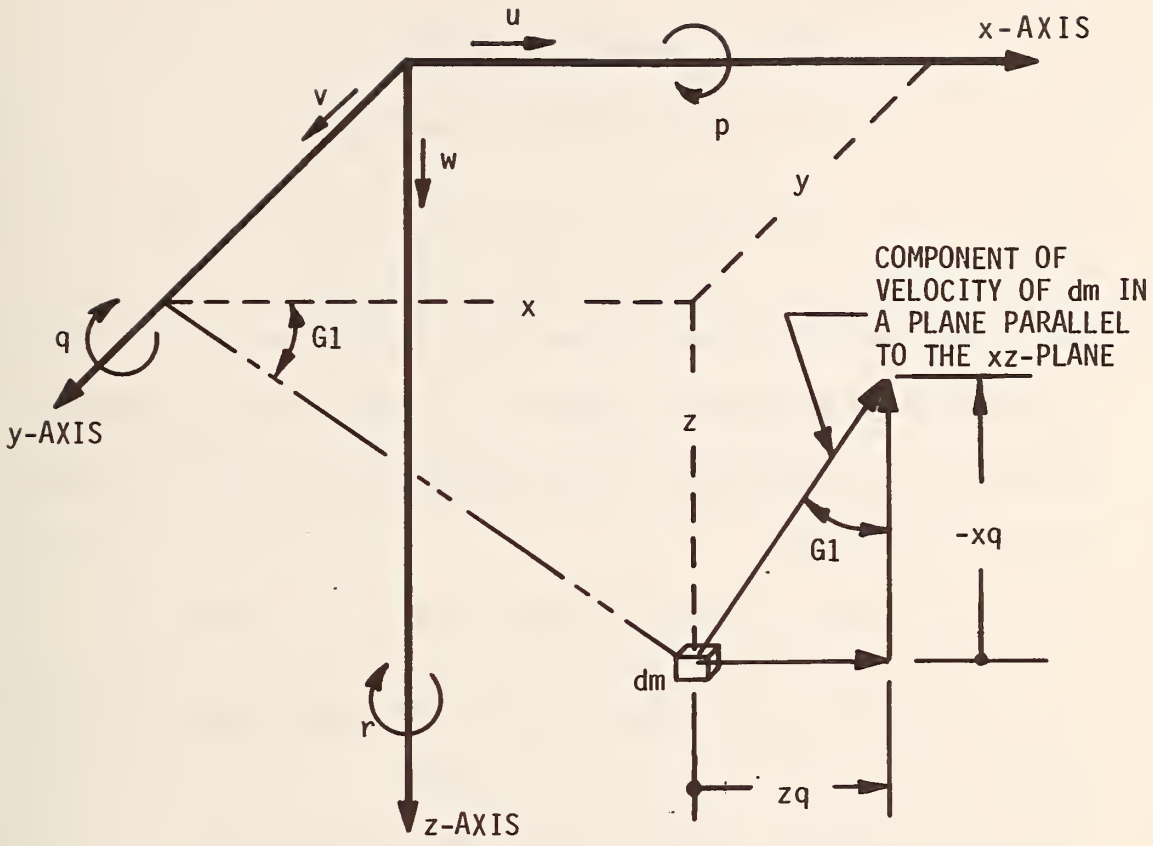

FIGURE 2.3 SCHEMATIC FOR ANALYSIS OF THE VELOCITY OF TYPICAL ELEMENT OF MASS, dm

respectively. The derivative of these velocity components with respect to time gives the components of acceleration acting on dm in the form

$$\dot{u} + wq + z\dot{q} - vr - y\dot{r} ,$$

$$\dot{v} + ur + x\dot{r} - wp - z\dot{p}$$

and

$$\dot{w} + vp + y\dot{p} - uq - x\dot{q} .$$

The forces acting on dm may be studied by applying d'Alembert's principle, which is a corollary of Newton's second and third laws. The components of inertia forces acting on dm are

$$dF_{xi} = -dm\ [\dot{u} + wq + z\dot{q} - vr - y\dot{r}] , \qquad (2.1)$$

$$dF_{yi} = -dm\ [\dot{v} + ur + x\dot{r} - wp - z\dot{p}] \qquad (2.2)$$

and

$$dF_{zi} = -dm\ [\dot{w} + vp + y\dot{p} - uq - x\dot{q}] . \qquad (2.3)$$

These inertia forces cause moments about the three axes. These moments are

$$dM_{xi} = ydF_{zi} - zdF_{yi} , \qquad (2.4)$$

$$dM_{yi} = zdF_{xi} - xdF_{zi} \qquad (2.5)$$

and

$$dM_{zi} = xdF_{yi} - ydF_{xi} . \qquad (2.6)$$

Substitution of Equations 2.1, 2.2 and 2.3 into Equations 2.4, 2.5 and 2.6 yields

$$dM_{xi} = [-\dot{w}y - yvp - y^2\dot{p} + yuq + yx\dot{q} + \dot{v}z + zur + zx\dot{r} - zwp - z^2\dot{p}]dm , \quad (2.7)$$

$$dM_{yi} = [-\dot{u}z - zwq - z^2\dot{q} + zvr + zy\dot{r} + \dot{w}x + xvp + xy\dot{p} - xuq - x^2\dot{q}]dm , \quad (2.8)$$

$$dM_{zi} = [-\dot{v}x - xur - x^2\dot{r} + xwp + xz\dot{p} + \dot{u}y + ywq + yz\dot{q} - yvr - y^2\dot{r}]dm . \quad (2.9)$$

Equations 2.7, 2.8 and 2.9 may be expressed in terms of moments of inertia and products of inertia if velocity relationships, such as,

$$u = -yr , \quad v = xr , \quad u = zq \quad \text{and} \quad w = -xq$$

are applied to these equations. Since the vehicle is usually assumed to be symmetrical about the xz plane, the products of inertia I_{xy} and I_{yz} are zero, as indicated by

$$I_{xy} \equiv \int xydm = 0$$

and

$$I_{yz} \equiv \int yzdm = 0 .$$

However, I_{xz} is not zero, where

$$I_{xz} \equiv \int xzdm .$$

Because the origin of the axes xyz is located at the center of gravity of the vehicle, the following integrals are zero:

$$\int xdm = 0 ,$$

$$\int ydm = 0$$

and

$$\int zdm = 0 .$$

The moments of inertia are given by

$$I_x \equiv \int (y^2 + z^2)dm ,$$

$$I_y \equiv \int (x^2 + z^2)dm$$

and

$$I_z \equiv \int (x^2 + y^2)dm .$$

If Equations 2.1, 2.2, 2.3, 2.7, 2.8 and 2.9 are integrated, and if the relationships mentioned in the above paragraph are applied to these equations, then the inertia forces and inertia moments acting on the vehicle are

$$F_{xi} = -M [\dot{u} + wq - vr] ,$$

$$F_{yi} = -M [\dot{v} - wp + ur] ,$$

$$F_{zi} = -M [\dot{w} - uq + vp] ,$$

$$M_{xi} = -\dot{p}I_x + qr [I_y - I_z] + [\dot{r} + pq] I_{xz} ,$$

$$M_{yi} = -\dot{q}I_y + pr [I_z - I_x] + [r^2 - p^2] I_{xz} ,$$

$$M_{zi} = -\dot{r}I_z + pq [I_x - I_y] + [\dot{p} - qr] I_{xz} .$$

The relationships between the inertia forces and the external forces acting on the vehicle are given by the following six equations according to d'Alembert's principle.

$$\sum F_x - M [\dot{u} + wq - vr] = 0 , \tag{2.10}$$

$$\sum F_y - M [\dot{v} - wp + ur] = 0 , \tag{2.11}$$

$$\sum F_z - M [\dot{w} - uq + vp] = 0 , \tag{2.12}$$

$$\sum M_x - \dot{p} I_x + qr [I_y - I_z] + [\dot{r} + pq] I_{xz} = 0 , \tag{2.13}$$

$$\sum M_y - \dot{q} I_y + pr [I_z - I_x] + [r^2 - p^2] I_{xz} = 0 , \tag{2.14}$$

$$\sum M_z - \dot{r} I_z + pq [I_x - I_y] + [\dot{p} - qr] I_{xz} . \tag{2.15}$$

The Equations 2.10 through 2.15 for the motion of the vehicle may be simplified by the following assumptions:

1- The motion of the vehicle is restricted to the xy plane. Therefore,

$$w = 0 \quad \text{and} \quad \dot{w} = 0 .$$

2- The roll of the vehicle about its x-axis is neglected, because the construction of the bicycle model can not support a moment about the x-axis. Therefore,

$$p = 0 \quad \text{and} \quad \dot{p} = 0 .$$

3- The pitch of the vehicle about the y-axis is neglected. Therefore,

$$q = 0 \quad \text{and} \quad \dot{q} = 0 \ .$$

4- The velocity, V, of the vehicle center of gravity is constant, and the angle between V and u is small. Therefore,

$$u \approx V \ ,$$

so

$$\dot{u} \approx 0 \ .$$

These simplifying assumptions may be applied to Equations 2.10 through 2.15 to obtain the following equations of motion:

$$\sum F_x + Mvr = 0 \ , \tag{2.16}$$

$$\sum F_y - M\,[\dot{v} + ur] = 0 \ , \tag{2.17}$$

$$\sum F_z = 0 \ , \tag{2.18}$$

$$\sum M_x + \dot{r} I_{xz} = 0 \ , \tag{2.19}$$

$$\sum M_y + r^2 I_{xz} = 0 \ , \tag{2.20}$$

$$\sum M_z - \dot{r} I_z = 0 \ . \tag{2.21}$$

The schematic of the simplified vehicle model, which is represented by these equations of motion, is shown in Figure 2.4.

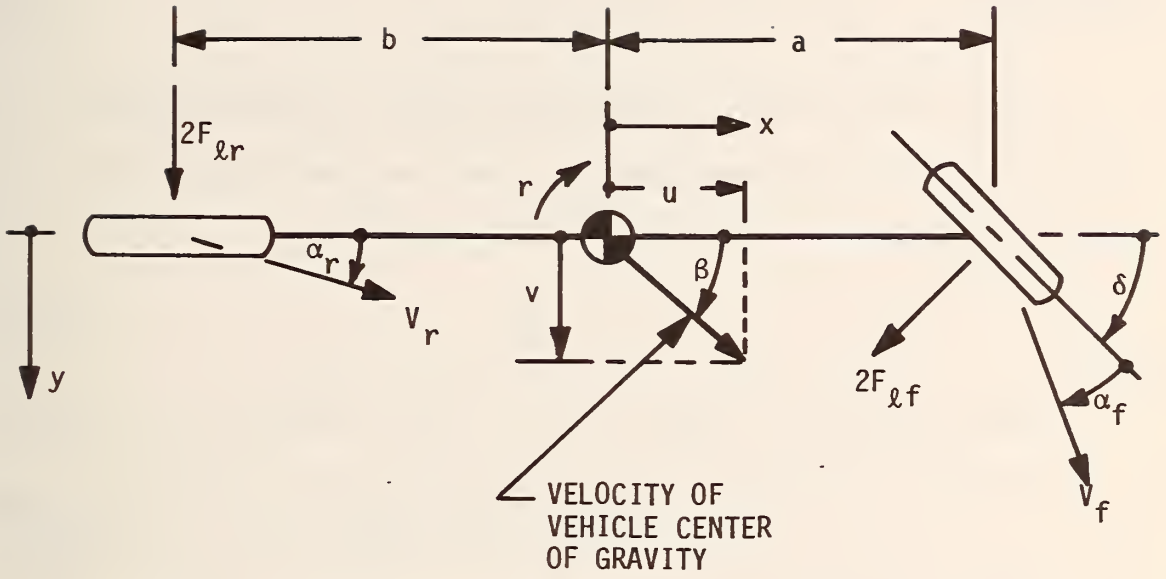

FIGURE 2.4 VEHICLE HANDLING MODEL

The vehicle sideslip angle, β, is

$$\beta = \text{Tan}^{-1}\left[\frac{v}{u}\right] \approx \frac{v}{u} ,$$

because β is small.

Therefore, $$v \approx u\beta . \qquad (2.22)$$

Since the velocity of the vehicle is assumed to be constant in this investigation, the time derivative of Equation 2.22 is

$$\dot{v} = u\dot{\beta} . \qquad (2.23)$$

Substitution of Equation 2.23 into Equation 2.17 gives

$$\sum F_y - M\,[u\dot{\beta} + ur] = 0 . \qquad (2.24)$$

The relationship between the lateral tire force and the tire slip angle, when the camber angle is negligible, is

$$F_{\ell f} = - C_{\alpha f}\,\alpha_f \qquad (2.25)$$

and

$$F_{\ell r} = - C_{\alpha r}\,\alpha_r \qquad (2.26)$$

as discussed at the end of this section. These forces are shown in Figure 2.4.

The steer angle is assumed to be small, so $F_{\ell f}$ will be approximately parallel to the y-axis. The plane of the rear wheel is assumed to remain parallel to the xz-plane,

so $F_{\ell r}$ will be parallel to the y-axis. Therefore, Equation 2.24 becomes

$$2F_{\ell f} + 2F_{\ell r} - M\,[u\dot{\beta} + ur] = 0 \ ,$$

or

$$-2C_{\alpha f}\,\alpha_f - 2C_{\alpha r}\,\alpha_r - M\,[u\dot{\beta} + ur] = 0 \ . \qquad (2.27)$$

Equation 2.21 takes the form

$$a\,[2F_{\ell f}] - b\,[2F_{\ell r}] - \dot{r}I_z = 0 \ ,$$

or

$$-2aC_{\alpha f}\,\alpha_f + 2bC_{\alpha r}\,\alpha_r - \dot{r}I_z = 0 \ . \qquad (2.28)$$

The rear tire slip angle may be obtained from components of the velocity vector V_r as

$$\alpha_r = \frac{V_r \text{ Sin } (\alpha_r)}{V_r \text{ Cos } (\alpha_r)} \approx \frac{v - br}{u} \ ,$$

or

$$\alpha_r = \frac{u\beta - br}{u} \ . \qquad (2.29)$$

The front tire slip angle may be obtained from components of the velocity vector V_f and the steer angle, δ, as

$$\alpha_f = \frac{u\beta + ar}{u} - \delta \ . \qquad (2.30)$$

It should be noted that the value of δ is small for normal conditions.

Substitution of Equations 2.29 and 2.30 into 2.28 gives

$$2aC_{\alpha f}\delta = \dot{r}I_z + \left[\frac{2a^2C_{\alpha f} + 2b^2C_{\alpha r}}{u}\right]r + \left[2aC_{\alpha f} - 2bC_{\alpha r}\right]\beta. \quad (2.31)$$

Substitution of Equations 2.29 and 2.30 into 2.27 gives

$$2C_{\alpha f}\delta = Mu\dot{\beta} + \left[Mu + \frac{2aC_{\alpha f} - 2bC_{\alpha r}}{u}\right]r + \left[2C_{\alpha f} + 2C_{\alpha r}\right]\beta. \quad (2.32)$$

Equation 2.32 may be expressed in the form

$$r = \frac{2C_{\alpha f}\delta - Mu\dot{\beta} - [2C_{\alpha f} + 2C_{\alpha r}]\beta}{Mu + \left[\frac{2aC_{\alpha f} - 2bC_{\alpha r}}{u}\right]}. \quad (2.33)$$

The value of $\dot{r}$ may be obtained by taking the time derivative of Equation 2.33, and $\dot{r}$ is given by

$$\dot{r} = \frac{2C_{\alpha f}\dot{\delta} - Mu\ddot{\beta} - [2C_{\alpha f} + 2C_{\alpha r}]\dot{\beta}}{Mu + \left[\frac{2aC_{\alpha f} - 2bC_{\alpha r}}{u}\right]}. \quad (2.34)$$

The Equation 2.31 may be expressed in terms of β, δ and the time derivatives of β and δ by using Equations 2.33 and 2.34 to eliminate r and $\dot{r}$. The resulting equation is

$$\ddot{\beta} = \frac{1}{MuI_z}\left\{[-2aC_{\alpha f}D_2 + 2C_{\alpha f}D_3]\delta + [2C_{\alpha f}I_z]\dot{\delta} + [-D_1I_z - D_3Mu]\dot{\beta} - [D_3D_1 - D_2(2aC_{\alpha f} - 2bC_{\alpha r})]\beta\right\}, \tag{2.35}$$

where

$$D_1 = 2C_{\alpha f} + 2C_{\alpha r} ,$$

$$D_2 = Mu + \frac{2aC_{\alpha f} - 2bC_{\alpha r}}{u}$$

and

$$D_3 = \frac{2a^2C_{\alpha f} + 2b^2C_{\alpha r}}{u} .$$

The coefficients of $\ddot{\beta}$, δ, $\dot{\delta}$, β and $\dot{\beta}$ are constants, since the vehicle is moving at a fixed speed. Consequently, Equation 2.35 may be solved for β for a given steer angle, δ, by using the Quinn Method (21) of numerical integration. If the steering wheel angle measurements are too far apart, the numerical integration of this equation may not converge. Sometimes it is possible to eliminate this convergence problem by reducing the time interval between data points, Δt, by ½ and adding a new data point between each of the original data points. The magnitude of this new data point may be taken as the average value of the two adjacent, original points.

The lateral velocity, v, of the center of gravity of the vehicle may now be obtained by Equation 2.22. Moreover, the x and y displacements of the vehicle center of gravity

may be obtained by

$$x = u \int_0^T dt \tag{2.36}$$

and

$$y = \int_0^T v \, dt \, . \tag{2.37}$$

The control input, δ, for the bicycle model is obtained by dividing measured values of the steering wheel angle, δ_{SW}, by the ratio of steering wheel rotation to front tire rotation. Therefore, this control input to the bicycle model is a function of the steering wheel rotation, and δ does not contain the sometimes erratic rotation associated with the front wheels of the vehicle.

If the vehicle motion is restricted to a circular path, the sideslip angle may be easily obtained as shown in Appendix B, and β is given by

$$\beta = 57.3 \frac{b}{R_c} - \frac{W_r V^2}{g C_{\alpha r} R_c} \, . \tag{2.38}$$

The simplified bicycle model does not include lateral weight transfer, compliance or geometric steer characteristics, unequal turning of the front tires due to the linkage, or wheel shimmy.

The sideslip angle can also be measured experimentally by making use of the instant center of the vehicle as indicated in Figure 2.5. The instant center may be located by using the geometric relationships illustrated in Figure

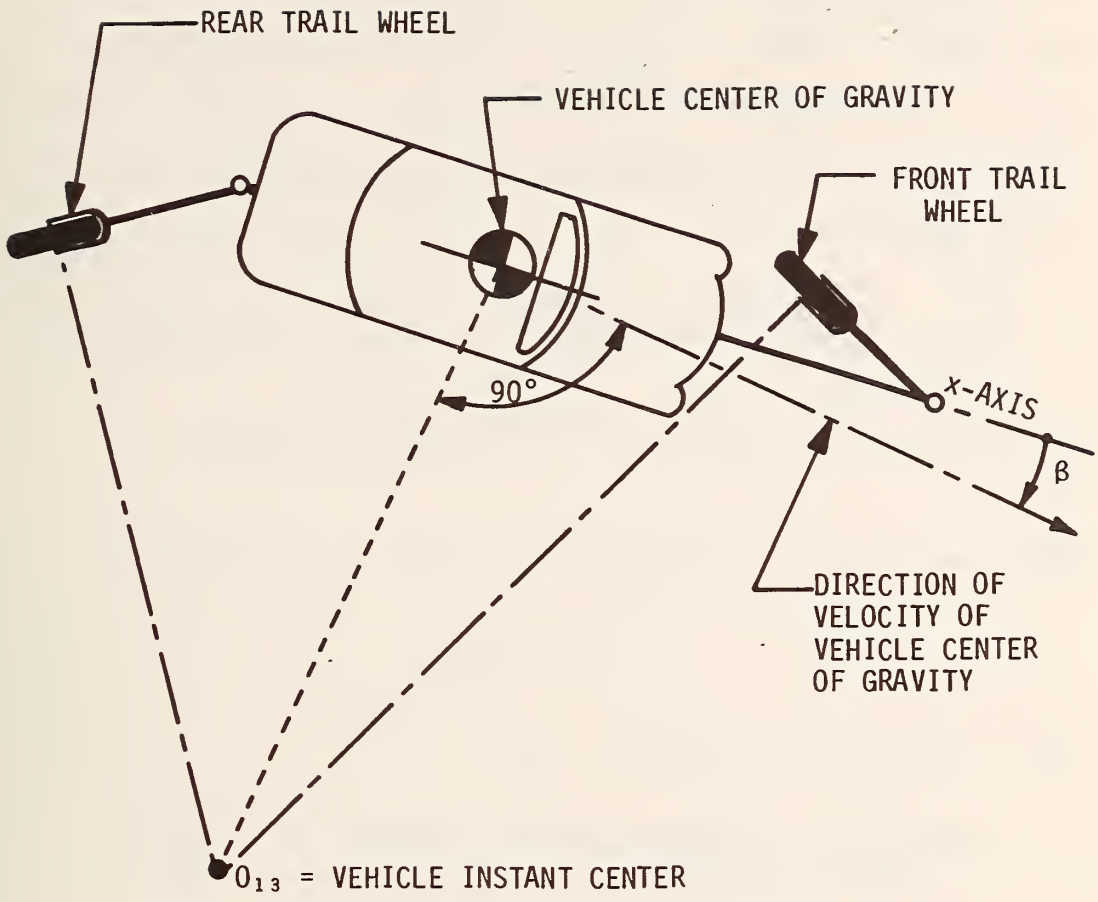

FIGURE 2.5 TRAIL WHEELS FOR OBTAINING THE SIDESLIP ANGLE AND THE CENTER OF PATH CURVATURE

2.6 if the vehicle is equipped with trail wheels as shown. The vehicle and trail wheels may be represented by vector polygons as shown in Figure 2.7. The distances R_f and R_r may be obtained by summing the x and y distances around the outer loop of the vector polygon. The vector equation for this outer loop is

$$(a + A_p)e^{j(0)} \mapsto P_f e^{j(A_f)} \mapsto R_f e^{j(F_2)} \mapsto R_r e^{j(F_1)}$$
$$\mapsto P_r e^{j(A_r)} \mapsto (B_p + b)e^{j(0)} = 0 .$$

The sum of the x-components is given by the equation

$$\sum X = 0 ,$$

and this equation gives

$$(a + A_p) + P_f \text{ Cos}(A_f) + R_f \text{ Cos}(F_2) + R_r \text{ Cos}(F_1)$$
$$+ P_r \text{ Cos}(A_r) + (B_p + b) = 0 . \qquad (2.39)$$

The sum of the y-components is given by the equation

$$\sum Y = 0 ,$$

and this equation gives

$$P_f \text{ Sin}(A_f) + R_f \text{ Sin}(F_2) + R_r \text{ Sin}(F_1)$$
$$+ P_r \text{ Sin}(A_r) = 0 . \qquad (2.40)$$

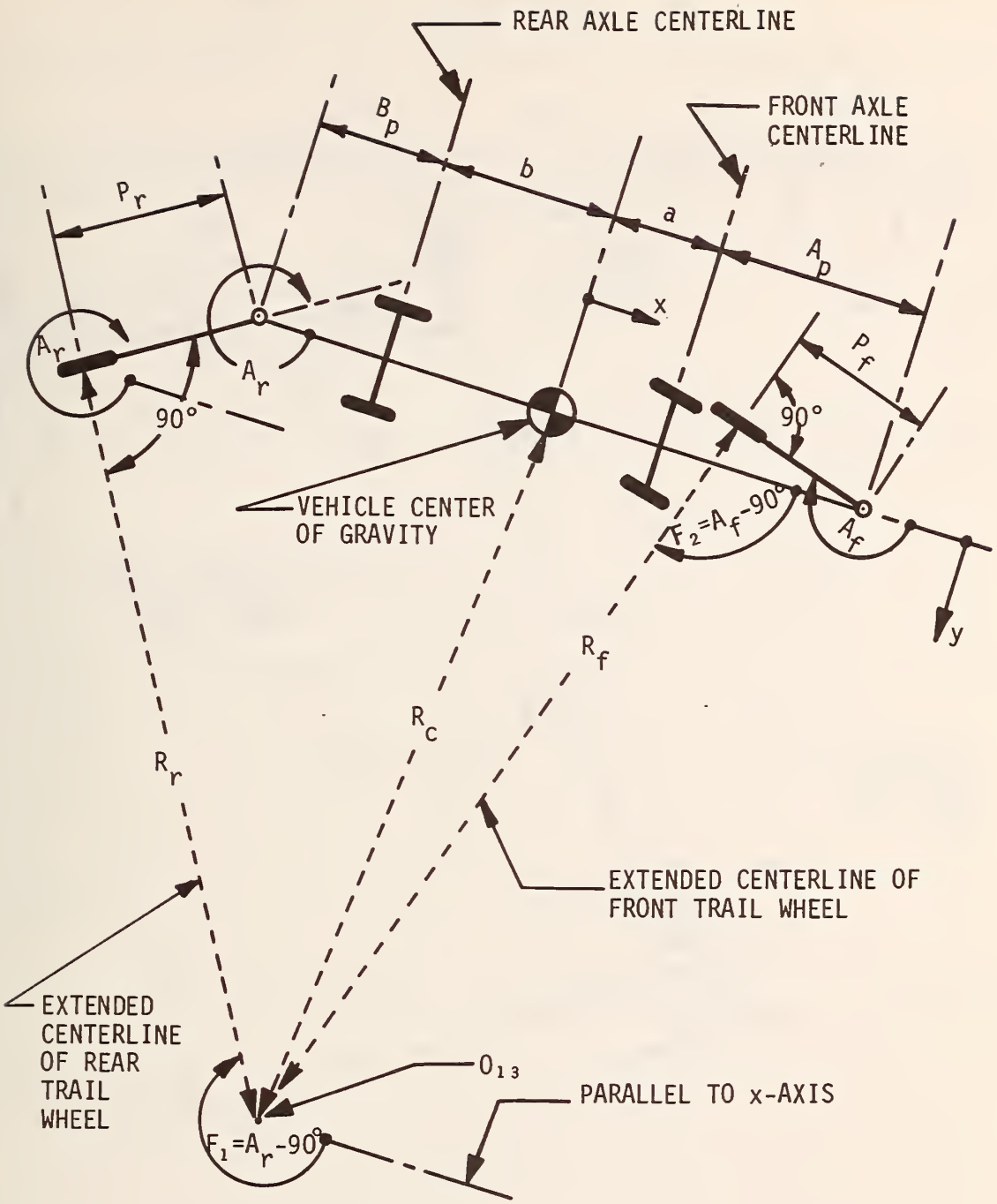

FIGURE 2.6 LOCATION OF INSTANT CENTER OF VEHICLE IN A RIGHT TURN BY TWO TRAILING WHEELS

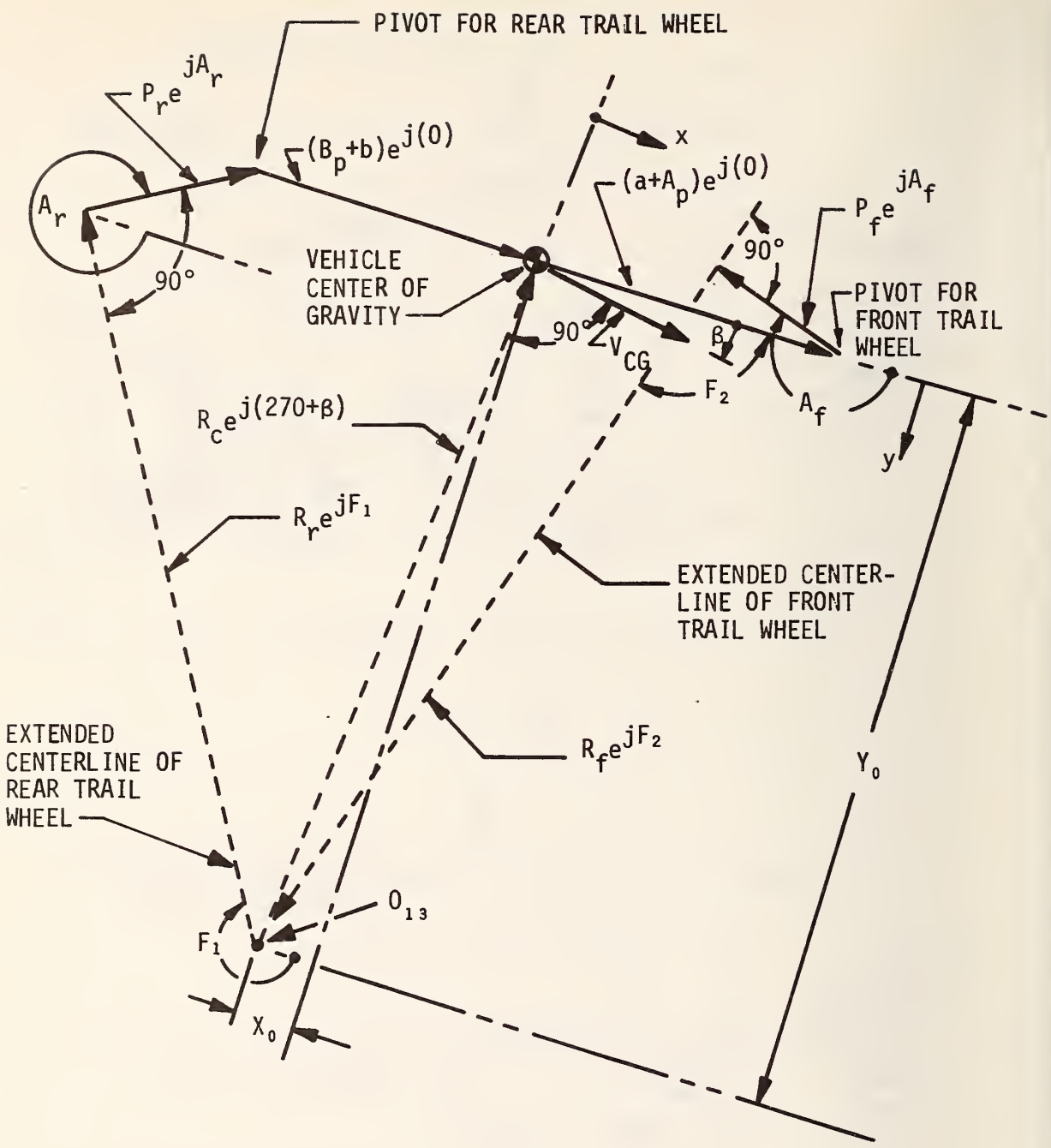

FIGURE 2.7 SPATIAL EQUIVALENT OF VEHICLE IN A RIGHT TURN WITH TRAILING WHEELS

These two equations may be combined to give

$$R_f = \frac{P_f \mathrm{Sin}(A_f) - \mathrm{Tan}(F_1)\left[a + A_p + P_f \mathrm{Cos}(A_f) + P_r \mathrm{Cos}(A_r) + B_p + b\right] + P_r \mathrm{Sin}(A_r)}{\mathrm{Cos}(F_2)\ \mathrm{Tan}(F_1) - \mathrm{Sin}(F_2)} \tag{2.41}$$

and

$$R_r = -\frac{1}{\mathrm{Cos}(F_1)}\left[a + A_p + P_f \mathrm{Cos}(A_f) + R_f \mathrm{Cos}(F_2) + P_r \mathrm{Cos}(A_r) + B_p + b\right]. \tag{2.42}$$

The coordinates, (x_0, y_0), of the instant center O_{13} of the vehicle may be located by summing the x and y components of displacement around the vector polygon containing lengths x_0, y_0, R_r, P_r, and $(B_p + b)$. The equation

$$\sum X = 0$$

gives

$$x_0 = -R_r \mathrm{Cos}(F_1) - P_r \mathrm{Cos}(A_r) - B_p - b\ . \tag{2.43}$$

The equation

$$\sum Y = 0$$

gives

$$y_0 = -R_r \mathrm{Sin}(F_1) - P_r \mathrm{Sin}(A_r)\ . \tag{2.44}$$

The sideslip angle may be obtained by the equation

$$\beta = \mathrm{Tan}^{-1}\left[-x_0/y_0\right]\ . \tag{2.45}$$

The radius of curvature, R_c, of the vehicle path may be evaluated by the equation

$$R_c = \sqrt{x_0^2 + y_0^2} \quad . \tag{2.46}$$

The slip angle, α, of the tire is the angle formed between the direction of travel of the center of tire contact and the X'-axis (Figure 2.8) (35). The magnitude of α may be calculated from the geometry of the vehicle and the coordinates of the instant center of the vehicle. The value of α for the right rear tire may be obtained by the following equation, which is based on Figure 2.9,

$$\alpha_{rr} = \text{Tan}^{-1} \left[-(b + x_0)/(y_0 - T_r/2)\right] \quad . \tag{2.47}$$

It should be recognized that x_0 is actually a negative value for the case shown, and the proper distance will result when this negative sign is included as part of x_0. Since α_{rr} is a negative angle for the case shown, an additional minus sign is required inside the brackets of Equation 2.47 as indicated. This equation is based on the assumption that the X'-axis of the rear wheel remains parallel to the x-axis of the vehicle. However, the roll steer (27) and deflection steer characteristics of the vehicle produce a significant change in the angular position of the X'-axis relative to the x-axis when centrifugal forces act on the vehicle. This change in the angle between the X'-axis and the x-axis may be reduced by replacing the shock absorbers with solid bars.

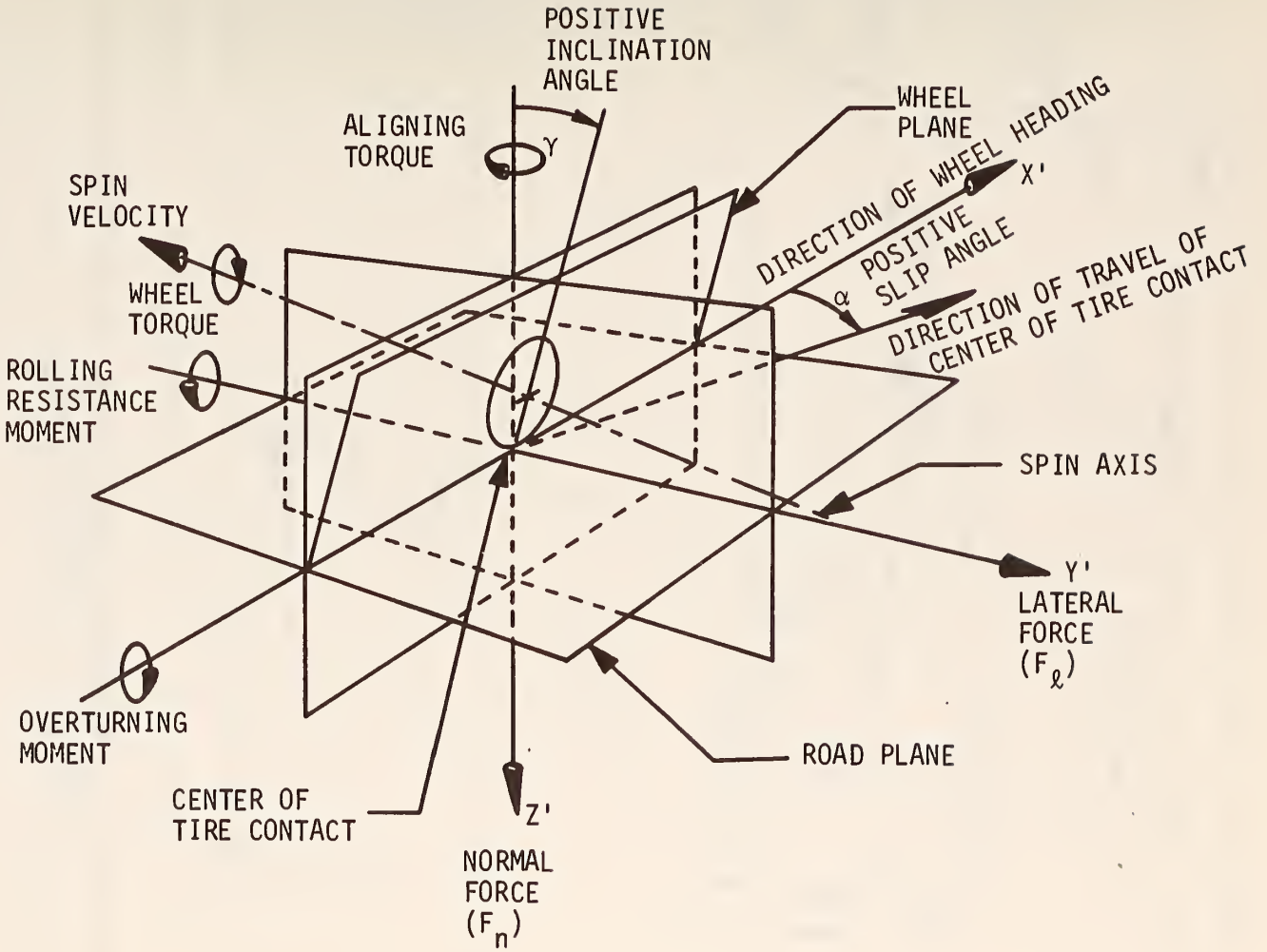

FIGURE 2.8 TIRE AXIS SYSTEM

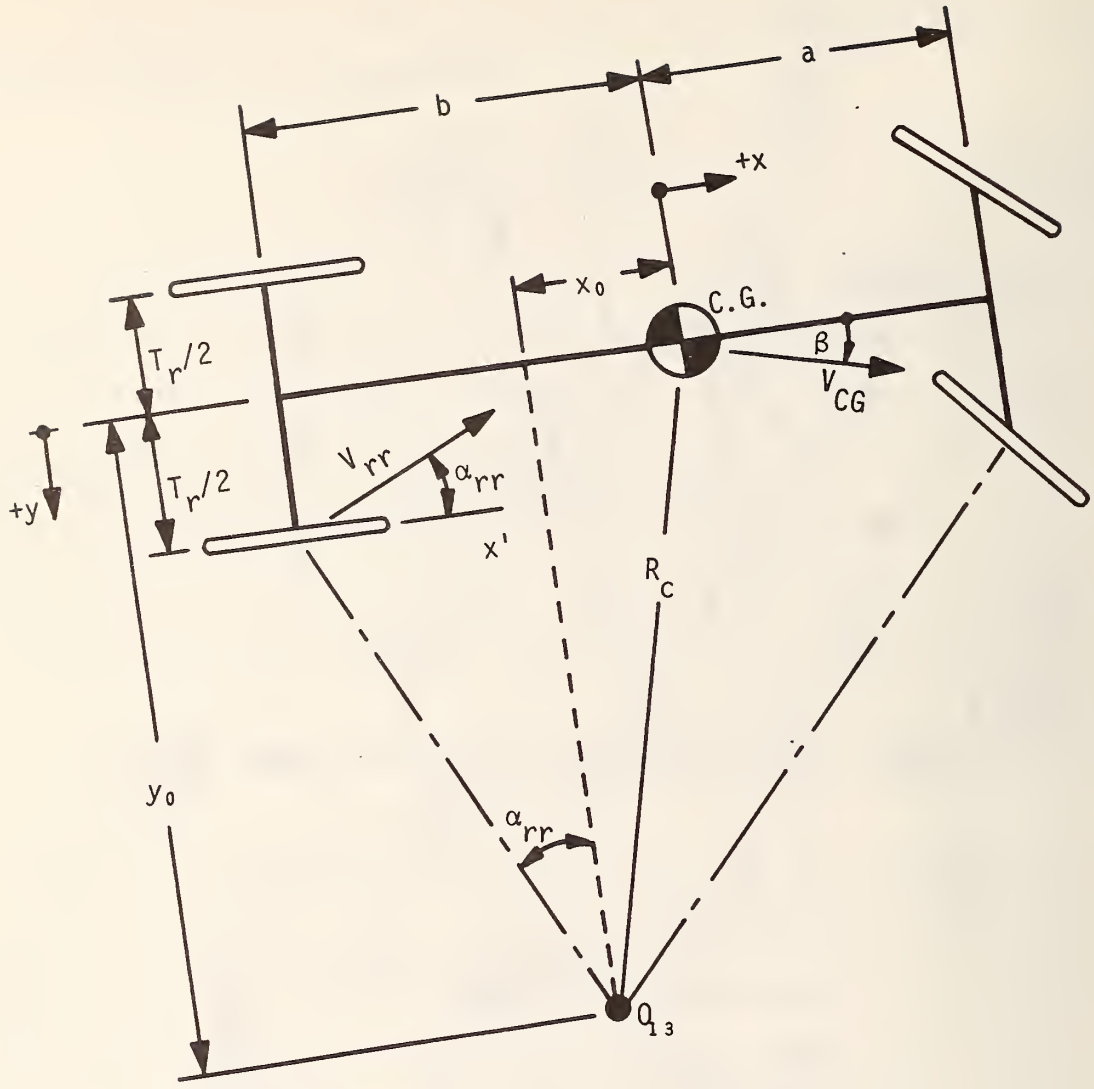

FIGURE 2.9 SCHEMATIC OF RIGHT REAR TIRE SLIP ANGLE FOR VEHICLE IN CIRCULAR PATH

The tire cornering stiffness and the tire camber stiffness are related to the lateral tire force, the tire slip angle and the inclination angle (camber) by the following equation

$$F_{\ell} = - C_{\alpha} \alpha + C_{\gamma} \gamma \, , \tag{2.48}$$

where

F_{ℓ} = lateral tire force (lbs)

C_{α} = tire cornering stiffness (lb/degree)

α = tire slip angle (degrees)

C_{γ} = tire camber stiffness (lb/degree)

γ = tire inclination angle (degrees).

This equation is a good approximation if the normal tire force is constant and if α and γ are small.

The lateral tire force, $F_{\ell r}$, on one rear tire may be calculated by applying d'Alembert's principle and summing moments about the center of the front axle as shown in Appendix B. This analysis applies to a vehicle with weight, W_t, which is operating at a constant speed, V, in a circular path. From Appendix B the lateral force on a rear tire is given by

$$F_{\ell r} = \frac{a}{2(a+b)} \frac{V^2}{R_c} \frac{W_t}{g} \, . \tag{2.49}$$

Substitution of Equation 2.48 into Equation 2.49 gives the result

$$- C_\alpha \alpha + C_\gamma \gamma = \frac{a}{2(a+b)} \frac{V^2}{R_c} \frac{W_t}{g} . \qquad (2.50)$$

The values of C_α and C_γ may be determined by fitting Equation 2.50 to experimental values of α and γ. The experimental values of α and γ should be obtained for two different vertical locations of the vehicle center of gravity in order to obtain values of γ which are not directly proportional to both α and the inertia force.

Vertical Acceleration of the Driver

The vertical acceleration of the driver is a function of the road roughness and the vehicle-driver system characteristics. If human tolerance to random vibration can be established, it would provide the basis for establishing allowable values of road roughness. It is desirable to establish the relationship between the acceleration of the driver and roughness of the road.

Human tolerance levels for vertical steady state sinusoidal vibration have been tabulated as a function of frequency and peak displacement (23). The maximum recommended mean square value of human acceleration for steady state sinusoidal vibration is

$$\overline{\ddot{X}}^2_{MAX} = \left[\frac{\ddot{X}_{MAX}(2\pi f)^2}{g_1} \left(\frac{1}{\sqrt{2}} \right) \right]^2 , \qquad (2.51)$$

where

$\overline{\ddot{X}}^2_{MAX}$ = the maximum recommended mean square value of sinusoidal vibration (g^2)

X_{MAX} = the maximum recommended displacement amplitude for sinusoidal vibration at frequency, f. This value is given in Ref. 23 (inches)

f = frequency of vibration (cps)

g_1 = 386 in/sec^2.

The principal ride problems of highway vehicles exist in well-defined frequency bands which correspond to the major natural frequencies of the vehicle or to the spacing of expansion strips in the pavement. Moreover, the frequency range in which ride problems occur is bounded by the response of humans to vibrations. Human response to vibration resembles a band pass filter, and frequencies below 0.8 cps are highly attenuated. The limits for sinusoidal vibration do not apply precisely to the acceleration of a driver on a highway, because the acceleration of the driver is random in nature and contains various amplitudes and frequencies. However, these limits may indicate the objectionable frequencies in many cases.

The acceleration of the driver may be estimated if the roughness of the road and the response characteristic of the vehicle-driver system are known. The roughness of the road may be expressed in terms of the roughness power spectral density, $P_{y_0}(f)$, which can be measured with the modified BPR

roughometer. The vehicle response characteristic, $[\ddot{Y}_3/Y_0]$, may be obtained by treating the entire vehicle as a single unit as described by Hamilton (14), or it may be based on the analysis of the system shown in Figure 2.10. If the response characteristics of the system are linear, the driver acceleration power spectral density, $P_{\ddot{Y}_3}(f)$, is given by the equation

$$P_{\ddot{Y}_3}(f) = \left|\frac{\ddot{Y}_3(f)}{Y_0(f)}\right|^2 P_{Y_0}(f) , \qquad (2.52)$$

where

$P_{\ddot{Y}_3}(f)$ = power spectral density of the driver acceleration (G^2/cps)

$P_{Y_0}(f)$ = power spectral density of the road roughness (in^2/cps)

$\ddot{Y}_3/Y_0$ = transfer function for the linear system (G/in)

$\ddot{Y}_3(f)$ = acceleration of the driver for a given excitation Y_0 at frequency f (g)

$Y_0(f)$ = displacement input into the system at frequency f (in)

f = frequency (cps).

Equations for the transfer functions for this system are developed in Appendix A. The equations of motion for this three degree of freedom system are

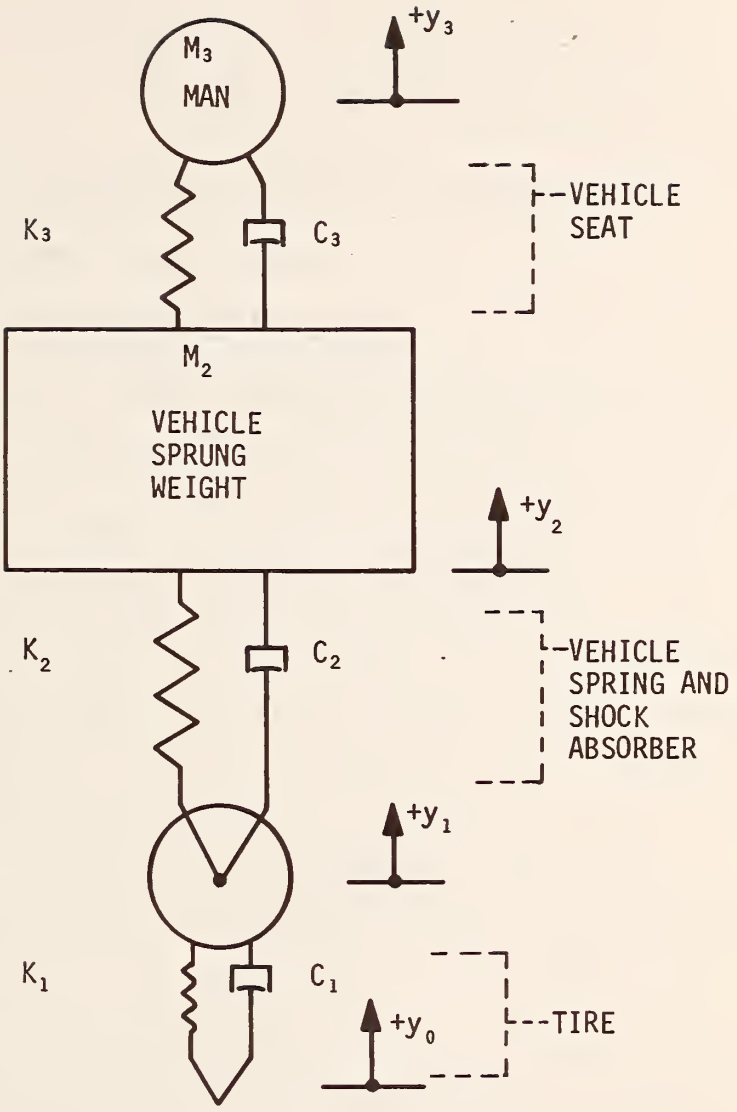

FIGURE 2.10 VEHICLE MODEL - THREE DEGREE OF FREEDOM SYSTEM

$$M_1\ddot{y}_1 = K_1(y_0-y_1) + C_1(\dot{y}_0-\dot{y}_1) - K_2(y_1-y_2) - C_2(\dot{y}_1-\dot{y}_2) , \quad (2.53)$$

$$M_2\ddot{y}_2 = K_2(y_1-y_2) + C_2(\dot{y}_1-\dot{y}_2) - K_3(y_2-y_3) - C_3(\dot{y}_2-\dot{y}_3) , \quad (2.54)$$

$$M_3\ddot{y}_3 = K_3(y_2-y_3) + C_3(\dot{y}_2-\dot{y}_3) . \quad (2.55)$$

The response of the actual system will only deviate slightly from that of the linear vehicle model for small displacements because of nonlinear spring rates and nonlinear damping. However, the assumption of a linear model is not acceptable for large displacements because rubber bumpers will limit the relative motion between wheel and frame for large body motions, and the tires will loose contact with the ground for large wheel hop displacements. One solution to this nonlinear problem may be obtained by solving the nonlinear equations of motion in the time domain. The solution in the time domain will require values of the road roughness, y_0, as a function of time. A method for estimating y_0 as a function of time will be discussed later.

The probability distribution of the driver acceleration for various roads provides information concerning the distribution of the amplitudes of acceleration. Random data are often assumed to have a Gaussian probability denstiy function because of the practical implications of the Central Limit Theorem, which implies that any physical phenomenon produced by the sum of numerous random effects will tend to be normally distributed (4).

The power spectral density function for the driver acceleration will identify the contribution of each frequency band to the total mean square value of the driver acceleration. The total area under the acceleration power spectrum curve will be equal to the mean square value of the driver acceleration.

Lateral Tire Forces

The lateral force, which is developed at the tire and road interface, produces the directional control for the vehicle. The lateral tire force, F_ℓ, is related to the normal force, F_n, exerted on the tire by the road. The direction of F_ℓ is tangent to the plane of the road as illustrated in Figure 2.8. If the surface of the road is rough, the normal force on the tire, F_n, will not be constant. In fact, the normal force may be zero for a large percent of the time if high amplitudes of wheel hop are occurring.

The probability density distribution for the lateral tire force may be calculated if the relationship between F_n, F_ℓ and α are known and if the probability density distribution of F_n is known.

If the tire inclination angle is fixed, the relationship between F_n and F_ℓ for a specific value of α may be expressed by the equation

$$F_\ell(I) = C(I,1)[F_n(I)]^1 + C(I,2)[F_n(I)]^2 + C(I,3)[F_n(I)]^3 + C(I,4)[F_n(I)]^4 . \quad (2.56)$$

The parameters C(I,1), C(I,2), C(I,3) and C(I,4) are constants for a given value of α. These constants are usually obtained by applying the Method of Least Squares Fit to tire data.

The standard deviation for the normal tire force was recorded on several roads by Sattaripour (36). The probability density distribution of the normal tire forces was shown to be approximately Gaussian by Hildebrand (16). The probability density of the lateral tire force may be calculated as shown in Reference (30) using

$$P_\ell(F_\ell) = \frac{P_n(F_{n_1})}{\left|\frac{dg(F_{n_1})}{d\,F_n}\right|} + \ldots + \frac{P_n(F_{nN})}{\left|\frac{dg(F_{nN})}{d\,F_n}\right|} , \quad (2.57)$$

where

$P_\ell(F_\ell)$ = probability density for lateral tire forces (lb^2/lb)

$P_n(F_{nN})$ = probability density for normal tire forces (lb^2/lb)

F_{nN} = normal tire force at station N (lb)

F_ℓ = lateral tire force at station N (lb).

The evaluation of $P_\ell(F_\ell)$ is illustrated in Figure 2.11. This illustration shows that the area under the curve of

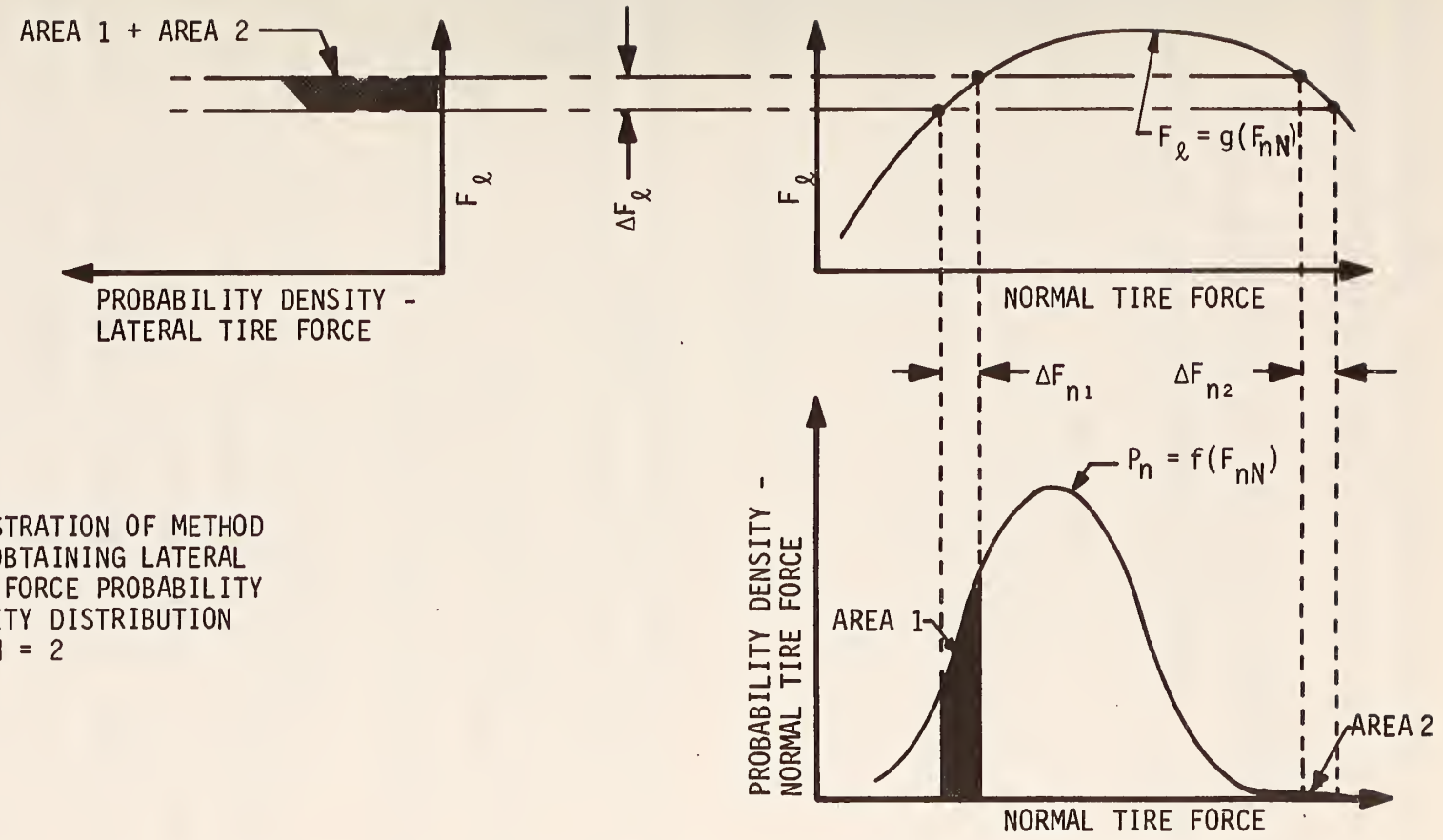

ILLUSTRATION OF METHOD FOR OBTAINING LATERAL TIRE FORCE PROBABILITY DENSITY DISTRIBUTION FOR N = 2

FIGURE 2.11 CALCULATION OF LATERAL TIRE FORCE PROBABILITY DENSITY DISTRIBUTION

$P_\ell(F_\ell)$ for an increment of lateral force, ΔF_ℓ, must be equal to the area under the curve of $P_n(F_{nN})$ inside the N related force increments ΔF_{nN}.

The area under the lateral tire force probability density curve and inside the range of lateral tire forces

$$a1 \leq F_\ell \leq b1$$

is equal to the probability, $p_r(F_\ell)$, of occurrence of lateral forces within this range. This relationship may be expressed in the form

$$p_r(a1 < F_\ell < b1) = \int_{a1}^{b1} P_\ell(F_\ell)dF_\ell \ . \qquad (2.58)$$

The cumulative probability distribution is formed by summing the area under the probability density distribution between $F_\ell = 0$ and some value $F_\ell = F_{\ell 1}$. The ordinate of the cumulative probability distribution at $F_\ell = F_{\ell 1}$ is equal to the probability that forces less than $F_{\ell 1}$ will occur.

The tire cornering stiffness, C_α, is often assumed to have a constant value when performing a dynamic analysis for a vehicle. For a perfectly smooth road, F_n would be constant and C_α would be constant for small angles. However, for a rough road C_α is not a constant, because F_ℓ is not a linear function of α when F_n is not constant. If the tire properties and normal load distribution are known, the error in the lateral tire force due to the assumption

that C_α is constant can be investigated. Results of such a study are included later.

The Use of P and Q to Synthesize a Pavement Profile

The roughness of road surfaces may be described in the frequency domain by the Zable Equation. Roughness is the vertical distance between the highway elevation and a base line. The Zable Equation is based on the parameters P and Q which must be determined experimentally. The Zable Equation, which expresses roughness in terms of its power spectral density is

$$P_y(f_d) = e^{[Q \ln(f_d)+P]}, \qquad (2.59)$$

where

$P_y(f_d)$ = power spectral density of road roughness ($ft^2/(cycles/ft)$)

f_d = distance based frequency (cycles/ft)

e = base of natural logarithms

Q and P = parameters for a specific highway.

The dimensions of the Zable Equation and the significance of the parameters P and Q may be easier to see if expressed in the form

$$P_y(f_d) = \left[\frac{f_d}{f_{d_1}}\right]^Q P_y(f_{d_1}), \qquad (2.60)$$

where

f_{d_1} = a specific value of the distance based frequency (cycles/ft)

$P_y(f_{d_1})$ = the roughness power spectral density evaluated at f_{d_1} ($ft^2/(cycles/ft)$)

$$P = \ln\left[\frac{P_y(f_{d_1})}{(f_{d_1})^Q}\right] . \qquad (2.61)$$

Equations 2.59 and 2.60 are identical. If f_{d_1} is assumed to be unity, the results of Equations 2.60 and 2.61 are simplified.

It is possible to generate a pavement profile from a pavement roughness spectrum by using Rice's Equation (33). In employing this procedure it is convenient to assume that the pavement profile is a time based random variable, x(t), defined by Equation 2.62.

The roughness spectrum is divided into frequency bands as shown in Figure 2.12, and the midfrequencies of these bands are specified by f_i. The area within each band is indicated by A_i. A time based frequency, ω_i, is obtained from f_i by using

$$\omega_i = 2\pi f_d V ,$$

where f_d is the distance based frequency discussed in Chapter 1, and V is the vehicle velocity.

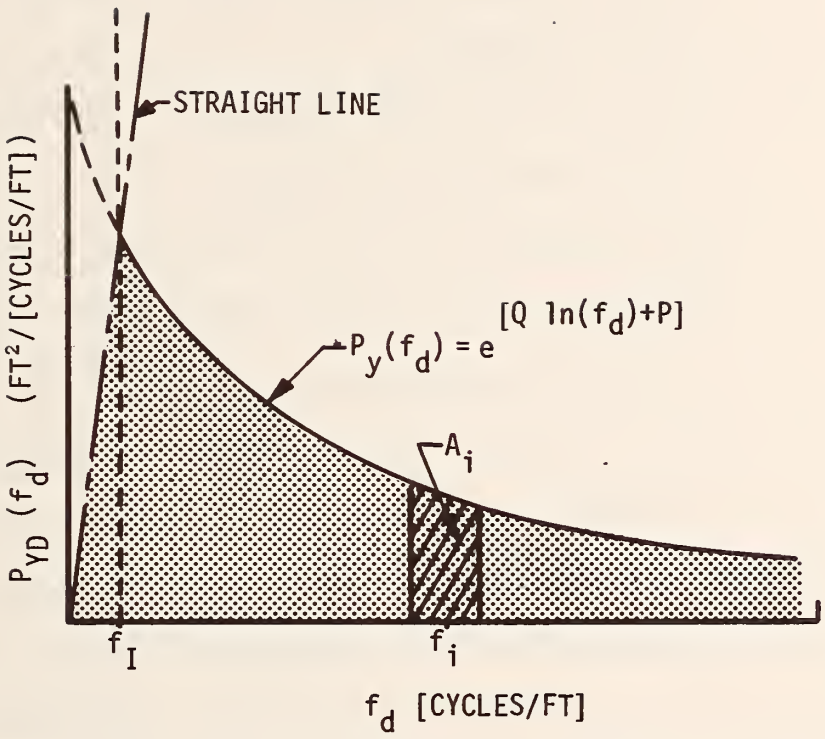

FIGURE 2.12 THE PAVEMENT ROUGHNESS SPECTRUM REPRESENTED BY THE MODIFIED ZABLE EQUATION

$$x(t) = \sum_{i=1}^{n} \sqrt{2A_i} \left[\text{Cos}(\omega_i t - \phi_i)\right] , \qquad (2.62)$$

where

$x(t)$ = the time based random variable representing a pavement profile (ft)

t = time (seconds)

A_i = area under the i^{th} interval of the roughness power spectrum curve (ft^2)

ω_i = midfrequency of the i^{th} interval (radians/second)

ϕ_i = uniformly distributed random number with $0 \leq \phi_i \leq 2\pi$.

The area, A_i, in each frequency band of the roughness power spectrum is required to generate a highway profile with Rice's equation. However, the area under the roughness power spectrum as described by Equation 2.60 is not defined as f_d approaches zero because Q is always negative. Therefore, it is desirable to modify the Zable Equation for small values of f_d to eliminate this problem. The relationship between f_d and the wavelength, λ, of the road profile is given by Equation 1.1 as

$$f_d = \frac{1}{\lambda} .$$

Long wavelengths are commonly removed from data by electronic high pass filters or by mathematical filters. For example, a mathematical filter in the form of a 300 foot long running mean baseline (Figure 2.13), was used to

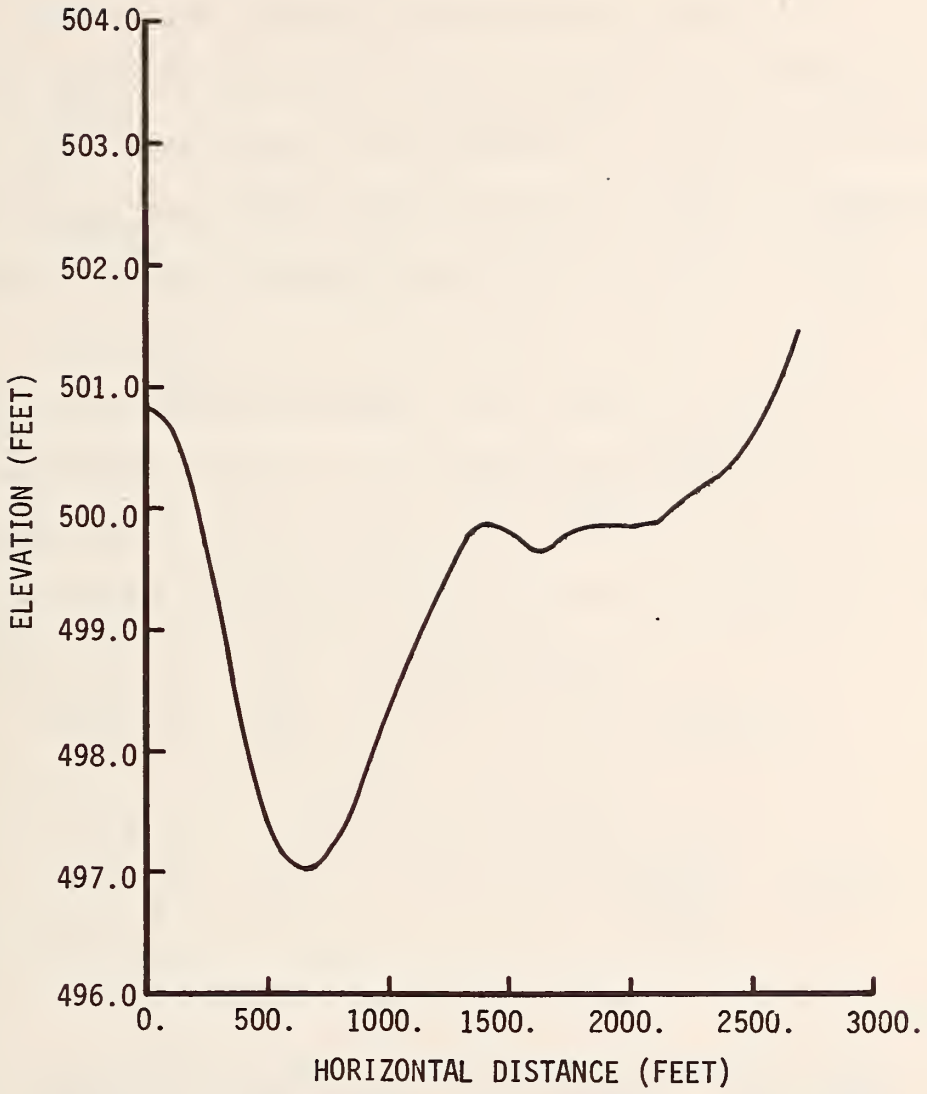

FIGURE 2.13 ELEVATION FILTER USING A 300 FOOT RUNNING MEAN BASELINE ON STATE ROAD 26

preprocess the elevation data (Figure 2.14) for State Road 26, and the resulting roughness values are shown in Figure 2.15. This process attenuates the high amplitude long wavelengths (e.g. mountains and long hills) which do not affect the vehicle's response, but which do affect the mathematical analysis by spilling power from one band into an adjacent band as discussed by Quinn (31) and Van Deusen (40).

A finite area under the roughness power spectrum curve may be obtained by modification of the low frequency end of the spectrum as indicated in Figure 2.12. The resulting power spectrum is defined by two equations

$$P_y(f_d) = e^{[Q \ln(f_d)+P]} \quad \text{for} \quad f_d \geq f_I \qquad (2.63)$$

and

$$P_y(f_d) = \left[\frac{f_d}{f_I}\right] e^{[Q \ln(f_I)+P]} \quad \text{for} \quad f_d < f_I, \qquad (2.64)$$

with

f_I = the frequency at the intersection between the straight and curves lines shown in Figure 2.12 (cycles/foot).

If f_I is too large, the roughness values generated by Rice's equation will be too small. If f_I is too low, the actual roughness may not fit the original Zable Equation, because measurements have not been obtained at very low frequencies.

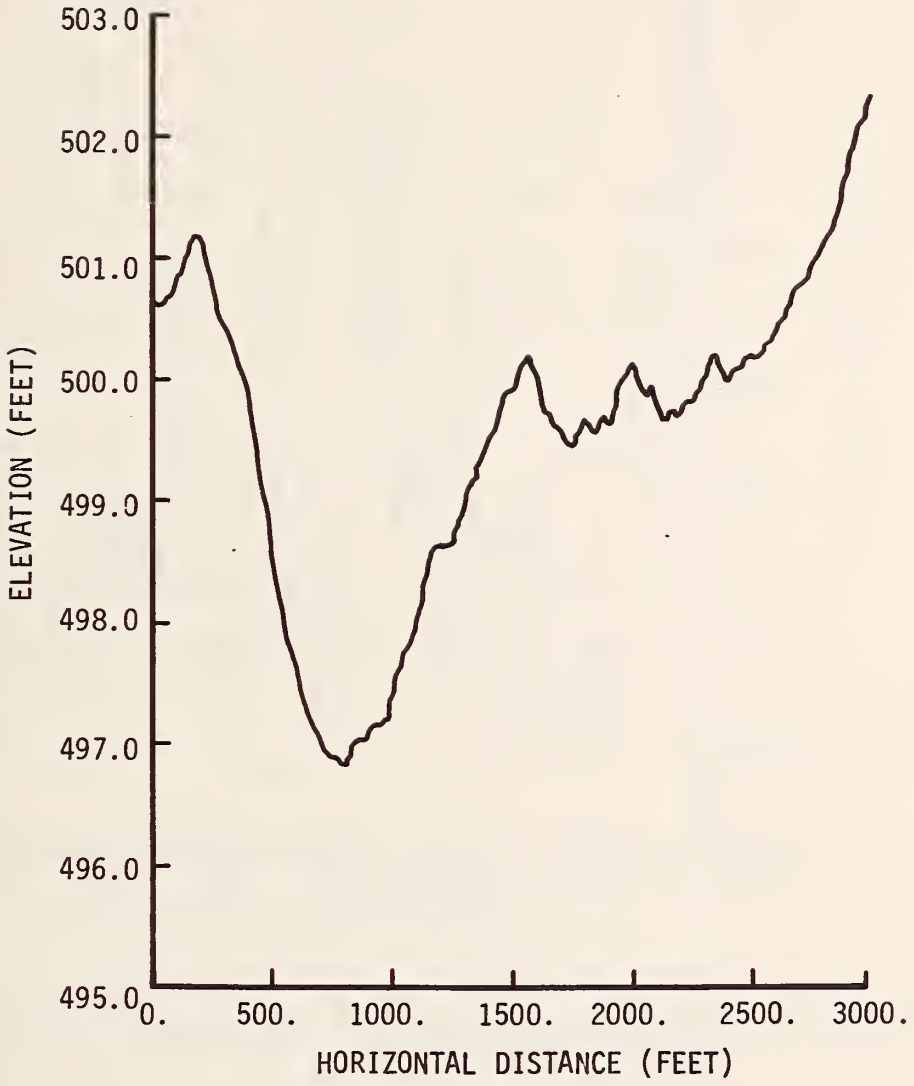

FIGURE 2.14 ROD AND LEVEL ELEVATION DATA FOR STATE ROAD 26

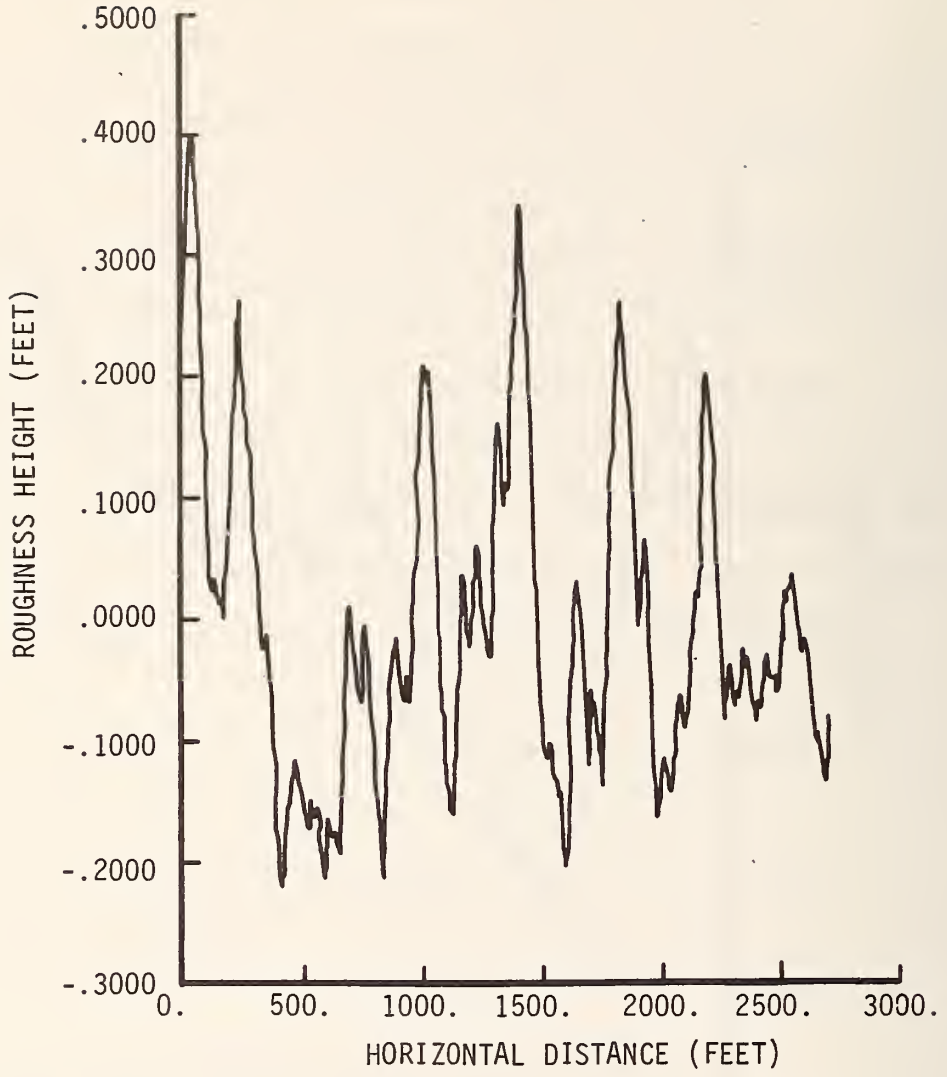

FIGURE 2.15 ROUGHNESS VALUES OBTAINED BY SUBTRACTING A 300 FOOT RUNNING MEAN BASELINE FROM THE ELEVATION DATA FOR STATE ROAD 26

Hudson (18) has suggested that wavelengths greater than 500 feet long (i.e. f_I = .002 cycles/ft) need not be recorded in highway roughness studies.

When applying Rice's equation, the number of points generated must be adequate from a statistical viewpoint, and the original roughness power spectrum must be accurate.

After a pavement profile has been generated, it is necessary to compute the power spectrum of the generated data. Comparison of the power spectrum of the generated data with the original power spectrum will provide a check on the accuracy of the generated pavement in the various frequency ranges. If these two power spectra are identical, the generated pavement will have roughness which will be statistically the same as the parent pavement profile.

It should be recognized that the use of Rice's Equation to reconstruct a pavement profile will, in general, not result in a unique pavement profile. It is possible to generate many different profiles which will have the same pavement roughness spectrum. This lack of uniqueness is due to the loss of the phase relationships when the pavement roughness spectrum is determined. Since the true phase relationships are not known, different random phase angles are selected when the construction of a profile is undertaken.

CHAPTER 3

INSTRUMENTATION

Introduction

The instruments which were developed for evaluating the steer angle, steering wheel angle, sideslip angle, and the vertical acceleration of the driver are described in this chapter. All measurements are based on tests of a 1967 Chevrolet automobile with 30,000 miles. Before conducting these tests, the gear box in the steering linkage was adjusted to remove the free play. This vehicle is equipped with Goodyear 8.25 × 14 tires with 0.20 inches of tread.

The test equipment is operated by a one kilowatt motor-generator set, which is mounted in the trunk of the vehicle. The test equipment includes the following items:

Strip Chart Recorder (115 v, 0.8 a)

DC Power Supply (± 15 v, 0.3 a)

Philbrick Model RP Manifold

Gyroscope

DC Power Supply for Gyroscope (26 v, 2 a starting current, 0.6 a running current)

Accelerometer (unbonded strain gage model)

Strain Gage Transducers

Rotary Potentiometer

Signal Processing Circuits

FM Tape Recorder (7 channels)

The road roughness measurements in this investigation were obtained with the modified BPR roughometer which is described by Smeyak (37).

All of the experimental data were recorded by the strip chart recorder. The strip chart data records were digitized by a manually triggered chart reader, which was attached to a PDP II computer. The digital data were then plotted by the CALCOMP plotting system. These plots were visually inspected for discontinuities before the data were analyzed.

Steer Angle

The steer angle of the left front wheel was measured by strain gages, which are attached to a frame as shown in Figure 3.1. The following comments about the mechanical and electrical aspects of the system will add to this description. One end of the frame is fixed to the front wheel. The opposite end of the frame is fixed to a solid bar, which connects the upper and lower control arms at the centers of the ball sockets. The frame was designed to have a minimum natural frequency of 33 cps to minimize strain signals caused by resonant vibrations. The material supporting the strain gages is through hardened steel, which will tend to break instead of yield. This virtually eliminates

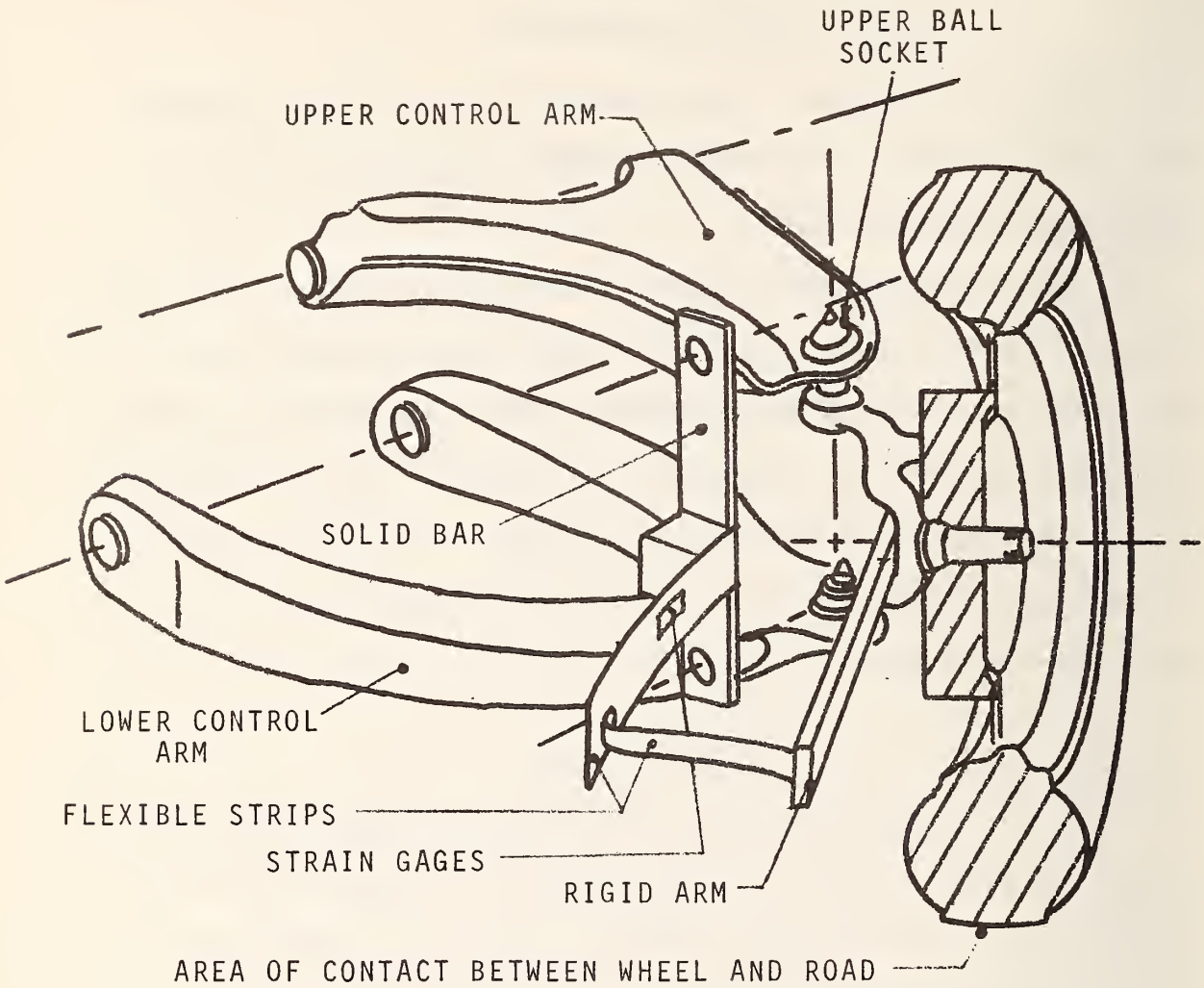

FIGURE 3.1 TRANSDUCER FOR SENSING THE STEER ANGLE OF THE LEFT FRONT WHEEL

the possibility of unidentified yielding by the gage support. The two strain gages are arranged to provide temperature compensation and to cancel axial strains. The current in the gages is set at approximately 20 ma by the 12 volt power source for the bridge circuit. The gages form the two active arms in the bridge circuit shown in Figure 3.2. The bridge is attached to the null balance potentiometer. The 200:1 amplifier, which follows the null balance, will remove noise induced into the leads. A second filter provides signal amplification and suppression of high frequency noise.

The block diagram of the steer angle measuring system is shown in Figure 3.3.

Static calibration tests show excellent agreement between the steer angle and the steering wheel angle. A static calibration curve for the system is shown in Figure 3.4. However, some of the records from dynamic tests show poor agreement between these two angles. This is due in part to the effects of rear end steering and the effects of body roll on the steer angles of both front wheels.

Steering Wheel Angle

The steering wheel angle measurement was performed by a rotary potentiometer, which is illustrated in Figure 3.5. The potentiometer is mounted on a leaf spring, and it is driven by a steel cable. This spring deflects to provide the proper cable tension. The cable is wrapped 1.5 turns around each pulley to prevent creep.

TWO ACTIVE ARM BRIDGE

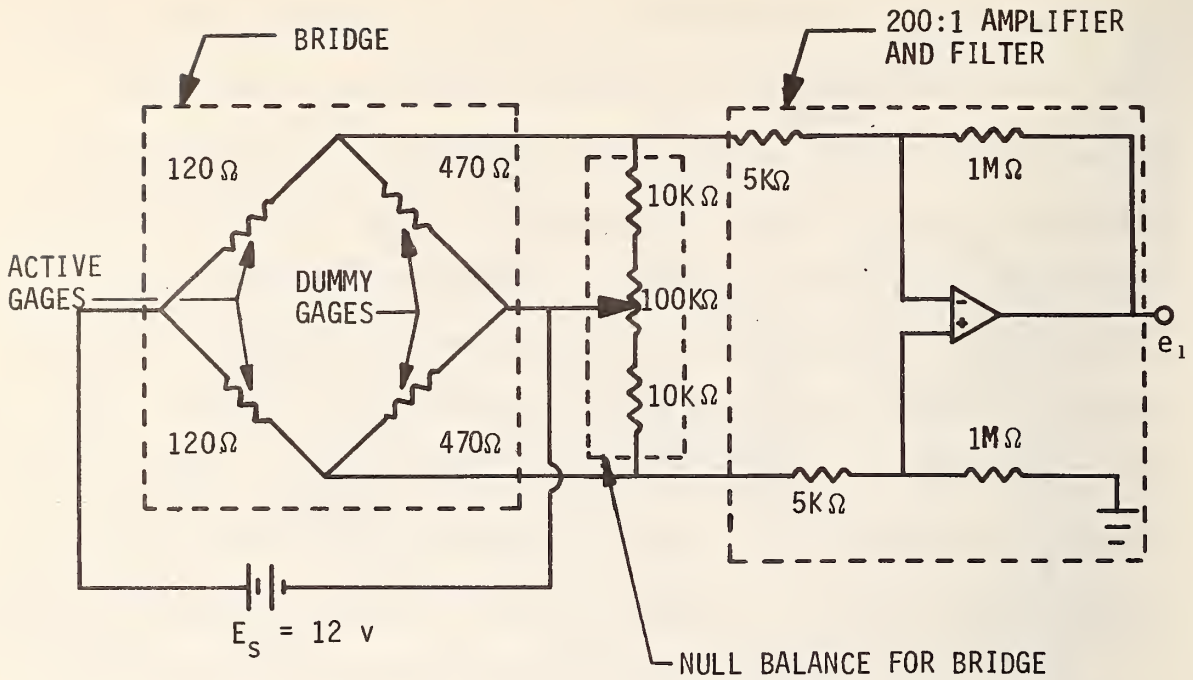

LOW PASS FILTER

R_2 = 39KΩ

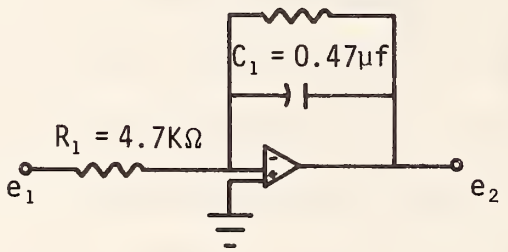

$$\omega_b = \frac{1}{R_2 C_1} = 171 \text{ RADIANS/SEC}$$

$$\text{GAIN} = \frac{R_2}{R_1} = 8.3:1$$

FIGURE 3.2 ELECTRONIC CIRCUIT FOR TWO ACTIVE ARM BRIDGE AND LOW PASS FILTER

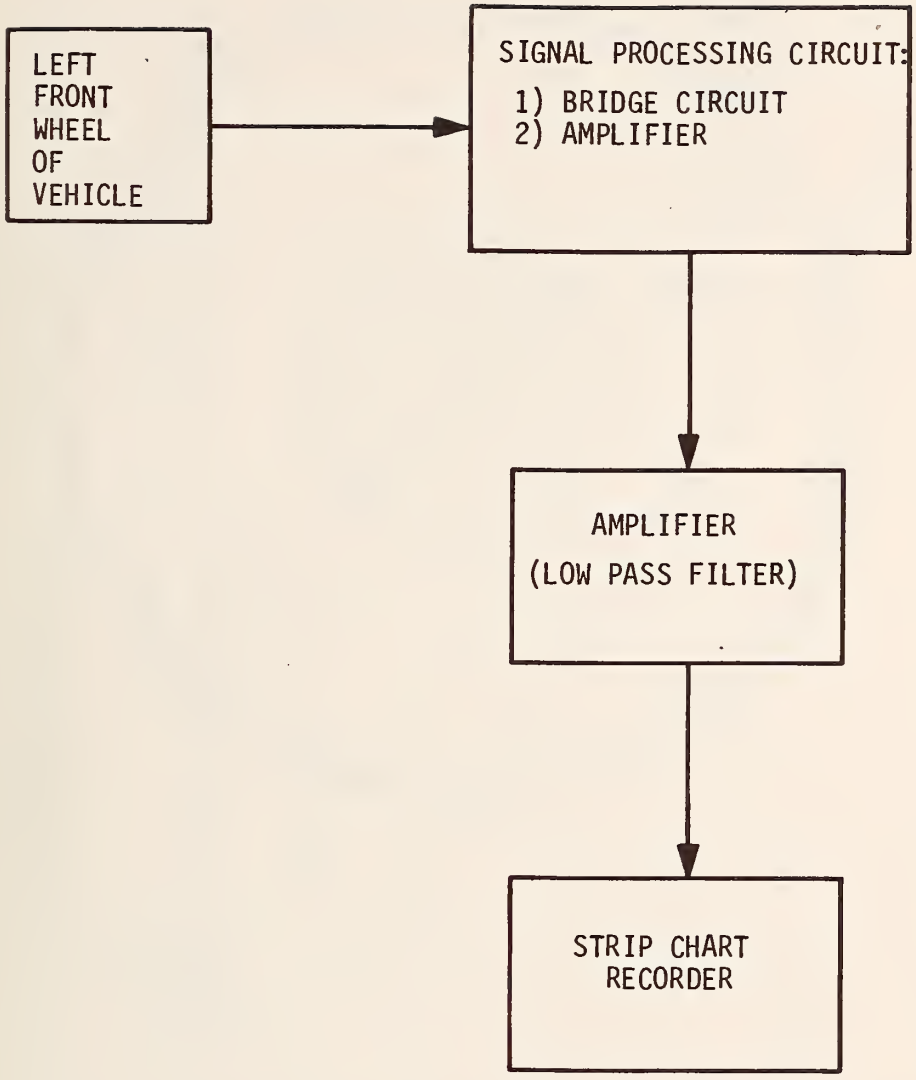

FIGURE 3.3 BLOCK DIAGRAM OF STEER ANGLE MEASURING SYSTEM

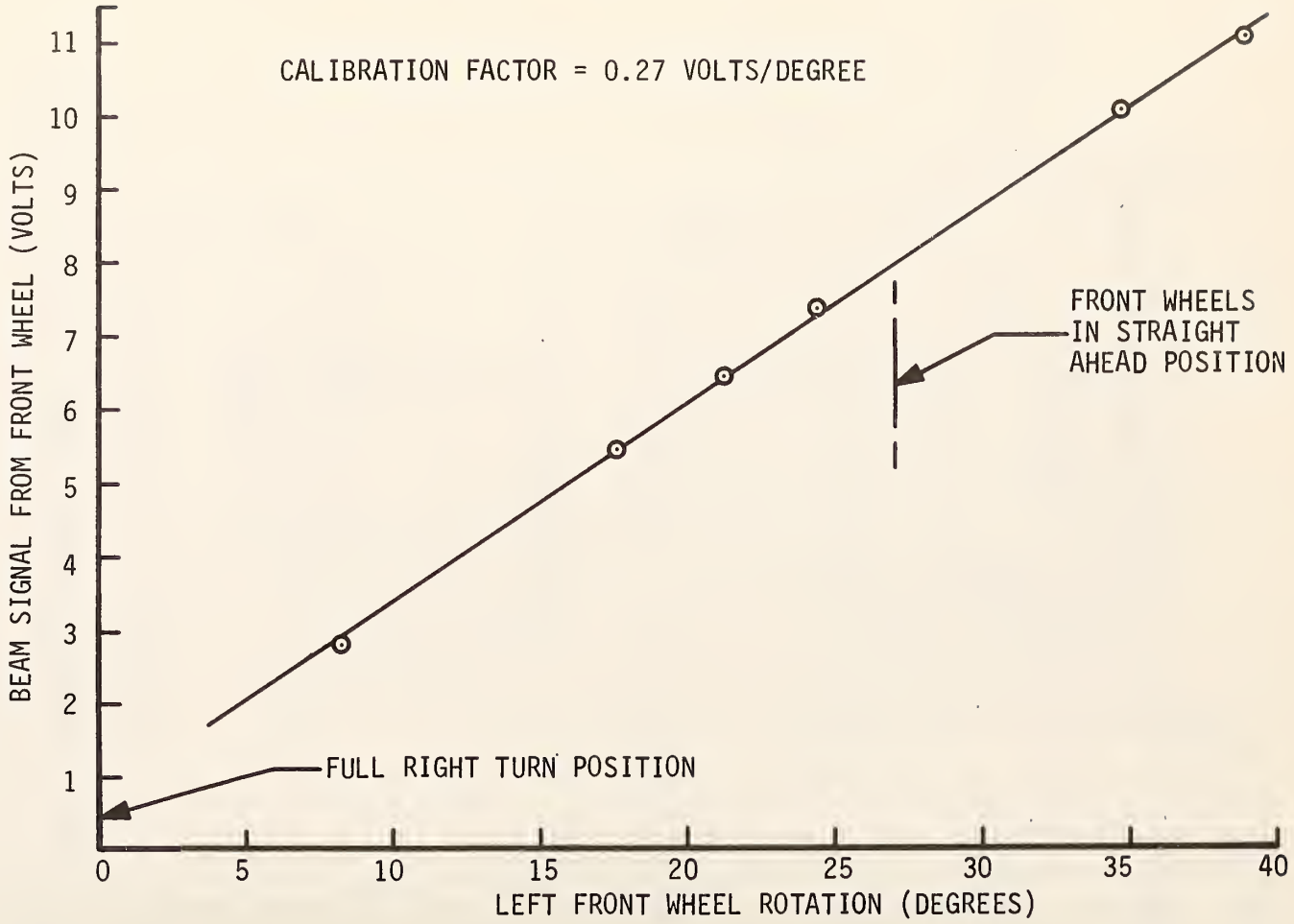

FIGURE 3.4 STATIC CALIBRATION CURVE FOR STEER ANGLE INSTRUMENTATION SYSTEM

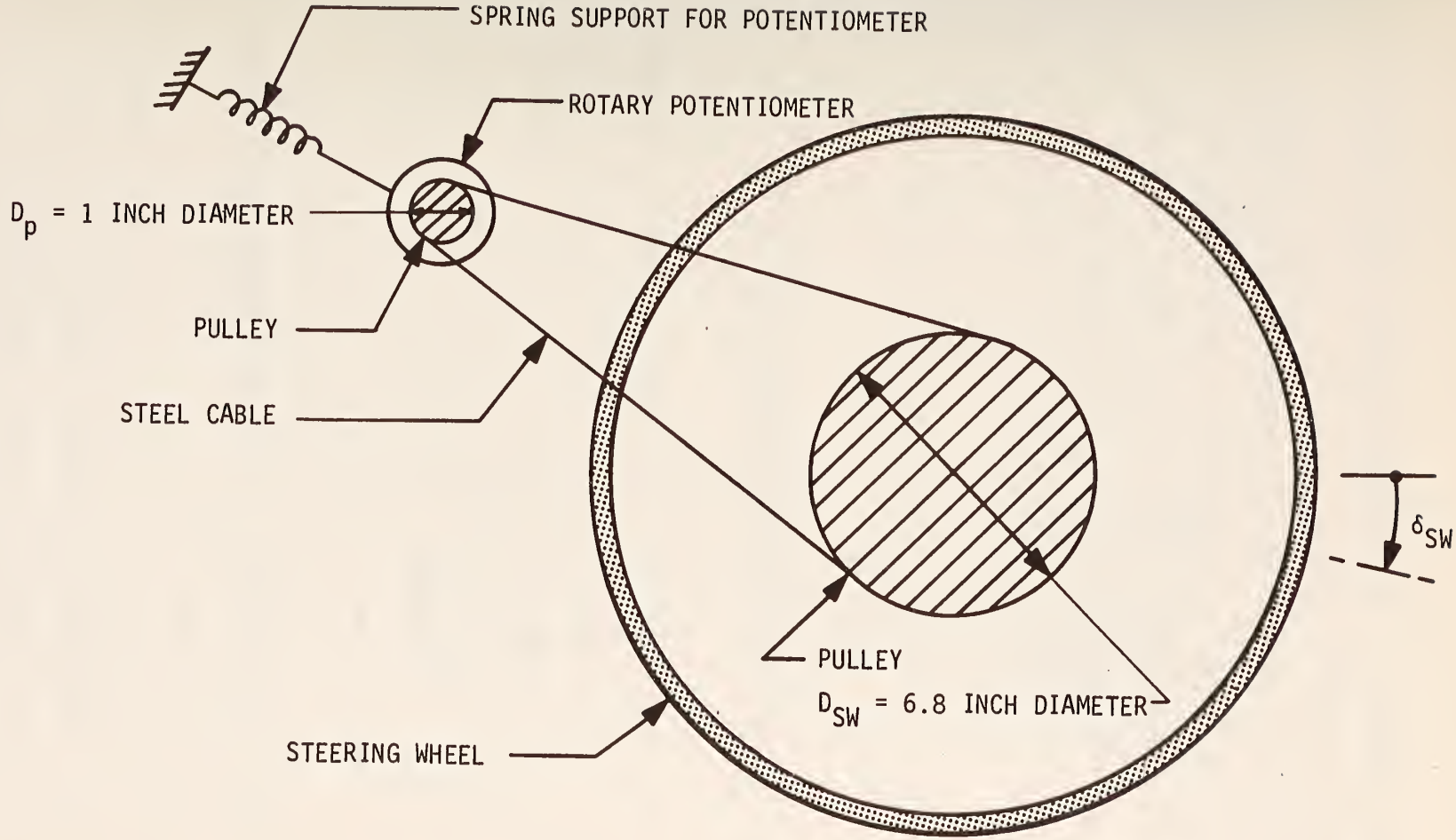

FIGURE 3.5 TRANSDUCER FOR SENSING THE STEERING WHEEL ANGLE

The block diagram of the steering wheel angle measuring system is shown in Figure 3.6.

The electronic circuit for the steering wheel angle instrumentation is shown in Figure 3.7. The two 6 volt batteries are arranged to provide a zero output when the slidewire is at the center position of the ten turn potentiometer. The signal is amplified by a low pass filter.

The relationship between steering wheel angle, δ_{SW}, and the output signal voltage, e_o, is

$$\frac{\delta_{SW}}{e_o} = \frac{R_2}{R_1}\left(\frac{\text{10 turns of potentiometer}}{\text{1 turn of steering wheel}}\right)\left(\frac{D_P}{D_{SW}}\right)\left(\frac{360°}{E_s}\right).$$

Since many roads usually have short, straight sections, several trips over the same section are required to accumulate a statistically desirable quantity of data. The data records are based on a 5 mm per second chart speed. The digital data points are spaced 0.2 seconds apart. The data from one trip over the road is defined as one piece of record. Each piece of record was adjusted to have a zero mean value prior to combining it with the other pieces of record for a given section of road.

The steering wheel angle is easy to measure, and this instrumentation system gives excellent results. If the potentiometer had more turns, it would facilitate the collection of data. This system is inconvenient because

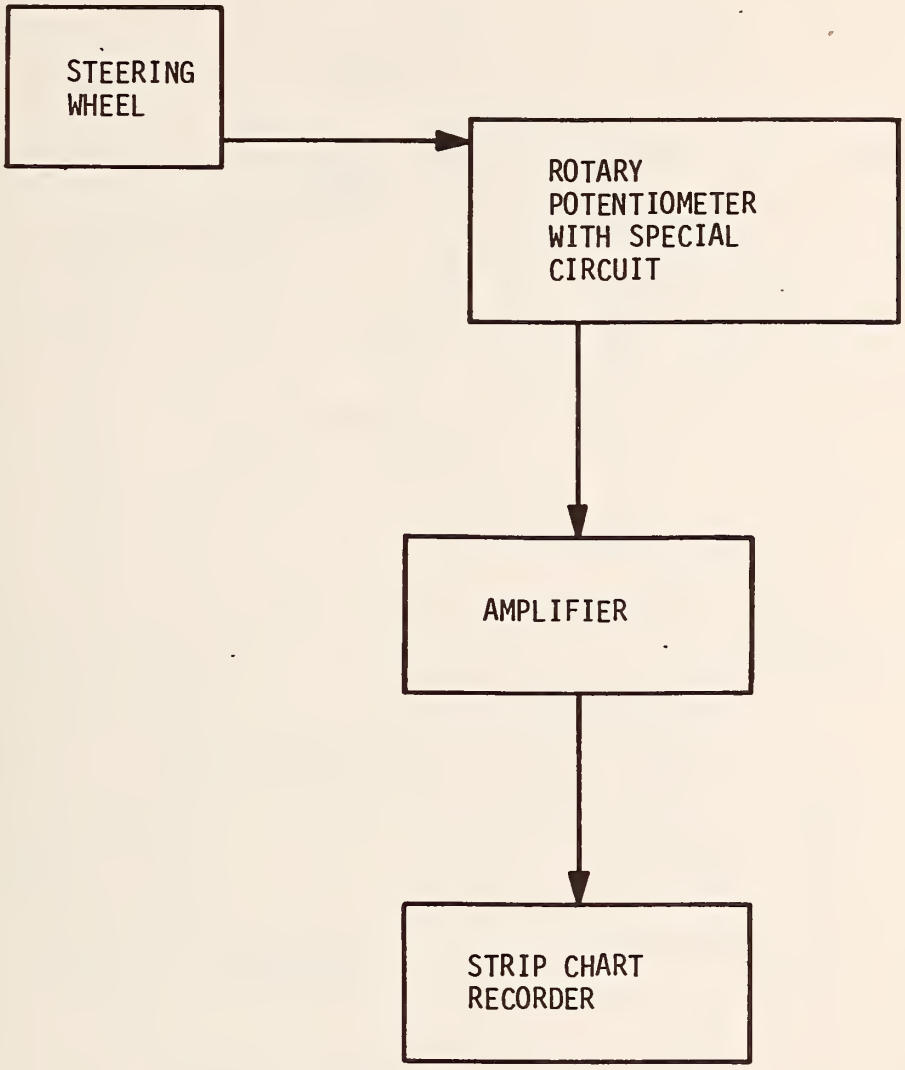

FIGURE 3.6 BLOCK DIAGRAM OF STEERING WHEEL ANGLE MEASURING SYSTEM

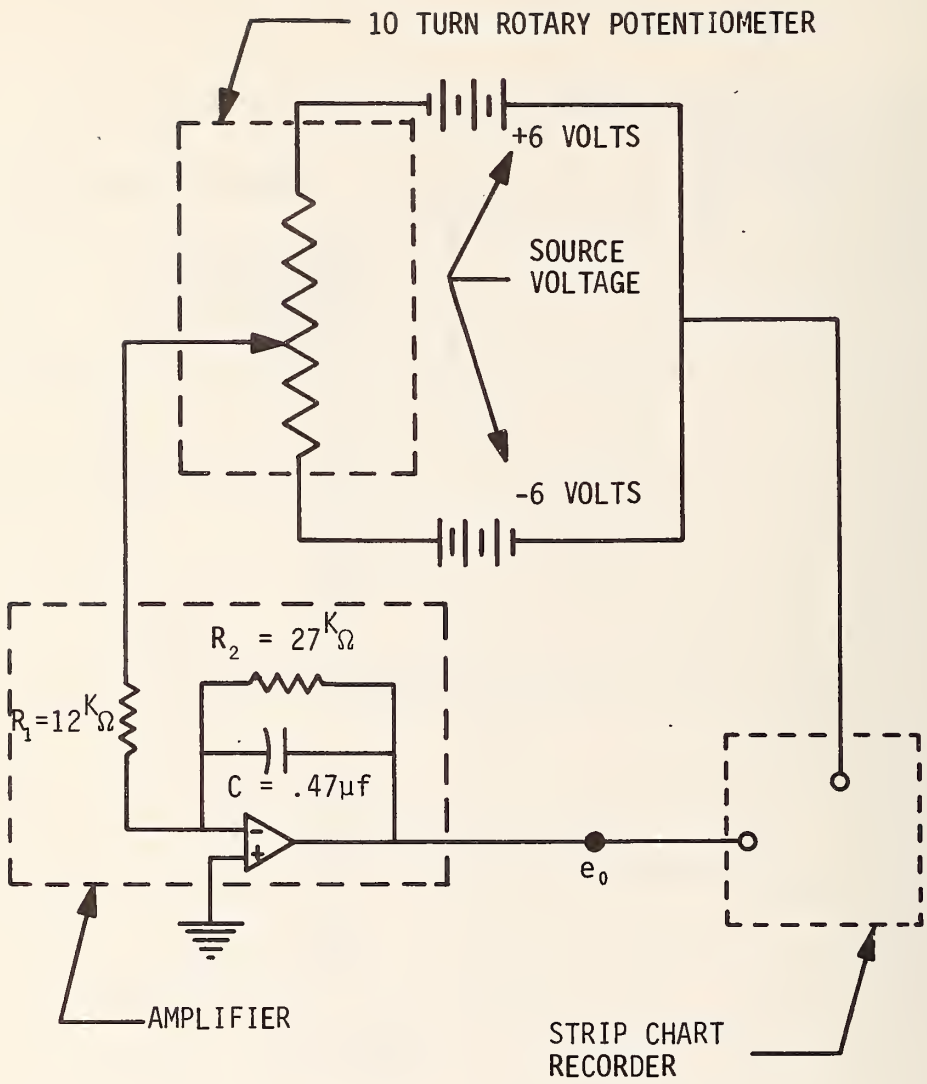

e_0 = OUTPUT VOLTAGE

E_S = TOTAL SOURCE VOLTAGE = 12 VOLTS

FIGURE 3.7 ELECTRONIC CIRCUIT FOR STEERING WHEEL ANGLE INSTRUMENTATION

the potentiometer reaches the end of its travel before the maximum steering wheel rotation is attained.

Sideslip Angle

The sideslip angle was obtained by using two trail wheels to locate the center of curvature of the vehicle's path as shown in Figures 2.5 and 2.6. The coordinates of this instant center are established if the trail wheel angles A_f and A_r are known. These two angles are sensed by strain gage and frame assemblies, which are similar to the arrangement described for the steer angle measurement.

Some design considerations, which affect the performance of the trail wheel assembly, are illustrated in Figure 3.8. The 20 inch wheel allows relatively high speed travel without producing excessive centrifugal forces on the tire carcass. The member, which connects the wheel to the pivot shaft, is of tubular construction to reduce torsional vibration. The distance from the wheel to the pivot shaft allows approximately 3/4 of an inch of lateral motion by the wheel per degree of change in the angles A_f or A_r. The hold down spring minimizes the time when the wheel is not in contact with the road. The counterbalance weight will annul the centrifugal force which acts on the trail wheel assembly in a turning maneuver. The frame, which supports the front trail wheel, is made of aluminum tube to provide a rigid, low mass structure.

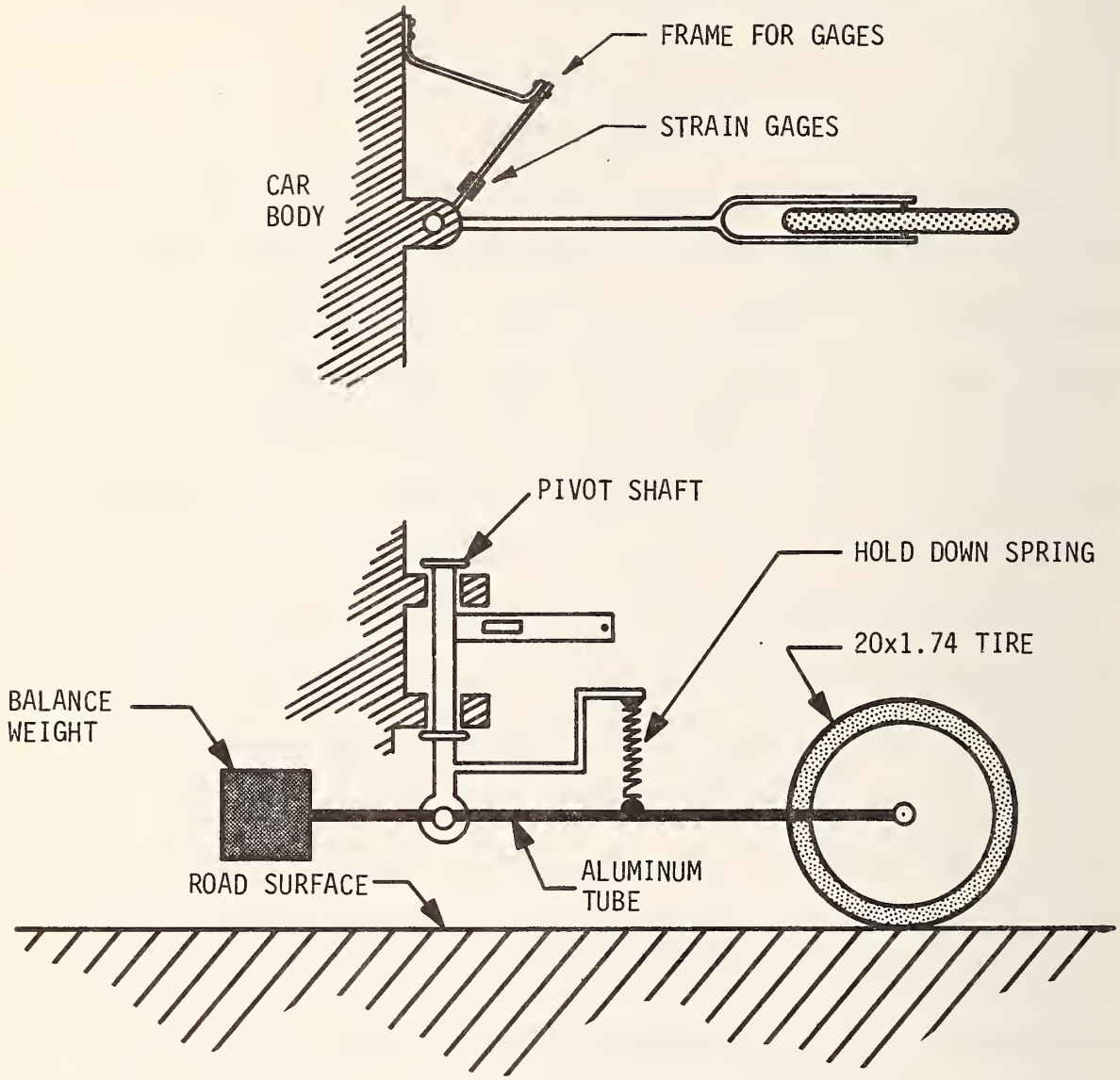

FIGURE 3.8 SCHEMATIC OF TRAIL WHEEL AND STRAIN GAGE INSTALLATION

A calibration curve for the front trail wheel is shown in Figure 3.9.

The block diagram of the trail wheel system is similar to the one used for the steer angle measurement.

An additional check on the performance of the trail wheel system was conducted by using the system to measure the path radius when driving the test vehicle around a circle of known radius at various speeds. The actual path radius was measured from a trail of water, which was deposited on the blacktop surface during the circular maneuver. The radius of the path of curvature was also obtained from the trail wheel signals. The variation in these two radii is less than five percent as shown in Figure 3.10.

The relationship between tire slip angle, tire inclination angle and lateral tire force is reported in this investigation. The steering action of the live rear axle produces secondary steering effects, which may be eliminated by replacing the shock absorbers with solid links. The solid links connect the rear axle to the sprung mass. This connection produces a large rear wheel caster angle when body roll occurs. The caster angle may be measured by a gyroscope. The tire slip angle may be obtained by the trail wheels. Values of α, γ, and R_c were recorded at various speeds for a circular maneuver with the solid links installed.

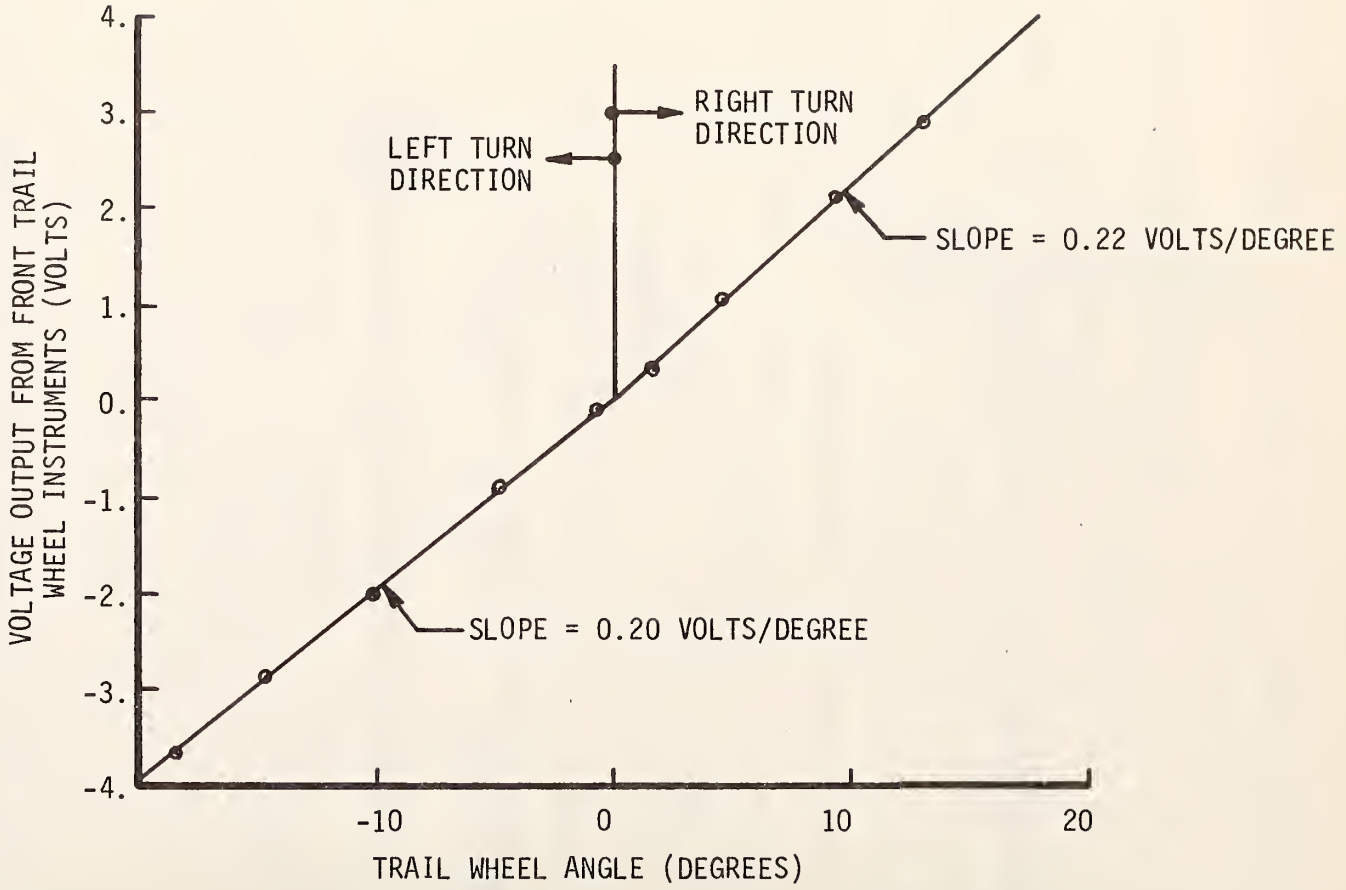

FIGURE 3.9 STATIC CALIBRATION CURVE FOR FRONT TRAIL WHEEL

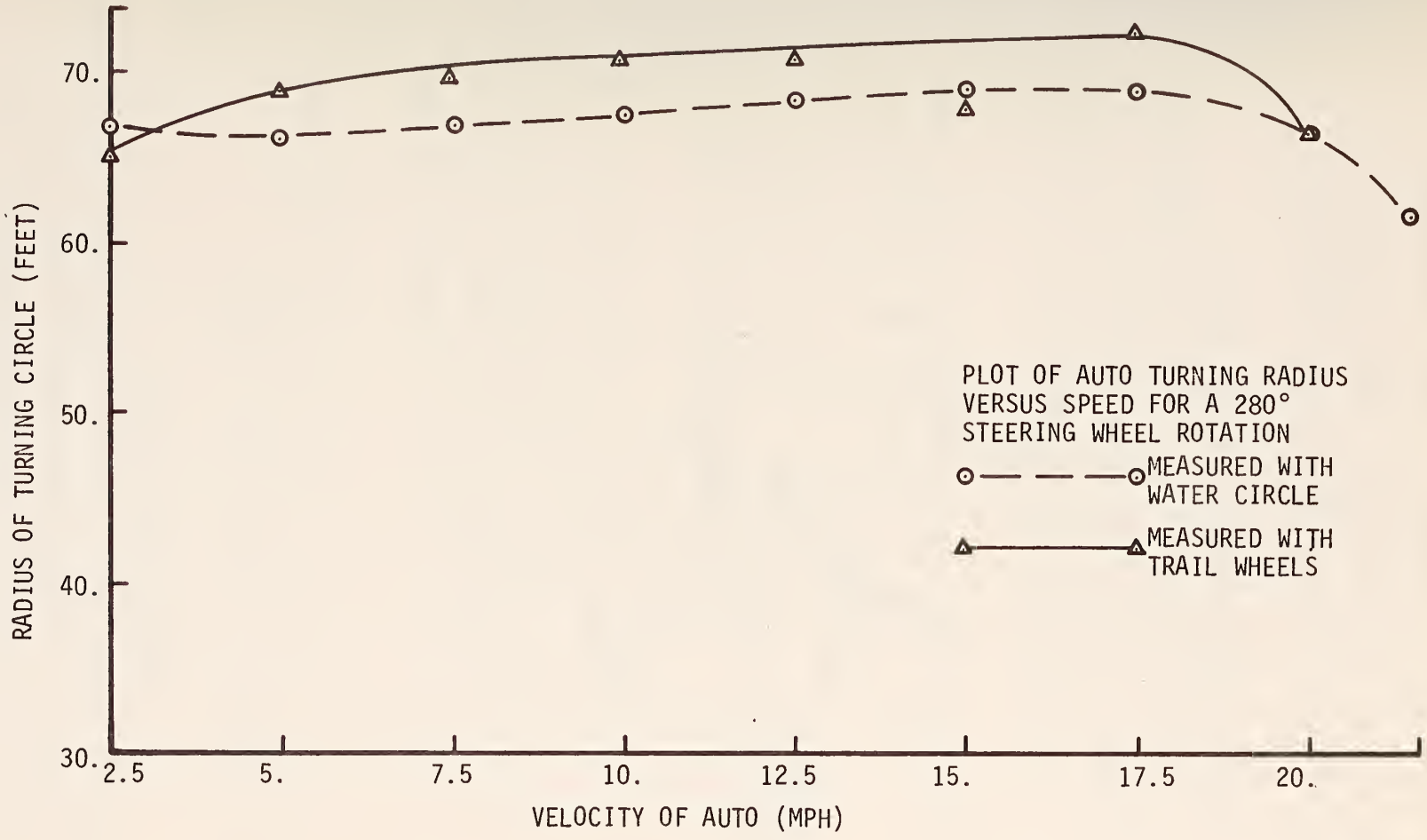

FIGURE 3.10 COMPARISON OF PATH RADIUS OF CURVATURE VALUES

The trail wheel system appears to give reasonably accurate values for β on hard surface roads; however, β is difficult to measure because of its low magnitude.

Vertical Acceleration of the Driver

The vertical acceleration of the driver was measured with an accelerometer as illustrated in Figure 3.11. The accelerometer is attached to a board between the driver and the vehicle seat.

The unbonded strain gage accelerometer contained four active arms of a bridge. The schematic of the electronic circuit for the accelerometer is identical to the circuit for the steer angle transducer if the bridge is replaced by the four active arms of the accelerometer and if the voltage source is changed to 4.5 volts.

The accelerometer was calibrated by inverting it in the earth's gravitational field to change the acceleration from +1 g to -1 g. The performance of the accelerometer was verified at various frequencies on the harmonic shaker table.

The acceleration data were recorded by the strip chart recorder with a 100 mm per second chart speed.

Lateral Tire Forces

The values of lateral tire forces, which are reported in this investigation, were not measured, but they were calculated from tire data and from normal (vertical) tire

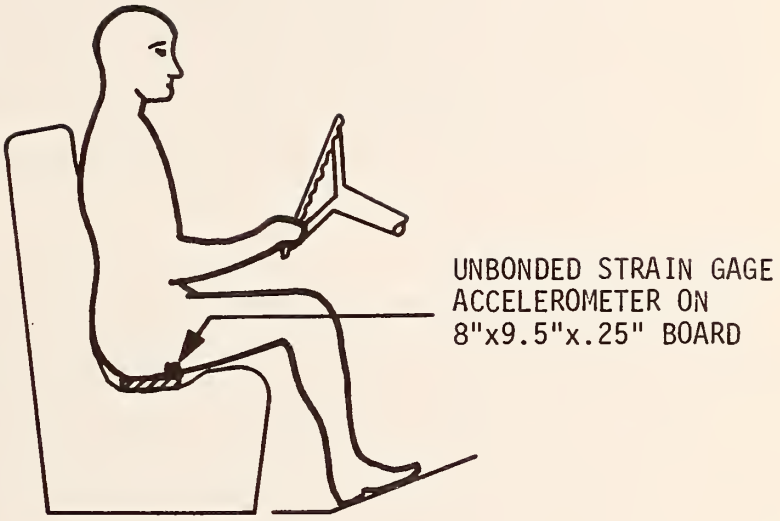

FIGURE 3.11 SKETCH OF ACCELEROMETER AND DRIVER

force values. The tire data were furnished by the B. F. Goodrich Company while the normal tire forces were measured by Sattaripour (36). The discussion of the procedure for determining the lateral tire forces is given in Chapter 2.

CHAPTER 4

DISCUSSION OF RESULTS

Steer Angle and Steering Wheel Angle

The measured relationships between the steer angle, the steering wheel angle and the roughness of the road identify some of the effects of roughness on the control of a vehicle. The values of road roughness used in this study were reported by Smeyak (37), and are given in Table 4.1.

The steer angle tracks the steering wheel angle for an oscillatory input (Figure 4.1) and for a vehicle maneuver around a curve (Figure 4.2). However, Figure 4.3 shows a case where the steer angle appears to be independent of the steering wheel angle. This independent change in the steer angle is caused by relative motion between the car frame and the wheel. The lack of a one to one correspondence between these two angles introduces a question concerning which angle is the best indicator of controllability. Since the driver rotates the steering wheel when he decides a control correction is required, the steering wheel angle is assumed to be a better indicator of controllability. Therefore, the remaining results are based on the steering wheel angle in lieu of the steer angle.

TABLE 4.1 SUMMARY OF INFORMATION PERTAINING TO THE DYNAMIC TIRE FORCE RECORDS AND THE MEASURED PAVEMENTS

PAVEMENT NAME AND TYPE	S. River Rd. (Rough Section) RIGID				S. River Rd. (Smooth Section) FLEXIBLE				State Rd. 26 FLEXIBLE				Lindberg Rd. FLEXIBLE				U.S. 52 (Overlay Section) FLEXIBLE				U.S. 52 (Concrete Section) RIGID				I-65 RIGID			
Speed (mph)	20	30	40	50	20	30	40	50	20	30	40	50	20	30	40	50	20	30	40	50	20	30	40	50	30	40	50	60
Direction	S	S	S	S	N	N	N	N	S	S	S	S	E	E	E	E	N	N	N	N	N	N	N	N	S	S	S	S
RMS Value of Dynamic Tire Force	80	115	156	-	29	55	81	104	28	42	68	83	-	40	-	69	-	50	66	73	-	51	70	97	42	43	53	58
Constants of the Zable Equation P	-17.67				-16.77				-21.6				-18.73				-19.79				-18.84				-16.7			
Constants of the Zable Equation Q	- 3.93				- 2.59				- 4.27				- 3.55				- 3.66				- 3.543				- 2.577			
Description of the Test Vehicle No. 755	1967 Chevrolet, 4 door, hard top, static weight: 4000 lbs. Right rear wheel was instrumented in making the dynamic tire force measurements between the tire and the pavement.																											

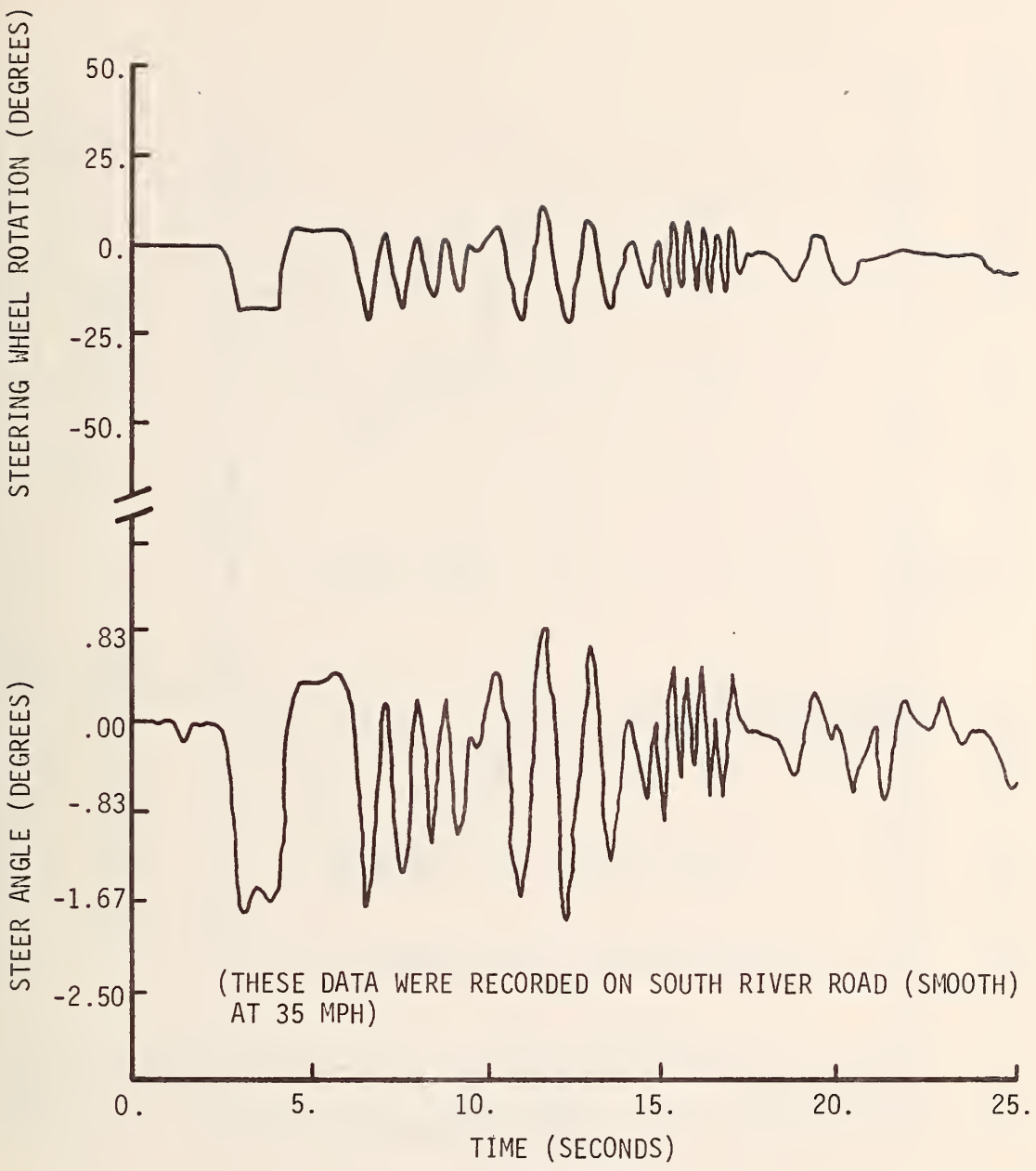

FIGURE 4.1 RESPONSE OF THE STEER ANGLE TO STEERING WHEEL ROTATION

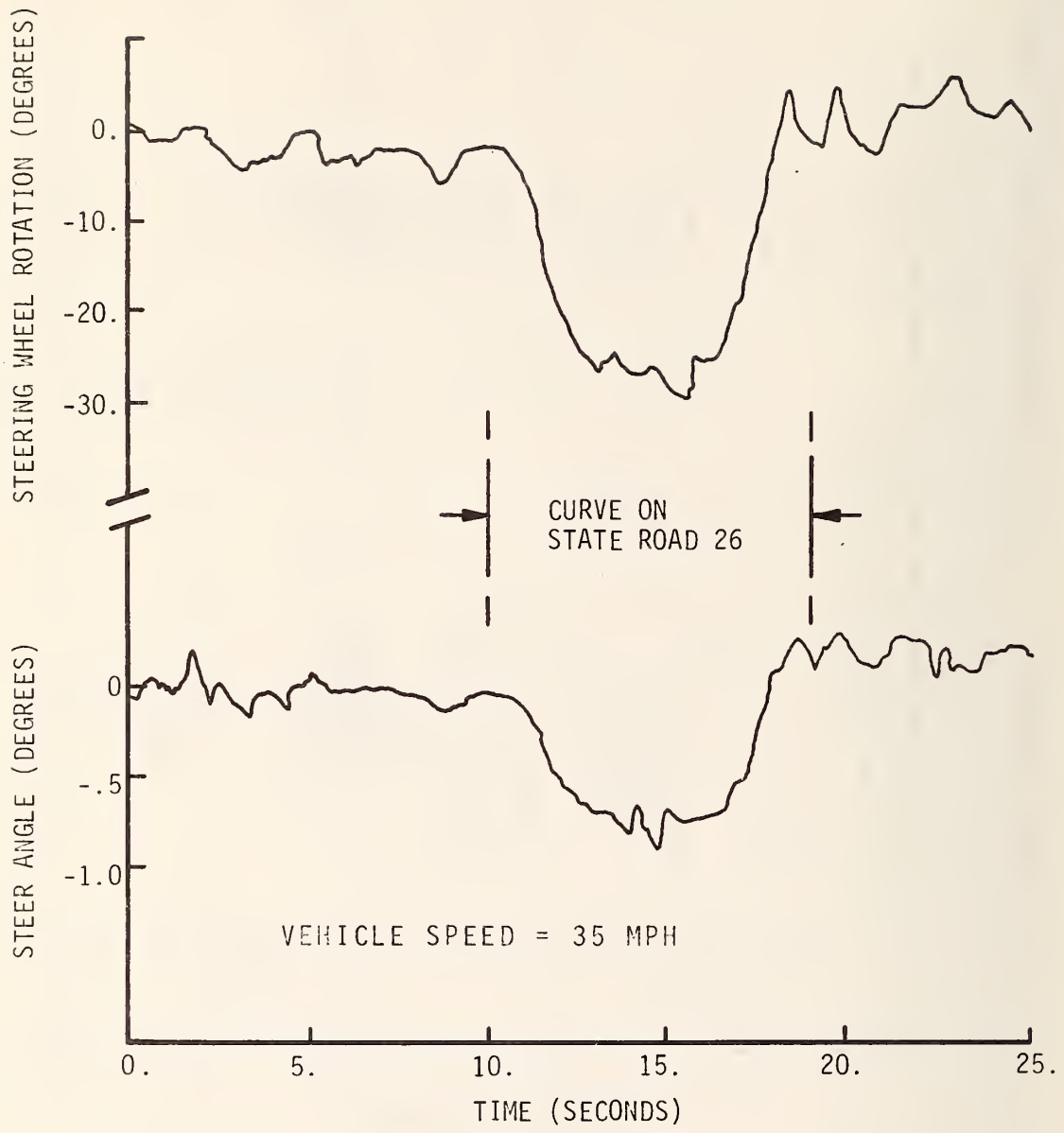

FIGURE 4.2 TYPICAL RECORDS FOR STEER ANGLE AND STEERING WHEEL ROTATION FOR A CURVE ON S. R. 26

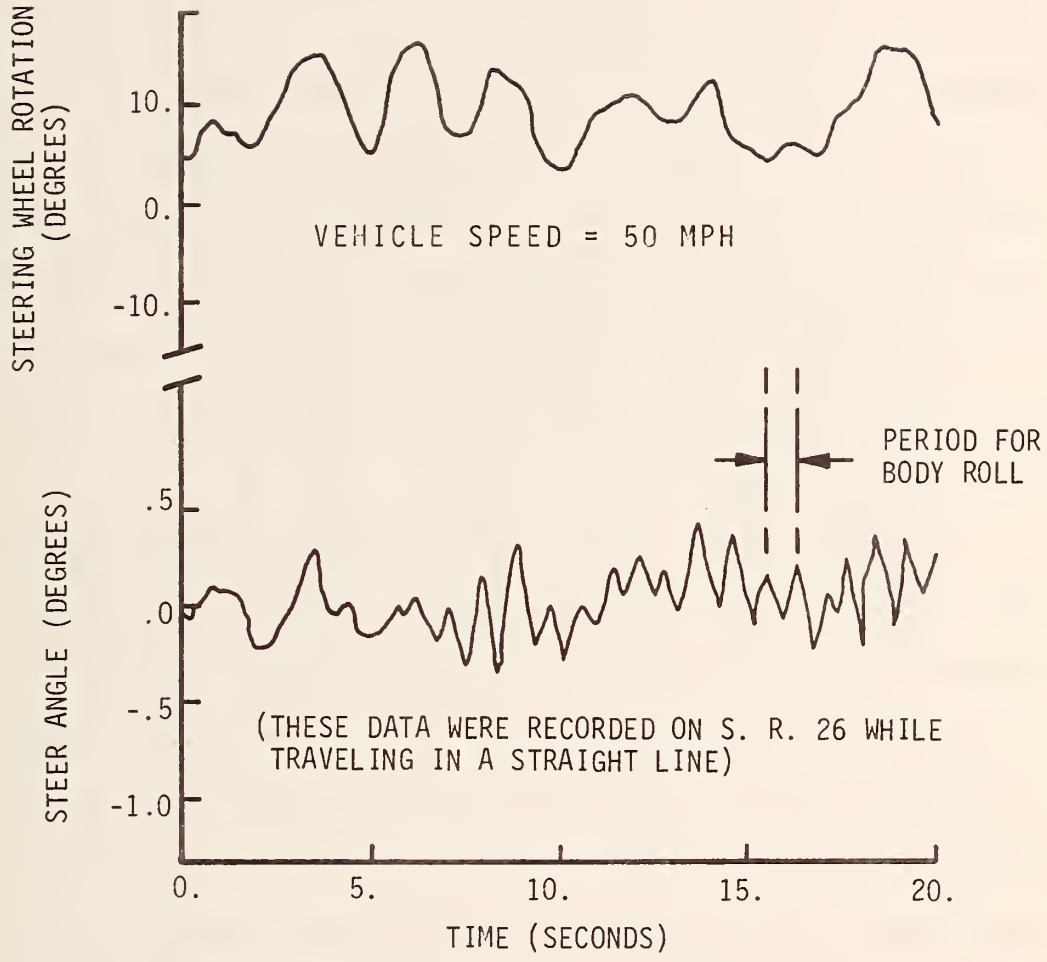

FIGURE 4.3 RECORDS FOR STEER ANGLE AND STEERING WHEEL ROTATION SHOWING THE EFFECT OF BODY ROLL

The steering wheel angle was measured continuously while traveling on straight roads at 50 mph. The steering wheel angle, which is shown as a function of time in Figure 4.4, for South River Road (Rough) contains large amplitudes; however, the corresponding record for South River Road (Smooth) (Figure 4.5) contains low amplitudes. The record of steering wheel angle for State Road 26 (Figure 4.6) contains dominant low frequency components, but the record for Cumberland Avenue (Figure 4.7) contains dominant high frequency components. The records of steering wheel angle for Lindberg Road and U. S. Highway 52 are shown in Figures 4.8 and 4.9 respectively.

The probability density distribution for the steering wheel angle identifies the amplitude content of these records. For example, the area under the probability density curve outside of the +5° to -5° range is equal to the probability of occurrence of a steering wheel angle greater than 5°. The probability density distribution for State Road 26 (Figure 4.10) shows a high probability of steering wheel angles with large amplitudes, but the probability density distribution for Cumberland Avenue (Figure 4.11) shows a high probability of relatively low amplitude steering wheel angles. The probability density distributions for the remaining four roads are shown in Figures 4.12, 4.13, 4.14 and 4.15. The summary of probability data shown in Table 4.2 provides a comparison

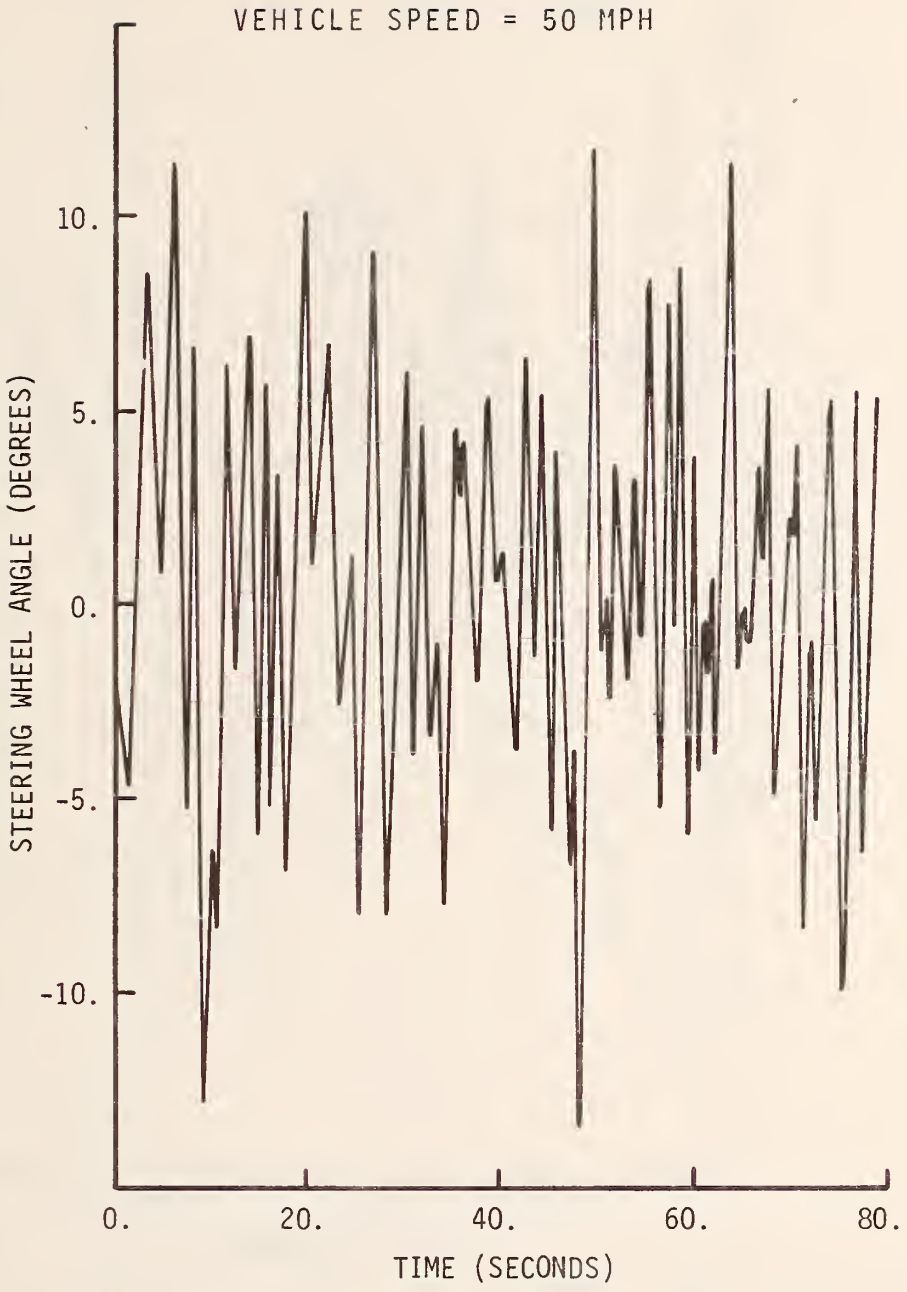

FIGURE 4.4 STEERING WHEEL ANGLE AS A FUNCTION OF TIME FOR SOUTH RIVER ROAD (ROUGH)

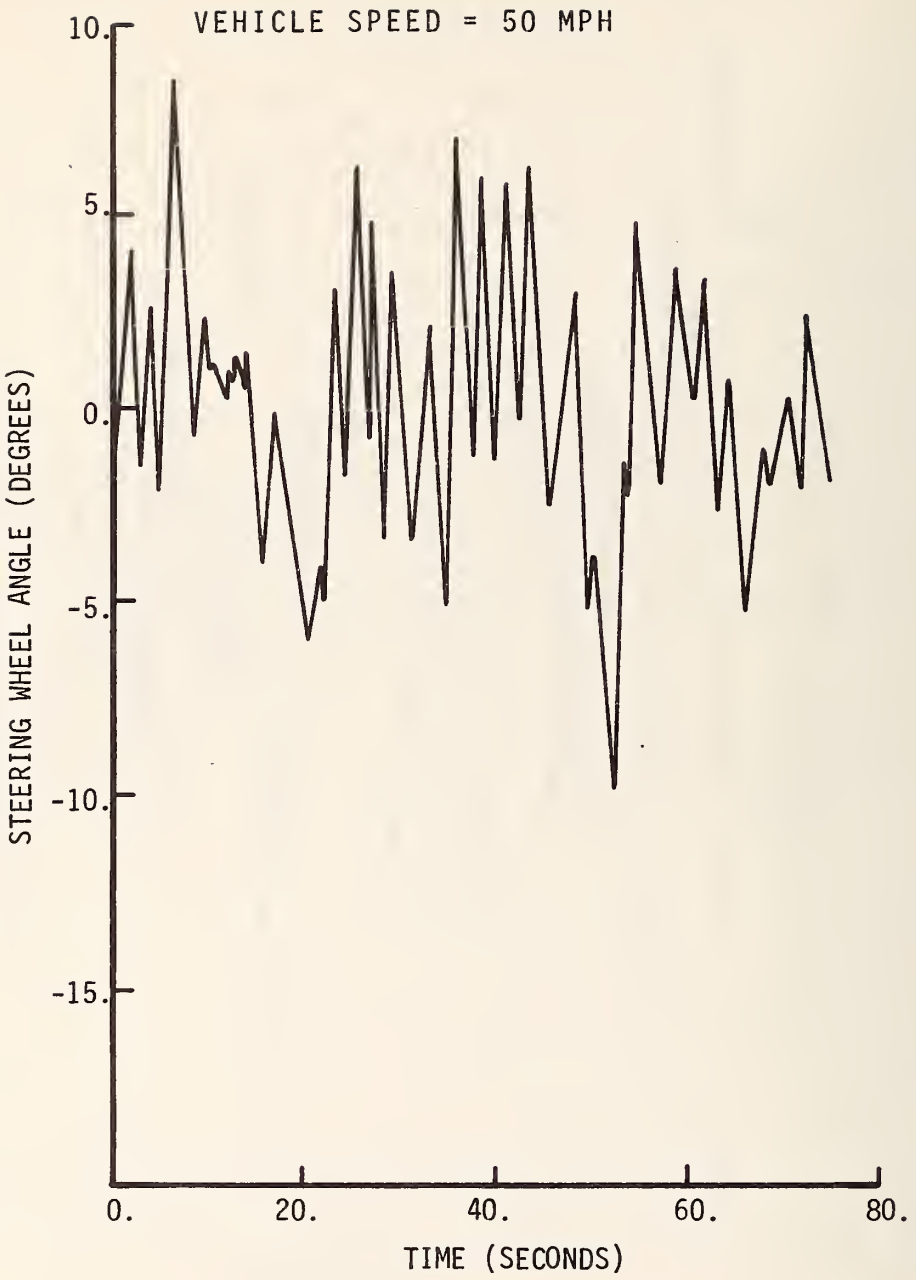

FIGURE 4.5 STEERING WHEEL ANGLE AS A FUNCTION OF TIME FOR SOUTH RIVER ROAD (SMOOTH)

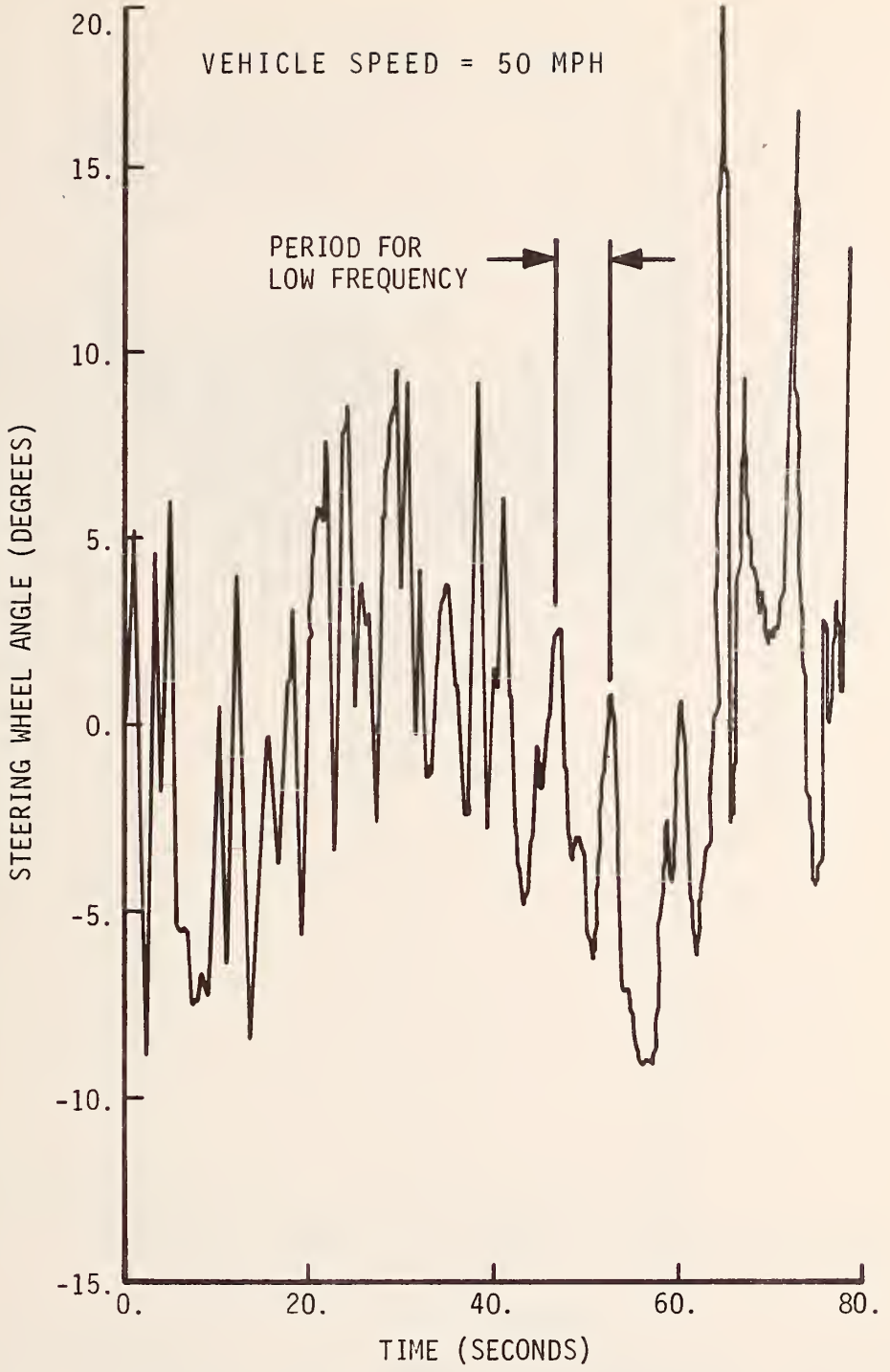

FIGURE 4.6 STEERING WHEEL ANGLE AS A FUNCTION OF TIME FOR S. R. 26

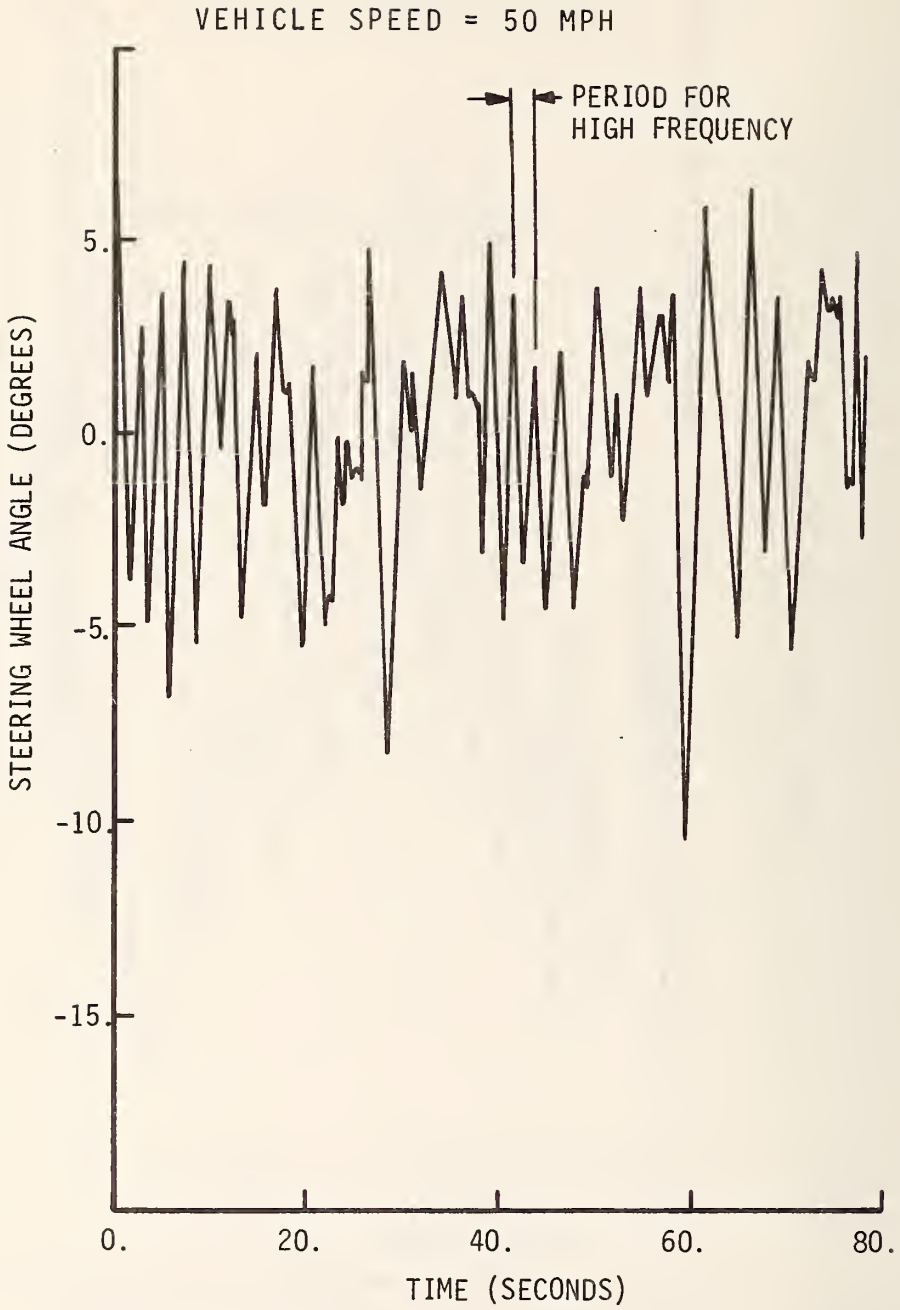

FIGURE 4.7 STEERING WHEEL ANGLE AS A FUNCTION OF TIME FOR CUMBERLAND AVENUE

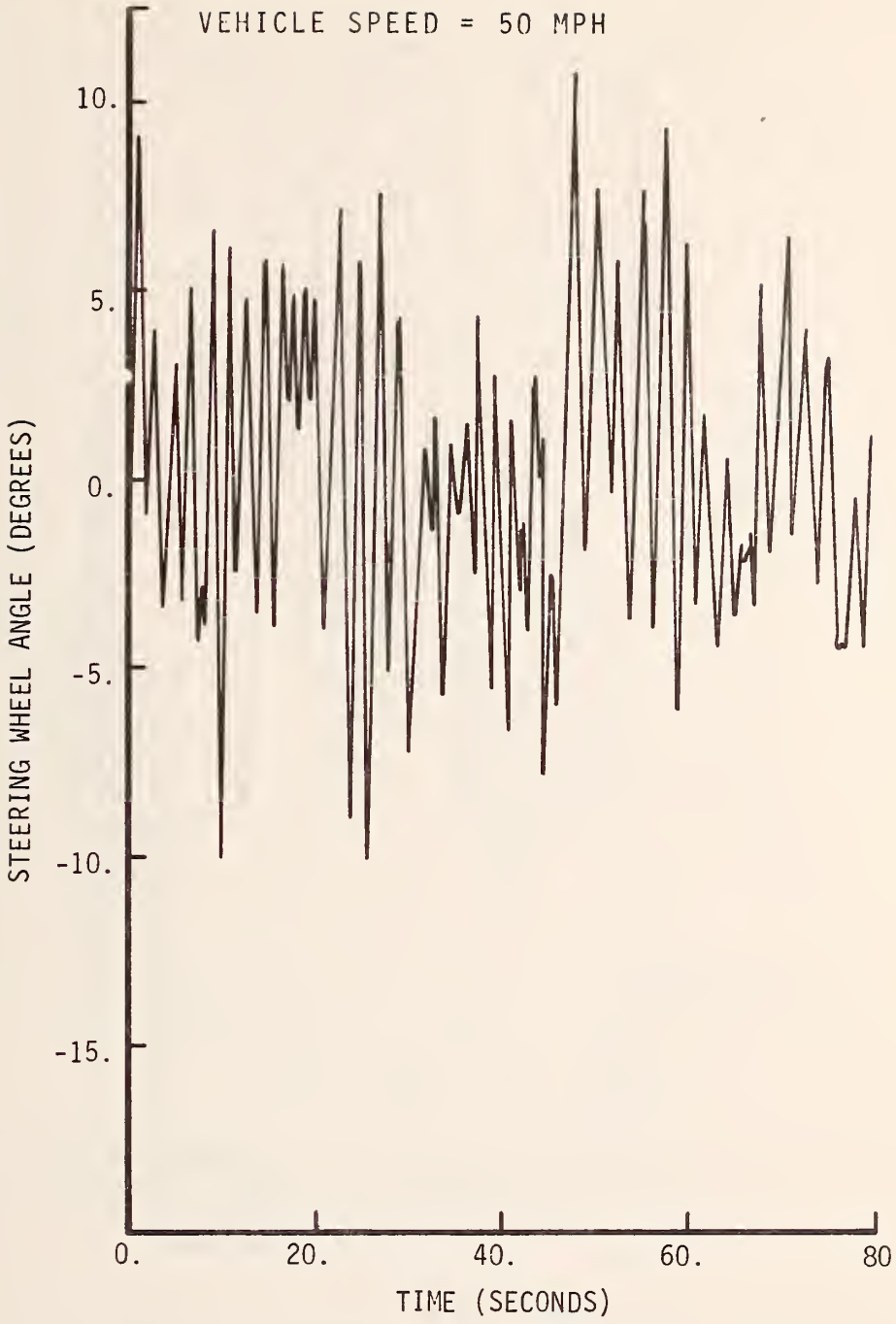

FIGURE 4.8 STEERING WHEEL ANGLE AS A FUNCTION OF TIME FOR LINDBERG ROAD

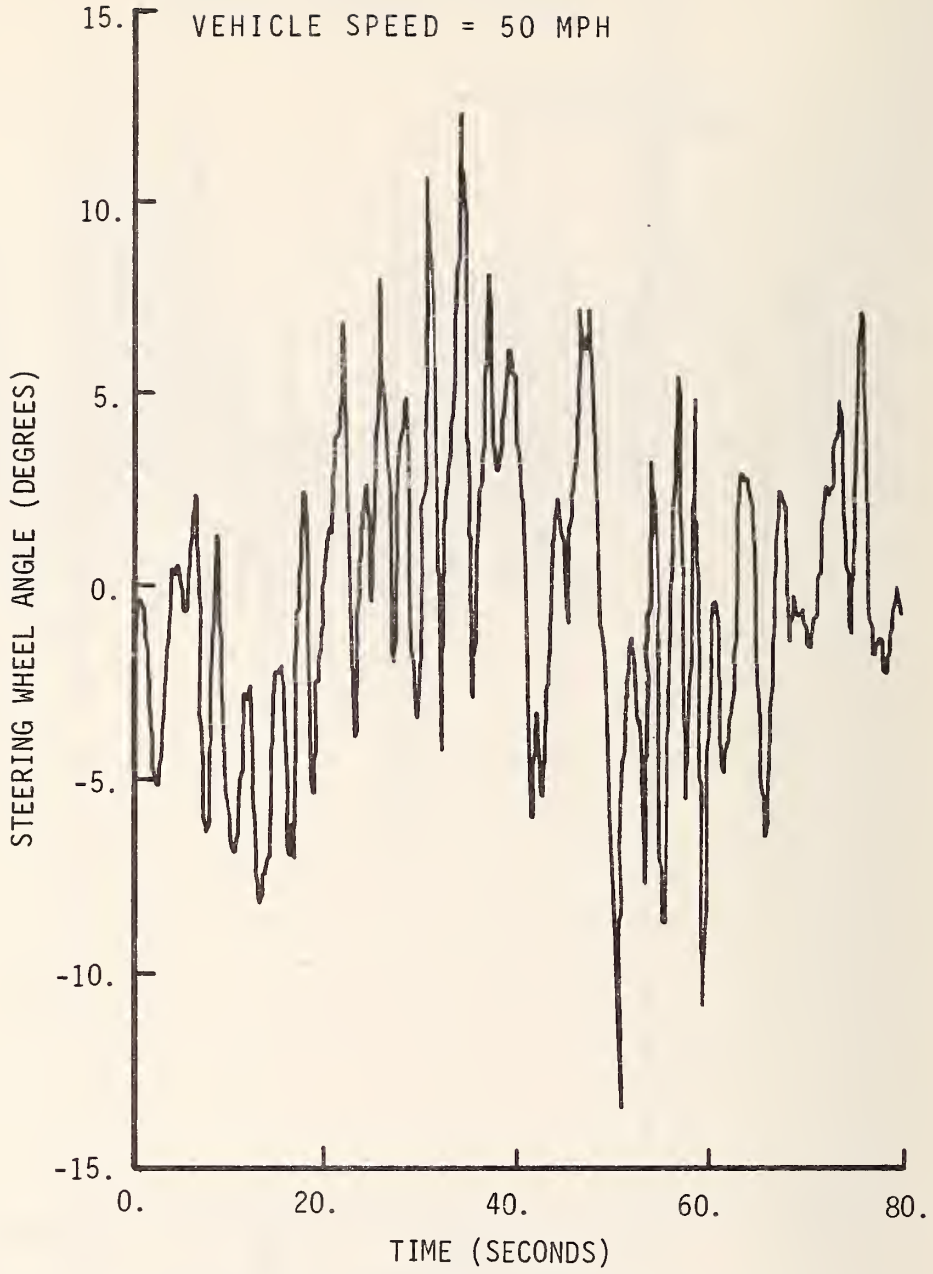

FIGURE 4.9 STEERING WHEEL ANGLE AS A FUNCTION OF TIME FOR U. S. 52

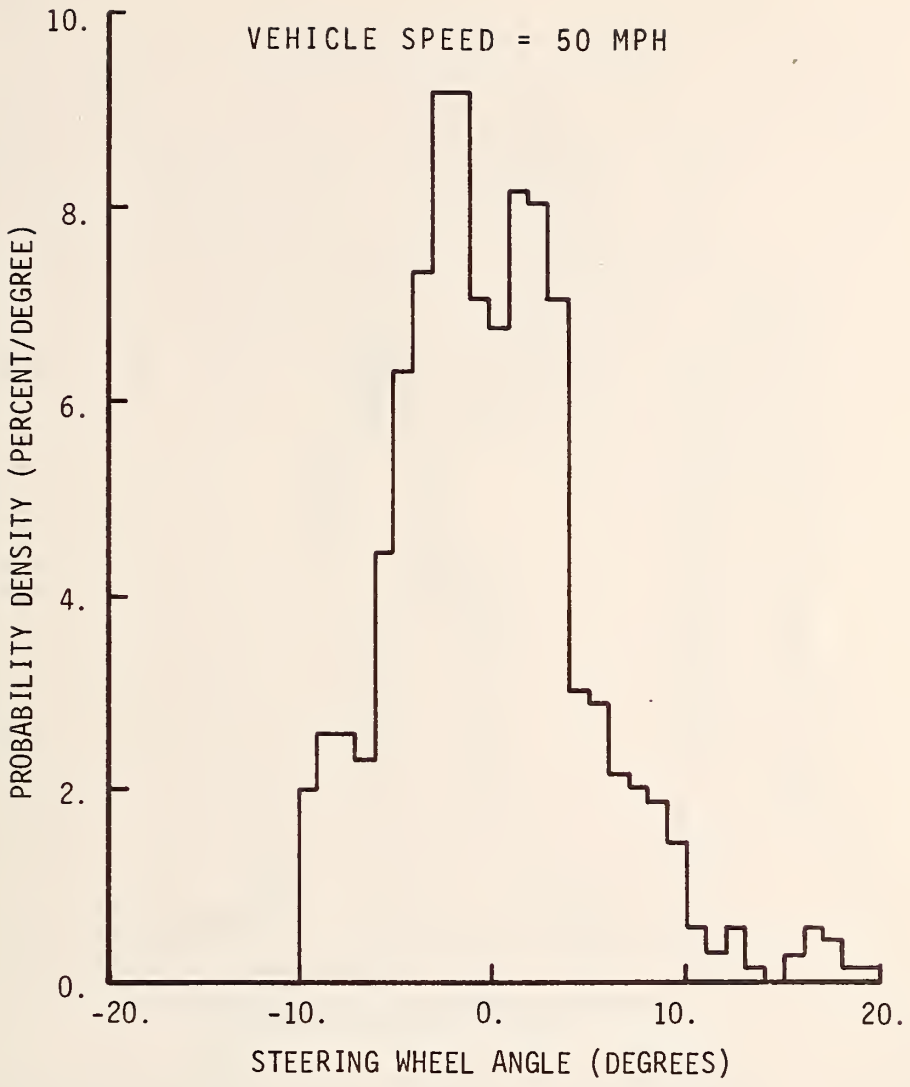

FIGURE 4.10 PROBABILITY DENSITY DISTRIBUTION FOR STEERING WHEEL ANGLE - S. R. 26

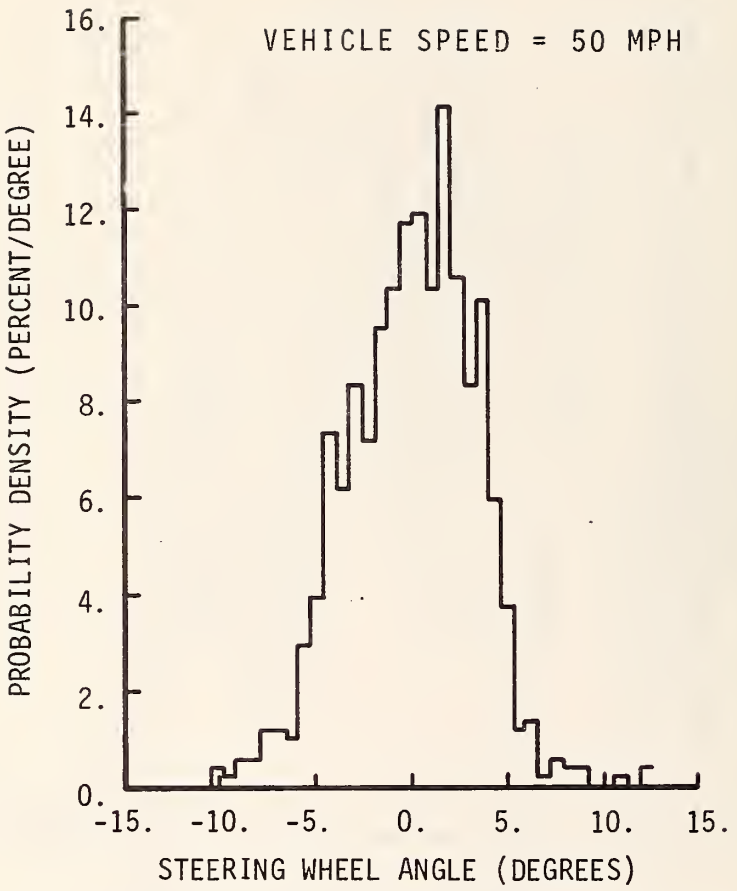

FIGURE 4.11 PROBABILITY DENSITY DISTRIBUTION FOR STEERING WHEEL ANGLE - CUMBERLAND AVENUE

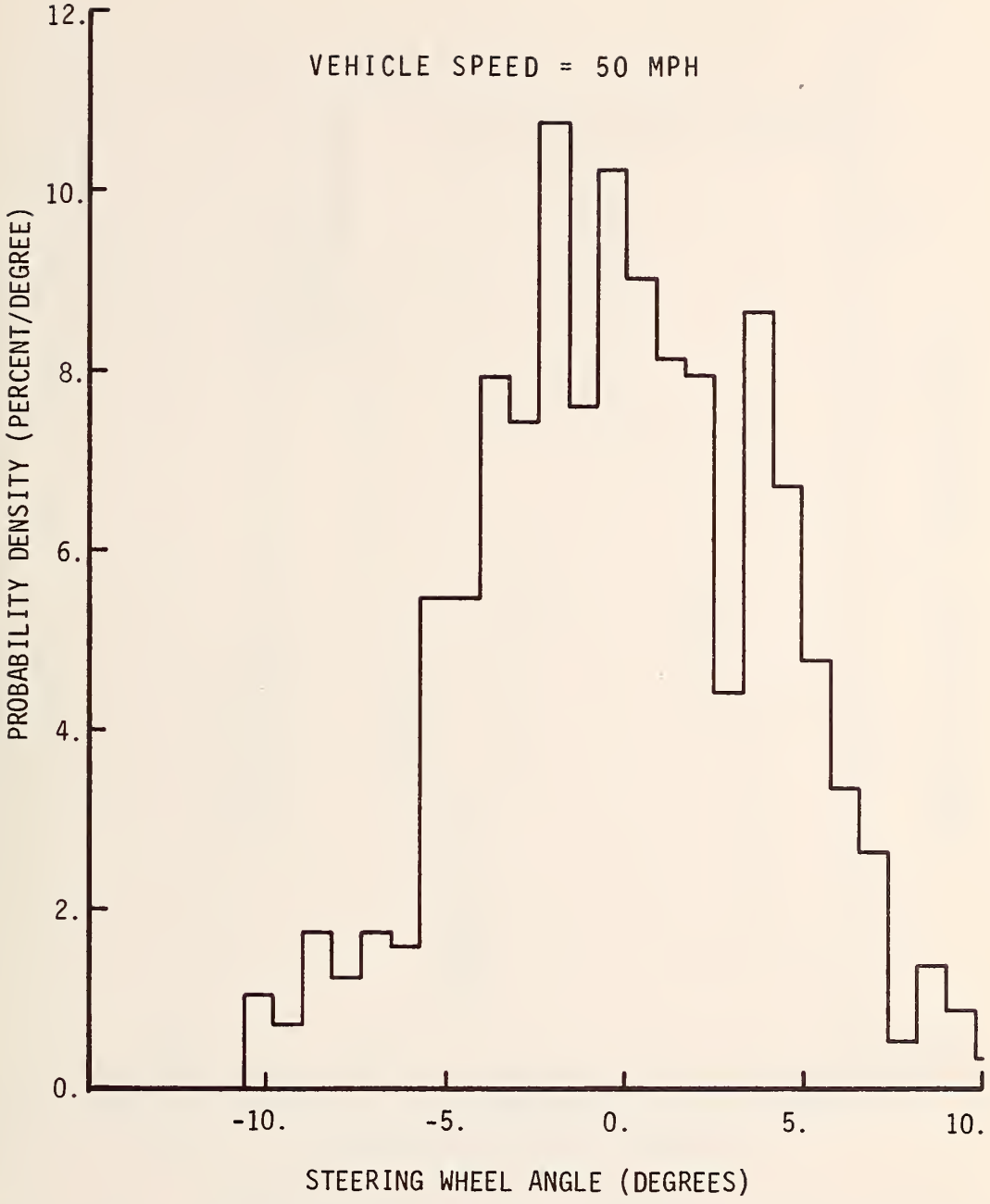

FIGURE 4.12 PROBABILITY DENSITY DISTRIBUTION FOR STEERING WHEEL ANGLE - LINDBERG ROAD

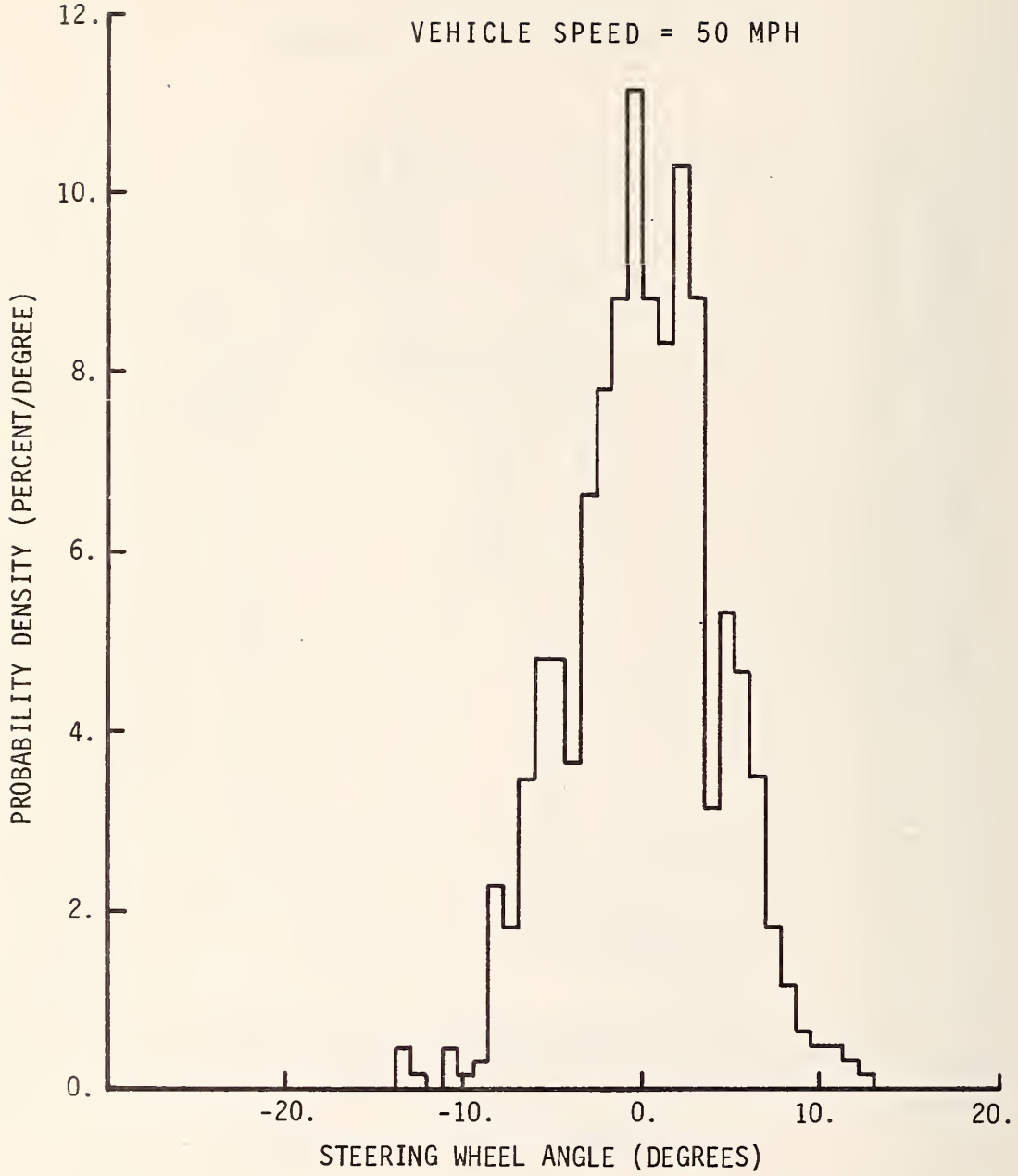

FIGURE 4.13 PROBABILITY DENSITY DISTRIBUTION FOR STEERING WHEEL ANGLE - U. S. 52

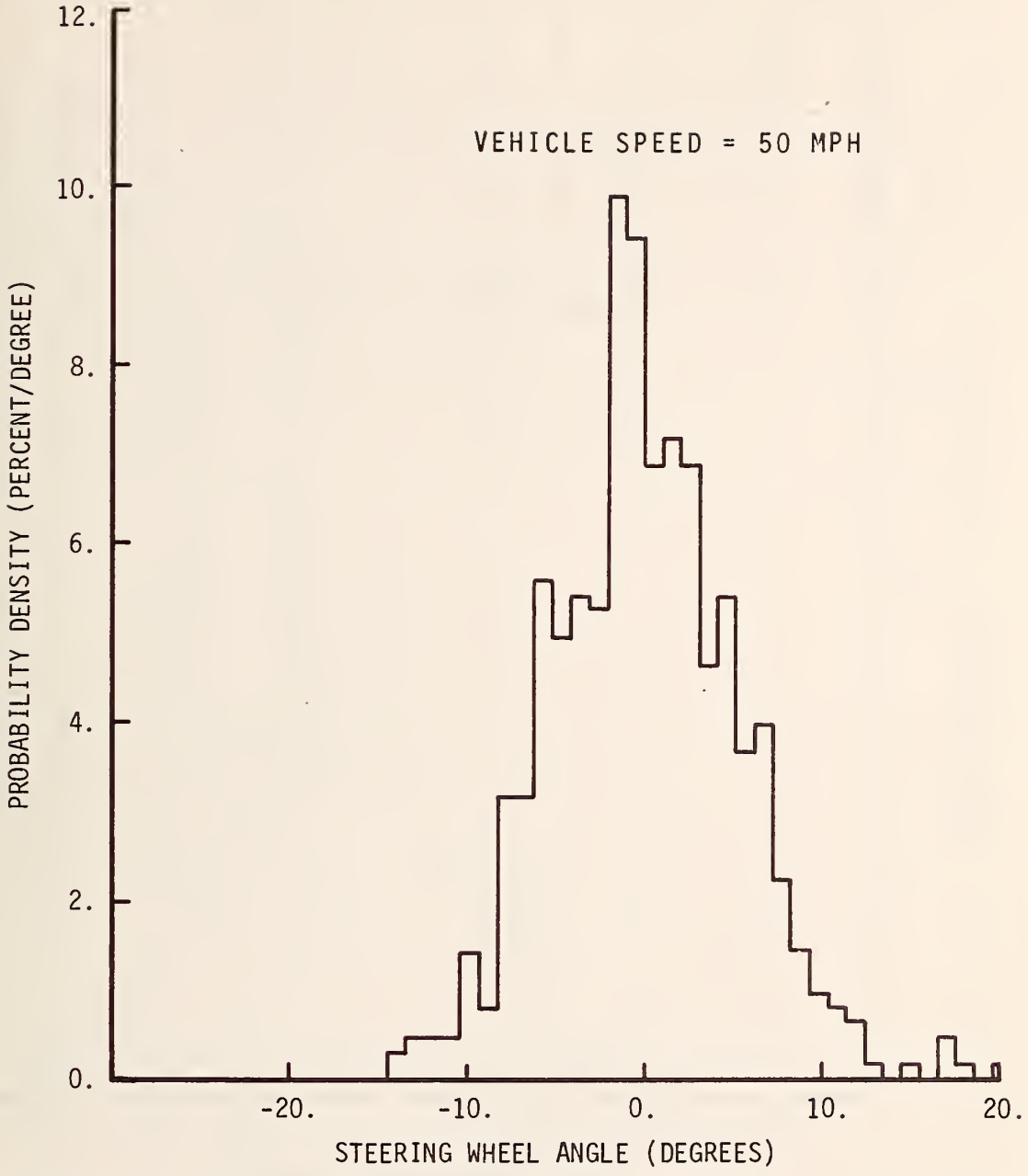

FIGURE 4.14 PROBABILITY DENSITY DISTRIBUTION FOR STEERING WHEEL ANGLE - SOUTH RIVER ROAD (ROUGH)

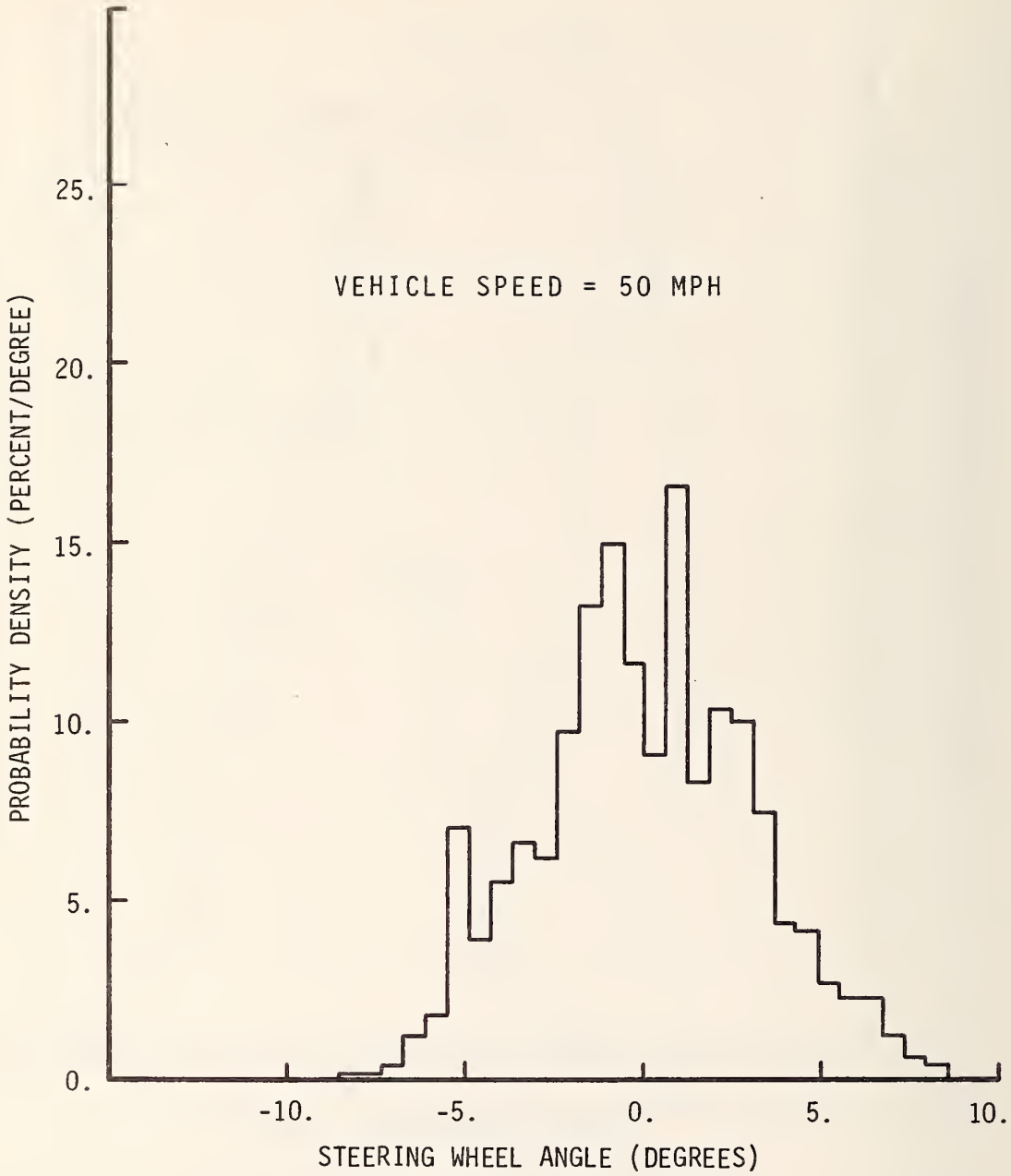

FIGURE 4.15 PROBABILITY DENSITY DISTRIBUTION FOR STEERING WHEEL ANGLE - SOUTH RIVER ROAD (SMOOTH)

TABLE 4.2 SUMMARY OF PROBABILITY DISTRIBUTION FOR STEERING WHEEL CORRECTION DATA

ROAD NAME	S* (degrees)	PROBABILITY OF OCCURRENCE OF STEERING WHEEL ANGLES FOR A GIVEN RANGE OF VALUES OF S								
		±S	±2S	±3S	0 to -S	0 to -2S	0 to -3S	0 to +S	0 to +2S	0 to +3S
Road with a Gaussian Distribution	S	68.3	95.4	99.7	34.1	47.7	49.9	34.1	47.7	49.9
South River Road - Rough	5.49	68.2	95.5	99.1	36.2	50.8	52.6	32.0	44.7	46.5
U.S. 52	4.25	67.3	96.8	99.6	33.1	48.2	49.2	34.2	48.6	50.4
State Road 26	5.23	72.4	96.8	98.4	39.2	53.2	53.2	33.2	43.6	45.2
Cumberland	3.37	67.9	96.6	100.0	30.9	44.9	47.4	37.0	51.7	52.6
Lindberg Road	4.02	67.1	94.5	100.0	35.9	48.6	51.5	31.2	45.9	48.5
South River Road - Smooth	3.23	67.5	95.8	99.9	34.2	49.6	50.9	33.3	46.2	49.0

* S = Standard deviation of the steering wheel angle (degrees)

between the distributions for the six test roads and the Gaussian distribution.

The autocovariance function (6, 36) for steering wheel angle on U. S. Highway 52 (Figure 4.16) approaches zero as the lag value is increased. This indicates that the steering wheel angle on U. S. 52 approximates a random phenomenon although some periodicity is indicated. Conversely, the autocovariance function for Cumberland Avenue (Figure 4.17) continues to oscillate as the lag values are increased. This indicates that the steering angle on Cumberland Avenue has a periodic oscillation instead of a random motion.

The power spectral density function for the steering wheel angle describes the general frequency composition. The power spectrum for Lindberg Road (Figure 4.18) identifies 0.5 cps as the frequency which makes the largest contribution to the mean square value of the steering wheel angle. The major contribution to the steering wheel angle for Cumberland Avenue (Figure 4.19) is also at a high value, 0.4 cps. The major contribution to the mean square value of the steering correction for South River Road - Smooth (Figure 4.20) occurs at the relatively low frequency of 0.05 cps. The steering correction for South River Road - Rough (Figure 4.21, note change of scale) has relatively large values at 0.12 cps, .25 cps, .37 cps and .56 cps. The power spectra for the steering wheel angles for State

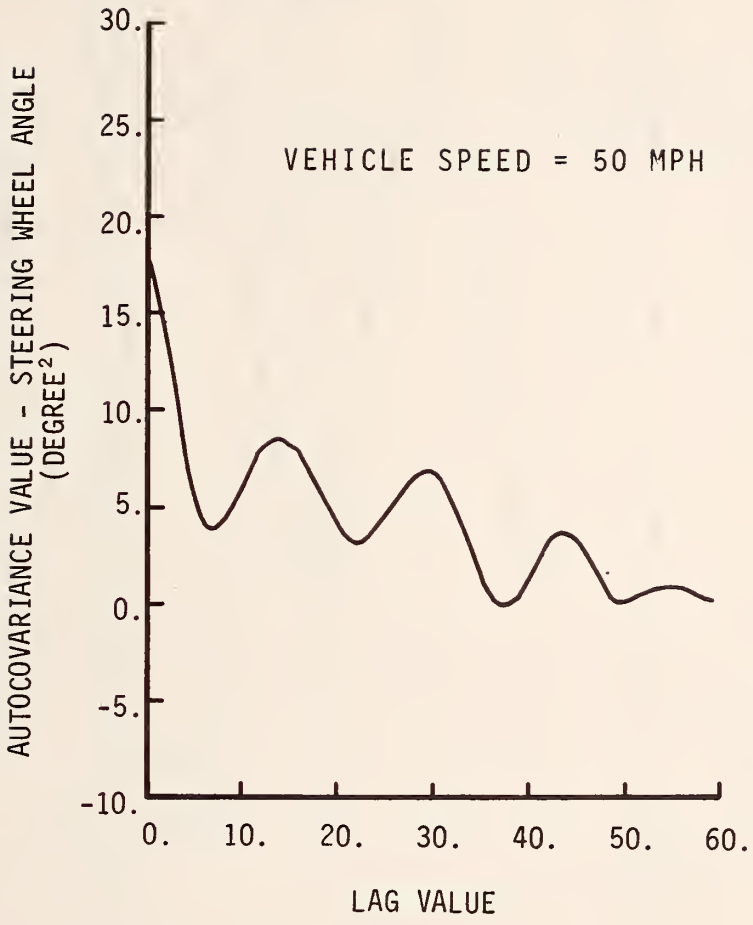

FIGURE 4.16 AUTOCOVARIANCE FUNCTION FOR STEERING WHEEL ANGLE - U. S. 52 HIGHWAY

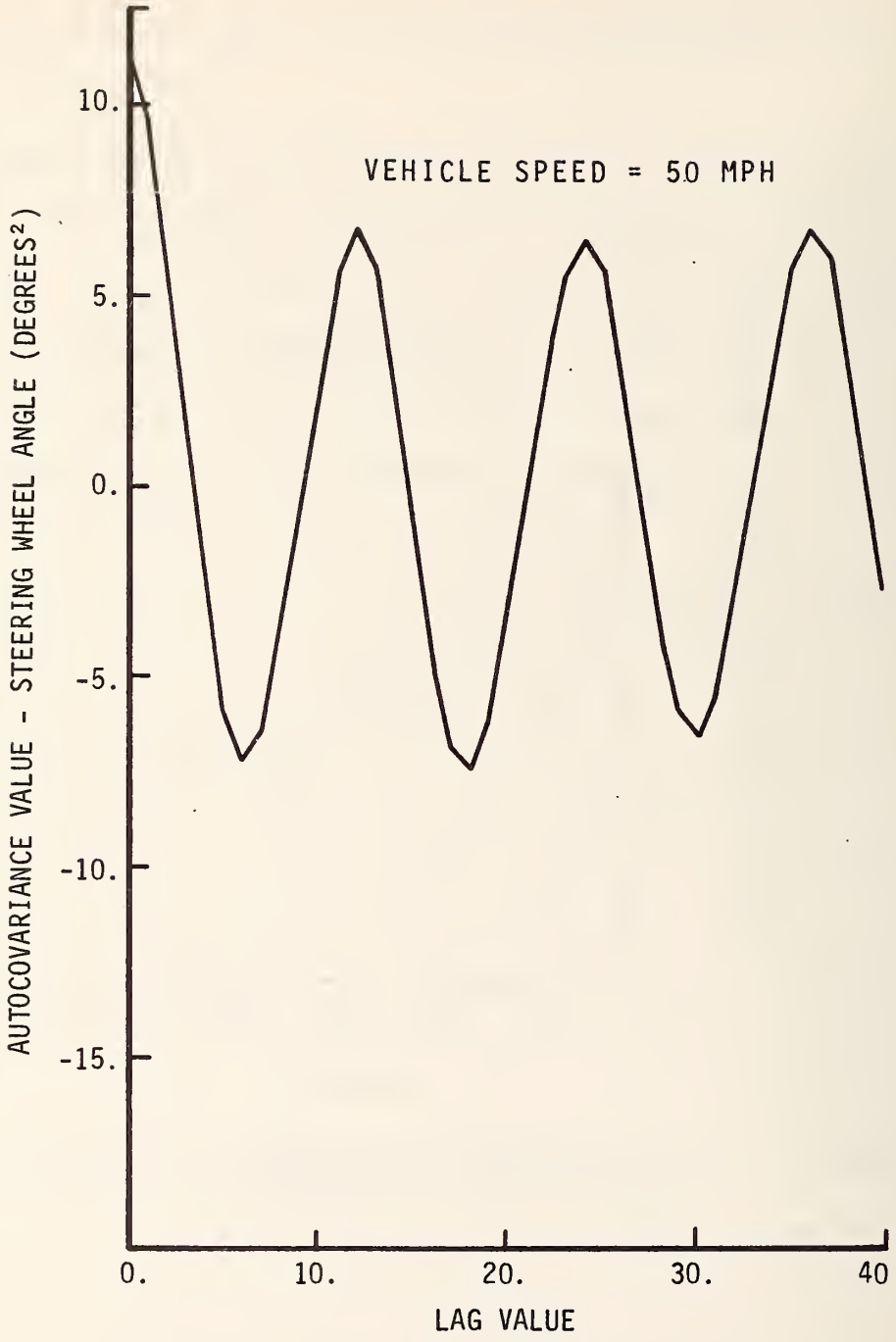

FIGURE 4.17 AUTOCOVARIANCE FUNCTION FOR STEERING WHEEL ANGLE - CUMBERLAND AVENUE

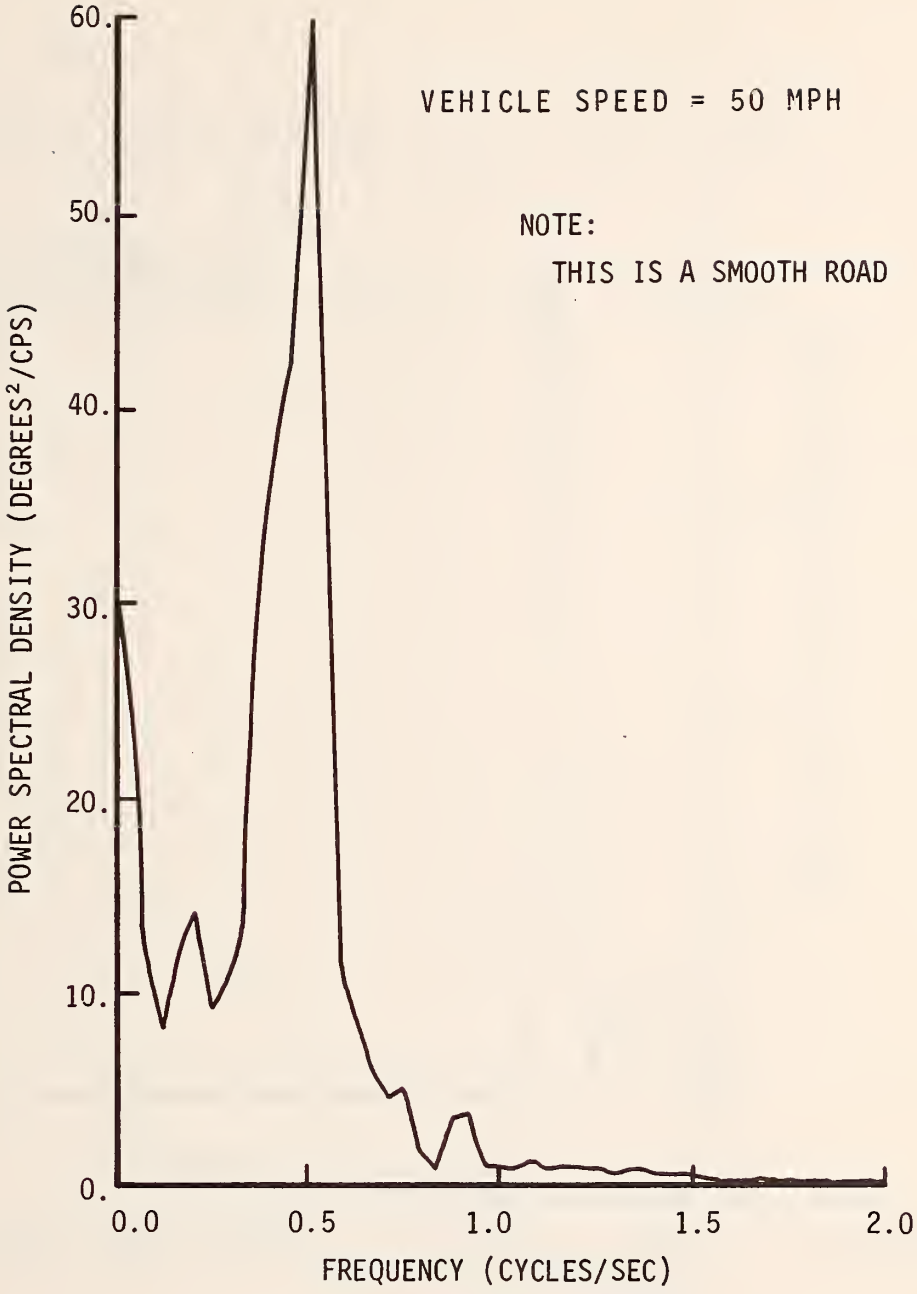

FIGURE 4.18 POWER SPECTRUM FOR STEERING WHEEL ANGLE - LINDBERG ROAD

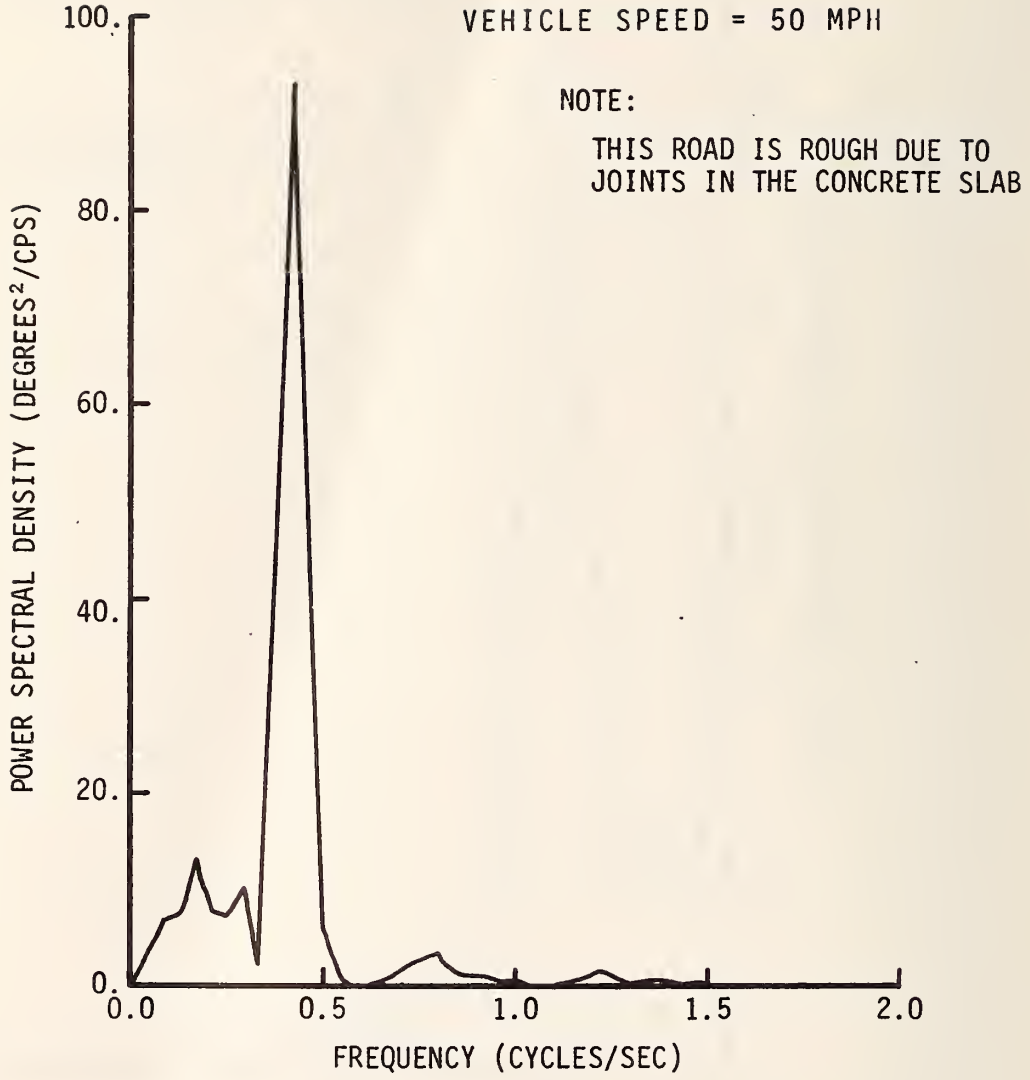

FIGURE 4.19 POWER SPECTRUM FOR STEERING WHEEL ANGLE - CUMBERLAND AVENUE

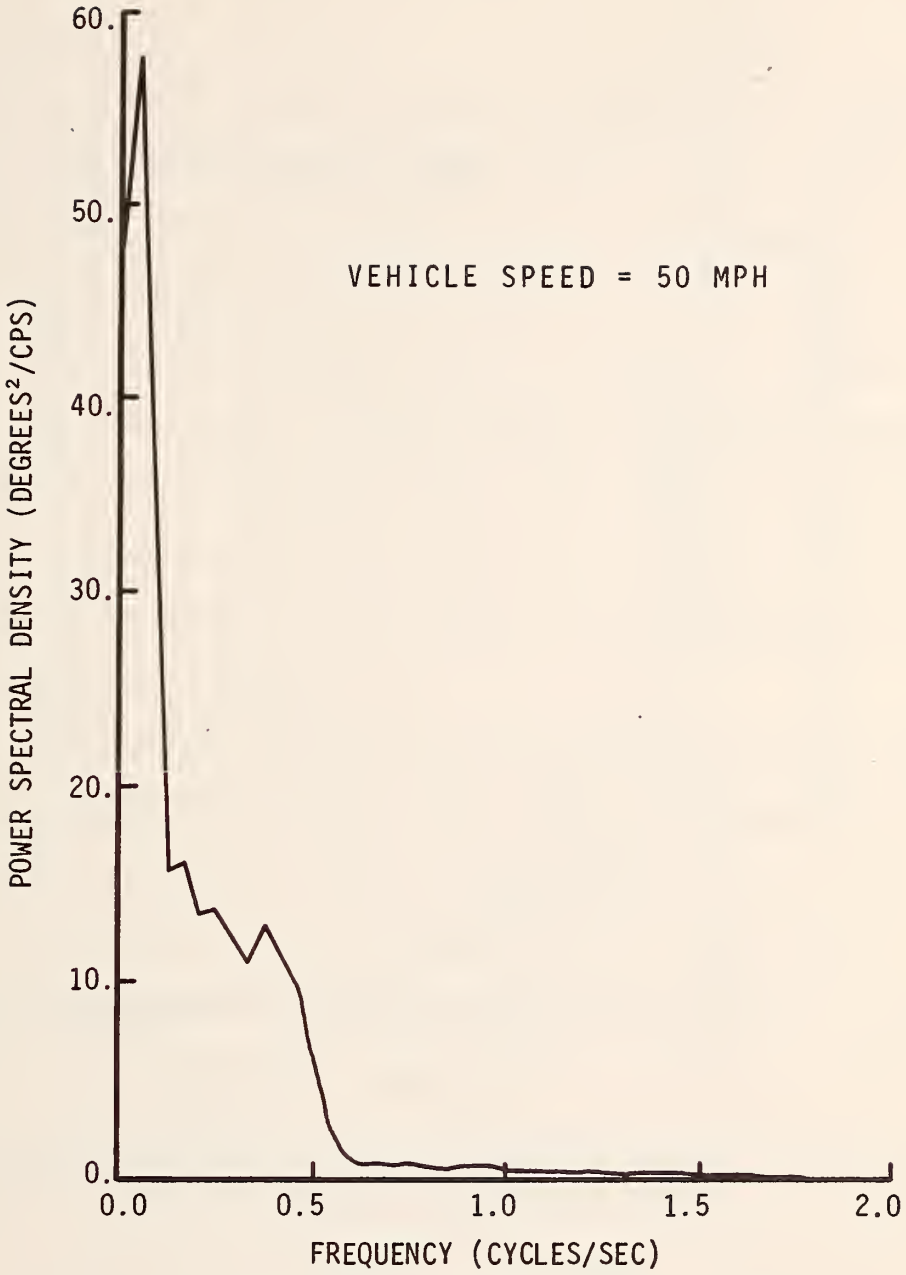

FIGURE 4.20 POWER SPECTRUM FOR STEERING WHEEL ANGLE - SOUTH RIVER ROAD (SMOOTH)

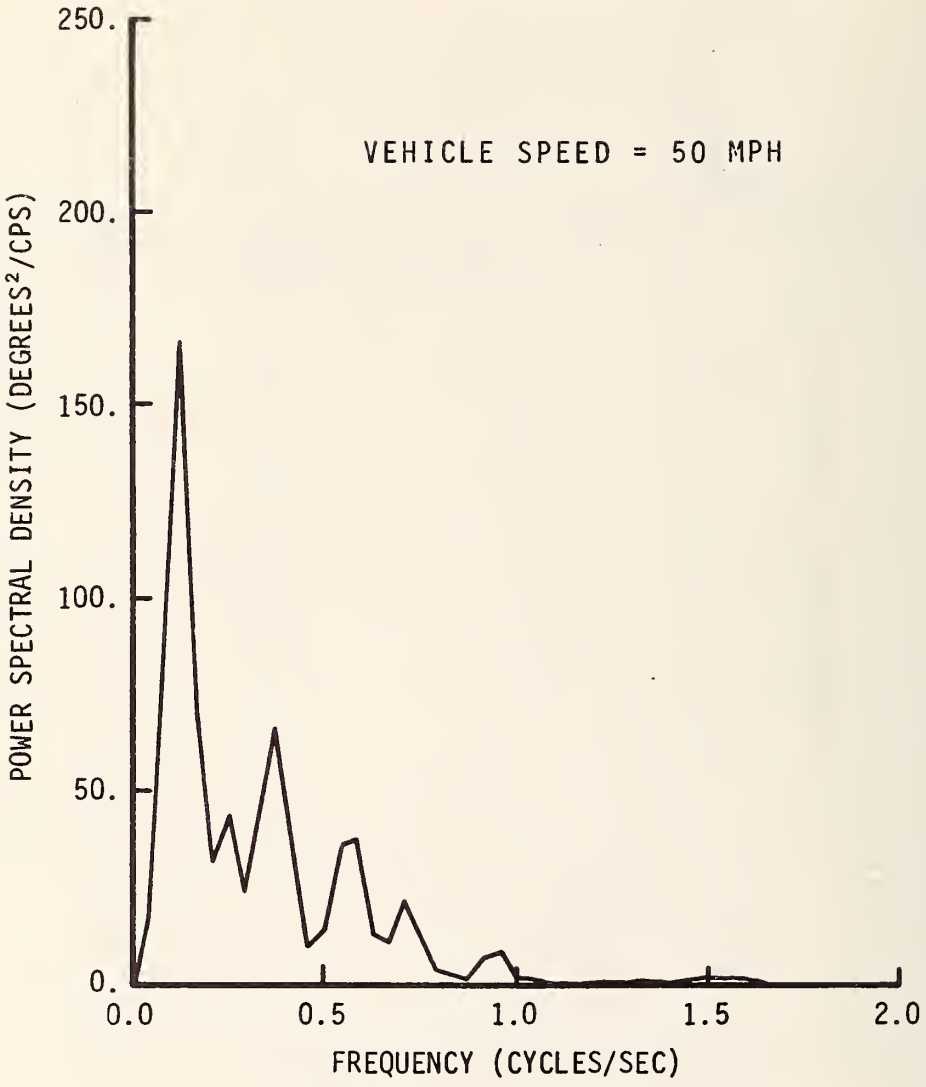

FIGURE 4.21 POWER SPECTRUM FOR STEERING WHEEL ANGLE - SOUTH RIVER ROAD (ROUGH)

Road 26 and U. S. Highway 52 are shown in Figures 4.22 and 4.23 respectively.

The roads with rough surfaces do require more steering correction than smooth roads. The steering wheel angle does not appear to be a function of the system's major natural frequencies: pitch (1.3 cps), roll (1.3 cps), yaw (2.0 cps), wheel hop (10. cps) and bounce (1.3 cps). However, the roads which contain dominant values of roughness in the short wavelength range (e.g. Cumberland Avenue) do require a higher frequency steering correction than roads with predominantly long roughness wavelengths (e.g. South River Road - Smooth).

The relationship between the mean square value of road roughness and the mean square value of steering wheel angle is shown in Figure 4.24. The two curves represent data taken on two different days under different conditions. The rear shock absorbers were removed when the data for the upper curve were recorded. These curves indicate a threshold level of roughness, S_{TH}. If the road roughness is below S_{TH}, the roughness has very little effect on steering angle. If the road roughness is above S_{TH}, the steering angle for this vehicle may be estimated by the following equation

$$\left[S_s\right]^2 = C_1 \text{Log}_{10}\left[S_y\right]^2 + C_2 \qquad \text{for} \quad S_y > S_{TH}, \quad (4.1)$$

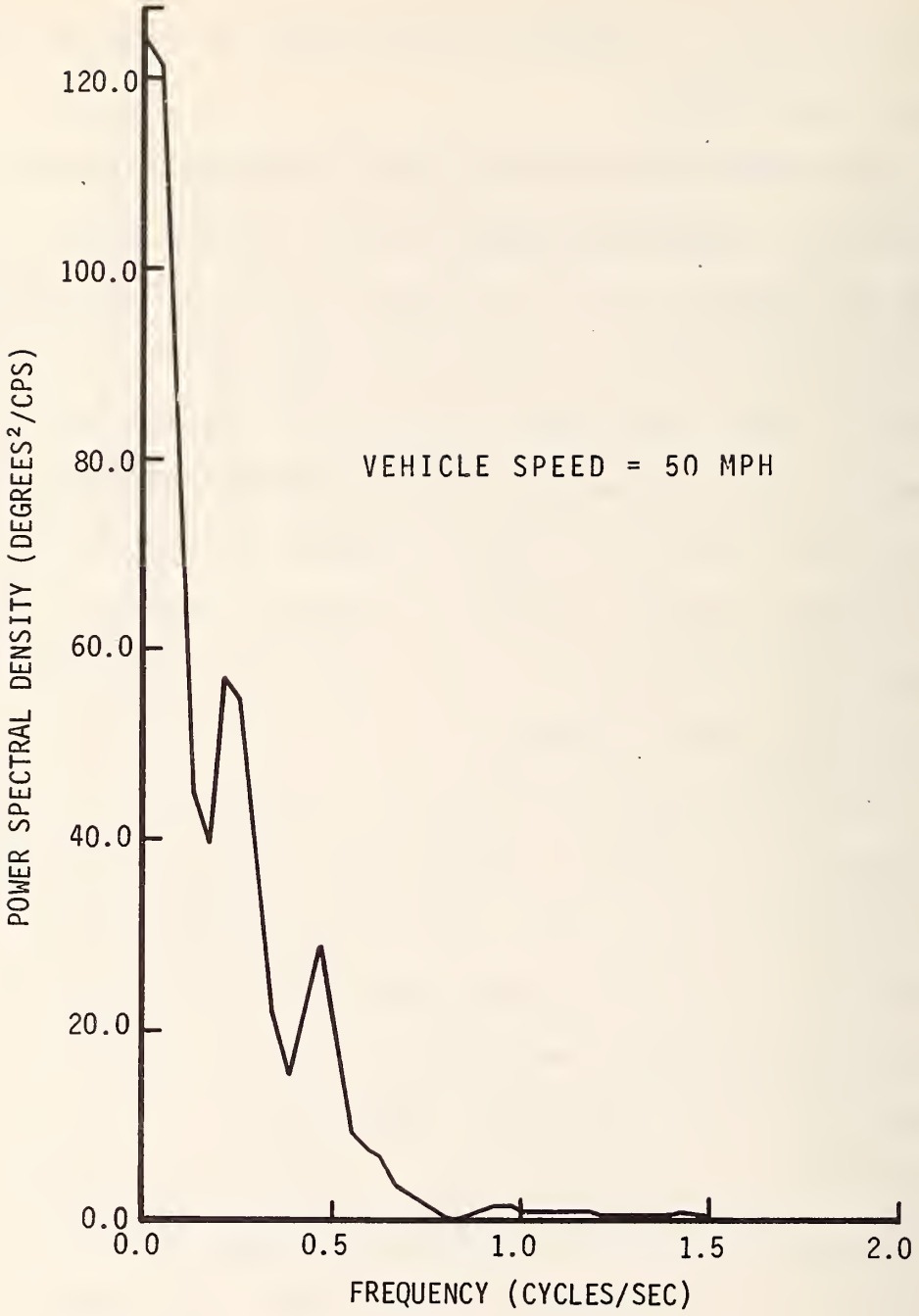

FIGURE 4.22 POWER SPECTRUM FOR STEERING WHEEL ANGLE-S. R. 26

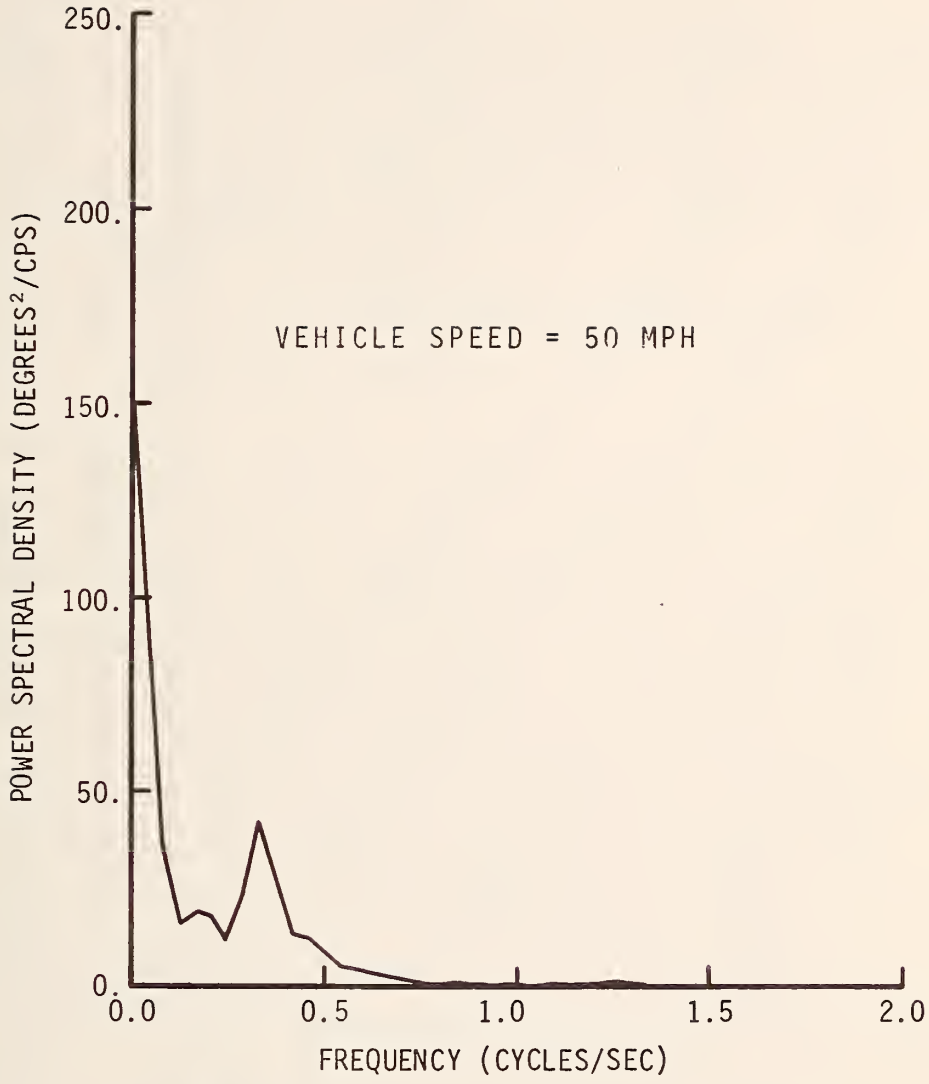

FIGURE 4.23 POWER SPECTRUM FOR STEERING WHEEL ANGLE - U. S. 52

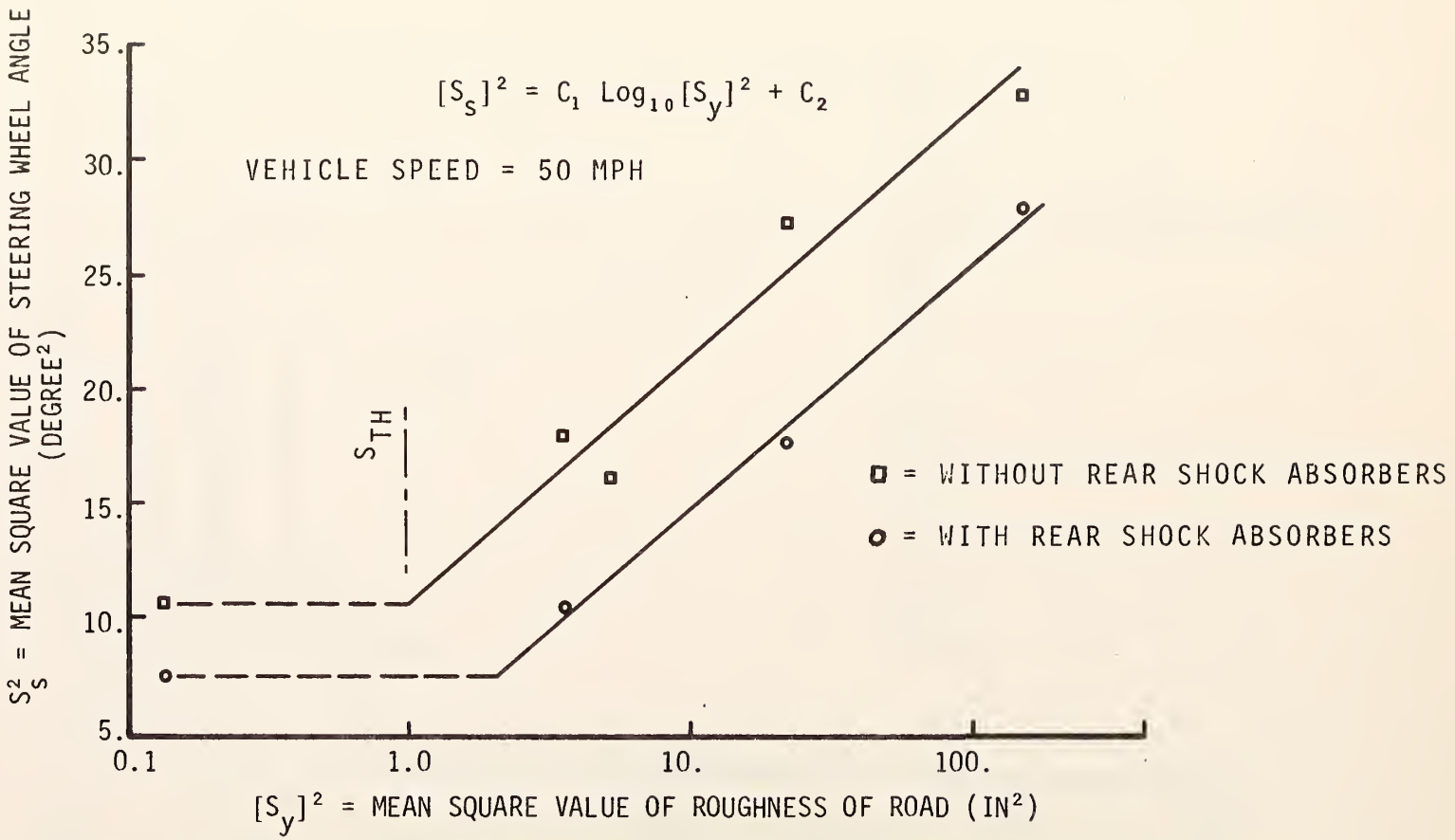

FIGURE 4.24 CORRELATION BETWEEN MEAN SQUARE VALUES OF STEERING WHEEL CORRECTION AND ROAD ROUGHNESS

where

$[S_s]^2$ = Mean square value of the steering wheel angle (degrees^2)

$[S_y]^2$ = Mean square value of road roughness (inches^2)

C_1 = Slope of $\text{Log}_{10}[S_y]^2$ versus $[S_s]^2$ represented by the straight line which has the units of $\left(\frac{\text{Deg}^2}{\text{Log}_{10}(\text{in}^2)}\right)$

C_2 = The $[S_s]^2$ coordinate at $\text{Log}_{10}[S_y]^2 = 0$ (degrees^2)

The roughness values used in the above relationship were obtained by modifying the Zable Equation as discussed in Chapter 2. The Zable Equation for the roughness power spectrum is not bounded at $f_d = 0$. The value of $[S_y]^2$ will approach infinity as frequency, f_d, approaches zero. Therefore, the Zable Equation was modified by a straight line between points [0, 0] and $[f_I, P_y(f_I)]$. The resulting values of $[S_y]^2$ are finite, but they are functions of the arbitrary intersection frequency, f_I. The value of f_I which was used to establish the steering wheel angle relationship given by Equation 4.1 is 0.005 cpf, which is 0.36 cps at 50 mph. This modification to the Zable Equation is based on the assumption that as the roughness wavelengths are increased above 1./.005 feet per cycle, the roughness has a decreasing effect on the steering wheel angle.

The steering wheel angle is related to the road roughness. It may serve to indicate the reduction in controllability due to roughness.

Sideslip Angle

The sideslip angle, β, and its time derivatives are related to the control of a vehicle, because β describes the orientation of the vehicle relative to the direction of velocity of the vehicle's center of gravity. The controllability of the vehicle as indicated by β may be a function of road roughness. Three methods for evaluating β are applied in this section:

1- The value of β is obtained analytically by using the bicycle model in a constant radius path.

2- The value of β is calculated from measured values of the steering wheel angle from which a steer angle can be determined for use in the bicycle model.

3- The value of β is measured experimentally by using two trail wheels on the vehicle to locate the center of curvature of the path along which the vehicle is moving.

The sideslip angle, which was obtained by the first of these three methods, is shown in Figure 4.25. Since the magnitude of β is small, it is difficult to measure. For example, the estimated value of β is 0.44 degrees for a circular path with a 290 foot radius at 18 mph.

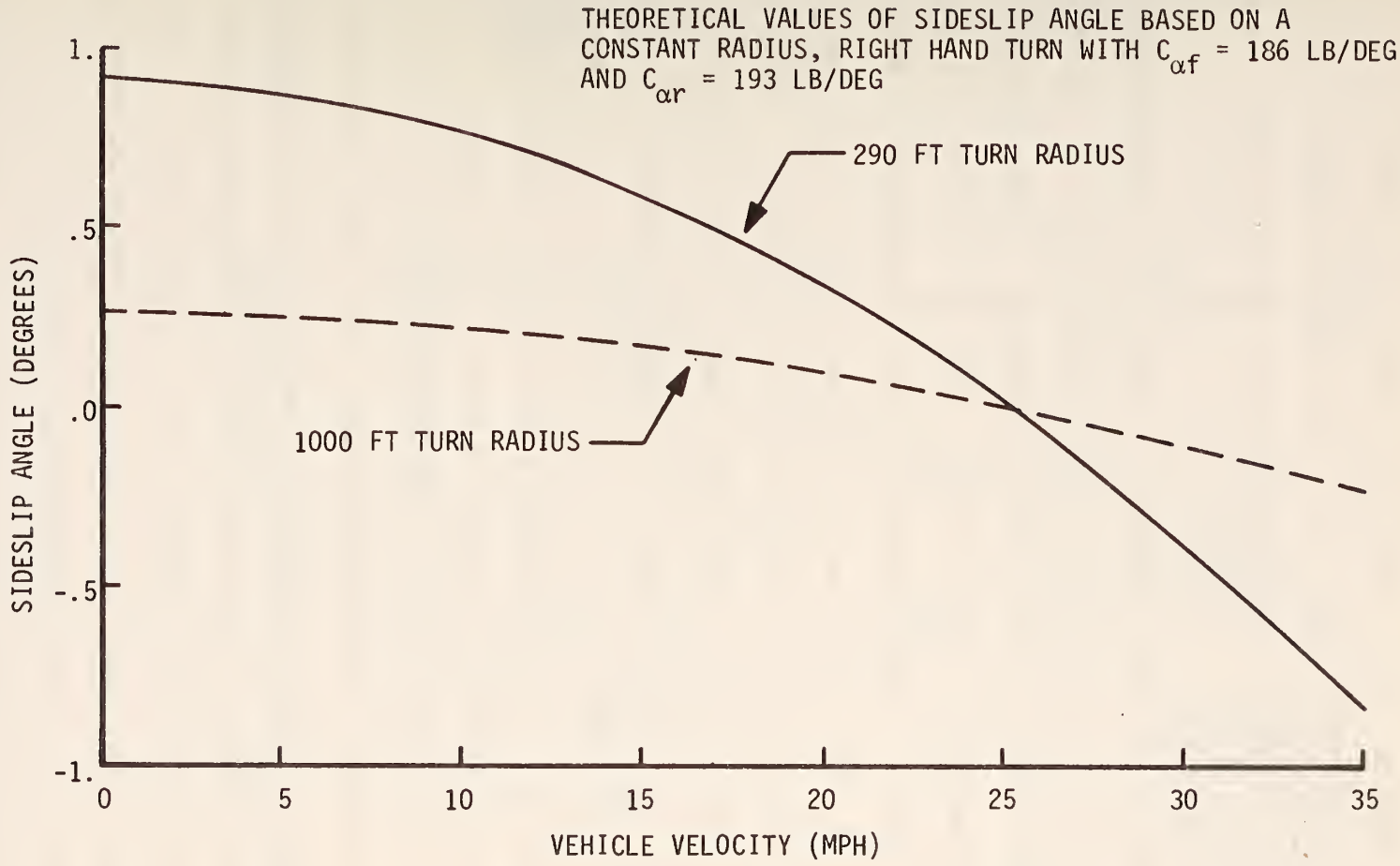

FIGURE 4.25 SIDESLIP ANGLE FOR BICYCLE MODEL IN A CONSTANT RADIUS PATH

The sideslip angle, which was obtained by the second method, is shown in Figure 4.26. The steering wheel data shown in this figure were recorded while driving west around a curve with a 290 foot radius. The effect of vehicle speed on sideslip angle is indicated in this figure. The magnitude of the sideslip angle obtained by this method is relatively close to the value estimated in the paragraph above. The westbound lane of this curve is smooth, but the eastbound lane has a washboard surface. The steering wheel data shown in Figure 4.27 were recorded while driving east around the curve with a 290 foot radius at 18 mph. The large peak shown in this steering record after approximately five seconds is typical for operation in this eastbound lane. The driver usually senses a loss of control at this location in the eastbound lane and he usually makes this type of sudden steering correction. The loss of control is not experienced in the smooth westbound lane.

The accuracy of the bicycle model for predicting the dynamic behavior of the vehicle is indicated by a comparison of the coordinates of the actual path of the vehicle with the coordinates of the predicted path of the vehicle. The actual path of the vehicle in the curve on State Road 26 is shown together with the path which was predicted from the measured steering wheel angle in Figure 4.28. These results indicate that the bicycle model may serve as a limited indicator of a vehicle's dynamic response.

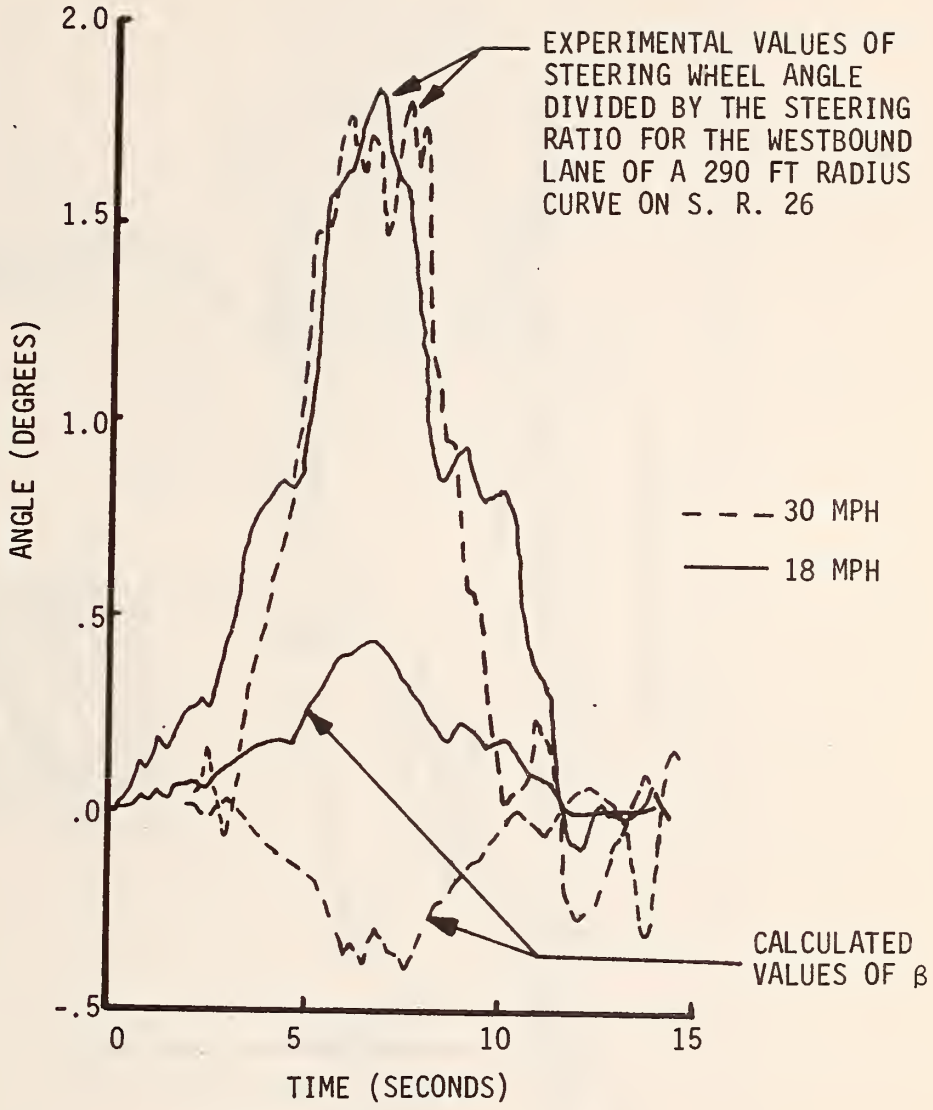

FIGURE 4.26 SIDESLIP ANGLE OBTAINED FROM MEASURED STEERING WHEEL ROTATION

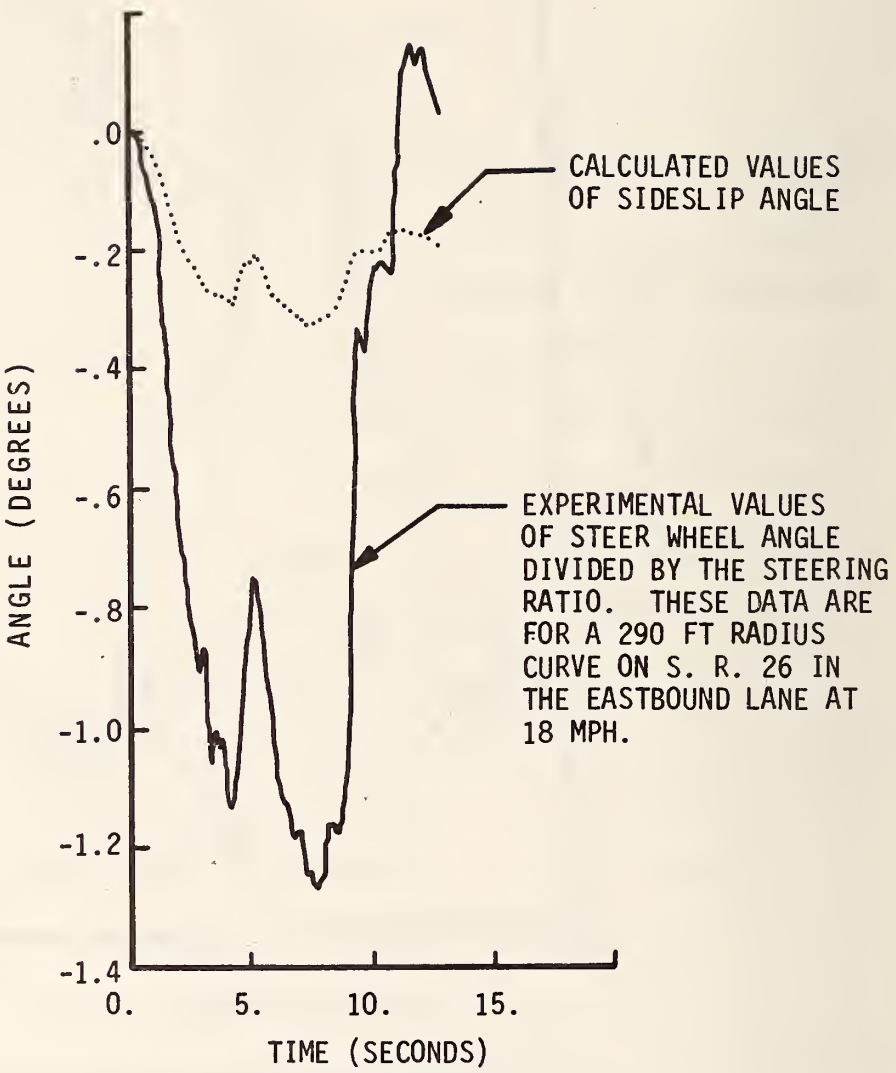

FIGURE 4.27 SIDESLIP ANGLE OBTAINED FROM MEASURED STEERING WHEEL ROTATION

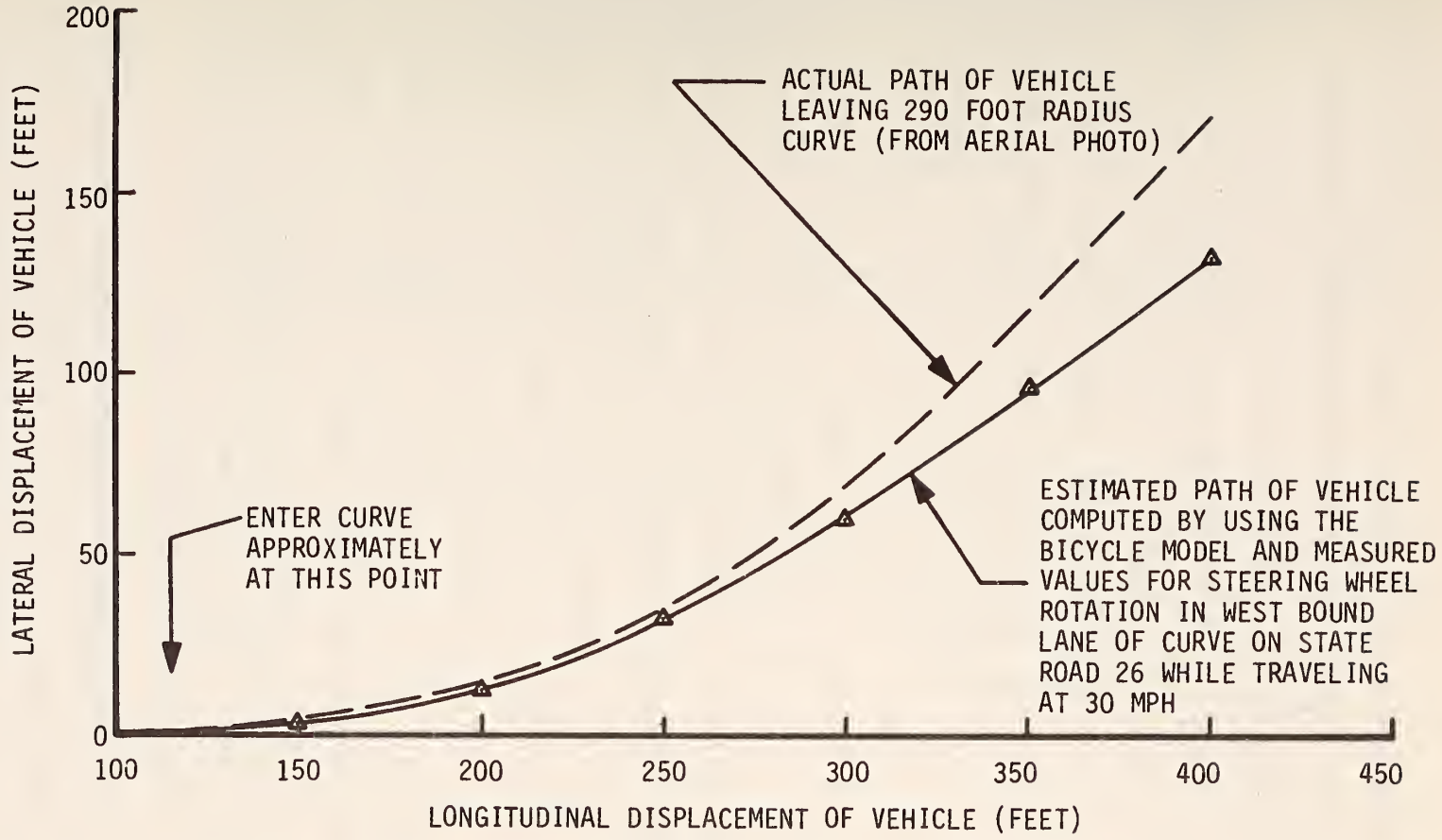

FIGURE 4.28 COMPARISON OF THE PATH PREDICTED BY THE BICYCLE MODEL WITH THE ACTUAL PATH

The sideslip angle which was obtained by using the two trail wheels while traveling in the eastbound lane around the 290 foot radius curve on State Road 26 at 30 mph is shown in Figure 4.29. The corresponding data for the front and rear trail wheels are shown in Figures 4.30 and 4.31 respectively. These data show the peaks corresponding to the sensation of a loss of control at approximately the 150 foot position. This sense of a loss of control is usually associated with sharp peaks in the values of β and with fast steering corrections. The sideslip angles measured during different runs do not correspond closely, because of changes in the vehicle's path and errors in the measurements.

The effect of low tire pressure on the control of a vehicle was studied by measuring the sideslip angle at various tire pressures. The vehicle was driven in a circular path with a radius of approximately 68 feet on smooth asphalt during this test. The values of β were evaluated at different speeds by data from the trail wheels. These experimental values of β are shown with theoretical values of β in Figure 4.32. The reduction in tire pressure causes a reduction in the tire cornering stiffness.

The empirical relationships between the tire angles (α and γ) and the lateral acceleration (A_{CG}) of the vehicle with GY 8.25-14 tires are shown in Figure 4.33. The shock absorbers were replaced by solid links for this test. This eliminated the rear axle roll steer, but it significantly

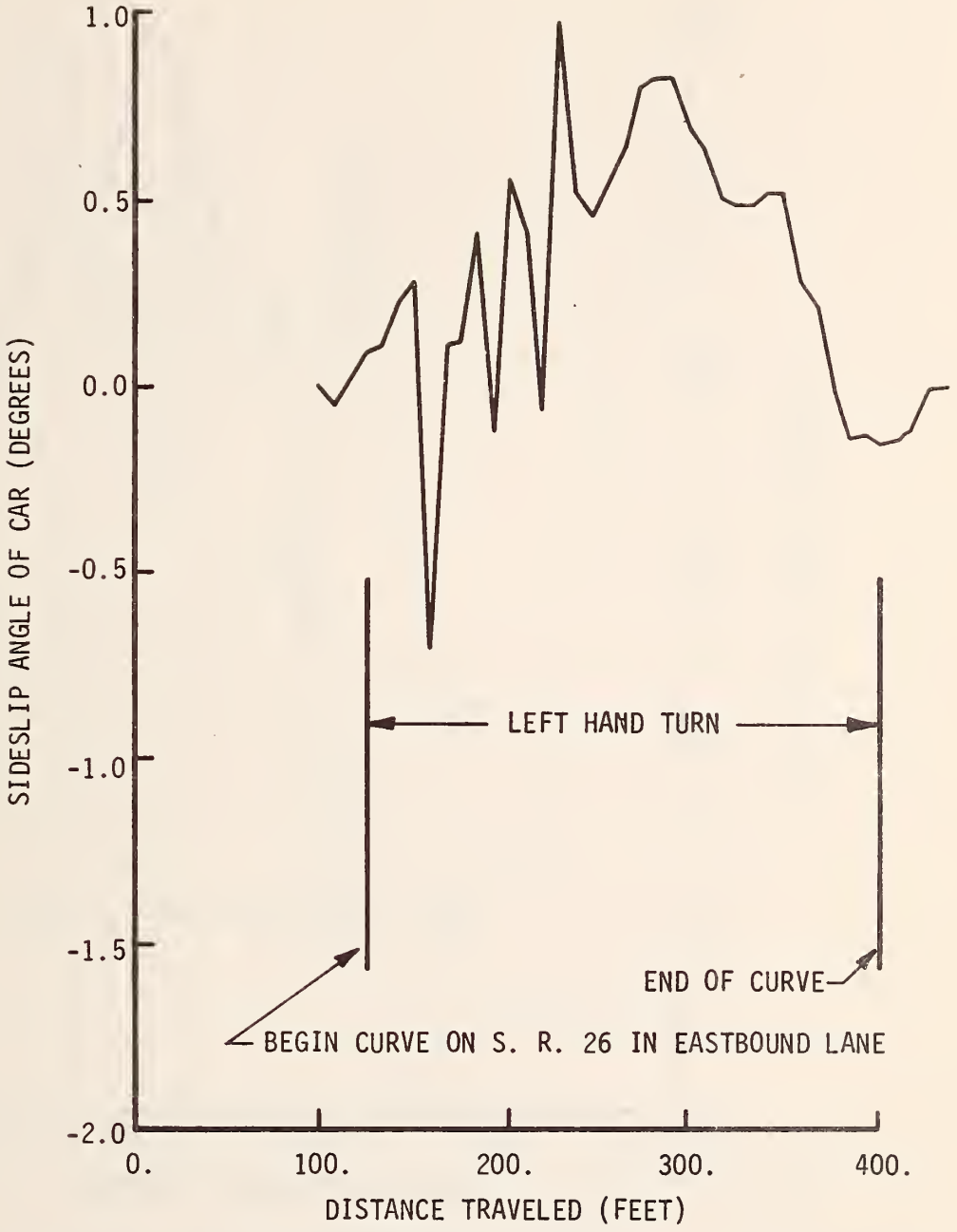

FIGURE 4.29 SIDESLIP ANGLE MEASURED WITH TRAIL WHEELS AT 30 MPH

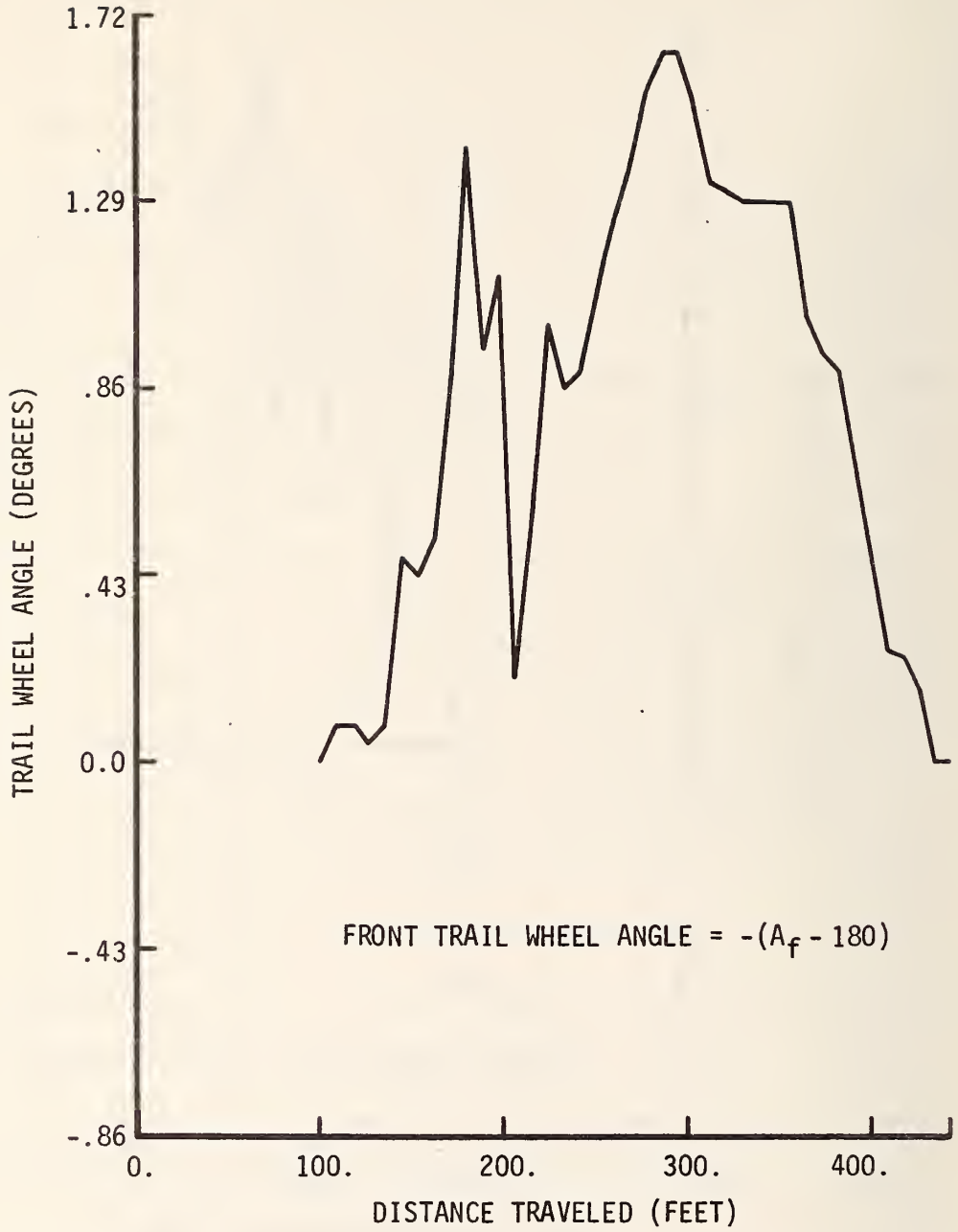

FIGURE 4.30 FRONT TRAIL WHEEL ANGLE FOR CURVE ON S. R. 26 IN EASTBOUND LANE AT 30 MPH

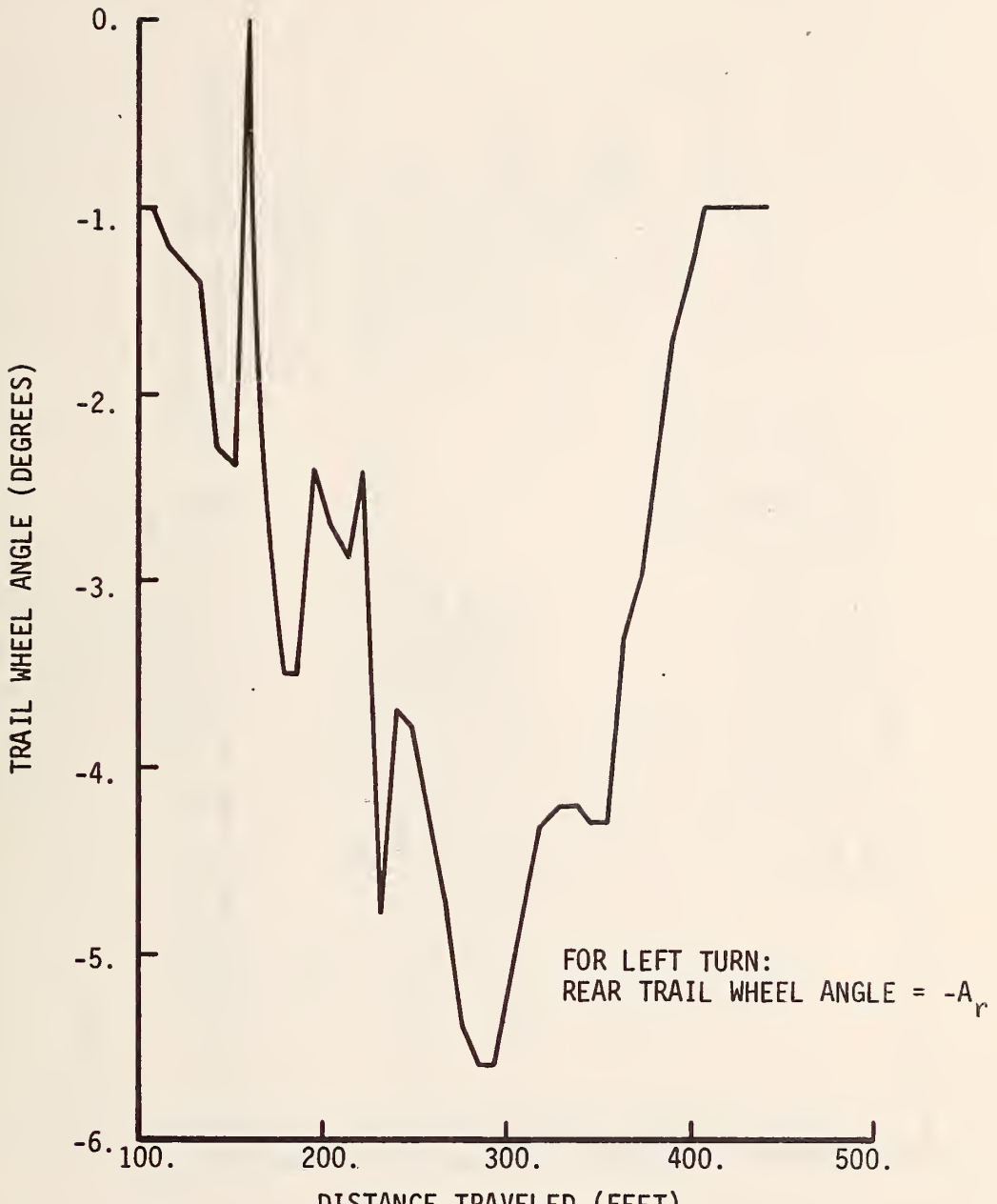

FIGURE 4.31 REAR TRAIL WHEEL ANGLE FOR CURVE ON S. R. 26 IN EASTBOUND LANE AT 30 MPH

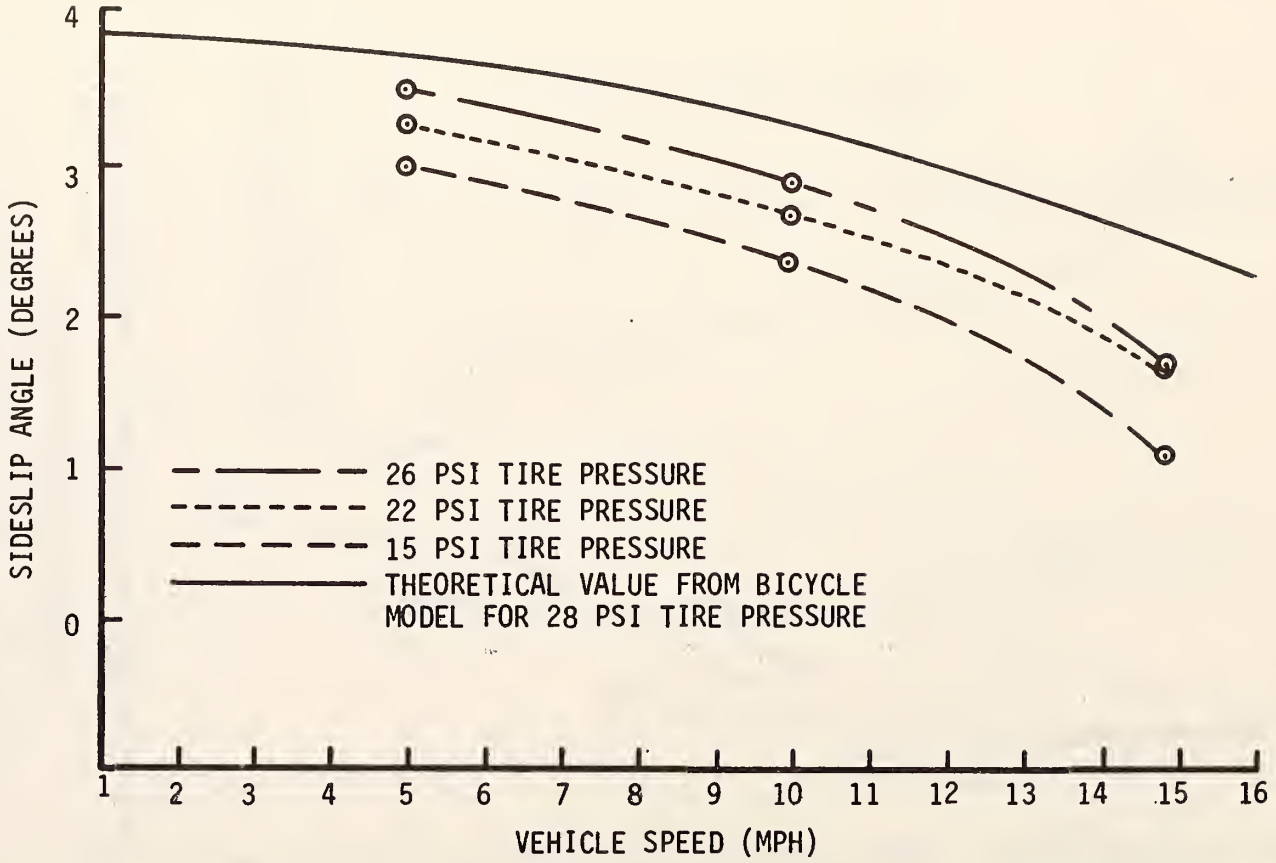

FIGURE 4.32 THE EFFECT OF LOW TIRE PRESSURE ON β

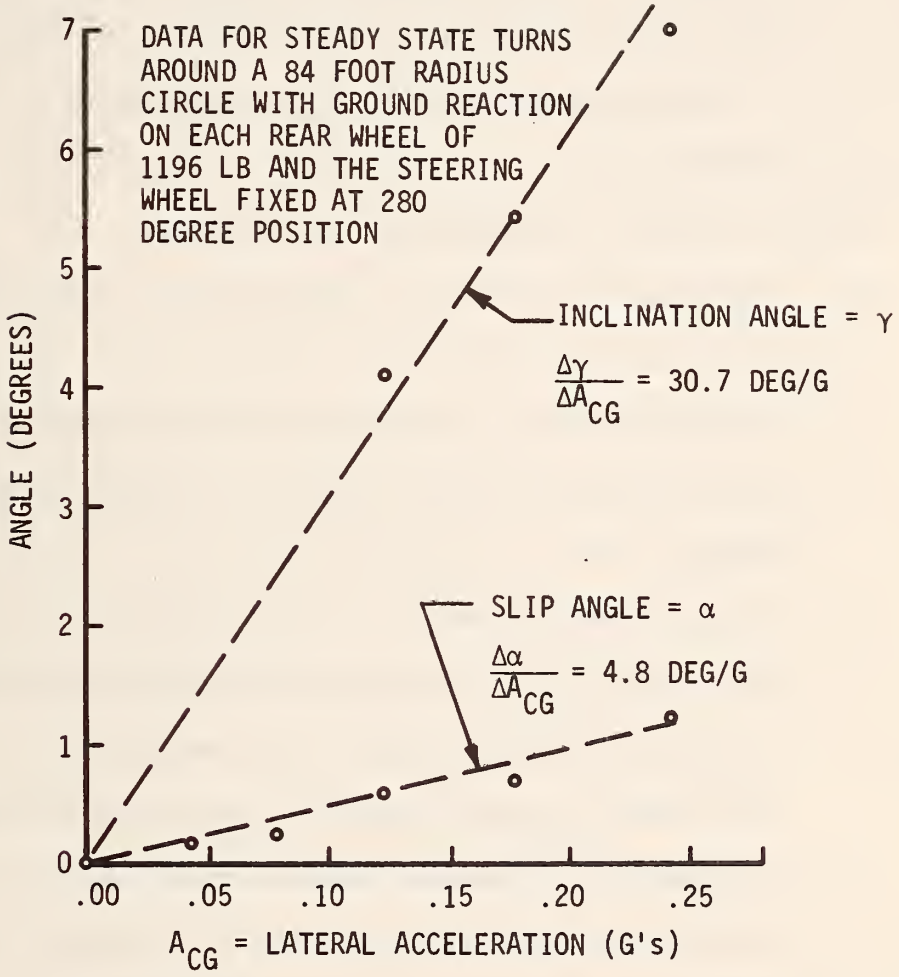

FIGURE 4.33 TIRE SLIP AND INCLINATION ANGLES VERSUS LATERAL ACCELERATION OF VEHICLE CENTER OF GRAVITY

increased the rear wheel caster. A second set of values for $\Delta\gamma/\Delta A_{CG}$ and $\Delta\alpha/\Delta A_{CG}$ for a different rear wheel ground reaction, W_r, should provide the information required to evaluate C_α and C_γ. (An example of the expected magnitudes for C_α and C_γ are indicated by the data for GR 70-15 tires with a 1196 pound normal force: C_α = 187 lb/deg, C_γ = 10.4 lb/deg.)

These results indicate the following:

1- The sideslip angle is affected by road roughness.

2- The sensation of loss of control of a vehicle, and the driver's response to this judgment may be reflected in high rates of change of sideslip angle.

3- Approximate estimates of the dynamic response characteristics of vehicles may be obtained by using the bicycle model with measured values of the steering wheel angle as the forcing function.

4- The two trail wheels furnish relatively accurate values for the location of the instant center for travel in a circular path. The sideslip angle can be calculated by using the instant center location. However, during transient maneuvers, the small magnitude of the sideslip angle and errors in measurement make β a difficult parameter to measure.

5- Measurement of the steering wheel angle in lieu of the sideslip angle may be a more desirable method of studying the controllability of a vehicle on pavements of different roughness.

Vertical Acceleration of the Driver

A relationship exists between the road roughness and the vertical acceleration of the driver. The displacement of the driver and its time derivatives are related to the comfort of the driver. Measured values of the vertical acceleration of the driver (with the acceleration due to gravity removed) are compared to values of road roughness in this section. The vehicle speed for these data is 50 mph.

The first set of driver acceleration data, which is reported in this investigation, was recorded with the front shock absorbers installed and without the rear shock absorbers in order to simulate badly worn shocks. The second set of data reported in this investigation was recorded with both the front and the rear shock absorbers installed on the vehicle.

Driver Acceleration without Rear Shocks

The records of driver acceleration contain low frequency components associated with the natural frequencies of the sprung mass (e.g. bounce and pitch) and high frequency components associated with the unsprung mass

and tire (e.g. wheel hop and tire thump) of the vehicle as shown in Figure 4.34 for operation on State Road 26. This record shows dominant low frequency vibrations. The record for U. S. 52 has dominant high frequency vibrations (Figure 4.35). The records for Cumberland Avenue and South River Road (Rough) are shown in Figures 4.36 and 4.37 respectively.

Probability density curves for the acceleration of the driver describe the percent of time spent in any band of acceleration amplitudes. The probability density curves for State Road 26 and Cumberland Avenue are shown in Figures 4.38 and 4.39. These curves show a 7% and 1.3% probability of exceeding 0.2 g's acceleration on State Road 26 and Cumberland Avenue respectively. The peak amplitudes of acceleration on South River Road (Rough) and U. S. 52 are approximately 0.4 g's and 0.15 g's respectively (Figures 4.40 and 4.41).

The probability density distributions for the driver acceleration on various roads are compared to a Gaussian distribution in Table 4.3. This comparison indicates that these distribution functions do approach a Gaussian distribution even though U. S. 52, State Road 26 and South River Road (Smooth) contain some marked deviations. The Chi-Square Goodness of Fit Test does not significantly add to these results.

The power spectral density curve for the driver acceleration identifies the contribution of each frequency band in

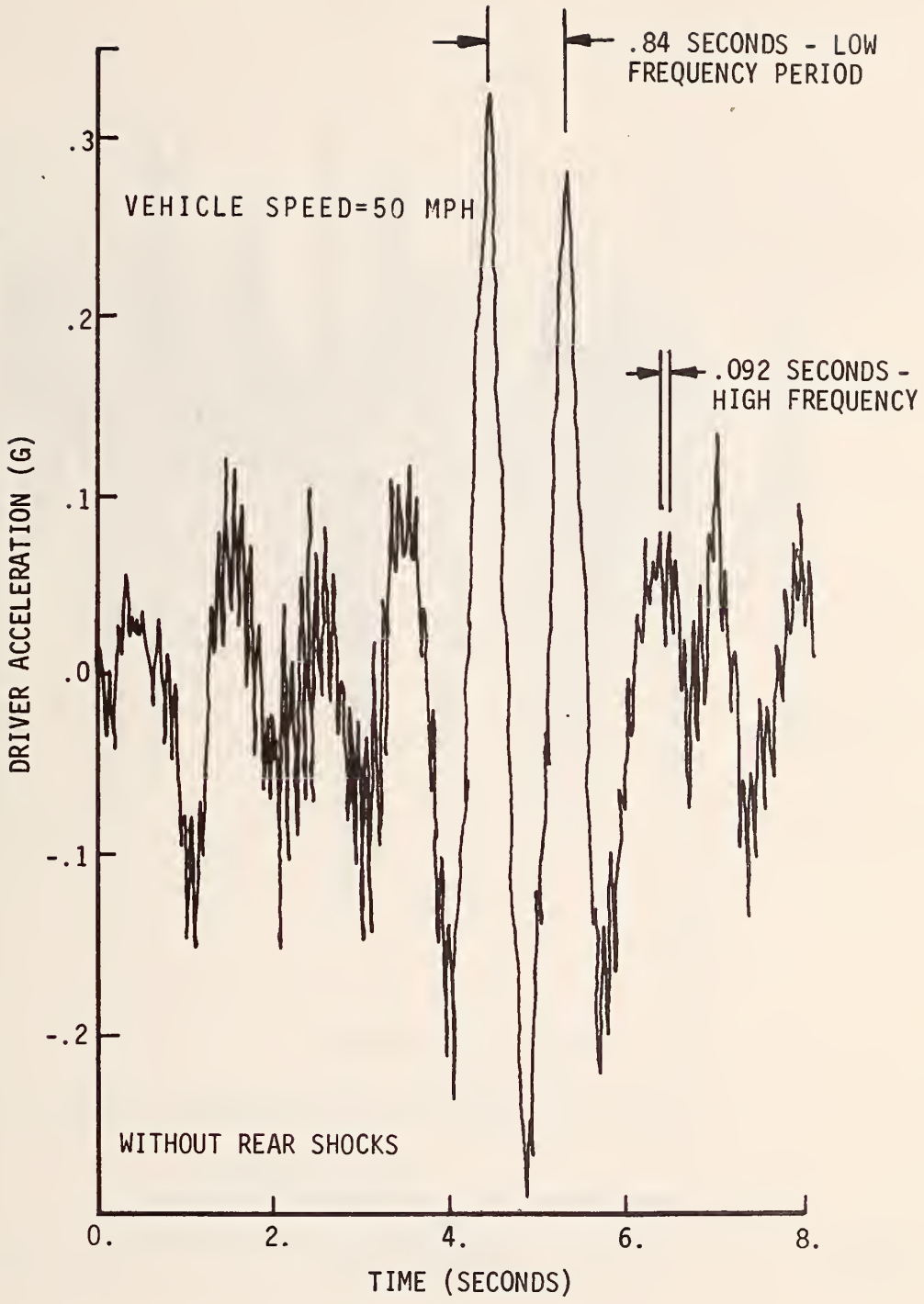

FIGURE 4.34 VERTICAL DRIVER ACCELERATION VERSUS TIME - S. R. 26

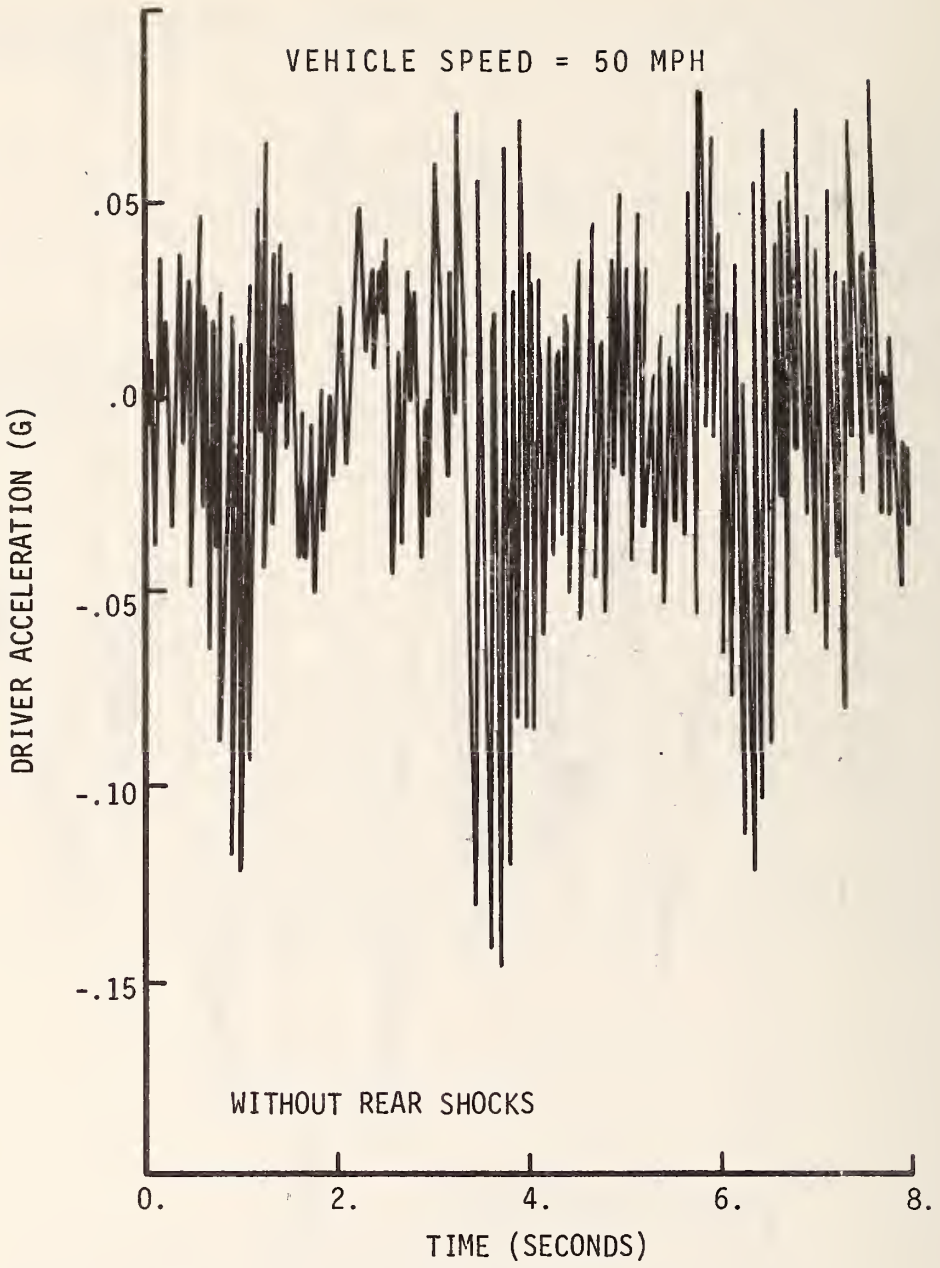

FIGURE 4.35 VERTICAL DRIVER ACCELERATION VERSUS TIME - U. S. 52 HIGHWAY

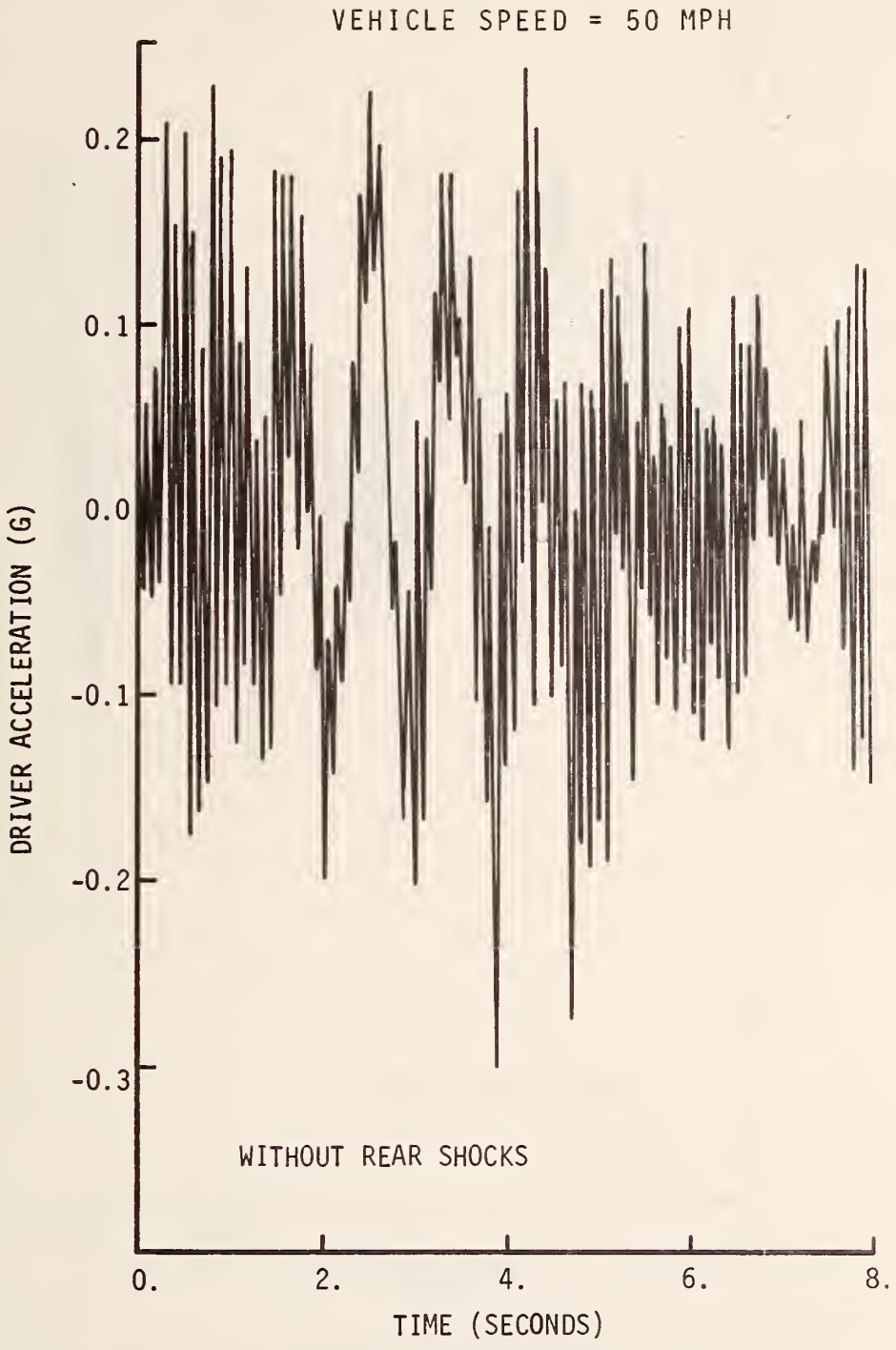

FIGURE 4.36 VERTICAL DRIVER ACCELERATION VERSUS TIME - CUMBERLAND AVENUE

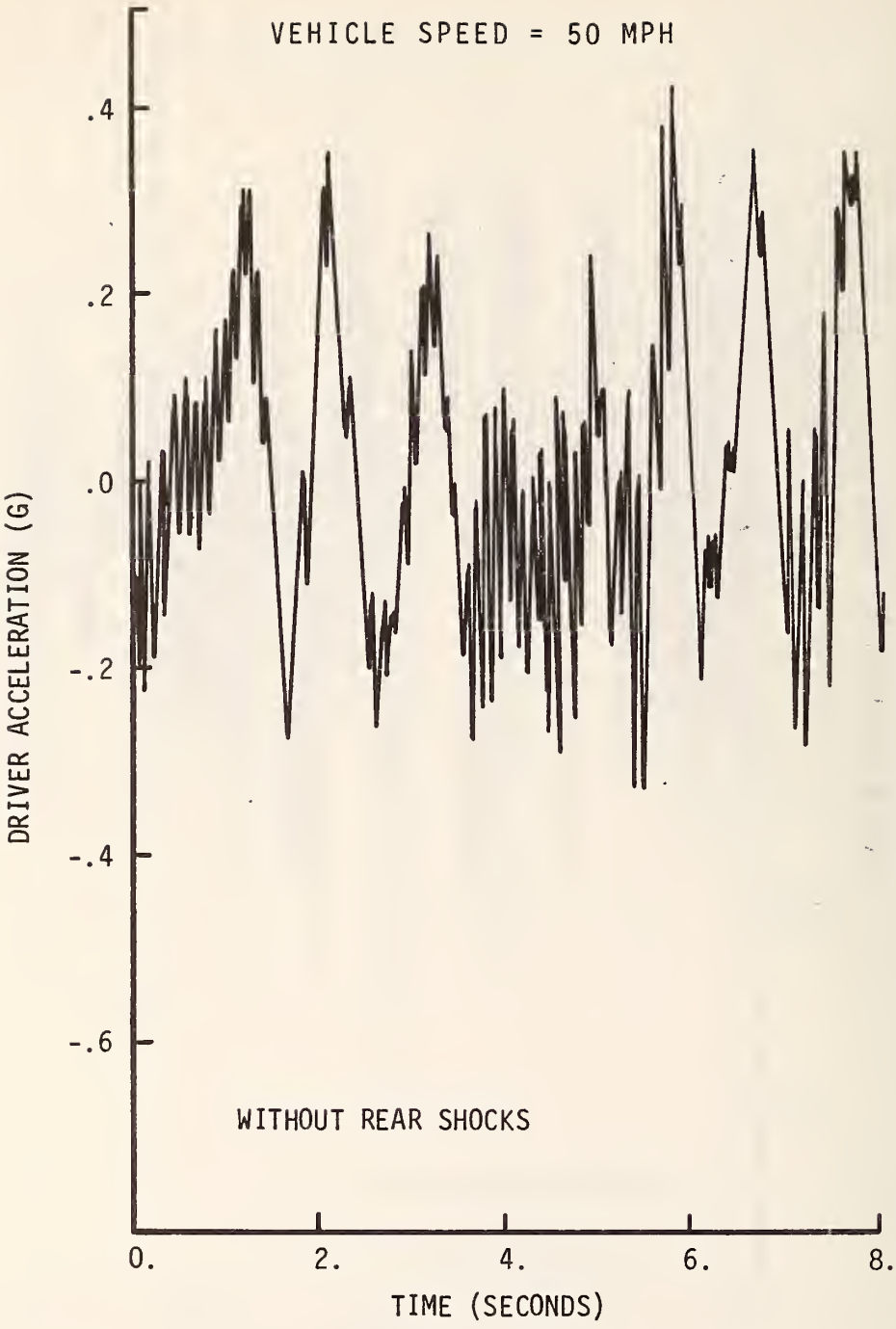

FIGURE 4.37 VERTICAL DRIVER ACCELERATION VERSUS TIME - SOUTH RIVER ROAD (ROUGH)

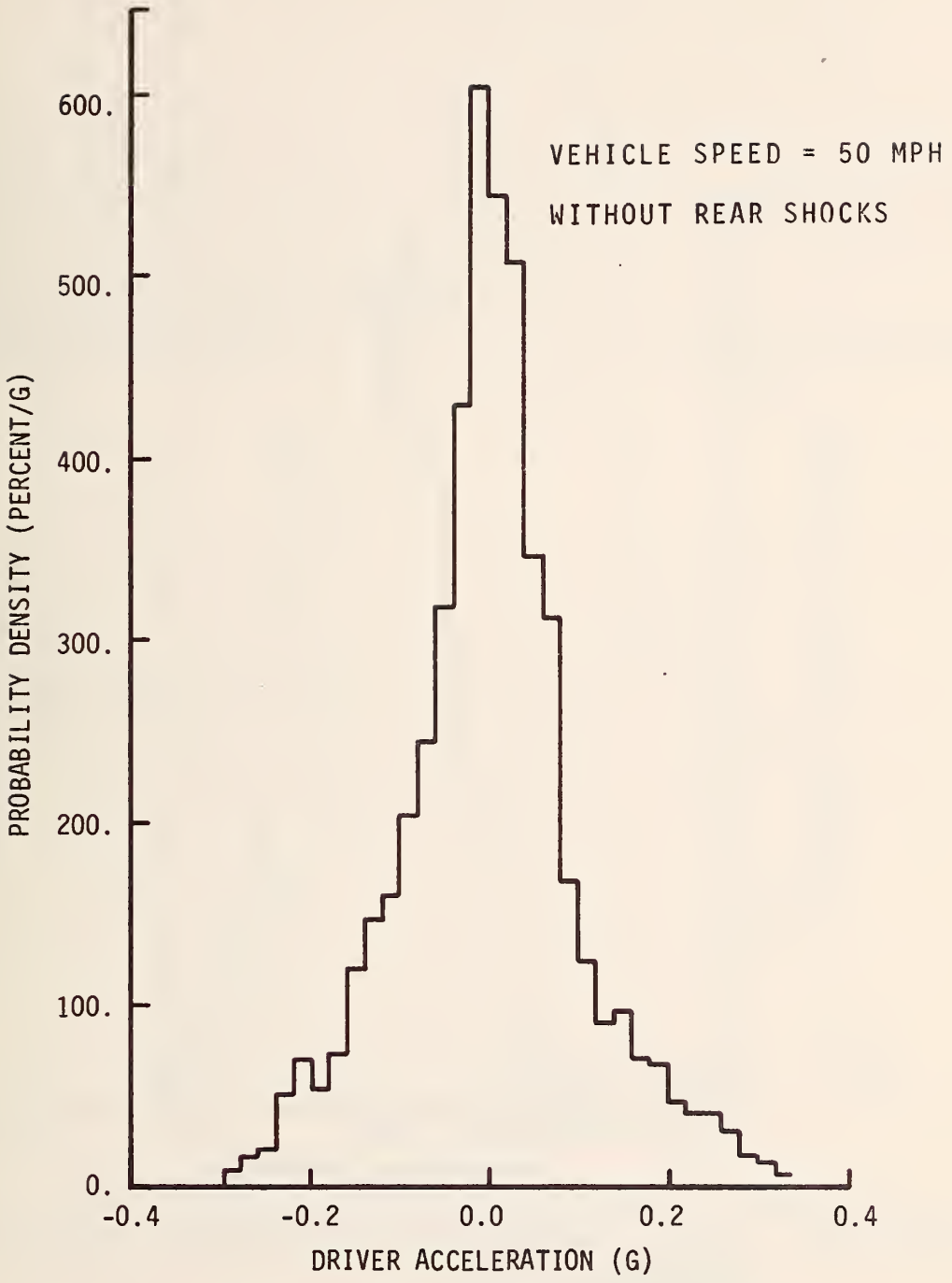

FIGURE 4.38 PROBABILITY DENSITY OF DRIVER ACCELERATION - S. R. 26

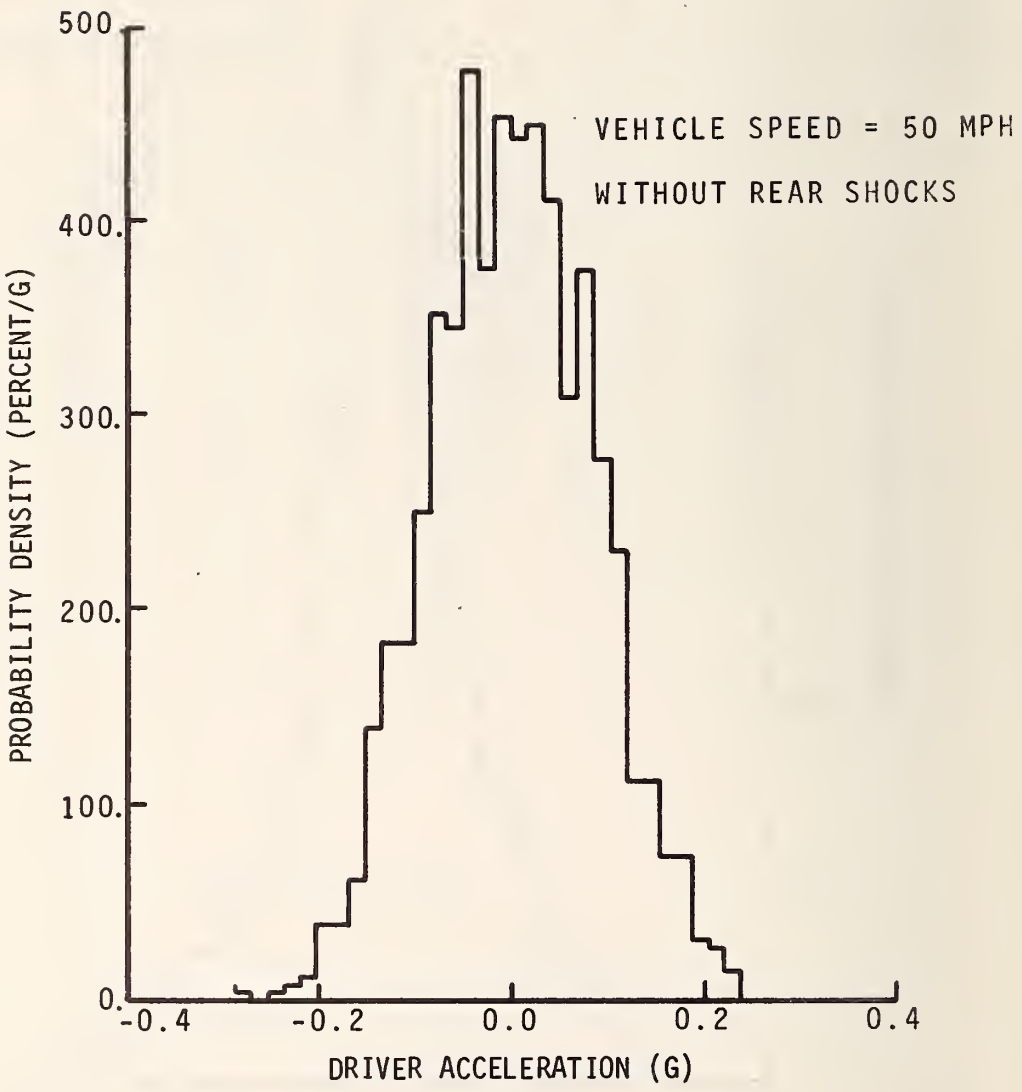

FIGURE 4.39 PROBABILITY DENSITY OF DRIVER ACCELERATION - CUMBERLAND AVENUE

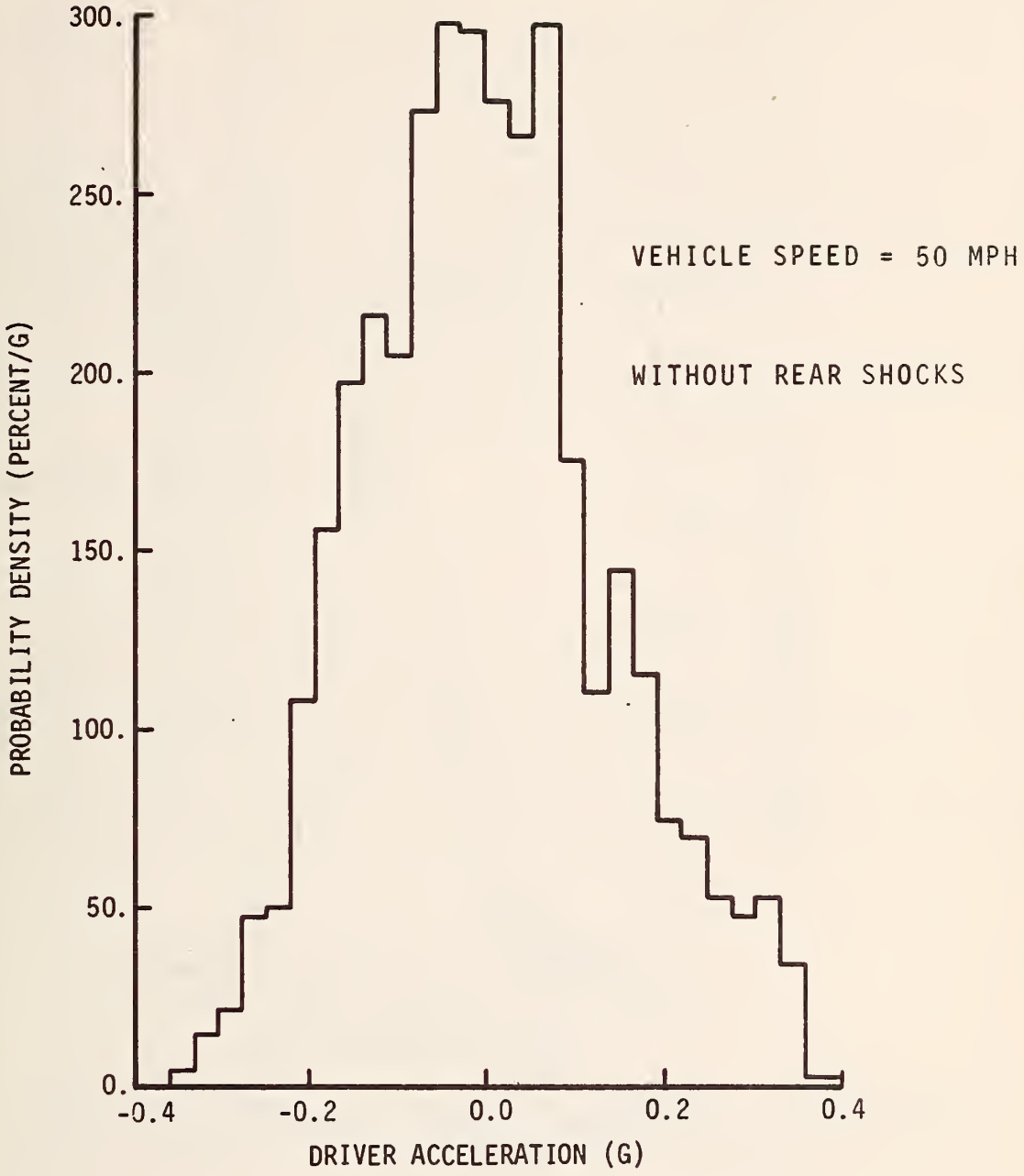

FIGURE 4.40 PROBABILITY DENSITY OF DRIVER ACCELERATION - SOUTH RIVER ROAD (ROUGH)

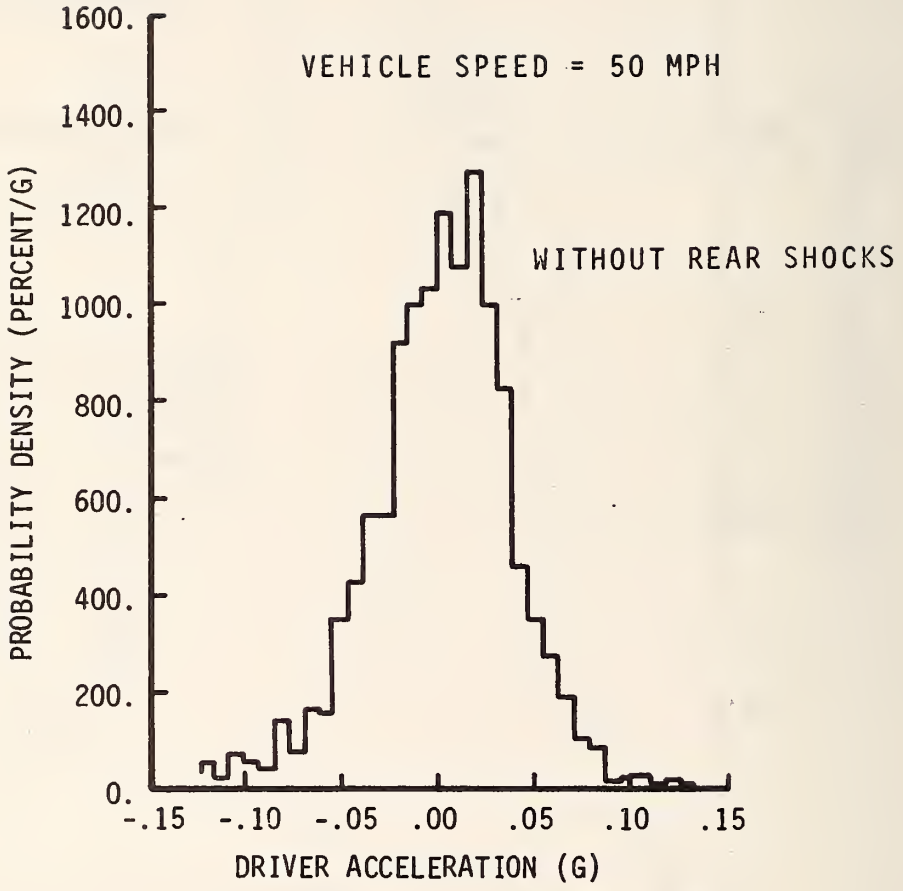

FIGURE 4.41 PROBABILITY DENSITY OF DRIVER ACCELERATION - U. S. 52 HIGHWAY

TABLE 4.3 SUMMARY OF PROBABILITY DATA FOR VERTICAL ACCELERATION OF AN AUTOMOBILE DRIVER IN AN AUTOMOBILE WITHOUT REAR SHOCK ABSORBERS

ROAD NAME	S* (g's)	PROBABILITY OF OCCURRENCE OF ACCELERATION FOR A GIVEN RANGE OF VALUES OF S								
		± S	± 2S	± 3S	0 to -S	0 to -2S	0 to -3S	0 to +S	0 to +2S	0 to +3S
Road with a Gaussian Distribution	S	68.3	95.4	99.7	34.1	47.7	49.9	34.1	47.7	49.9
South River Road - Rough**	.138	66.7	94.8	99.9	35.6	51.	52.2	31.1	43.8	47.7
U. S. 52	.039	74.2	94.4	98.2	32.1	41.5	44.2	42.1	52.9	54.
State Road 26	.098	72.8	92.8	99.6	35.7	46.7	50.1	37.1	46.1	49.5
Cumberland	.084	67.8	95.5	99.7	34.	48.	49.7	33.8	47.5	50.
Lindberg Road	.038	68.2	95.7	99.5	32.3	45.	47.5	35.9	50.7	52.
South River Road-Smooth**	.049	67.1	93.6	97.6	34.2	49.1	50.4	32.9	44.5	47.2

* S = Standard deviation of driver acceleration (g's)

** Vehicle heading is east.

the spectrum to the total mean square value of the driver acceleration. The acceleration power spectra are based on 1500 data points at .01 second intervals and a maximum lag number, M, of 150. The power spectrum for State Road 26 (Figure 4.42) has peaks at 1 cps and 10 cps which are associated with the natural frequencies of the sprung mass and unsprung mass of the vehicle respectively. The major contribution to the mean square value of the driver acceleration on State Road 26 occurs at 1 cps, because the area under the acceleration power spectrum is concentrated at this frequency. However, the major contribution to the driver acceleration on U. S. 52 occurs at 10 cps (Figure 4.43). The driver acceleration on Cumberland Avenue is made up of approximately equal contributions at 1 cps and 10 cps (Figure 4.44). The power spectrum for South River Road (Rough) shows higher magnitudes of acceleration in the low frequency band and in the high frequency band than any other road (Figure 4.45).

The areas under the driver acceleration power spectrum for low and high frequency ranges are compared with the areas under the road roughness power spectrum for corresponding frequency ranges in Figures 4.46 and 4.47 respectively. These two ranges divide the acceleration power spectrum into two exclusive frequency ranges which include different natural frequencies of the vehicle. The area under the acceleration power spectrum between 0.8 cps and 2.4 cps

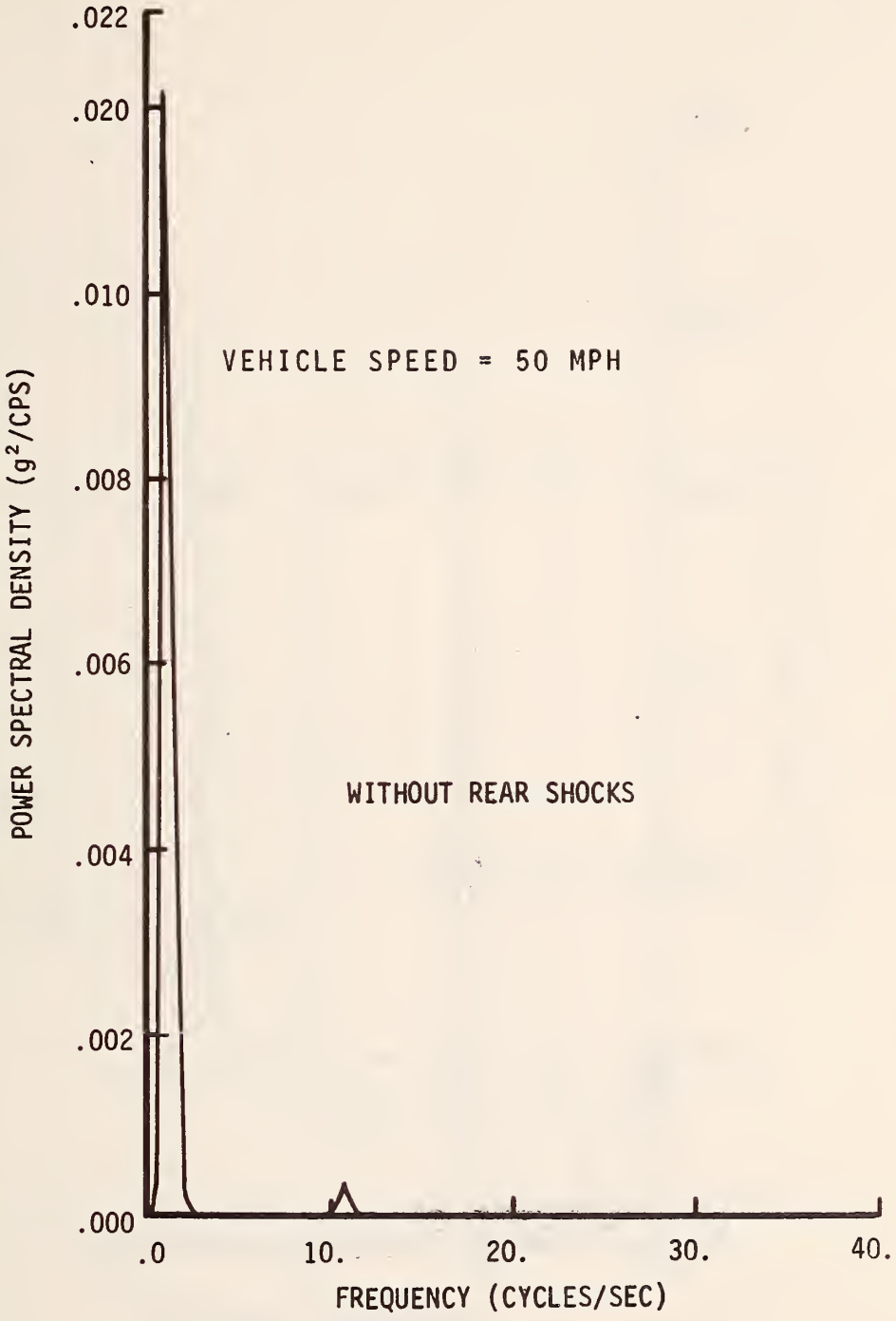

FIGURE 4.42 POWER SPECTRUM OF DRIVER ACCELERATION - S. R. 26

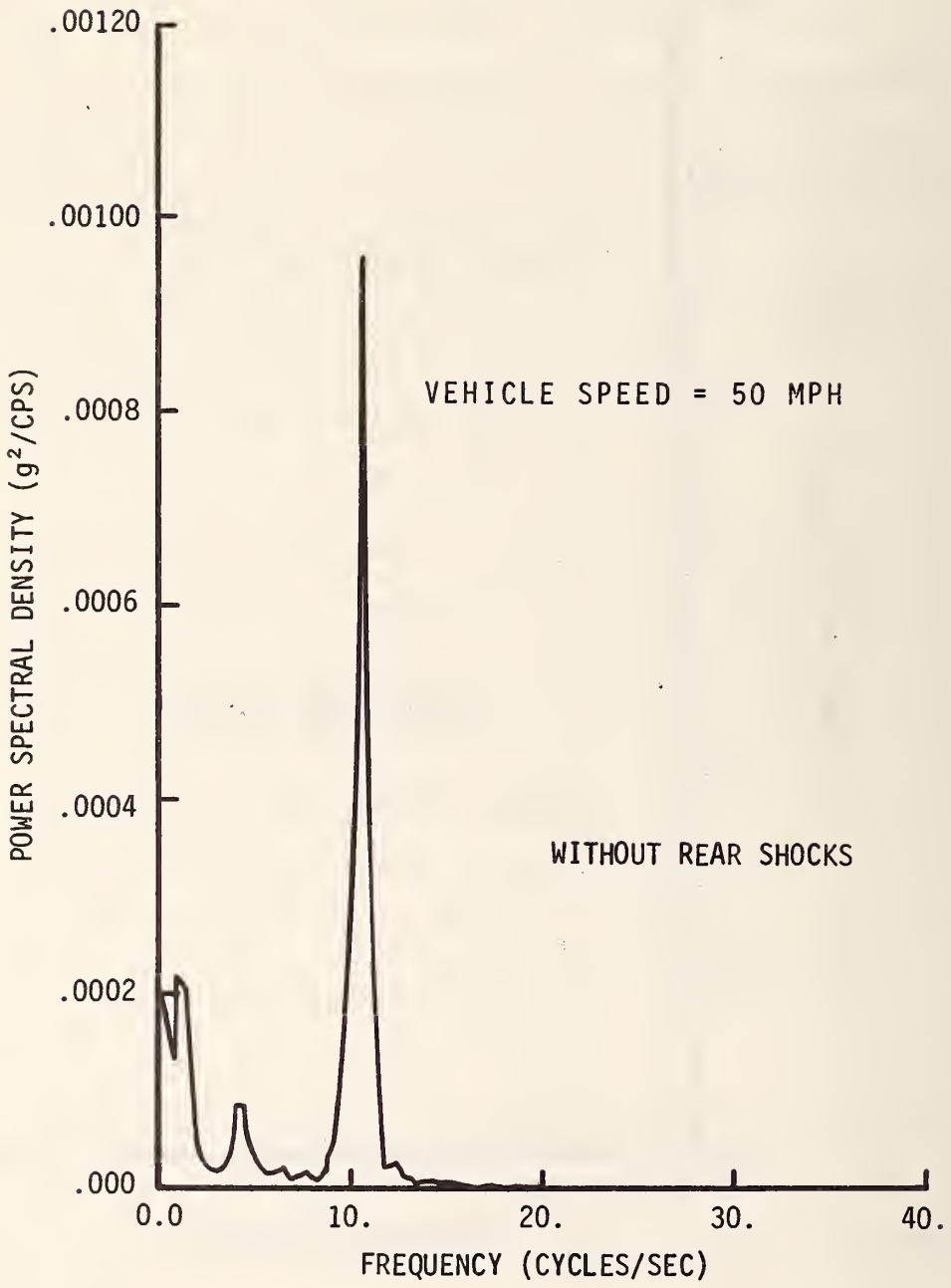

FIGURE 4.43 POWER SPECTRUM OF DRIVER ACCELERATION - U. S. 52

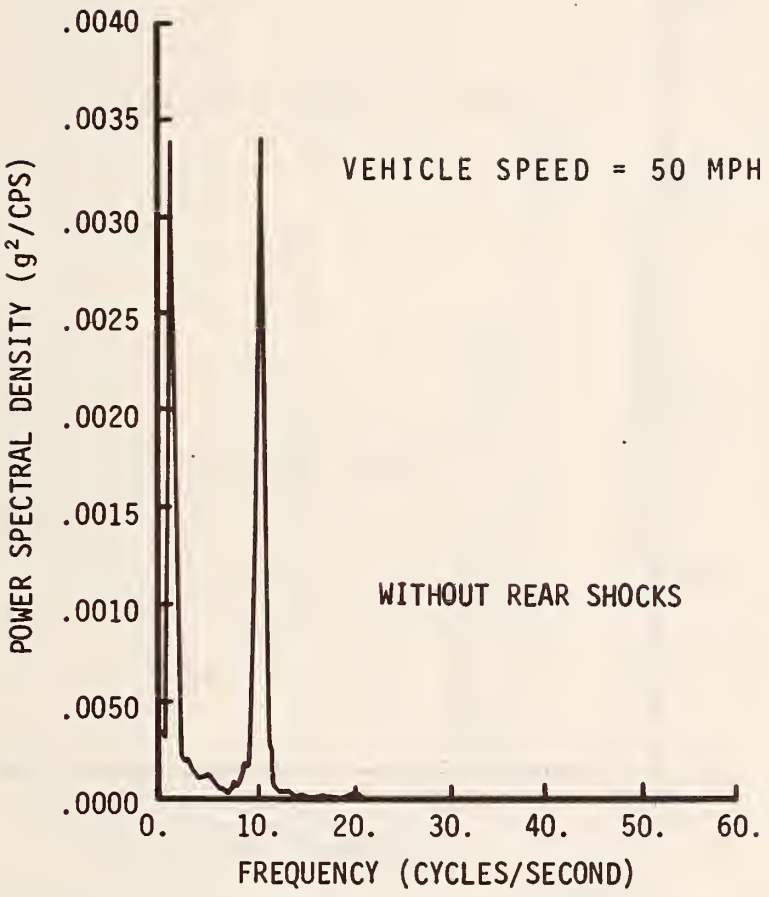

FIGURE 4.44 POWER SPECTRUM OF DRIVER ACCELERATION - CUMBERLAND AVENUE

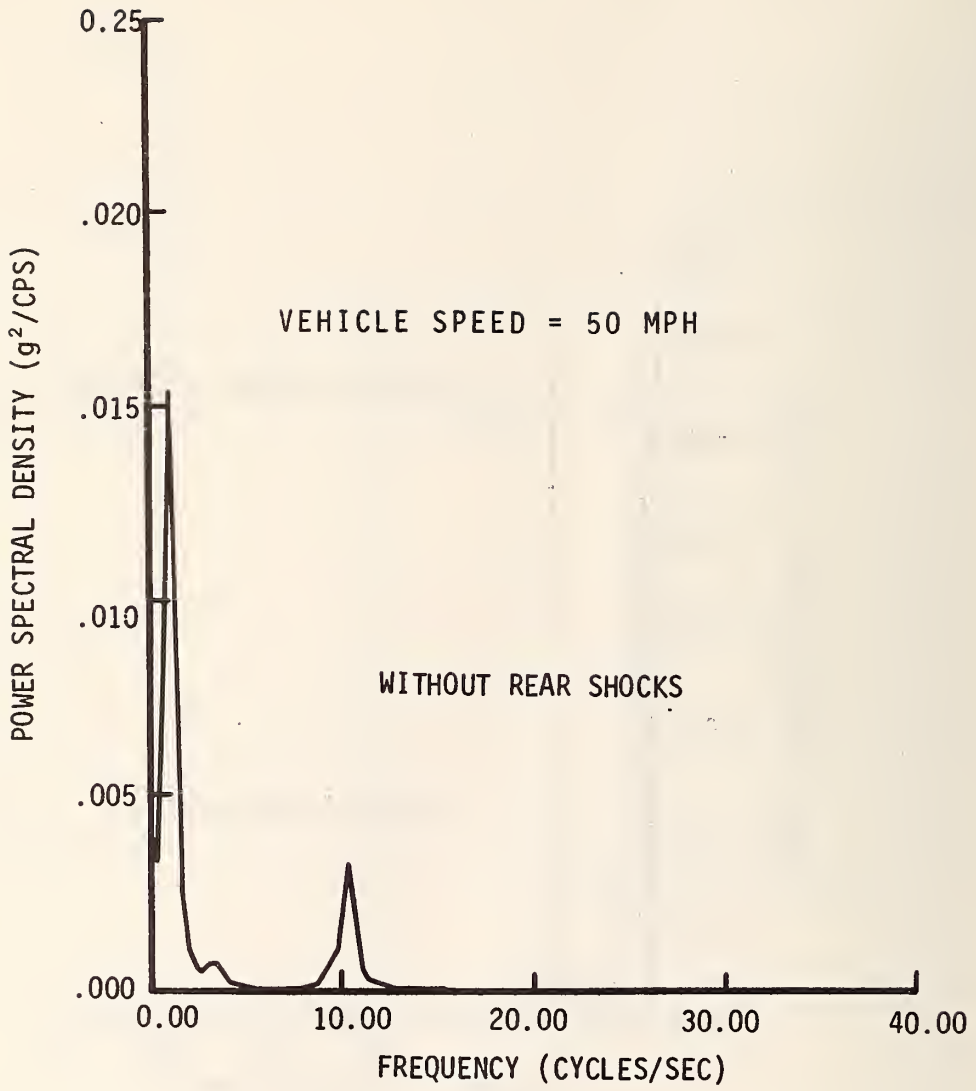

FIGURE 4.45 POWER SPECTRUM OF DRIVER ACCELERATION - SOUTH RIVER ROAD (ROUGH)

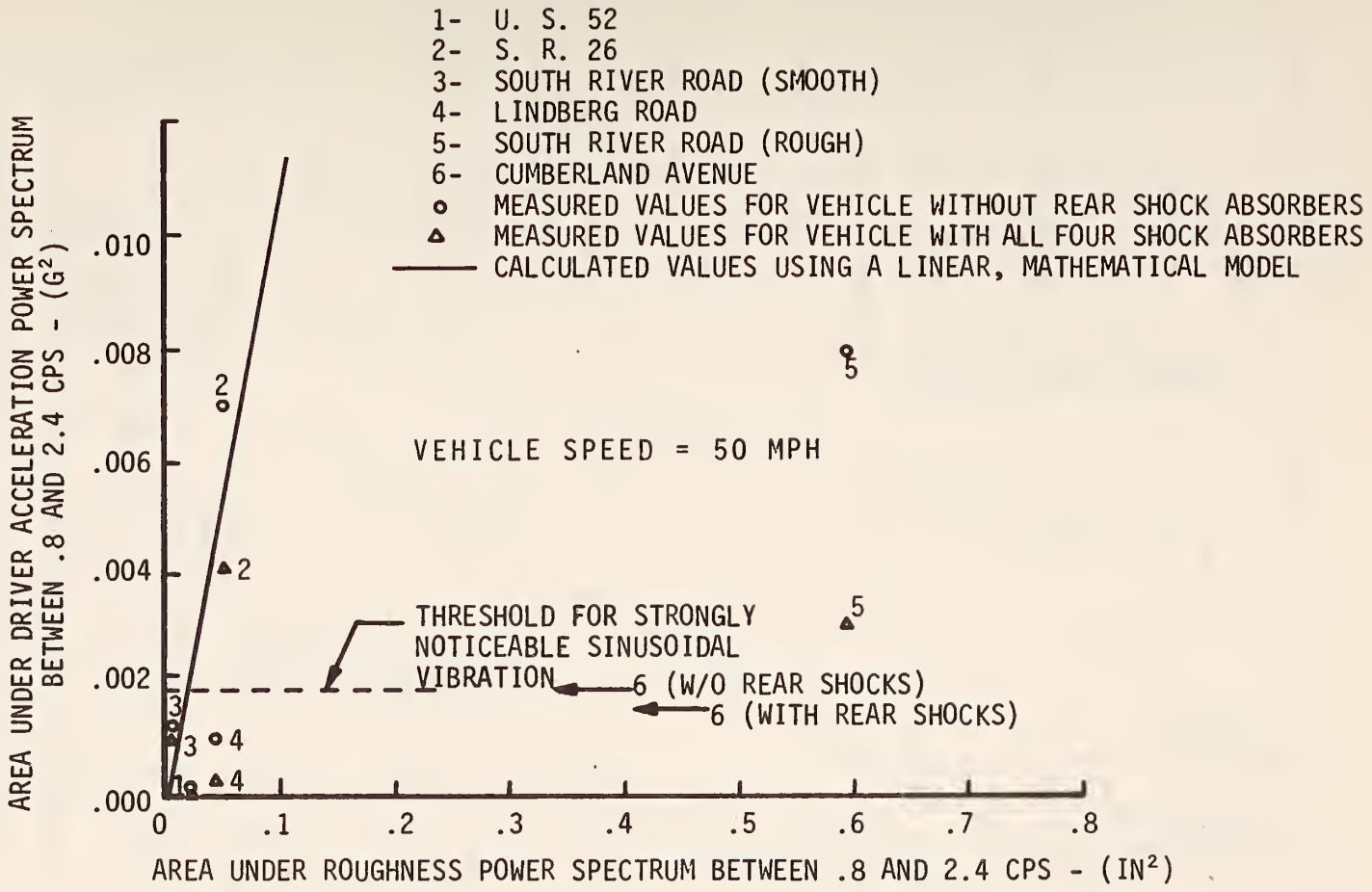

FIGURE 4.46 COMPARISON OF DRIVER ACCELERATION AND ROAD ROUGHNESS AT LOW FREQUENCIES

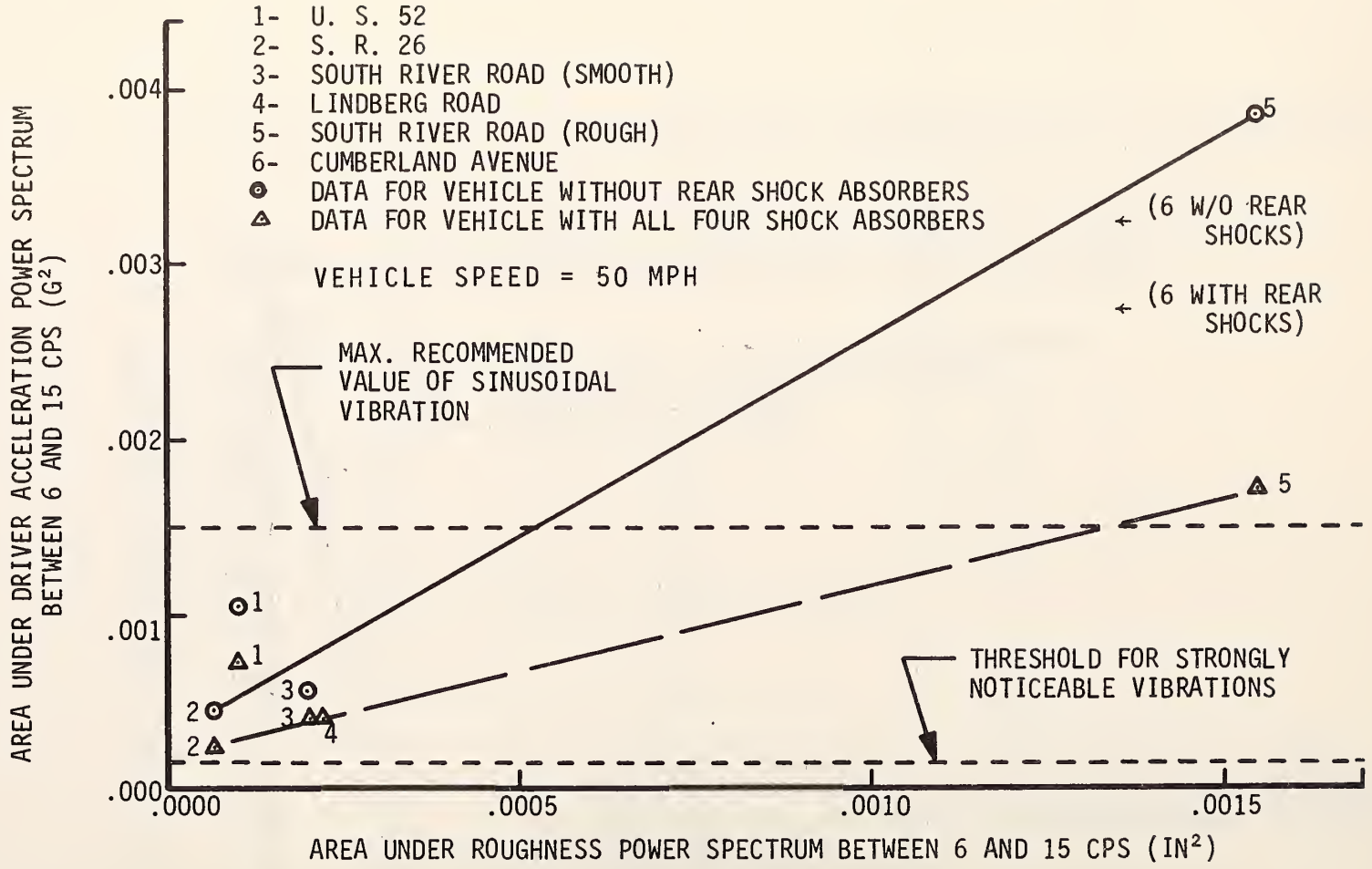

FIGURE 4.47 COMPARISON OF DRIVER ACCELERATION AND ROAD ROUGHNESS AT HIGH FREQUENCIES

encompasses the low frequency peak and forms the low frequency range. The area between 6 cps and 15 cps encompasses the high frequency peak and forms the high frequency range. Unfortunately the measurements of driver acceleration and pavement roughness were not taken at the same time, and the different rates of weathering during the three years since the roughness values were recorded introduces some error. The nonlinear response of the vehicle at extreme amplitudes is evident in these results. The system characteristics are responsible for the major differences in response rates at high and low frequencies.

A subjective evaluation of the ride on these test roads is as given below.

1- South River Road (Rough)

This was the most objectionable road and is not suitable for travel at 50 mph.

2- U. S. 52

The high frequency disturbance is noticeable, but it is not objectionable. There are bumps at 0.1 mile intervals which give annoying pulse excitations.

3- State Road 26

The low frequency, high amplitude vibration due to low hills is excessive; however, high frequency vibration is not objectionable.

4- Cumberland Avenue

The ride is objectionably harsh due to the high frequency excitation caused by the junctions of the concrete slabs.

5- Lindberg Road

The ride was not objectionable.

6- South River Road (Smooth)

The ride was not objectionable.

These observations indicate that the ride may be objectionable due to a high frequency vibration, a low frequency vibration, or a combination of high and low frequency vibrations.

Driver Acceleration with Front and Rear Shocks

The following results are based on measurements of the acceleration of the driver when both the front and rear shock absorbers are installed. The probability density distributions for the driver acceleration on South River Road (Rough), U. S. 52, State Road 26, Cumberland Avenue, Lindberg Road, and South River Road (Smooth) are shown in Figures 4.48 through 4.53 respectively. The probability data are summarized in Table 4.4. Comparison of the values of standard deviations for the driver acceleration in Table 4.4 with the values in Table 4.3 shows the effect of the rear shock absorbers in reducing peak amplitudes of driver acceleration. The data in Tables 4.3 and 4.4 for South River Road were recorded in different traffic lanes.

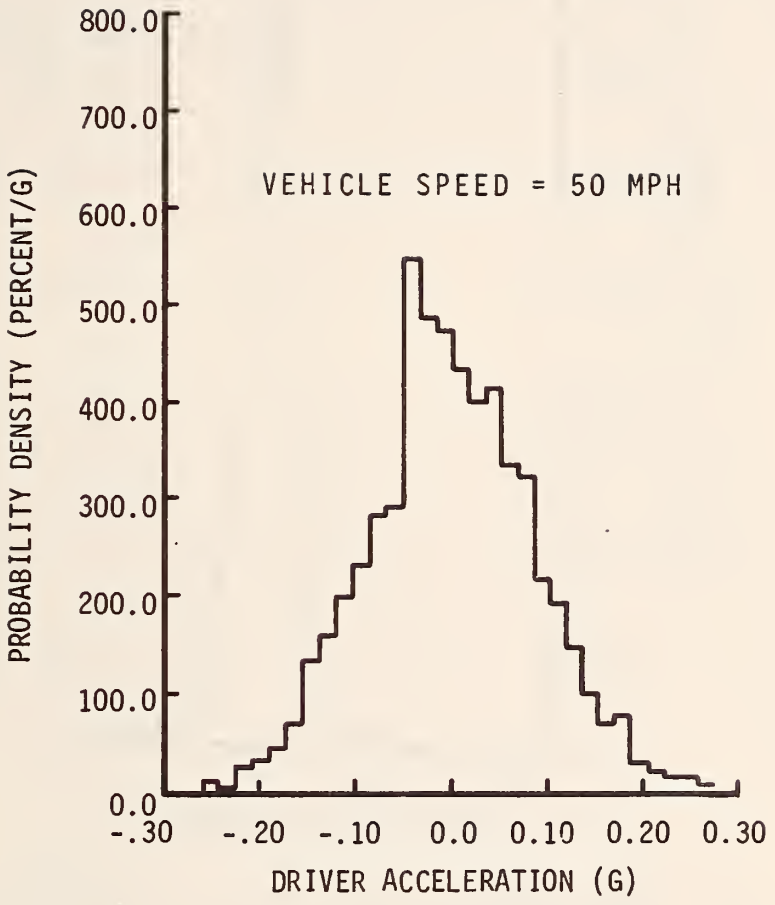

FIGURE 4.48 PROBABILITY DENSITY OF DRIVER ACCELERATION WITH SHOCKS - SOUTH RIVER ROAD (ROUGH)

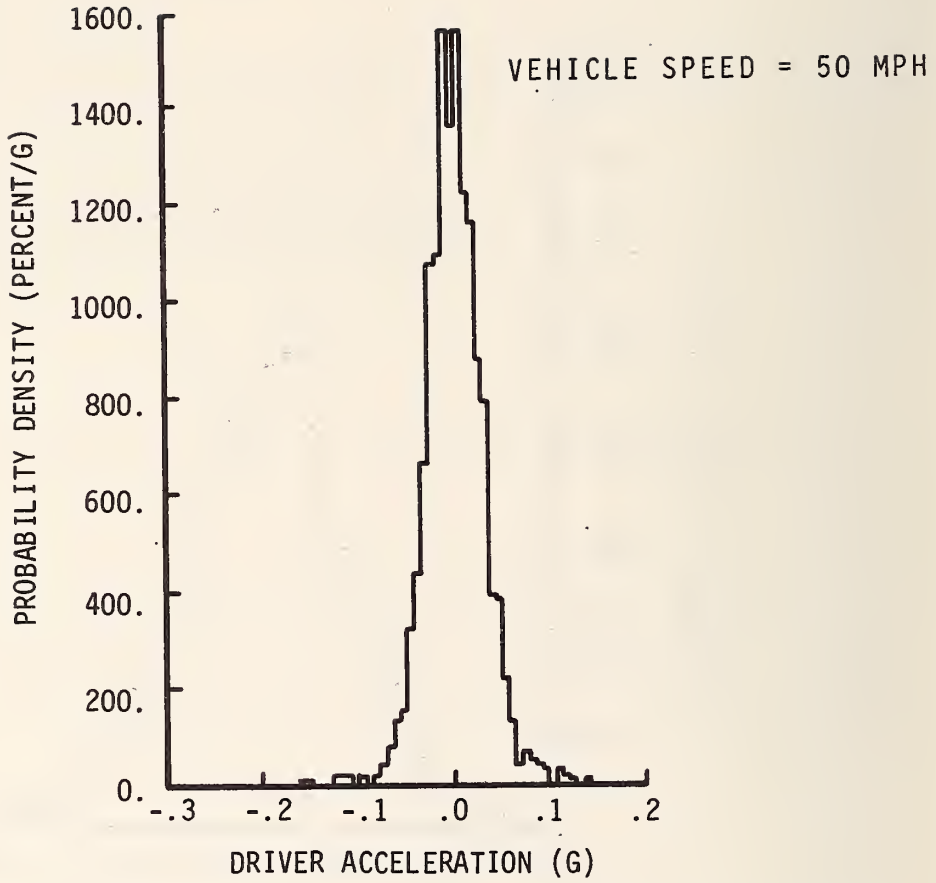

FIGURE 4.49 PROBABILITY DENSITY OF DRIVER ACCELERATION WITH SHOCKS - U. S. 52

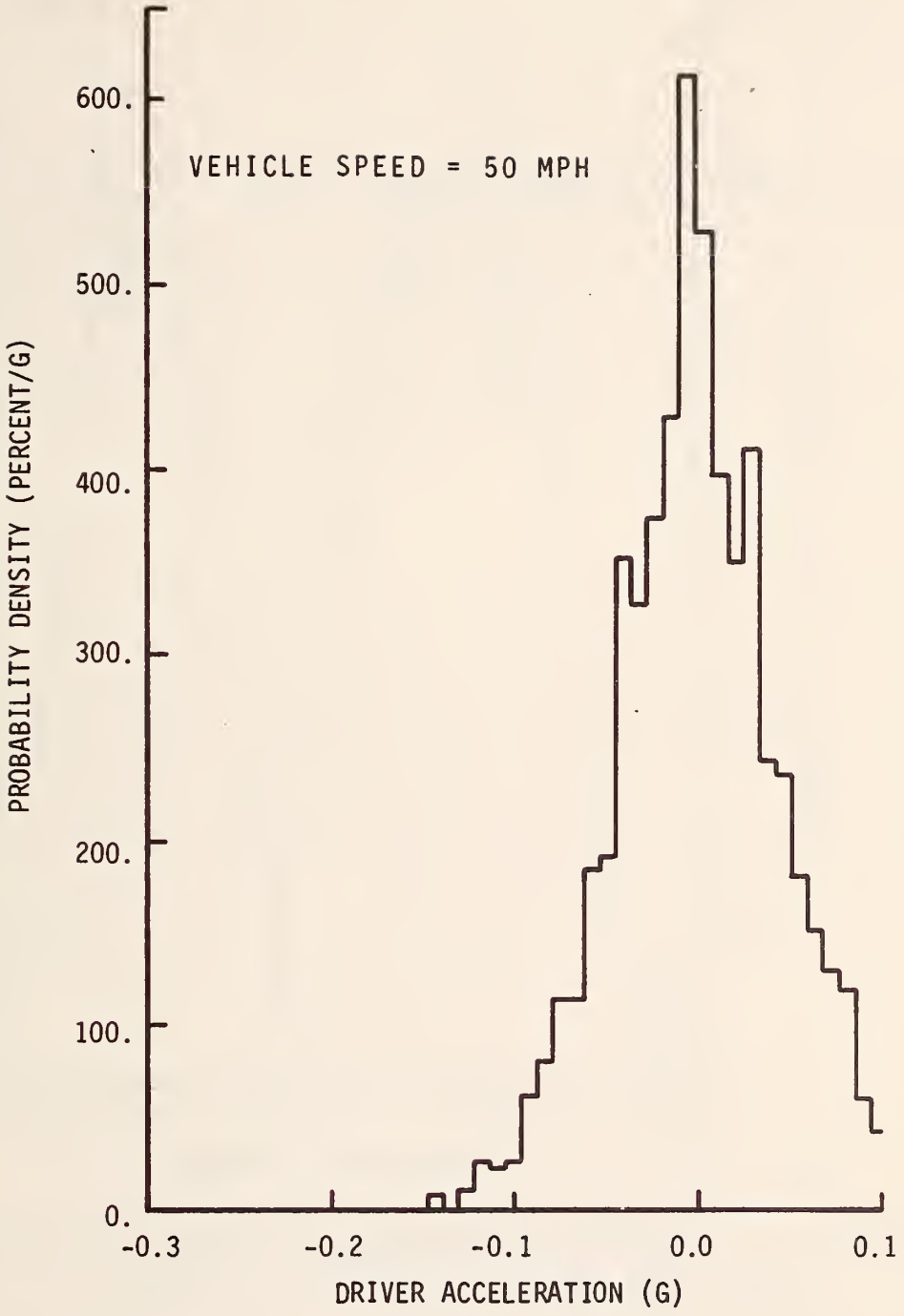

FIGURE 4.50 PROBABILITY DENSITY OF DRIVER ACCELERATION WITH SHOCKS - S. R. 26

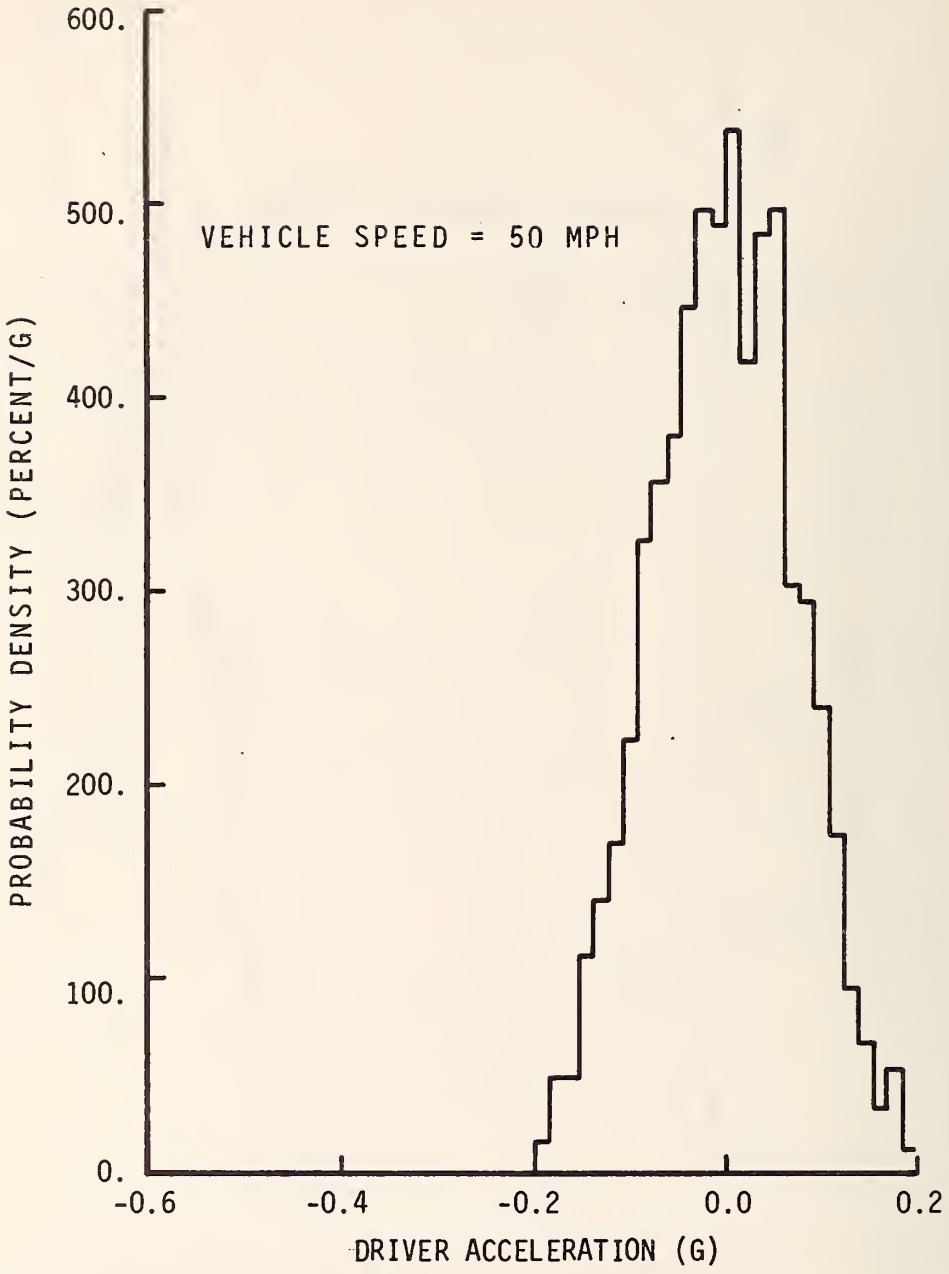

FIGURE 4.51 PROBABILITY DENSITY OF DRIVER ACCELERATION WITH SHOCKS - CUMBERLAND AVENUE

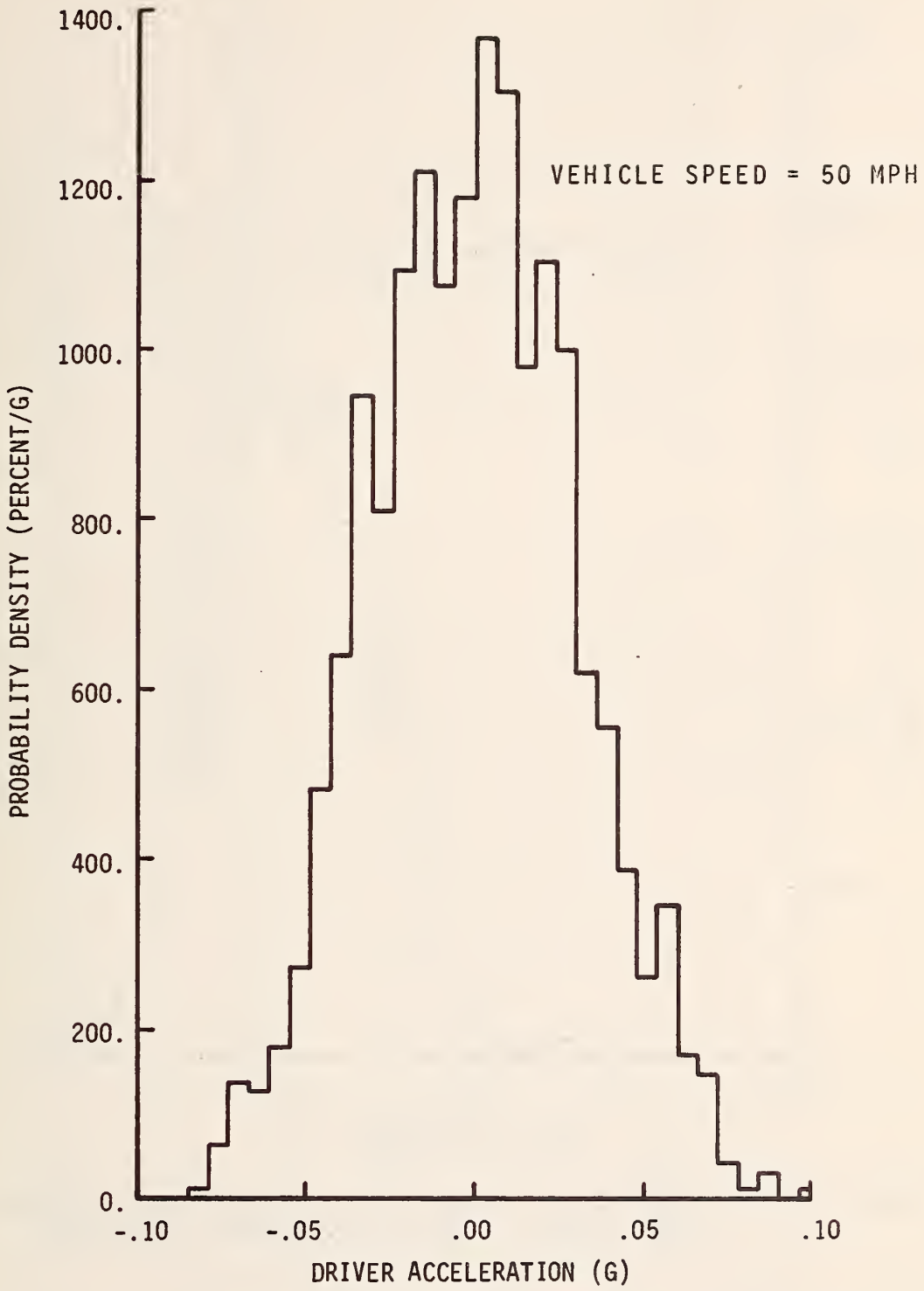

FIGURE 4.52 PROBABILITY DENSITY OF DRIVER ACCELERATION WITH SHOCKS - LINDBERG ROAD

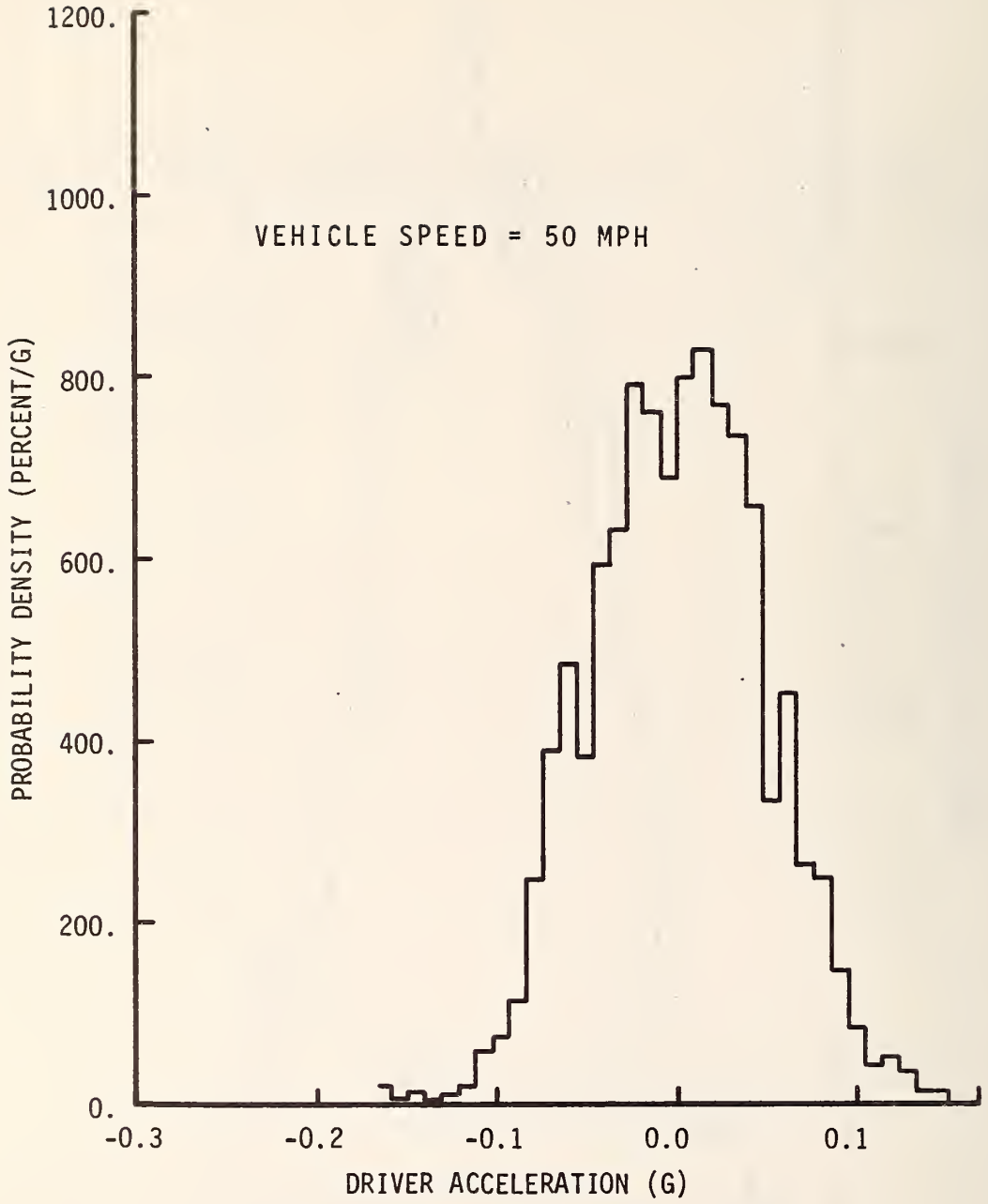

FIGURE 4.53 PROBABILITY DENSITY OF DRIVER ACCELERATION WITH SHOCKS - SOUTH RIVER ROAD (SMOOTH)

TABLE 4.4 SUMMARY OF PROBABILITY DATA FOR VERTICAL ACCELERATION OF AN AUTOMOBILE DRIVER IN AN AUTOMOBILE WITH FRONT AND REAR SHOCK ABSORBERS

ROAD NAME	S* (g's)	PROBABILITY OF OCCURRENCE OF ACCELERATION FOR A GIVEN RANGE OF VALUES OF S								
		± S	± 2S	± 3S	0 to -S	0 to -2S	0 to -3S	0 to +S	0 to +2S	0 to +3S
Road with a Gaussian Distribution	S	68.3	95.4	99.7	34.1	47.7	49.9	34.1	47.7	49.9
South River Road - Rough**	.086	68.8	95.1	99.8	35.9	49.6	51.6	32.9	45.5	48.2
U. S. 52	.035	80.2	96.6	98.6	40.6	48.6	49.2	39.6	48.0	49.4
State Road 26	.086	69.0	94.8	99.3	36.3	48.1	50.8	32.7	46.7	48.5
Cumberland	.076	67.6	95.9	99.6	33.2	48.2	49.9	34.4	47.7	49.7
Lindberg Road	.030	67.1	94.8	99.2	32.4	47.6	49.6	34.7	47.2	49.6
South River Road-Smooth**	.047	67.9	96.3	99.6	32.5	47.5	48.8	35.4	48.8	50.8

* S = Standard deviation of driver acceleration (g's)

** Vehicle heading is west.

The power spectral density curves of the driver acceleration on South River Road (Rough), U. S. 52, State Road 26, Cumberland Avenue, Lindberg Road, and South River Road (Smooth) are shown in Figures 4.54 through 4.59. The shape of the spectrum is usually similar to the spectrum shape which is obtained without the rear shocks. However, the peaks in the spectrum show large reductions in amplitude when the rear shock absorbers are installed.

A subjective evaluation of the ride when all four shocks are installed gives results which are the same as the subjective evaluation of the ride with the rear shocks removed; however, there is a large difference in the degree of objectionableness. This difference is apparent in the reduced amplitudes of gross body movement and in the reduction in the harshness of the ride.

Human tolerance levels for constant amplitude, sinusoidal vibrations are shown in Figures 4.46 and 4.47 which relate driver acceleration to road roughness. These tolerance levels can not be applied directly to the variable amplitude, random vibrations measured in this study. However, these tolerances are valuable reference points.

The roughness of the road may be used as the excitation for a linear mathematical model of the vehicle to evaluate the ride. This excitation was applied to a simple three mass model. The calculated values for driver acceleration are shown in Figure 4.46.

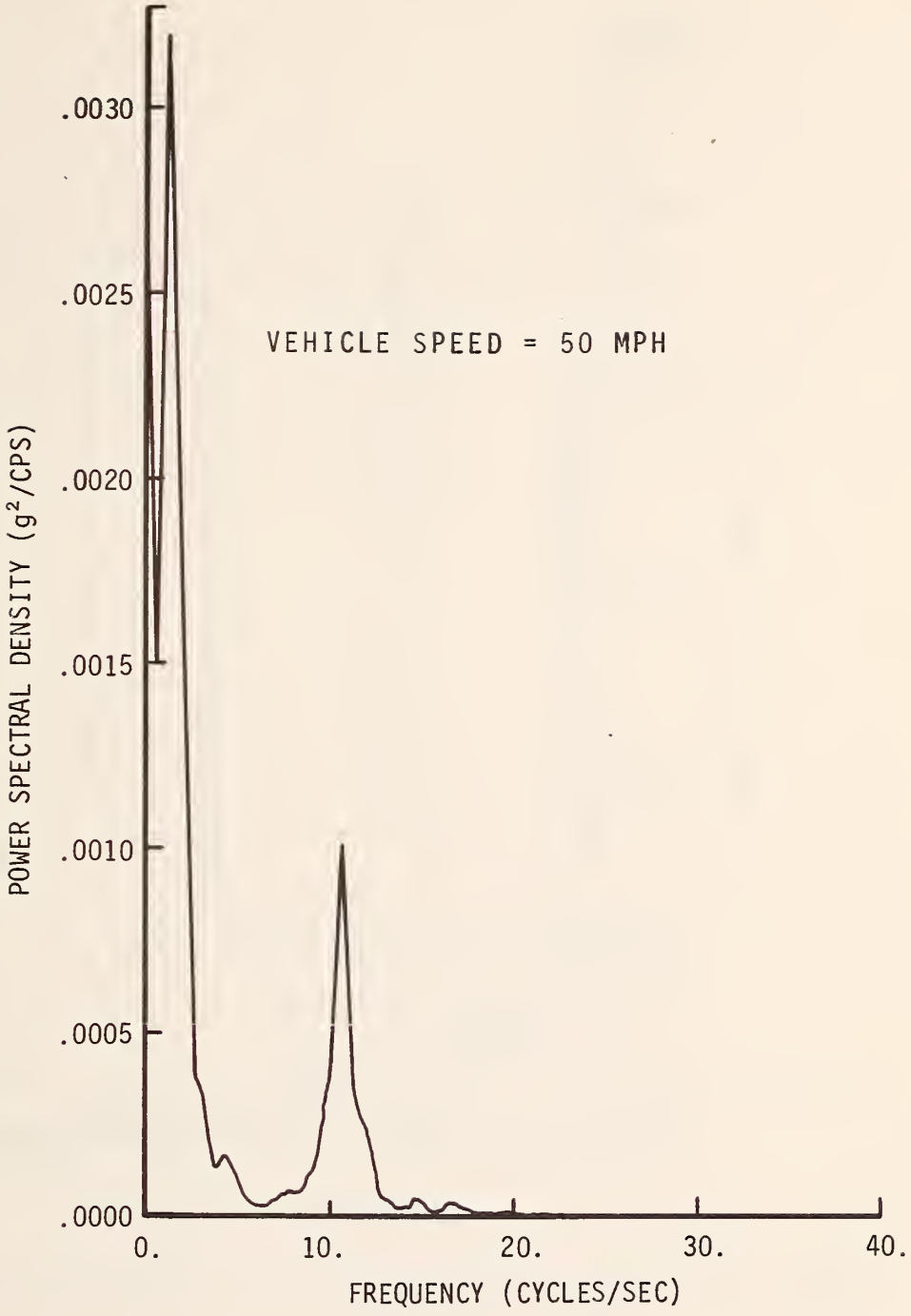

FIGURE 4.54 POWER SPECTRUM OF DRIVER ACCELERATION WITH SHOCKS - SOUTH RIVER ROAD (ROUGH)

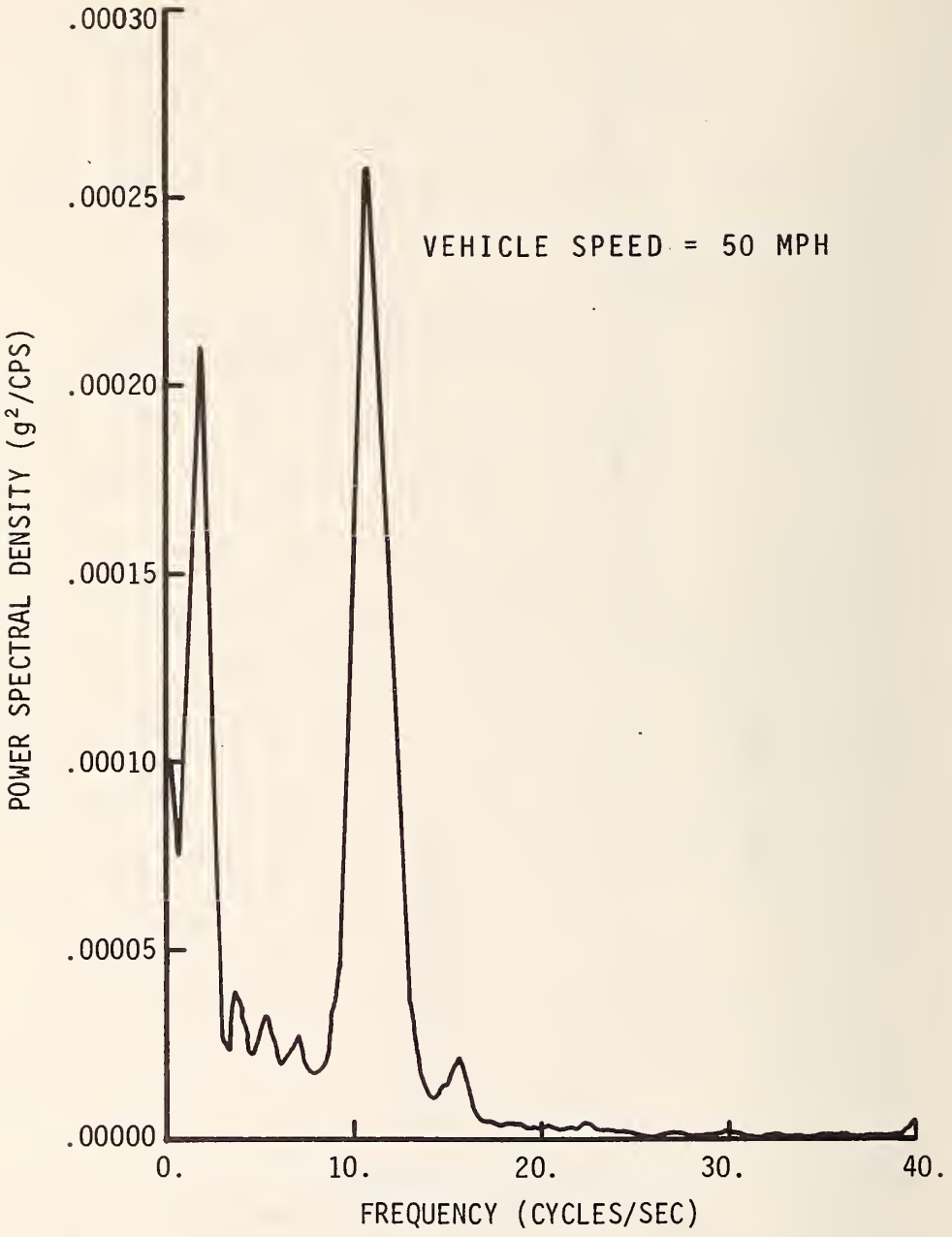

FIGURE 4.55 POWER SPECTRUM OF DRIVER ACCELERATION WITH SHOCKS - U. S. 52

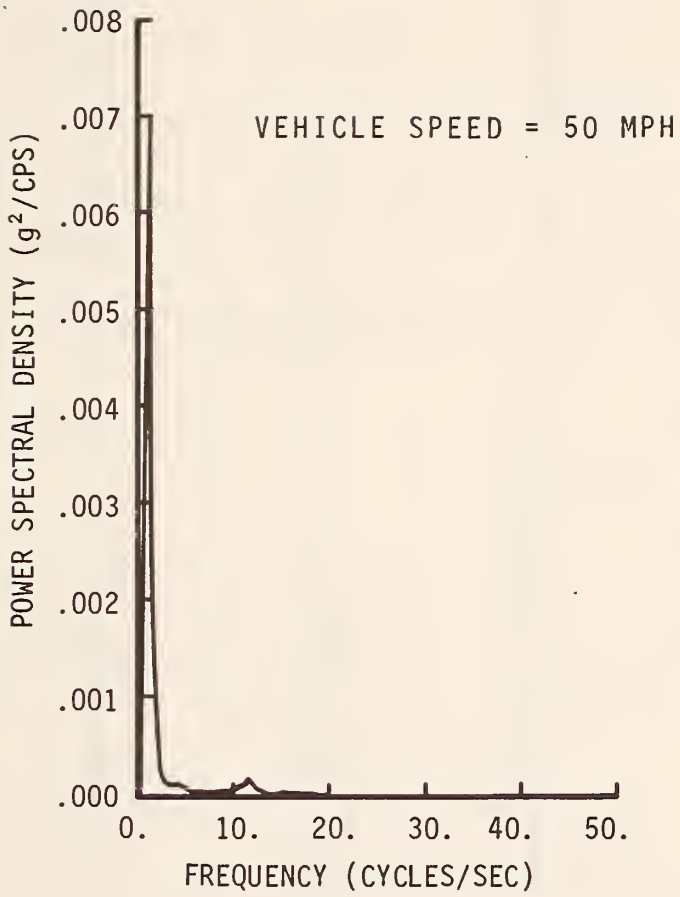

FIGURE 4.56 POWER SPECTRUM OF DRIVER ACCELERATION WITH SHOCKS - S. R. 26

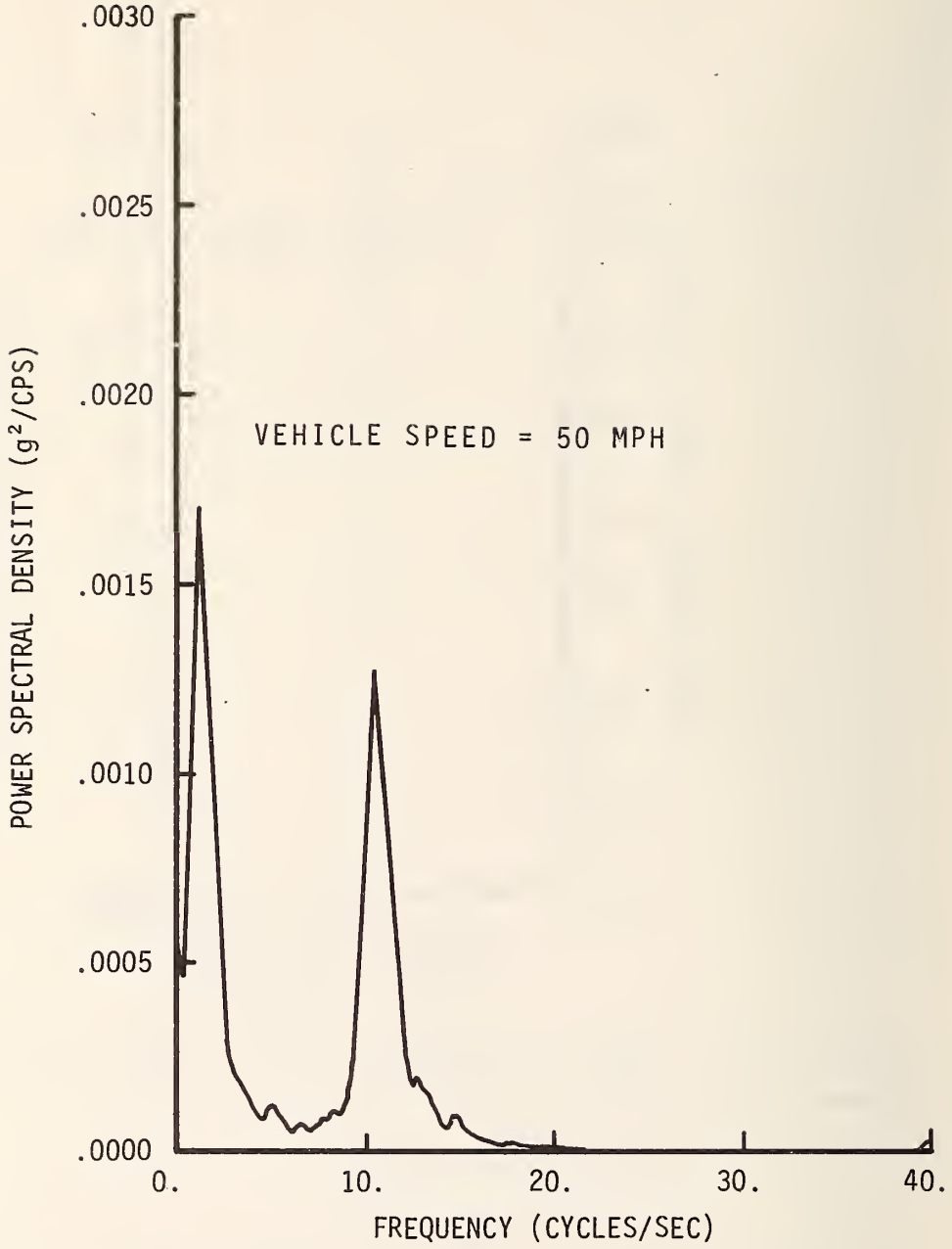

FIGURE 4.57 POWER SPECTRUM OF DRIVER ACCELERATION WITH SHOCKS - CUMBERLAND AVENUE

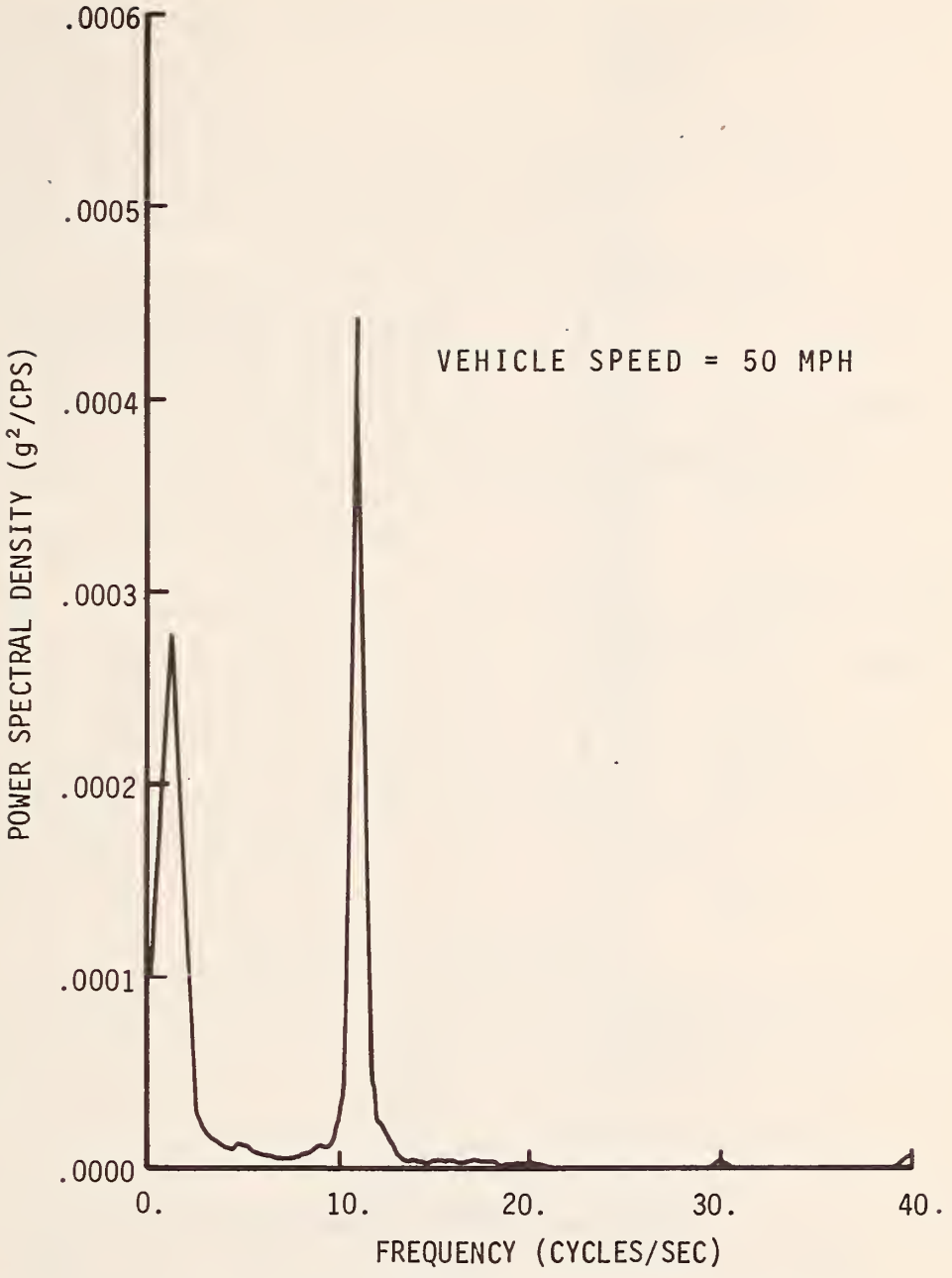

FIGURE 4.58 POWER SPECTRUM OF DRIVER ACCELERATION WITH SHOCKS - LINDBERG ROAD

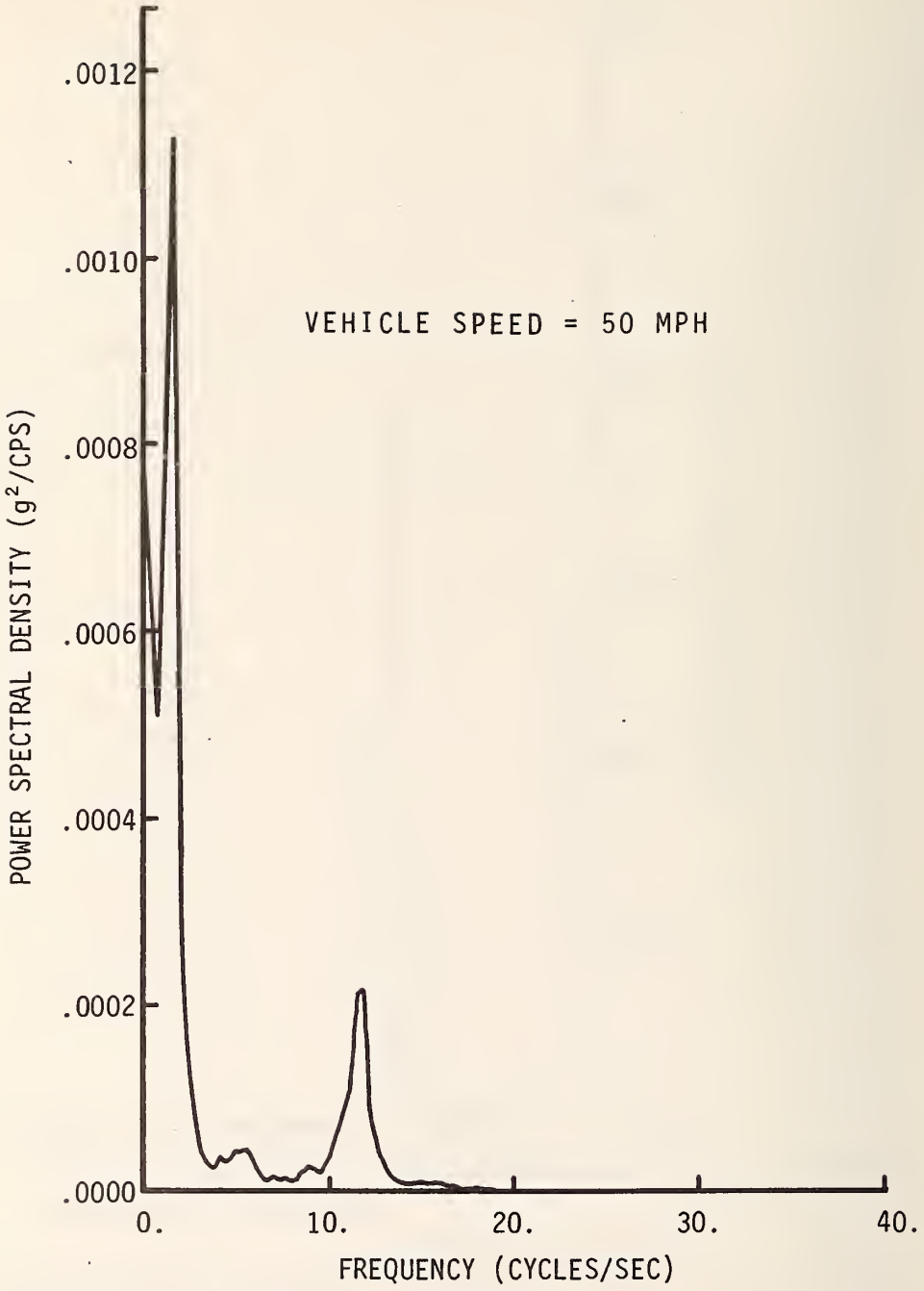

FIGURE 4.59 POWER SPECTRUM OF DRIVER ACCELERATION WITH SHOCKS - SOUTH RIVER ROAD (SMOOTH)

The results of this study of driver acceleration indicate the following:

1- It is feasible to correlate the driver acceleration with the roughness of the road.

2- The driver acceleration in the low frequency range should be evaluated by a different criteria than the driver acceleration in the high frequency range, because these two ranges have different human comfort tolerances.

3- The driver acceleration (or passenger acceleration) will probably serve as a good gauge of road roughness, because it is responsive to the changes in roughness and it identifies roughness problems in two frequency ranges.

Lateral Tire Forces

The lateral tire forces, which can be developed by a vehicle, are a function of the road roughness, the tire characteristics, and the vehicle characteristics. The probability distribution of the normal (vertical) tire force was shown to be reasonably Gaussian by Hildebrand (16). The standard deviation of the normal tire forces on several roads, which were reported by Sattaripour (36), are given in Table 4.1. The probability density distributions for the normal tire forces on State Road 26, U. S. 52, and South River Road (Rough) are shown in Figure 4.60.

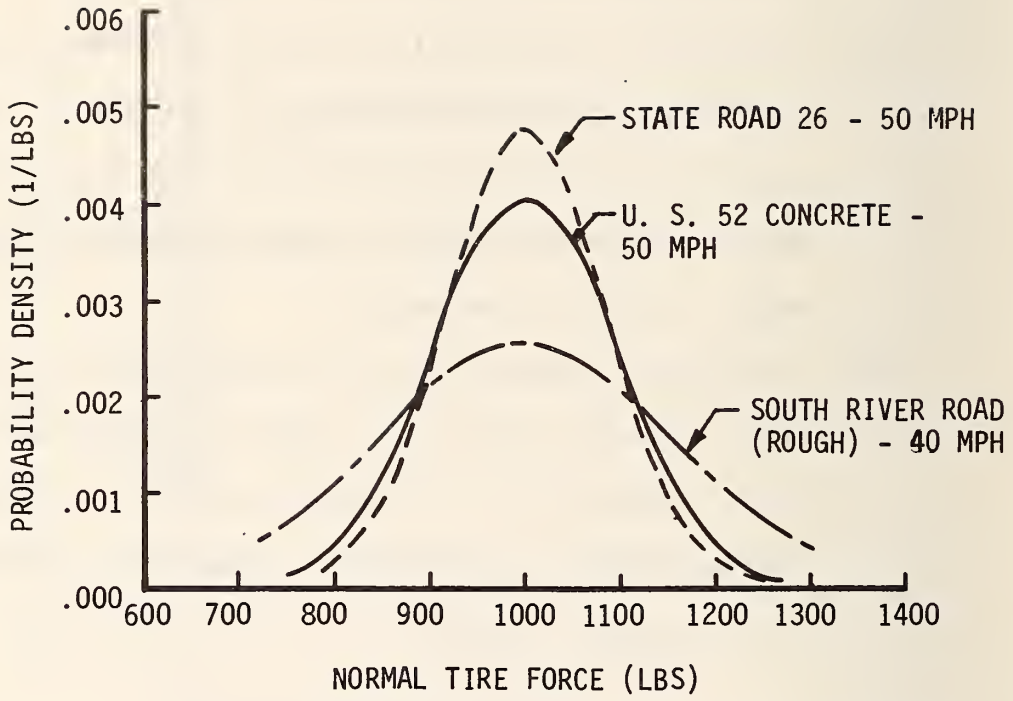

FIGURE 4.60 PROBABILITY DENSITY DISTRIBUTION FOR NORMAL TIRE FORCES

The lateral tire force probability density distribution may be evaluated by using the normal tire force distribution and the tire characteristics (Figure 4.61). The lateral tire force probability density distributions for three roads are shown in Figure 4.62.

The cumulative probability distributions of the lateral tire forces on South River Road (Rough) and State Road 26 are shown in Figure 4.63. The probability of developing a lateral tire force below 340 pounds is 18.5% on South River Road (Rough) and 5.5% on State Road 26 for a two degree tire slip angle and a mean normal load of 1000 pounds. Curves shown in Figures 4.60 and 4.61 provide a means for estimating the probability of encountering lateral forces that may result in loss of control of the vehicle during maneuvers on rough roads.

The tire cornering stiffness, C_α, on a perfectly smooth road would be constant for a fixed tire slip angle, because the normal tire force would be constant. The value of C_α is often assumed to be constant for a given slip angle. The error in the tire lateral force due to neglecting the effect of road roughness on the value of C_α is illustrated in Figure 4.64.

The Use of P and Q to Synthesize a Pavement Profile

The profile of a pavement may be generated from the roughness power spectrum of the pavement by using Rice's

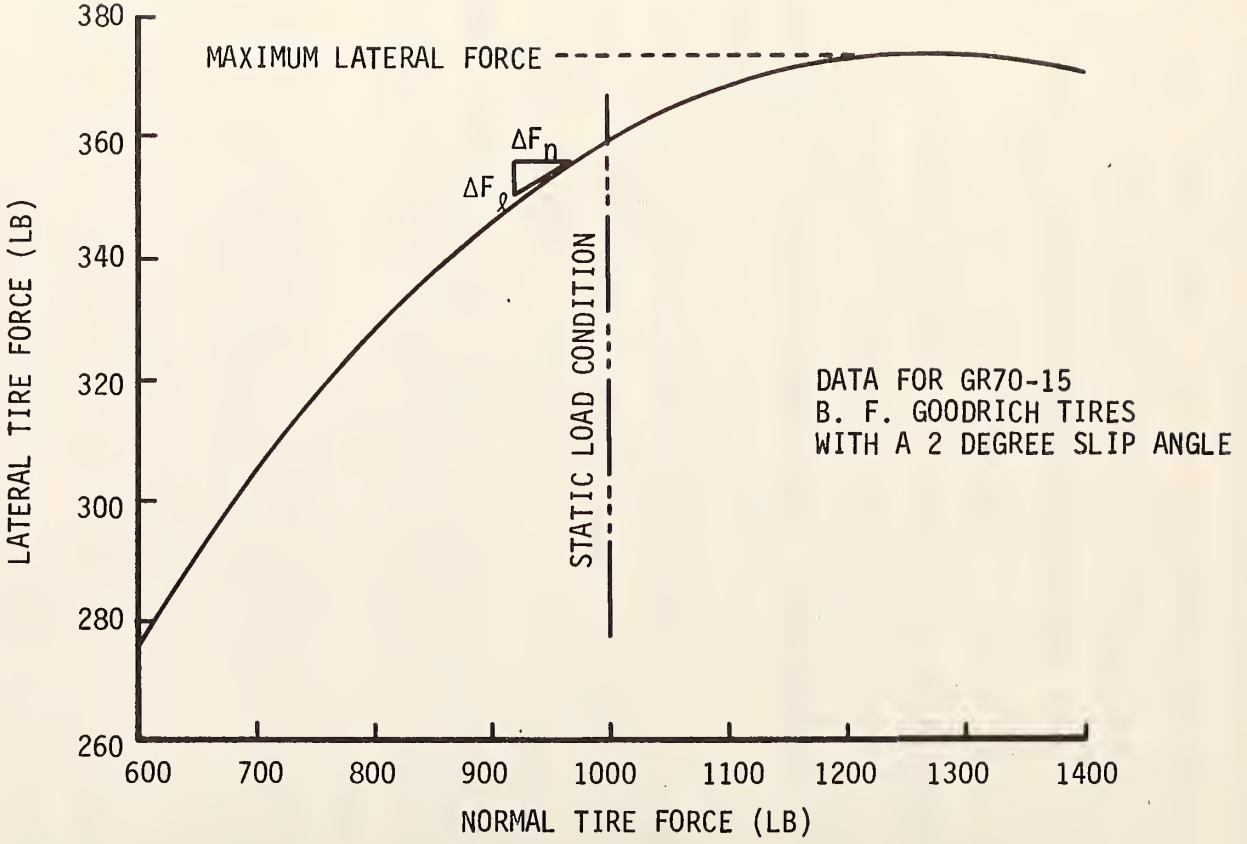

FIGURE 4.61 TIRE CHARACTERISTICS

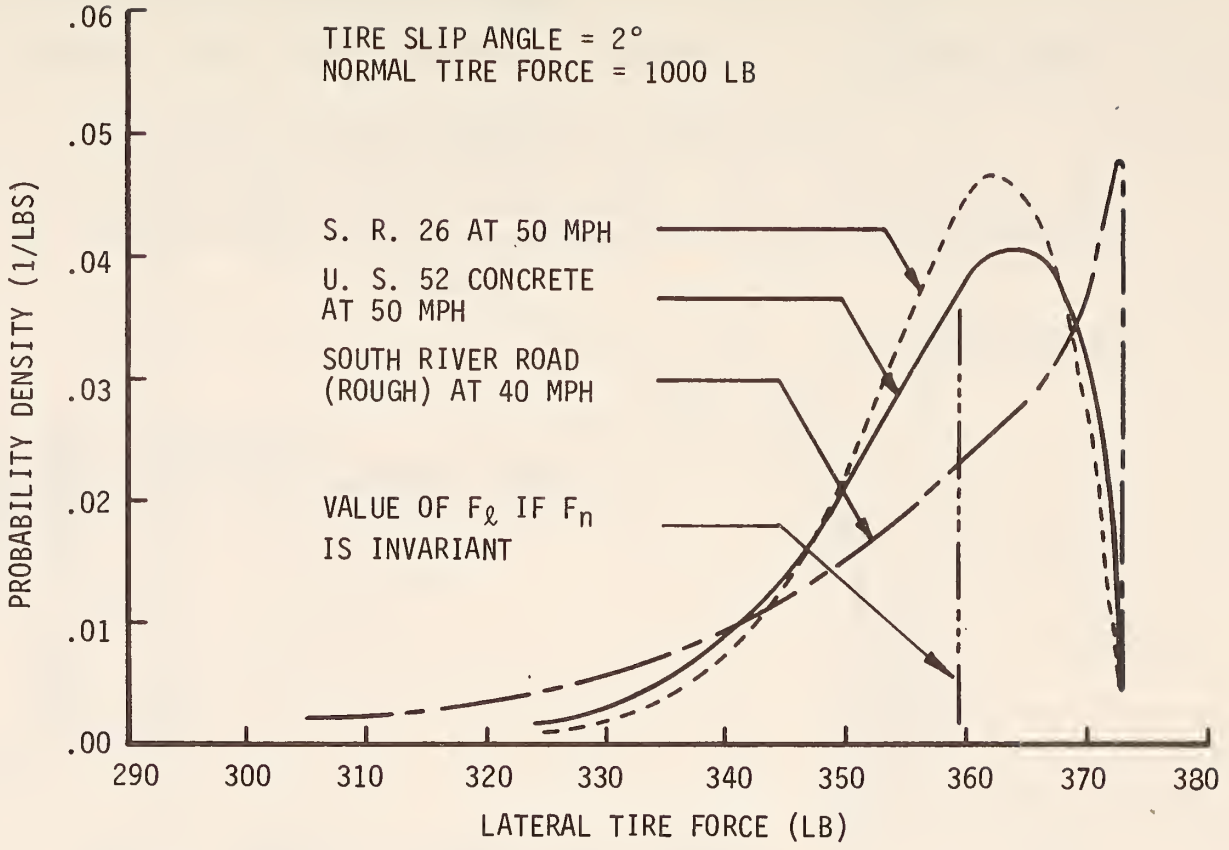

FIGURE 4.62 LATERAL TIRE FORCE PROBABILITY DENSITY DISTRIBUTIONS

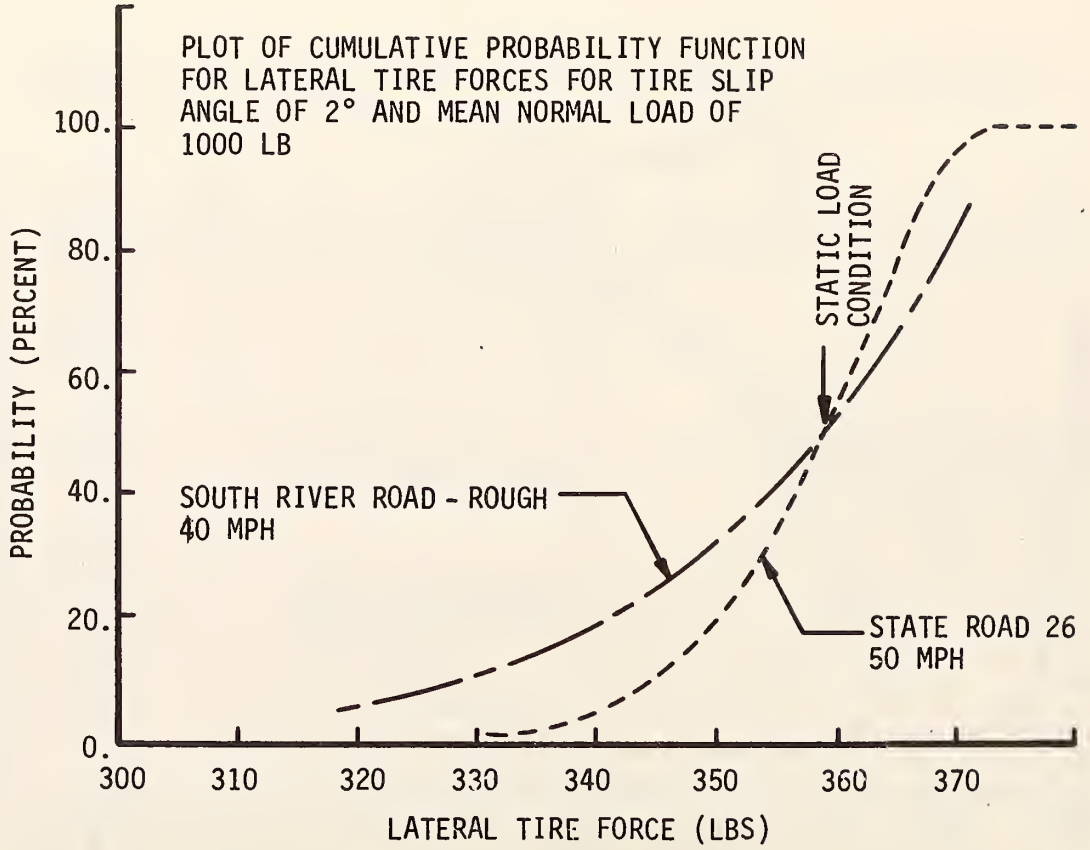

FIGURE 4.63 LATERAL TIRE FORCE CUMULATIVE PROBABILITY DISTRIBUTIONS

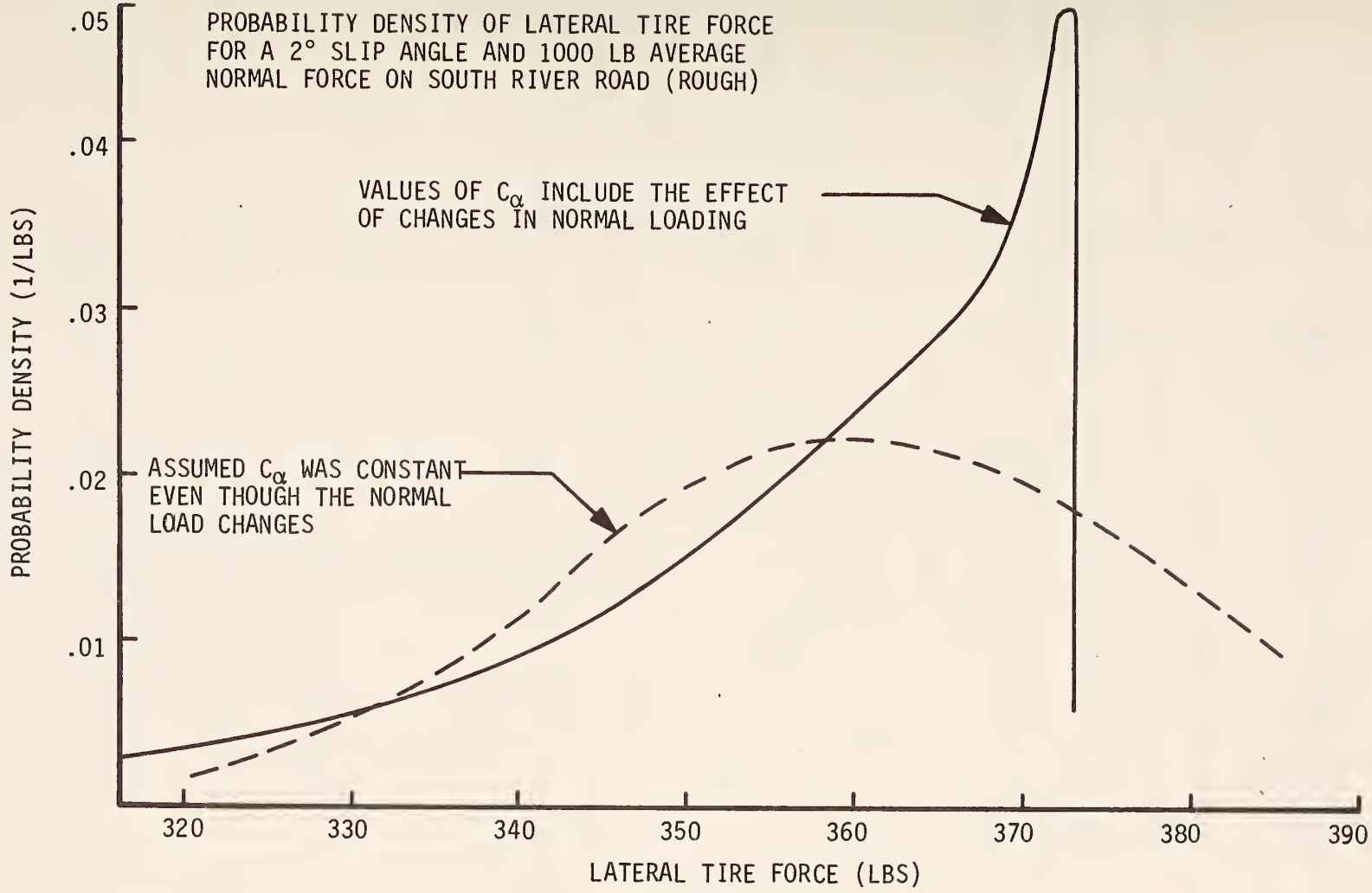

FIGURE 4.64 THE EFFECT OF ROAD ROUGHNESS AND TIRE CORNERING STIFFNESS ON LATERAL TIRE FORCES

equation. The roughness power spectra for certain pavements are available in the form of Zable's Equation, Equation 2.59.

The pavement profile generated with P = -21.6, Q = -4.27 and f_I = 0.005, as previously described, is shown in Figure 4.65. Random numbers with a uniform distribution are used for the phase angle. The probability density distribution and the roughness power spectral density for this generated profile are shown in Figures 4.66 and 4.67 respectively. The power spectral density calculation at high frequencies is very sensitive to the accuracy of the elevation data. The Hanning lag window (6) was used to evaluate the power spectrum.

Rice's Equation may be used to generate pavement elevation values with the same mean square value for roughness, and with the same roughness power spectral density distribution as the parent power spectrum.

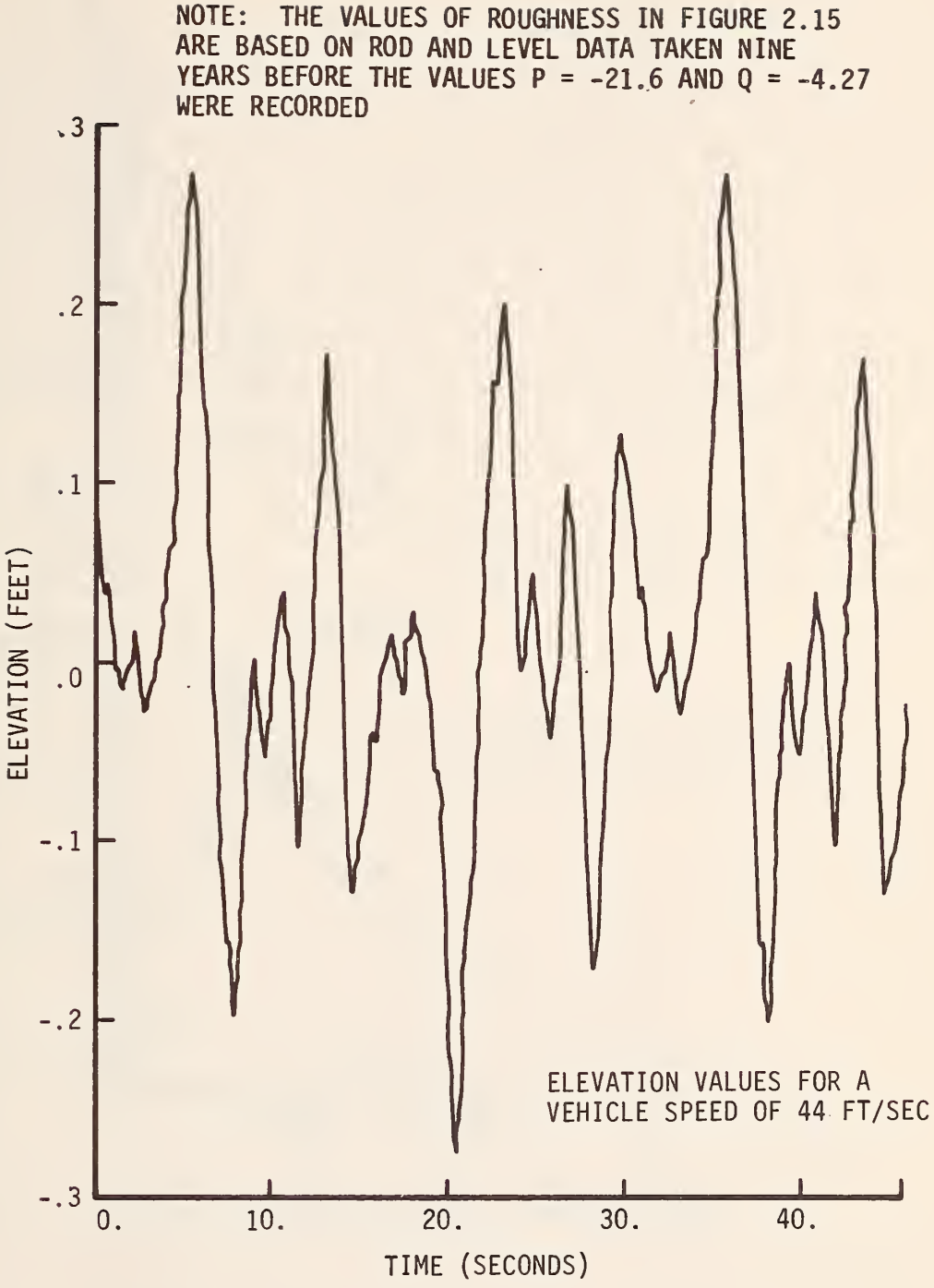

FIGURE 4.65 GENERATED PAVEMENT PROFILE BASED ON P AND Q FOR S. R. 26

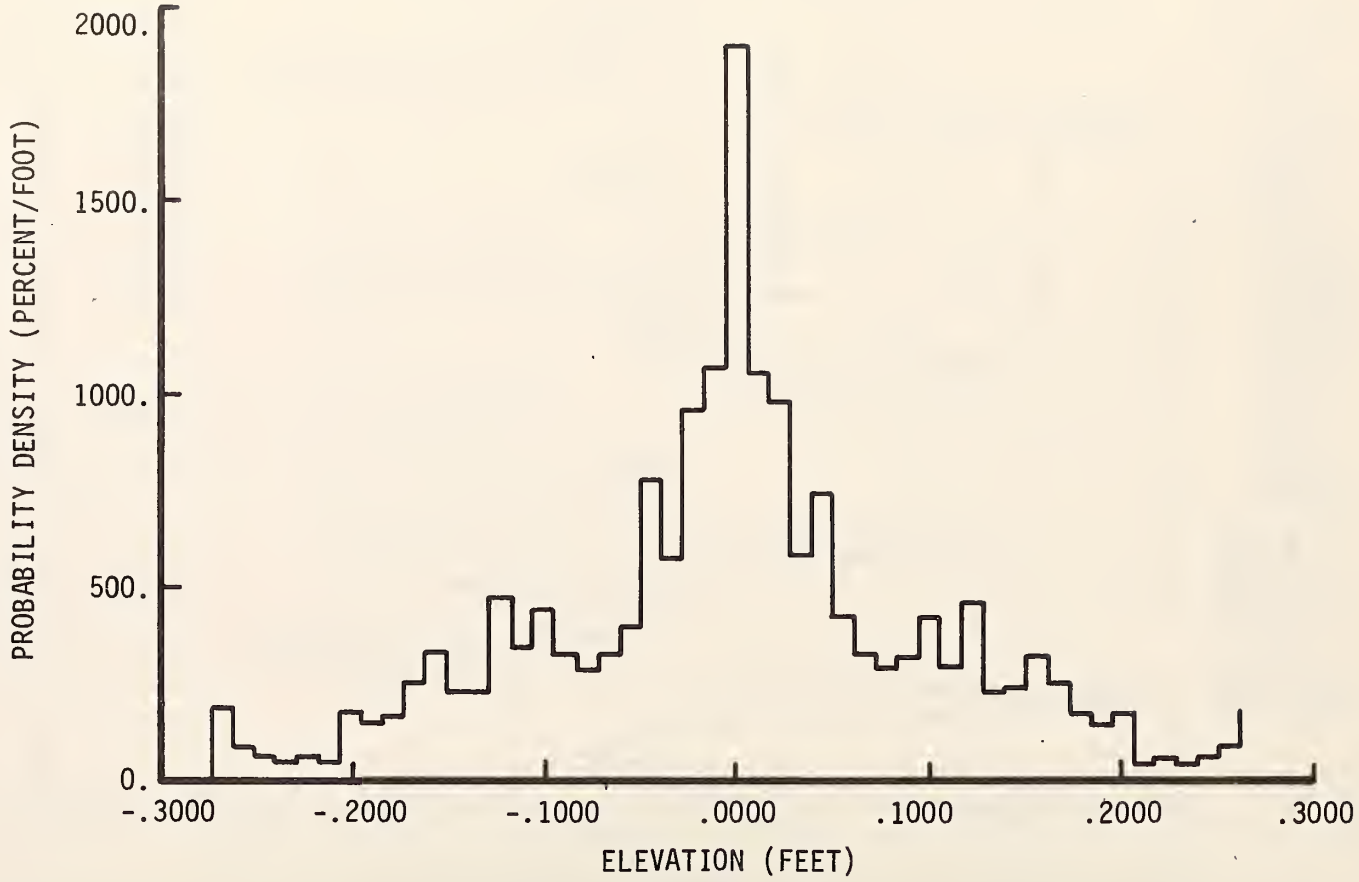

FIGURE 4.66 PROBABILITY DENSITY DISTRIBUTION OF ROUGHNESS FOR GENERATED ELEVATION DATA

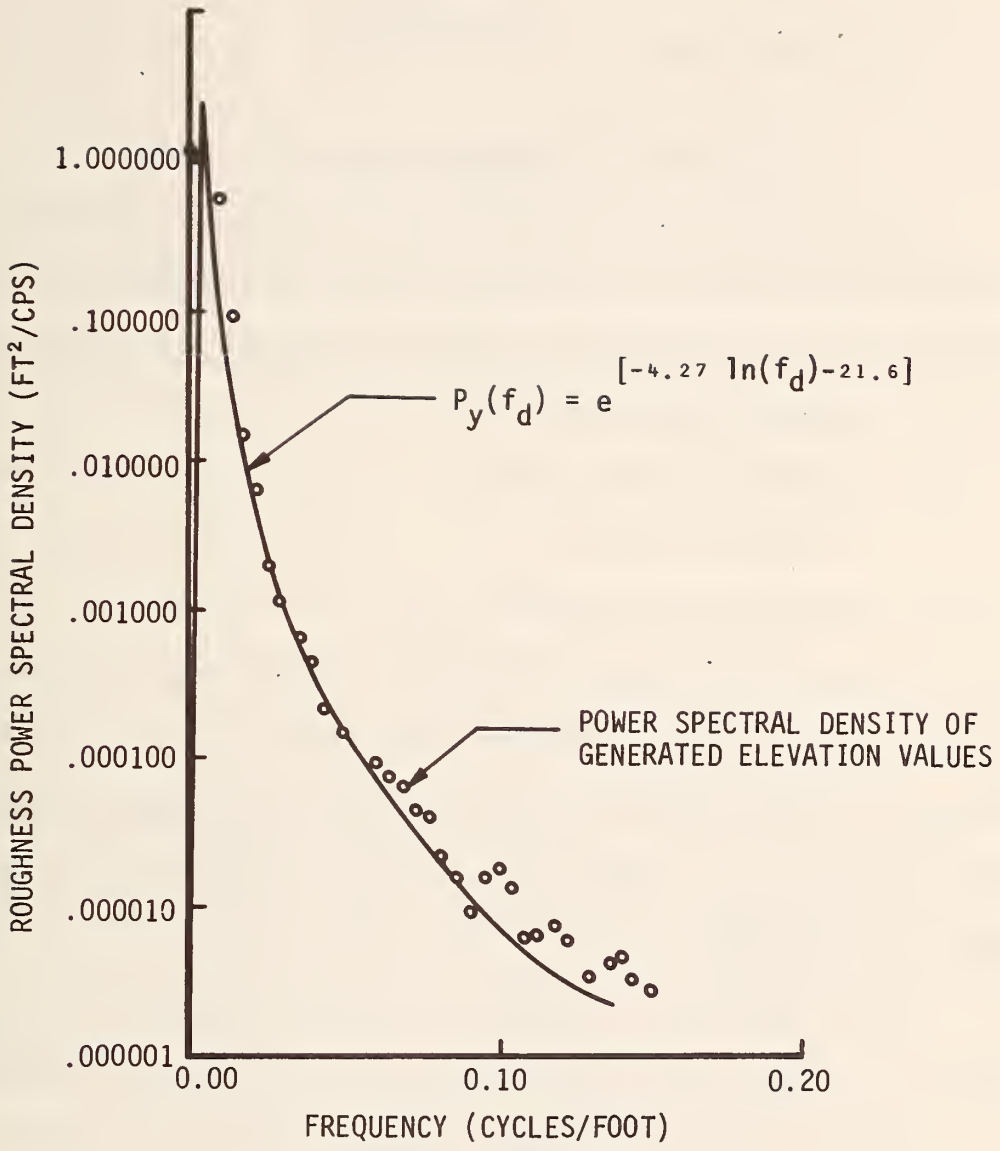

FIGURE 4.67 ROUGHNESS POWER SPECTRUM FOR GENERATED PAVEMENT

CHAPTER 5

CONCLUSIONS

Introduction

This investigation has been concerned with the relationship between road roughness and the behaviour of the vehicle-driver system in terms of the following factors:

1- Steer Angle

2- Steering Wheel Angle

3- Sideslip Angle

4- Driver Acceleration

5- Lateral Tire Forces

6- P and Q of the Zable Equation

In this investigation, the practicality of using each of these factors as an indicator of the roughness of a pavement is evaluated.

The effects of roughness on vehicle behaviour may provide criteria for establishing the allowable roughness of various classes of roads. Those effects of roughness which adversely influence the controllability of the vehicle and the comfort of the operator and passengers are best suited to serve as criteria for roughness. The effects of roughness on the behaviour of the vehicle are highly

dependent upon the vehicle and its operating speed. The measurements of vehicle behaviour in this investigation are based on the characteristics of a 1967 Chevrolet.

Steer Angle and Steering Wheel Angle

The steer angle is affected by oscillation of the front wheel about its kingpin, by deflection of the suspension system, and by wheel hop. Therefore, the steer angle is not a good criterion of road roughness, because a change in the steer angle may not correspond to a change in the direction of the vehicle.

The steering wheel angle serves as a relatively sensitive measure of pavement roughness, and it is a relatively easy quantity to measure. If the mean square value of the steering correction is high, then the mean square value of road roughness will be high. The larger steering wheel angles, which are associated with rougher roads, demonstrate that the operator must exert more effort to control the vehicle on the rougher roads.

Sideslip Angle

The sideslip angle is affected by road roughness, but due to the small magnitude of this angle it is difficult to measure under normal operating conditions. Moreover, large changes in the sideslip angle are usually associated with corresponding changes in the steering wheel angle because of the effort which is exerted by the driver to maintain

control of the vehicle. It appears that other vehicle parameters, such as the steering wheel angle, are easier to measure than the sideslip angle, and these other parameters may be equally as effective as the sideslip angle in demonstrating the effect of road roughness on the controllability of the vehicle.

Vertical Acceleration of the Driver

The vertical acceleration of the driver occurs within two frequency ranges, which are 0.8 to 2.4 cps and 6.0 to 15.0 cps. High vibration amplitudes occur in these two ranges because the natural frequency of the sprung mass of the vehicle and the wheel hop natural frequency occur within these two ranges. The relationship between pavement roughness and driver acceleration in these two frequency ranges may be observed by comparing the areas under the driver acceleration power spectrum curve within these two ranges with the corresponding areas under the roughness power spectrum curve for a given vehicle speed.

Therefore, the vertical acceleration of the driver provides an extremely useful and easily measured criterion for evaluating the allowable pavement roughness, because it is sensitive to roughness in two different ranges of wavelength. The long wavelengths are associated with shifting of the pavement foundation or short hills, and the short wavelengths are associated with small discontinuities, such as pot holes and cracks.

Lateral Tire Force

For a selected tire slip angle, there is more variation in the lateral tire force on a rough road than on a smooth road. Since the controllability of a vehicle depends on the ability to develop lateral forces at the tires, the lateral tire force variation is an important criterion for establishing the allowable level of pavement roughness. The lateral tire force is a relatively difficult quantity to measure, but it can be evaluated analytically for a given slip angle if the tire cornering stiffness values and the normal tire forces are known.

The Use of P and Q to Synthesize a Pavement Profile

The constants P and Q of the Zable Equation are functions of pavement roughness, but the relationship between P and Q and the mean square value of pavement roughness is not a simple relationship. However, P and Q do uniquely establish the roughness spectrum for a given pavement. Values of P and Q may be used to generate a pavement profile; which can be used to obtain time domain response information.

Values of P and Q can serve as criteria for pavement roughness. Values of P and Q are readily obtained with the modified BPR roughometer. However, additional work is required to set the tolerance limits for roughness based on values of P and Q.

Closure

Of the quantities studied in this investigation, the steering wheel angle, the acceleration of the driver, and the lateral tire force appear to have high potential for establishing allowable limits for pavement roughness.

In addition to the three items identified in this investigation, the dynamic tire force should also be considered as a significant factor for establishing allowable levels of pavement roughness.

Throughout this investigation it is apparent that the roughness power spectrum representation of the pavement profile is a valuable aid, because it allows the experimental work on vehicle behaviour to be extended by the use of mathematical models which can thus have measured values of roughness as the input excitation.

BIBLIOGRAPHY

1. Beauchamp, K. G., Signal Processing Using Analog and Digital Techniques, George Allen and Unwin Ltd., London, 1973.

2. Beauvais, F. N., Garelis, C., Iacovoni, D. H., "An Improved Analog for Vehicle Stability Analysis," SAE Paper 295-C, Jan. 1961.

3. Belsdorf, M. R., Rice, R. S., Bird, K. D., "Performance Tasks as Measures of Vehicle Handling Qualities at the Limit of Performance," SAE Paper 710081, 1971.

4. Bendat, J. S. and Piersol, A. G., Measurement and Analysis of Random Data, John Wiley & Sons Inc., New York, 1966.

5. Bergman, W., "Measurement and Subjective Evaluation of Vehicle Handling," SAE Paper 730492, 1973.

6. Blackman, R. B. and Tukey, J. W., The Measurement of Power Spectra, Dover Publications, New York, 1959.

7. Bundorf, R. T., "A Primer on Vehicle Directional Control," General Motors Engineering Staff Publication A-2730, 1968.

8. Bundorf, R. T., "The Influence of Vehicle Design Parameters on Characteristic Speed and Understeer," General Motors Engineering Staff Publication 3203.

9. Bundorf, R. T., Pollock, D. E., and Hardin, M. C., "Vehicle Handling Response to Aerodynamic Inputs," SAE Paper 716B, June 1963.

10. Butkunas, A. A., "Power Spectral Density and Ride Evaluation," SAE Paper 660138, 1966.

11. Carey, W. N., Jr. and Irick, P. E., "The Pavement Serviceability - Performance Concept," Highway Research Board Bull. 250, 40-58, 1960.

12. DeVries, T. W., "A Statistical Method for Estimating Dynamic Vehicle Loads on Highways," Ph.D. Thesis, Purdue University, 1961.

13. Gronberg, G. D., "Use of Pavement Condition Data in Highway Planning and Road Life Studies," Highway Research Record Number 40, 1963.

14. Hamilton, J. F., "Determination of Vehicle Characteristics Influencing Dynamic Reactions on Highways," Ph.D. Thesis, Purdue University, 1963.

15. Hansson, J. E., Sjøflot, L., Suggs, C. W., "Matching the Farm Machine to Operator's Capabilities and Limitations," Implement and Tractor, Aug. 21, 1970.

16. Hildebrand, S. E., "The Effect of Pavement Roughness on Safe Vehicle Handling Characteristics," M. S. Thesis, Purdue University, 1971, PB 180 600.*

17. Holbrook, L. F., "Prediction of Subjective Response to Road Roughness by Use of the Rapid Travel Profilometer," Highway Research Record Number 291, 1969.

18. Hudson, W. R., "High Speed Road Profile Equipment Evaluation," Highway Research Record Number 189, 1967.

19. Hveem, F. N., "Devices for Recording and Evaluating Pavement Roughness," Highway Research Board Bulletin 264, 1960.

20. Ingimarsson, G. R., "Computation of True Highway Elevations from an Elevation Profilometer," Highway Research Record Number 46, 1963.

21. James, M. L., Smith, G. M., Wolford, J. C., Applied Numerical Methods for Digital Computation with Fortran, International Textbook Company, Scranton, Pennsylvania, 1967.

22. Janeway, R. N., "A Practical Approach to Truck Ride Instrumentation and Evaluation - A Summary," SAE Paper 660140, SAE Transactions, 1967.

23. Janeway, R. N., LeFevre, W., Oswald, W. C., Versace, J., "Ride and Vibration Data Manual - SAE J6a," SAE Vehicle Dynamics Committee, Dec., 1965.

24. Jones, B. J., Flinn, R. H., Hammond, E. C., "Fatigue and Hours of Service of Interstate Truck Drivers," U. S. Public Health Service, 1941.

25. McHenry, R. R. and DeLeys, N. J., "Vehicle Dynamics in Single Vehicle Accidents - Validation and Extensions of a Computer Simulation," CAL Report Number VJ-2251-V-3, Cornell Aeronautical Laboratory, Inc., Dec. 1968.

26. Milliken, W. F., Whitcomb, D. W., Segel, L., et al., "Research in Automobile Stability and Control and in Tyre Performance," Institute of Mechanical Engineers, London, 1956.

27. Mola, S., Fundamentals of Vehicle Dynamics, General Motors Institute, 1969.

28. Morgan, C. T., Cook, J. S., Chapanis, A., Lund, M. W., Human Engineering Guide to Equipment Design, McGraw-Hill Book Co., New York, 1963.

29. Nakamura, V. F., and Michael, H. L., "Serviceability Rating of Highway Pavements," Highway Research Record Number 40, Jan. 1963.

30. Papoulis, A., Probability, Random Variables and Stochastic Processes, McGraw-Hill Book Co., New York, 1965.

31. Quinn, B. E., Hagen, K., "Problems Encountered in Using Elevation Power Spectra as Criteria of Pavement Condition," Highway Research Record Number 189, 1967.

32. Rasmussen, R. E., Hill, F. W., and Riede, P. M., "Typical Vehicle Parameters for Dynamics Studies," A-2542, General Motors Proving Grounds, April 1970.

33. Rice, S. O., "Mathematical Analysis of Random Noise," Bell System Technical Journal, Vol. 23, 1944, and Vol. 24, 1945.

34. Rizenbergs, R. L., "Accelerometer Method of Riding Quality Testing - An Interim Report," Kentucky Department of Highways Research Report, KYHPR-64-24; HPS-HPR-1(26), Feb., 1965.

35. SAE Committee, "Vehicle Dynamics Terminology," SAE Recommended Practice SAE J670a, 1965.

36. Quinn, B. E. and Sattaripour, S. A., "Measurement and Prediction of the Dynamic Tire Forces of a Passenger Vehicle on a Highway," Report No. FHWA-RD-72-26, PB 221 120.*

37. Quinn, B. E. And Smeyak, L. M., "Measuring Pavement Roughness Spectra Using the Modified BPR Roughometer with Additional Refinements," Report No. FHWA-RD-72-27, PB 223 695/AS.*

38. Steeds, W., Mechanics of Road Vehicles, Iliffe and Sons, Ltd., London, 1960.

39. Tsao, M. C., "The Skidding of Vehicles: A Dynamic Analysis," Ph.D. Thesis, Carnegie-Mellon University, 1969.

40. Van Deusen, B. D., "Analytical Techniques for Designing Riding Quality into Automotive Vehicles," SAE Paper 670021, 1967.

41. Van Deusen, B. D., "Human Response to Vehicle Vibration," SAE Paper 680090, 1968.

42. Yoder, E. J., "Comparison of Different Methods of Measuring Pavement Condition - Interim Report," National Cooperative Highway Research Program Report 7, HRB, 1964.

43. Zable, J., "Design of a Linear Vibrating System to Measure Low Frequency Random Excitation," Ph.D. Thesis, Purdue University, 1969.

*Available to the public through the National Technical Information Service, Springfield, Virginia 22161.

APPENDIX A

DERIVATION OF A MATHEMATICAL MODEL FOR RIDE

The ride of a vehicle may be investigated with a mathematical model which uses the road roughness as the excitation. The simplified model shown in Figure 2.10 will provide some insight into the vertical acceleration of the driver. This model is sensitive to the bounce mode of body motion and to wheel hop. It is based on the assumption that the road excitation at all four tires is identical at any given time.

The following three equations of motion for this system were obtained by applying Newton's Law for the summation of the vertical forces:

$$M_1\ddot{y}_1 = K_1(y_0-y_1) + C_1(\dot{y}_0-\dot{y}_1) - K_2(y_1-y_2) - C_2(\dot{y}_1-\dot{y}_2), \tag{A.1}$$

$$M_2\ddot{y}_2 = K_2(y_1-y_2) + C_2(\dot{y}_1-\dot{y}_2) - K_3(y_2-y_3) - C_3(\dot{y}_2-\dot{y}_3), \tag{A.2}$$

$$M_3\ddot{y}_3 = K_3(y_2-y_3) + C_3(\dot{y}_2-\dot{y}_3). \tag{A.3}$$

This system is assumed to be a linear system. These three equations can be expressed in terms of frequency, ω, by taking the Laplace Transform with zero initial conditions

and then replacing S by $j\omega$. This transformation produces the following three algebraic equations:

$$Y_1[(K_1+K_2-M_1\omega^2) + j\omega(C_1+C_2)] = (K_1+j\omega C_1)Y_0 + (K_2+j\omega C_2)Y_2 \ , \tag{A.4}$$

$$Y_2[(K_2+K_3-M_2\omega^2) + j\omega(C_2+C_3)] = (K_2+j\omega C_2)Y_1 + (K_3+j\omega C_3)Y_3 \ , \tag{A.5}$$

$$Y_3[(K_3-M_3\omega^2) + j\omega C_3] = (K_3+j\omega C_3)Y_2 \ . \tag{A.6}$$

These three algebraic equations may be expressed in exponential form. This change in form is facilitated by substitution of variables A_i and T_i for the amplitude and phase angle of each complex term of these equations, where

$$A_i = \left[[\text{Real Part}]^2 + [\text{Imaginary Part}]^2\right]^{\frac{1}{2}}$$

and

$$T_i = \text{Tan}^{-1}\left[\frac{\text{Imaginary Part}}{\text{Real Part}}\right].$$

For Equation A.4, let

$$A_1 = \left[[K_1+K_2-M_1\omega^2]^2 + [(C_1+C_2)\omega]^2\right]^{\frac{1}{2}} \ ,$$

$$T_1 = \text{Tan}^{-1}\left[\frac{(C_1+C_2)\omega}{K_1+K_2-M_1\omega^2}\right] \ ,$$

$$A_2 = \left[[K_1]^2 + (C_1\omega)^2\right]^{\frac{1}{2}} \ ,$$

$$T_2 = \text{Tan}^{-1}\left[\frac{C_1\omega}{K_1}\right]$$

$$A_3 = \left[[K_2]^2 + [C_2\omega]^2 \right]^{\frac{1}{2}}$$

and

$$T_3 = \text{Tan}^{-1} \left[\frac{C_2\omega}{K_2} \right] .$$

For Equation A.5, let

$$A_4 = \left[[K_2+K_3-M_2\omega^2]^2 + [(C_2+C_3)\omega]^2 \right]^{\frac{1}{2}} ,$$

$$T_4 = \text{Tan}^{-1} \left[\frac{(C_2+C_3)\omega}{K_2+K_3-M_2\omega^2} \right] ,$$

$$A_6 = \left[[K_3]^2 + [C_3\omega]^2 \right]^{\frac{1}{2}}$$

and

$$T_6 = \text{Tan}^{-1} \left[\frac{C_3\omega}{K_3} \right] .$$

For Equation A.6, let

$$A_7 = \left[(K_3-M_3\omega^2)^2 + (C_3\omega)^2 \right]^{\frac{1}{2}}$$

and

$$T_7 = \text{Tan}^{-1} \left[\frac{C_3\omega}{K_3-M_3\omega^2} \right] .$$

Substitution of these new variables into the three algebraic equations gives the following equations in exponential form:

$$A_1 e^{T_1} Y_1 = A_2 e^{T_2} Y_0 + A_3 e^{T_3} Y_2 , \qquad (A.7)$$

$$A_4 e^{T_4} Y_2 = A_3 e^{T_3} Y_1 + A_6 e^{T_6} Y_3 , \qquad (A.8)$$

$$A_7 e^{T_7} Y_3 = A_6 e^{T_6} Y_2 . \qquad (A.9)$$

The frequency response relationship between Y_3 and Y_2 is obtained from Equation A.9 as

$$\frac{Y_3}{Y_2} = \frac{A_6}{A_7} e^{(T_6-T_7)} . \qquad (A.10)$$

The combination of Equations A.8 and A.10 gives the frequency response relationship between Y_1 and Y_2 in the form

$$\frac{Y_2}{Y_1} = \frac{A_3 e^{T_3}}{\left[A_4 e^{T_4} - \frac{(A_6)^2}{A_7} e^{(2T_6-T_7)}\right]} . \qquad (A.11)$$

Substitution of Equation A.11 into Equation A.7 gives the frequency response relationship between the vertical displacement of the wheels and a change in road roughness by the equation

$$\frac{Y_1}{Y_0} = \frac{A_2 e^{T_2}}{\left[A_1 e^{T_1} - \frac{(A_3)^2 e^{2T_3}}{A_4 e^{T_4} - \frac{(A_6)^2}{A_7} e^{(2T_6-T_7)}}\right]} . \qquad (A.12)$$

Equations A.10, A.11, and A.12 may be multiplied together to give the frequency response relationship between the vertical displacement of the driver and a change in road roughness in the form

$$\frac{Y_3}{Y_0} = \left[\frac{A_6}{A_7}\, e^{(T_6-T_7)}\right] \left[\frac{A_3\, e^{T_3}}{A_4\, e^{T_4} - \frac{(A_6)^2}{A_7}\, e^{(2T_6-T_7)}}\right]$$

$$\left[\frac{A_2\, e^{T_2}}{A_1\, e^{T_1} - \frac{(A_3)^2\, e^{2T_3}}{A_4\, e^{T_4} - \frac{(A_6)^2}{A_7}\, e^{(2T_6-T_7)}}}\right] . \qquad (A.13)$$

This equation may be simplified by using the following terms

$$A_{32} = \frac{A_6}{A_7} ,$$

$$T_{32} = T_6 - T_7 ,$$

$$A_{10} = \left[[A_4\mathrm{Cos}(T_4) - A_6A_{32}\mathrm{Cos}(T_6+T_{32})]^2 + [A_4\mathrm{Sin}(T_4) - A_6A_{32}\mathrm{Sin}(T_6+T_{32})]^2\right]^{\frac{1}{2}} ,$$

and

$$T_{10} = \mathrm{Tan}^{-1}\left[\frac{A_4\mathrm{Sin}(T_4) - A_6A_{32}\mathrm{Sin}(T_6+T_{32})}{A_4\mathrm{Cos}(T_4) - A_6A_{32}\mathrm{Cos}(T_6+T_{32})}\right] .$$

Therefore, Equation A.13 takes the form

$$\frac{Y_3}{Y_0} = \left[A_{32}\, e^{T_{32}}\right] \left[\frac{A_3\, e^{T_3}}{A_{10}\, e^{T_{10}}}\right] \left[\frac{A_2\, e^{T_2}}{A_1\, e^{T_1} - \frac{(A_3)^2\, e^{2T_3}}{A_{10}\, e^{T_{10}}}}\right] . \qquad (A.14)$$

Let

$$A_{17} = \left[\left(A_1 \mathrm{Cos}(T_1) - \frac{(A_3)^2}{A_{10}} \mathrm{Cos}(2T_3 - T_{10})\right)^2 + \left(A_1 \mathrm{Sin}(T_1) - \frac{(A_3)^2}{A_{10}} \mathrm{Sin}(2T_3 - T_{10})\right)^2\right]^{\frac{1}{2}} ,$$

$$T_{17} = \mathrm{Tan}^{-1} \left[\frac{A_1 \mathrm{Sin}(T_1) - \frac{(A_3)^2}{A_{10}} \mathrm{Sin}(2T_3 - T_{10})}{A_1 \mathrm{Cos}(T_1) - \frac{(A_3)^2}{A_{10}} \mathrm{Cos}(2T_3 - T_{10})}\right] ,$$

$$A_{31} = \frac{A_{32}\, A_3\, A_2}{A_{10}\, A_{17}} ,$$

and

$$T_{31} = T_{32} + T_3 + T_2 - T_{17} - T_{10} .$$

Substitution of these four relationships into Equation A.14 will give an expression for the frequency response of the vertical displacement of the driver, Y_3, for a given change in road profile, Y_0, in the form

$$\frac{Y_3}{Y_0} = A_{31}\, e^{T_{31}} . \qquad (A.15)$$

For a sinusoidal excitation, the peak amplitude of acceleration, $\ddot{Y}_{3max}$, is given by the equation

$$\ddot{Y}_{3max} = \omega^2 Y_3 \ , \qquad (A.16)$$

where

ω = the steady state excitation frequency (rad/sec)

Y_3 = the peak amplitude of driver displacement (inches).

The magnitude ratio for driver acceleration and road roughness may be obtained from Equations A.15 and A.16 as follows

$$\left| \frac{\ddot{Y}_3 \ (f)}{Y_0 \ (f)} \right| = \omega^2 \ A_{31} \ .$$

APPENDIX B

BICYCLE MODEL FOR STUDY OF STEADY STATE VEHICLE RESPONSE IN A CIRCULAR PATH

The simplified bicycle model (7) is used to obtain an equation for the sideslip angle in this appendix. This derivation is based on motion of the bicycle model in a circular path at constant velocity. The simplified bicycle model consists of a single mass and two wheels as shown in Figure B.2. This mathematical model has been used for preliminary investigations concerning the dynamic behaviour of an automobile.

The sum of the moments about the front axle in Figure B.1 gives the rear ground reaction

$$2\ W_r = \frac{a}{a + b}\ W_t\ . \qquad (B.1)$$

The quantities $2\ W_r$, $2\ W_f$, $2\ F_{\ell r}$, and $2\ F_{\ell f}$ are used because the mathematical model has two wheels instead of four.

The sum of the moments about the front axle in Figure B.2 gives the lateral force on the rear tire

$$2\ F_{\ell r} = \frac{a\ W_t}{(a+b)g}\ \frac{V_{CG}^2}{R_c}\ . \qquad (B.2)$$

a = Distance from front axle to center of gravity of vehicle (inches)

b = Distance from rear axle to center of gravity of vehicle (inches)

$2W_f$ = The reaction of the ground on the front wheel of the bicycle model (lbs)

$2W_r$ = The reaction of the ground on the rear wheel of the bicycle model (lbs)

W_t = The total weight of the vehicle (lbs)

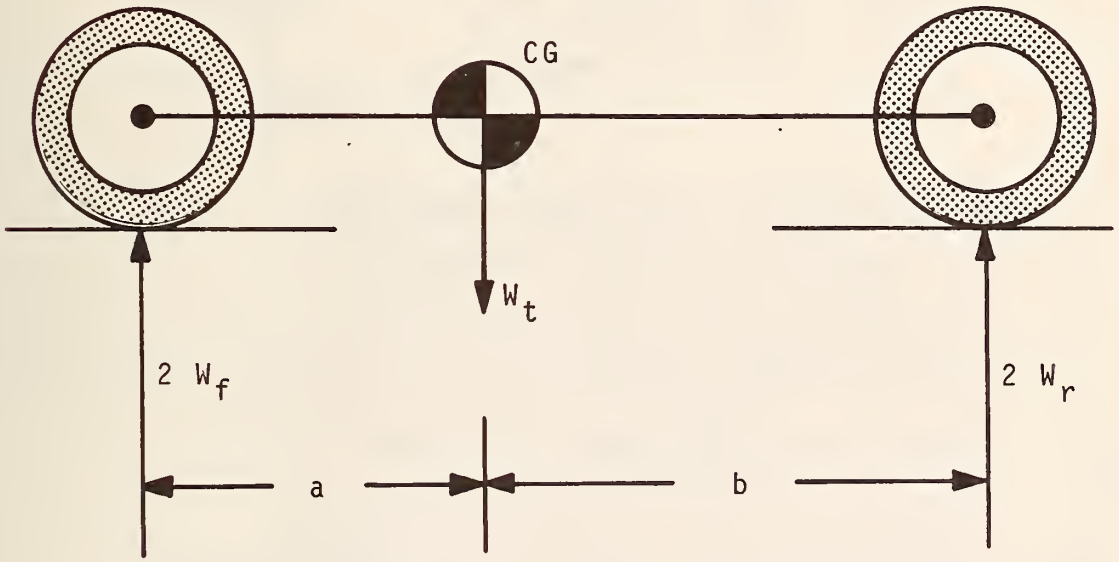

FIGURE B.1 THE BICYCLE MODEL - SIDE VIEW

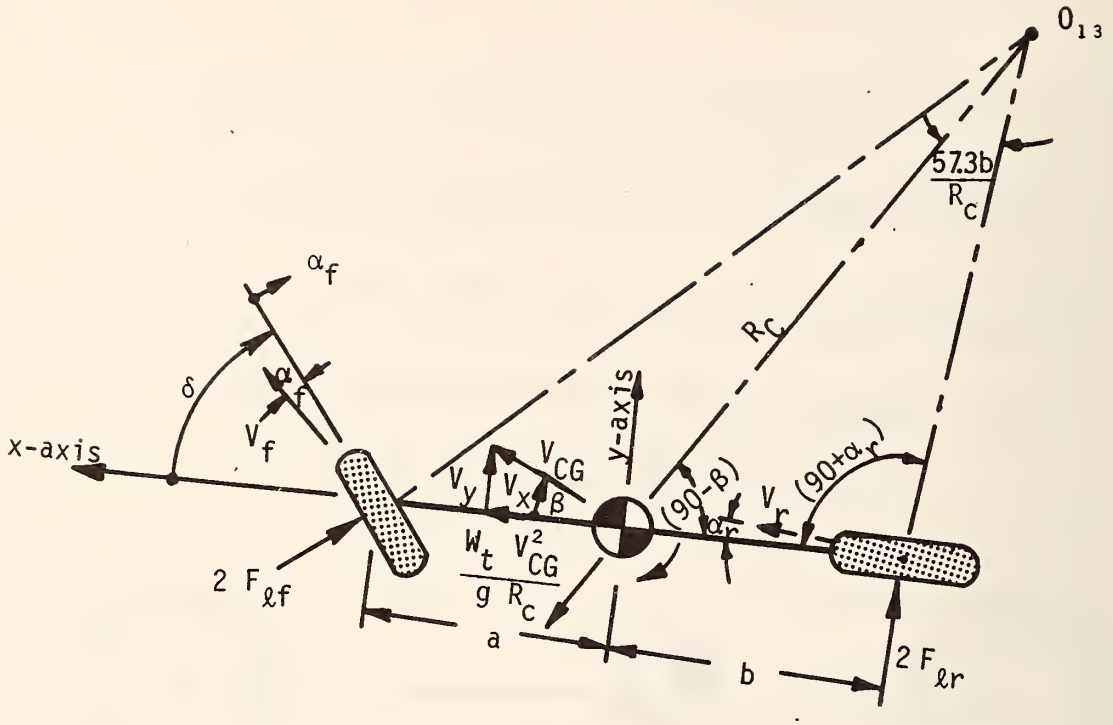

δ = Steer angle of front wheel (degrees)
α_f = Slip angle of front tire (degrees)
α_r = Slip angle of rear tire (degrees)
β = Sideslip angle (degrees)
R_c = Radius of curvature of vehicle path (feet)
$2\,F_{\ell f}$ = Lateral force on front tire (lbs)
$2\,F_{\ell r}$ = Lateral force on rear tire (lbs)
V_{CG} = Velocity of center of gravity (ft/sec)
V_y = Component of V_{CG} in the y direction (ft/sec)
V_x = Component of V_{CG} in the x direction (ft/sec)
r = Angular velocity of vehicle about the z-axis (rad/sec)
g = 32.17 ft/sec^2

FIGURE B.2 THE BICYCLE MODEL IN A CIRCULAR TURN - TOP VIEW

This result is based on the assumption that the angles α and β and the change in lateral force due to a change in camber are small quantities.

Equation B.1 may be substituted into B.2 to give

$$2 F_{\ell r} = \frac{2 W_r}{g} \frac{V_{CG}^2}{R_c} . \qquad (B.3)$$

The rear tire cornering stiffness, $C_{\alpha r}$, for small slip angles is

$$C_{\alpha r} = - \frac{d F_{\ell r}}{d \alpha_r} ,$$

or

$$C_{\alpha r} = - \frac{F_{\ell r}}{\alpha_r} . \qquad (B.4)$$

Equations B.3 and B.4 may be combined to give

$$\alpha_r = - \frac{W_r}{g} \frac{V_{CG}^2}{R_c C_{\alpha r}} . \qquad (B.5)$$

The path radius, R_c, is large relative to the distance b, and the magnitudes of β and α_r are small. Therefore, b may be considered as a cord which subtends an angle with magnitude

$$57.3 \frac{b}{R_c} \qquad \text{(degrees)}$$

as shown in Figure B.2.

The sum of the angles in the rear triangle of Figure B.2 is given by the equation

$$57.3 \frac{b}{R_c} + (90° - \beta) + (90° + \alpha_r) = 180° . \qquad (B.6)$$

This equation may be placed in the form

$$\beta = 57.3 \frac{b}{R_c} + \alpha_r . \qquad (B.7)$$

The desired equation for sideslip angle may be obtained from Equations B.7 and B.5, and it has the form

$$\beta = 57.3 \frac{b}{R_c} - \frac{W_r}{g} \frac{V_{CG}^2}{R_c C_{\alpha r}} . \qquad (B.8)$$

GPO 901-487